DNA Nanostructures as Templates for Hybrid Supramolecular Assemblies

by

Thomas G. W. Edwardson

A thesis submitted to McGill University in partial fulfillment of the requirements of the degree of

Doctor of Philosophy

Department of Chemistry
McGill University
Montréal, Québec, Canada

December 2014

To my parents, Janis and Doogie, and my wife Hee-un – I dedicate my work to you.

Abstract

DNA is used for the storage and propagation of genetic information in all living organisms. It is the programmability and molecular recognition properties of DNA which make this possible. Taking advantage of these properties, researchers have developed DNA self-assembly as a highly predictable method of bottom-up nanofabrication. The resulting nanostructures have the potential to solve important problems in diverse fields, from nanophotonics to gene therapy. To date most DNA nanostructures have been made purely from unmodified, natural DNA. To achieve structural complexity needed for functional devices, researchers have created intricate designs which often require a large number of DNA strands of different sequence,with increased cost and assembly error rates. This thesis examines the chemical modification of nucleic acids and their integration into DNA nanostructures. This approach is expected to simplify design and significantly reduce the number of DNA components, while adding functional complexity. Specifically, the introduction of orthogonal supramolecular interactions to DNA nanostructures and the resultant properties of these hybrid systems is investigated. Firstly, the synthesis of novel dendritic DNA amphiphiles and their self-assembly properties are investigated. The site-specific positioning of the amphiphiles on a cubic DNA scaffold allows the anisotropic organization of hydrophobic 'residues', in a manner similar to the side-chains on a protein backbone. A new set of self-assembly rules is discovered, in which these nanostructures show a geometry-dependent inter- or intra-molecular association. This is used to create the first example of a DNA nanostructure which can encapsulate and release small molecule drugs, an important challenge in nanomedicine. Secondly, this synthetic methodology is developed to produce a family of DNA-polymer conjugates, with sequence-defined polymers appended to DNA. These conjugates exhibit tunable self-assembly properties, dependent on the sequence of monomers in the polymer portion. Finally, the modular synthetic approaches developed are used to produce novel gold-binding DNA conjugates. The organization of these on prismatic DNA scaffolds creates patterns of DNA strands which can be efficiently transferred to gold nanoparticles. This template-guided 'printing' approach provides control over the number, directionality, geometry and sequence asymmetry of DNA strands bound to gold nanoparticle. Overall, the development of new synthetically modified oligonucleotides and their incorporation into nanostructures is shown to augment the field of DNA nanotechnology, introducing protein-inspired interactions and

providing new tools for the creation of functional nanodevices for applications in the fields of nanophotonics, nanoelectronics and biological sensing, as well as drug and oligonucleotide delivery.

Résumé

L'ADN est utilisé pour stocker et propager l'information génétique dans tous les organismes vivants. Ce sont les propriétés de programmabilité et de reconnaissance moléculaire de l'ADN qui rendent cela possible. Ces propriétés ont été mises à profit par les chercheurs qui utilisent l'auto-assemblage de l'ADN comme méthode hautement prévisible pour la nanofabrication ascendante. Les nanostructures résultantes ont le potentiel de résoudre des problèmes importants dans divers domaines, de la nanophotonique à la thérapie génique. A ce jour, la plupart des nanostructures d'ADN ont été faites uniquement à partir d'ADN non-modifié et naturel. Pour atteindre le niveau de complexité structurelle nécessaire pour des dispositifs fonctionnels, les chercheurs ont créé des modèles complexes qui nécessitent souvent un grand nombre de brins d'ADN de séquences différentes, ce qui est associé à une augmentation du taux d'erreur et du coût d'assemblage. Cette thèse examine la modification chimique des acides nucléiques et leur intégration dans des nanostructures d'ADN. Cette approche devrait simplifier la conception et réduire considérablement le nombre de composants ADN, tout en augmentant la complexité fonctionnelle. Plus précisément, cette thèse porte sur la mise en place d'intéractions supramoléculaires orthogonales dans les nanostructures d'ADN et les propriétés résultantes de ces systèmes hybrides. La première partie de cette thèse est dédiée à la synthèse de nouveaux amphiphiles d'ADN dendritique et à l'étude de leurs propriétés d'auto-assemblage. Le positionnement des amphiphiles sur certains sites spécifiques d'un échafaudage cubique d'ADN permet aux «résidus» hydrophobes de s'organiser de façon anisotrope, plus précisément d'une manière similaire aux chaines latérales sur un squelette de protéine. Les nanostructures qui ont été générées ont une géométrie qui est dépendante des associations intermoléculaires et intramoléculaires, ce qui fait parti d'un nouvel ensemble de règles d'auto-assemblage. Grâce à cette découverte, le premier exemple de nanostructure d'ADN ayant la capacité d'encapsuler et de libérer des médicaments à petites molécules a été créé. Ceci représente un défi majeur dans le domaine de la nanomédecine. De plus, cette méthodologie synthétique a aussi été développée pour produire une famille de conjugués polymères-ADN, avec des polymères

à séquences définies attachés à l'ADN. Ces conjugués possèdent des propriétés d'auto-assemblage modifiables selon la séquence de monomères présente dans les polymères. Enfin, les approches synthétiques modulaires développées ont aussi été utilisées pour produire de nouveaux conjugués d'ADN qui ont la capacité de se lier à l'or. L'organisation de ces derniers sur des échafaudages d'ADN prismatiques crée des motifs de brins d'ADN qui peuvent être efficacement transférés à des nanoparticules d'or. Cette approche qui est basée sur « l'impression » guidée par une matrice permet de contrôler le nombre, la directivité, la géométrie et l'asymétrie de la séquence des brins d'ADN liés aux nanoparticules d'or. Dans l'ensemble, l'élaboration de nouvelles modifications synthétiques d'acides nucléiques, et l'incorporation de celles-ci dans des nanostructures, a permis de contribuer au domaine de la nanotechnologie de l'ADN. Ceci a notamment débouché à l'instauration d'interactions semblables à celles généralement propres aux protéines et à la mise en place de nouveaux outils pour la création de nano-dispositifs fonctionnels qui pourront être appliqués dans les domaines de la nanophotonique, la nanoélectronique, la détection biologique et l'administration de médicaments et d'oligonucléotides.

- *Translation by Dr. Mehdi Belgnaoui*

Acknowledgements

Firstly, I would like to thank my research supervisor Dr. Hanadi Sleiman, whose enthusiasm for research led me to join the group as a Ph.D. student. I have been lucky to have been trained in an excellent research group, studying an area of chemistry which I find fascinating. I am evermore grateful for the fine balance of guidance, motivation, constructive criticism and creative encouragement I have received from Dr. Sleiman, which has directed my growth as a researcher. Thank you!

I would never have ventured this far into the world of science was it not for my great experience in the chemistry department at the University of Edinburgh, I would like to acknowledge in particular the group of Prof. David Leigh. It was while carrying out my Masters' project in the Leigh group that I developed an appetite for research. It was most likely due to the joy of working with my mentor at the time, Kevin, that I considered coming back to enter a Ph.D. program. Cheers pal!

Next, I would like to thank my fellow members of the Sleiman lab (Sleimanites?) who have been amazing from my first day ongoing. I am grateful to my initial mentors, Christopher McLaughlin, Graham Hamblin and Karina Carneiro for schooling me in the ways of DNA synthesis and assembly. I especially thank Karina for teaching me how to make modified DNA, giving me invaluable insights into every aspect of my graduate studies and for always giving me (false?) hope for AFM. I would also like to thank Chris M. for many fruitful discussions on research, from the fine details to the bigger picture. I would also like to thank Christopher Serpell for his help, guidance and motivation – it was a pleasure and a privilege. I would also like to thank Justin Conway, not only as a collaborator and colleague, but for many useful discussions on the art of brewing, music and the arcane science of temporal exploration. I thank Johans Fakhoury for both his biochemical and IT knowledge as well as his constant efforts to make our day-to-day lab life a little easier, you are a gentleman and a scholar. To Kai my long-term island buddy, it has been a pleasure to share a bench with you comrade, keep it black. Danny, thanks for all the cool stories, bro. To my lab son Donatien, you've made your father proud. And to all members of the Sleiman lab past and present – thank you for your unending help and companionship, it has truly been a pleasure.

I have also had the pleasure to work in various other laboratories in the chemistry department and I would like to thank those people involved. I would like to thank Dr. Masad Damha for allowing me access to and use of the HPLC instrument. I would like to

thank Matt Hassler and Glen Deleavey for teaching me the incredibly useful technique of HPLC. I thank Petr Fiurasek and CSACS for the use of and help with analytical instruments. I am grateful to Nadim Saade and Alexander Wahba for training and assistance in mass spectrometry and Mohini Ramkaran and Beatrice Lego for training and help with atomic force microscopy. I would like to thank the group of Dr. Albert Berghuis for access to their DLS instrument. I would also like to thank the Management and staff of Thomson House and PGSS for maintaining the inebriation and sanity of all graduate students.

I would also like to express my gratitude to Chantal Marotte who has been extremely helpful, from before I ever arrived at the department right to the end.

I would like to thank CIHR, CSACS, FQRNT and McGill University for the financial support during my doctoral studies. I would especially like to extend my gratitude to the McGill CIHR Drug Development Training Program.

Finally, I would like to thank my family for their love, understanding and encouragement from half-way across the world to home.

Contribution of authors

Chapter 2, **Thomas G. W. Edwardson** helped develop the project and primarily contributed to the production of experimental data from DNA synthesis, HPLC, mass spectrometry, electrophoresis, dynamic light scattering, atomic force microscopy and absorption and fluorescence spectroscopies and writing of the paper. **Karina M. M. Carneiro** helped design the project, developed the synthesis of modified DNA, aided data interpretation and co-wrote the paper. **Christopher K. McLaughlin** designed and synthesized the sequences for the DNA scaffold and additional unmodified DNA, data interpretation and co-wrote the paper. **Christopher J. Serpell** aided in the interpretation of data, discussion of results and co-wrote the paper. **Hanadi F. Sleiman** designed the project, guided interpretation of data, discussion of results and concepts and co-wrote the paper.

Chapter 3, **Thomas G.W. Edwardson** contributed to the synthesis, characterization and self-assembly studies of the DNA-polymer conjugates, production of experimental data, interpretation of results and co-wrote the paper. **Karina M. M. Carneiro** contributed to the synthesis of modified DNA, interpretation of data and co-wrote the paper. **Christopher J. Serpell** designed the project, carried out fluorescence experiments, aided in the interpretation of data, discussion of results and concepts and co-wrote the paper. **Hanadi F. Sleiman** designed the project, guided interpretation of data, discussion of results and concepts and co-wrote the paper.

Chapter 4, **Thomas G. W. Edwardson** helped develop the project and primarily contributed to the production of experimental data from DNA synthesis, HPLC, gel electrophoresis, dynamic light scattering, fluorescence spectroscopy and writing of the paper. **Kai Lin Lau** carried out gold nanoparticle synthesis, the majority of transmission electron microscopy analysis, prepared patterned gold nanoparticles for fluorescence spectroscopy, aided data interpretation and co-wrote the paper. **Danny Bousmail** carried out all dynamic light scattering experiments and data interpretation and co-wrote the paper. **Christopher J. Serpell** synthesized clip strands TC3-AB, PC4-AB and PP5-AB. **Hanadi F. Sleiman** designed the project, guided interpretation of data, discussion of results and concepts and co-wrote the paper.

Appendix, **Thomas G.W. Edwardson** helped design the project and carried out all experimental work. **Hanadi F. Sleiman** designed the project and guided interpretation of data, discussion of results and concepts.

Table of Contents

List of abbreviations

1D	One dimensional
2D	Two dimensional
3D	Three dimensional
AFM	Atomic force microscopy
AGE	Agarose gel electrophoresis
AuNP	Gold nanoparticle
BSA	Bovine serum albumin
CMC	Critical micelle concentration
CPG	Controlled pore glass
D-DNA	Dendritic DNA amphiphile
DMEM	Dulbecco's modified eagle's medium
DLS	Dynamic light scattering
ds	double-stranded
DTPA	Dithiol Phosphoramidite
EDTA	Ethylenediaminetetraacetic acid
ESI	Electrospray ionization
FBS	Fetal bovine serum
HE	Hexaethylene
HEG	Hexa(ethylene)glycol
HPLC	High performance (or pressure) liquid chromatography
HSA	Human serum albumin
R_h	Hydrodynamic radius
LC-MS	Liquid chromatography-mass spectrometry
MALDI	Matrix-assisted laser desorption ionization
MeCN	Acetonitrile
Min	Minute
MW	Molecular weight
PAGE	Polyacrylamide gel electrophoresis
PDI	Polydispersity index
PEG	Poly(ethylene)glycol
PPO	Polypropylene oxide
ROMP	Ring opening metathesis polymerization
TAMg	Tris-acetate-magnesium
TBE	Tris-boric acid-EDTA
TEM	Transmission electron microscopy
THF	Tetrahyrdofuran
rt	Room temperature
ss	single-stranded
UV/Vis	Ultraviolet-visible

1 Introduction

1.1 Origins

The dynamic organization of molecules and macromolecules is the underlying theme which ties together all life. This important regime lies within the realm of chemistry and molecular biology. Historically, chemists have sought to create, transform and control new forms of matter. The assemblage of individual atoms into molecules of almost any desired structure has been mastered, and as our capabilities have advanced so have our ambitions. Inspired by discoveries in the natural world, many chemists are now approaching the most complex forms of matter in an attempt to gain understanding, and ultimately control over such materials. This challenging prospect requires that chemists graduate from the creation of individual molecules to the precise engineering of interactions between molecules and macromolecules – the realm of supramolecular chemistry.

1.2 Bio-inspiration

It is clear that supramolecular chemistry is inspired by natural systems. Supramolecular complexes are held together by non-covalent forces, analogous to the receptor-substrate interactions seen in biological systems.[1] The creation of new synthetic molecules which are rationally designed from basic chemical principles may have produced the bulk of common materials used in current technology. However, the majority of our chemical inventory is at least in some respect derived from biology, whether it is the petrochemicals derived from decomposed biological matter or pharmaceuticals based on natural products. As our goals as chemists become more ambitious we look around us for inspiration from discoveries in biology. For example, to address energy concerns we look into photosynthesis,[2] to create new therapies we look into inherent regulatory mechanisms present in biological systems.[3]

1.3 The machinery of Nature

Upon looking at biological systems across all size regimes a common theme is evident; function is dependent on structure. This is how the machinery of natural systems works, whether looking at the height of a tree which can rise above the canopy of the forest to harvest light, or the molecular structure of a lipid molecule which forces it to create bilayer structures for compartmentalization. Chemists have gladly taken up the challenge and tried to mimic some of the fundamental mechanization and computational ability of biological components, and with a great deal of success. This begins with understanding Nature's design assembly strategy; how do things come together? The answer is by self-assembly, both inter- and intramolecular, of different units into the required structure. Fundamentally, this relies on local, weak interactions to guide the reversible assembly of structures, thus retaining dynamic character.

One essential aspect of the self-assembled systems found in nature is the breadth of interactions used to create the various components. This starts with covalent bonds which make up primary structures, i.e. peptide linkages and phosphodiester bonds - the backbone of our genes. Indeed, the making and breaking of covalent bonds is important in growth, metabolism and reproduction of living organisms. However, of equal importance, and arguably more far-reaching, are the variety of weak non-covalent interactions which organize the molecules, transforming them into functional entities. These consist of electrostatics, hydrogen bonding, dipole-dipole, Van der Waals and the hydrophobic effect. Protein folding represents the most exquisite application of these interactions in concert, to produce well-defined structures extremely selectively and quickly. The efficiency of this process largely remains a mystery to researchers.[4]

As much as we would like to be able to produce self-assembling systems of this complexity, we are limited by our understanding to produce a reasonable prediction of the structure based on the components when so many interactions are involved – *it's simply just too complicated.* For this reason, as a starting point it is best to limit our palette of interactions so that we can design building blocks with a good idea of the result of their self-organization. DNA has emerged as a very promising candidate in this respect. The concepts, assembly strategies and applications of the resulting DNA materials will be discussed herein.

1.4 Structural DNA Nanotechnology

The use of DNA as a construction material in nanotechnology has become well established since its inception in the '80s. As with many innovative ideas the inspiration and original purpose of using DNA to build nanomaterials was overtaken by the broad potential of the strategy, which has far-reaching practical applications. In 1982 Seeman proposed that DNA could be a potential solution to the problem of protein crystallization.[5] The ideas and discoveries in this early work can be distilled into one powerful concept: DNA scaffolds could be used to position other materials precisely on the nanoscale. Building upon this idea has resulted in rapid expansion of the field in recent decades.

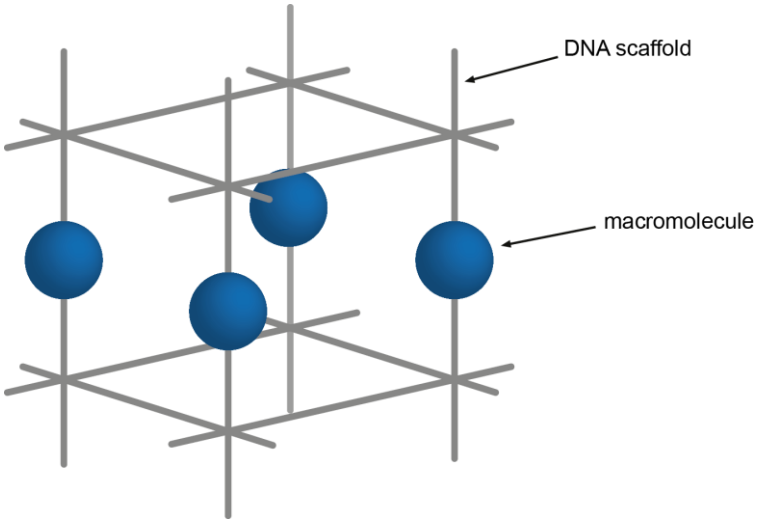

Figure 1.1 - The concept of DNA nanotechnology. The original idea proposed by Seeman was to organize proteins on a DNA framework to aid structure determination by x-ray diffraction.

Nature has developed proteins as the material of choice for construction of the majority of structural and functional components, while nucleic acids hold the information necessary to create that assortment of polypeptides. The reason that nucleic acids are well-suited for information storage can be attributed to their incredible molecular recognition properties. Upon determination of the structure of duplex DNA, Watson and Crick proposed that the specific base-pairing seen between complementary DNA strands may be the key to the copying mechanism which permits propagation of genetic information.[6] This process is now well understood and forms the foundation for the central dogma of molecular biology, Figure 1.2.[7]

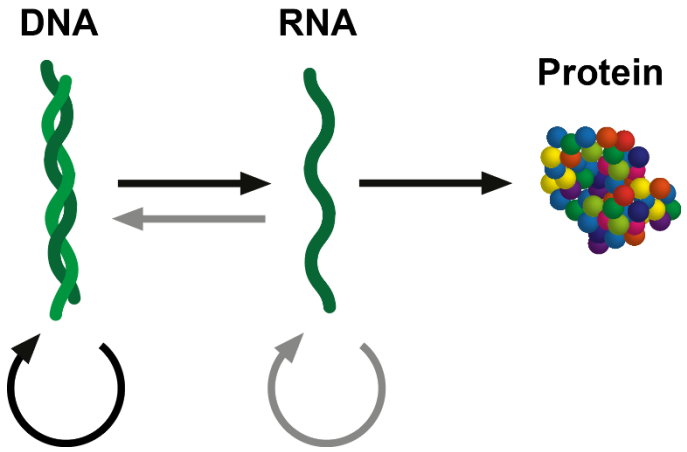

Figure 1.2 - The central dogma of molecular biology. The role of DNA in nature. Black arrows represent the normal flow of genetic information and grey arrows represent special circumstances.

In the context of self-assembly it is the highly specific, and importantly, predictable molecular recognition of DNA which makes it a fantastic building block for nanofabrication. In fact, its specificity and efficiency of self-assembly is only rivaled by its natural counterpart, the polypeptide. The structure of B-form DNA is shown in Figure 1.3.

As a starting point, let us consider the structural parameters of DNA from the bottom-up. It is a polymer in which the repeat unit comprises a deoxyribose sugar ring with a nucleobase attached through an N-glycosidic bond at the 1 position and a phosphate group at the 5' position. This monomer unit is termed a nucleotide (nt). Thus it follows that long chains should be referred to as polynucleotides, although it is now common to see the term oligonucleotide used for synthetic DNA molecules of various lengths.

DNA sequences are determined by the identity and order of the four heterocyclic nucleobases; the pyrimidines Cytosine (C) and Thymine (T), and the purines Adenine (A) and Guanine (G). The canonical base-pairing is between A:T and C:G, and is mediated by hydrogen bonding between the nucleobases. Free energies of the A:T and C:G bonds in aqueous solution have been determined as -4.3 and -5.8 kcal/mol, respectively.[8] Therefore the percentage of G/C bases (GC-content) is a useful indicator of the relative stability of DNA duplexes. In the double helical structure of duplex DNA, electrostatic and

hydrophobic/Van der Waals interactions between the stacked bases also substantially stabilize the duplex.

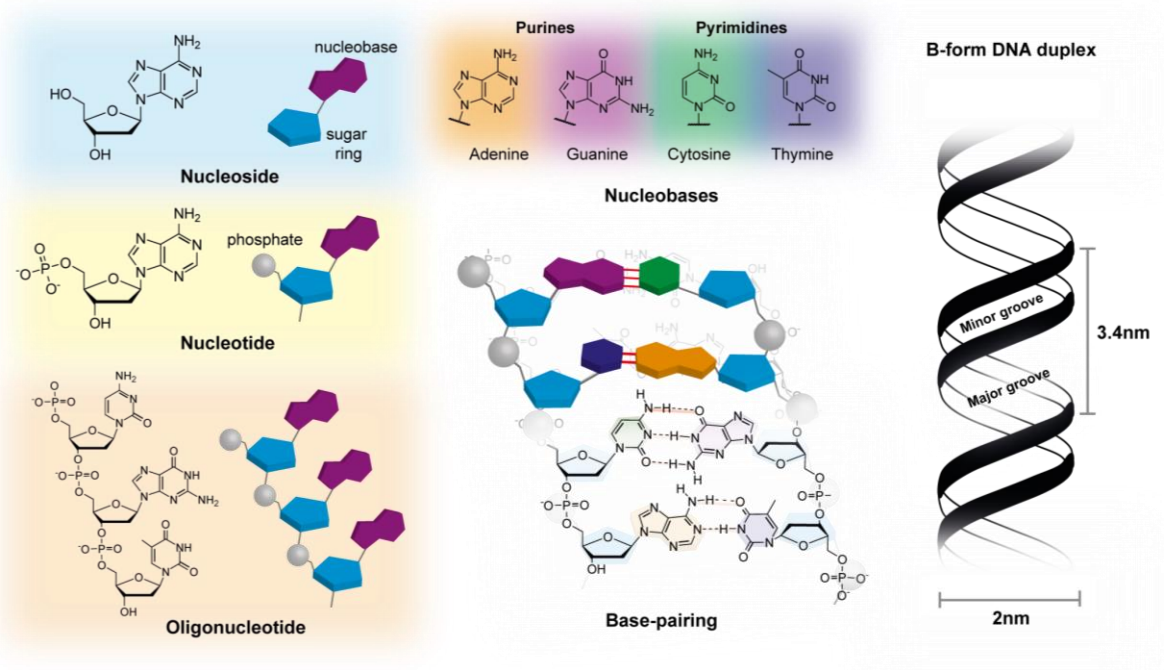

Figure 1.3 – Structure of DNA as a molecule. On the left are shown the individual building blocks of DNA, nucleosides and nucleotides, which include a 5' phosphate group. In the middle are the four nucleobases and the Watson-Crick base-pairs A:T and C:G. On the right are the dimensions of duplex DNA.

Double-stranded DNA (dsDNA) has very well-defined dimensions, which make it useful as a building block for nanomaterials. The most common conformation, B-form, is coiled in a right-handed double helix with 0.34nm between each base and a helical pitch of 10.5 base pairs. The diameter of B-form dsDNA is 2nm. At lengths of under 10nm dsDNA behaves as a rigid-rod and over larger length scales it has a persistence length of approximately 50nm.[9] These are important parameters with implications in the design and resulting structures of DNA self-assembly.

1.4.1 DNA synthesis

Although an in-depth chronological discussion is beyond the scope of this introduction, it is important to note that the thriving development of not only DNA nanotechnology but biotechnology as a whole would not be possible if it were not for the tremendous advances in oligonucleotide synthesis over the last fifty years. Now taken for granted by researchers spanning various disciplines, the affordable availability of large amounts of custom oligonucleotides has enabled a wealth of scientific progress which would not have been possible otherwise.

As the application of solid-phase oligonucleotide synthesis in the creation of new DNA-conjugates is an underlying theme in this thesis, the reasons for its success will be briefly summarized here. The fundamental requirement for oligonucleotide synthesis is quantitative coupling chemistry which can be carried out in a stepwise manner to allow sequence definition. Comparable to peptide synthesis, a strategy employing monomers with orthogonally protected functional groups has been developed. A crucial aspect of the synthesis is that it is carried out on a solid-support, typically controlled-pore glass or polystyrene beads. This has made the process amenable to high-throughput automation.

A variety of different approaches to the coupling chemistry have been researched,[10] with the most widely used now being the phosphoramidite method,[11,12] see Figure 1.4. Phosphoramidites are highly reactive, thus allowing each coupling step to be carried out quickly in high yield. Another practical consideration is that a single chemical treatment of the solid support can be used post-synthesis to liberate the molecules from the support and remove the nucleobase and phosphate protecting groups. The use of base-labile protecting groups and solid-support linkers allows this.

The synthetic cycle consists of four major steps, Deblocking, Coupling, Capping and Oxidation (Figure 1.4). Deblocking, or detritylation, removes the trityl group from the 5' hydroxyl under acidic conditions. The most commonly used trityl group is dimethoxytrityl, which is removed easily with dichloroacetic acid. Coupling introduces the next monomer as a 5' DMT-protected deoxynucleoside (2-cyanoethyl, N,N-diisopropyl) phosphoramidite, this step is also carried out under acidic conditions, typically using tetrazole derivatives as the 'activator'. The capping step is important to reduce side-products caused by unreacted 5' hydroxyl groups. If free 5' hydroxyl groups were left uncapped they could participate in the next coupling cycle and produce a

complex mixture of products, thus complicating purification. Next, the oxidation step converts the phosphite triester to a phosphate triester, this must be carried out after each coupling step due to the instability of phosphite triesters to acid. The cycle then begins again with deblocking and introduction of the next monomer, the process repeated until the desired product is fully grown on the solid support. Finally, treatment with aqueous ammonia or methylamine mixtures releases the oligonucleotides from the solid support and removes the base-labile nucleobase and cyanoethyl protecting groups, giving the crude oligonucleotide ready for purification.

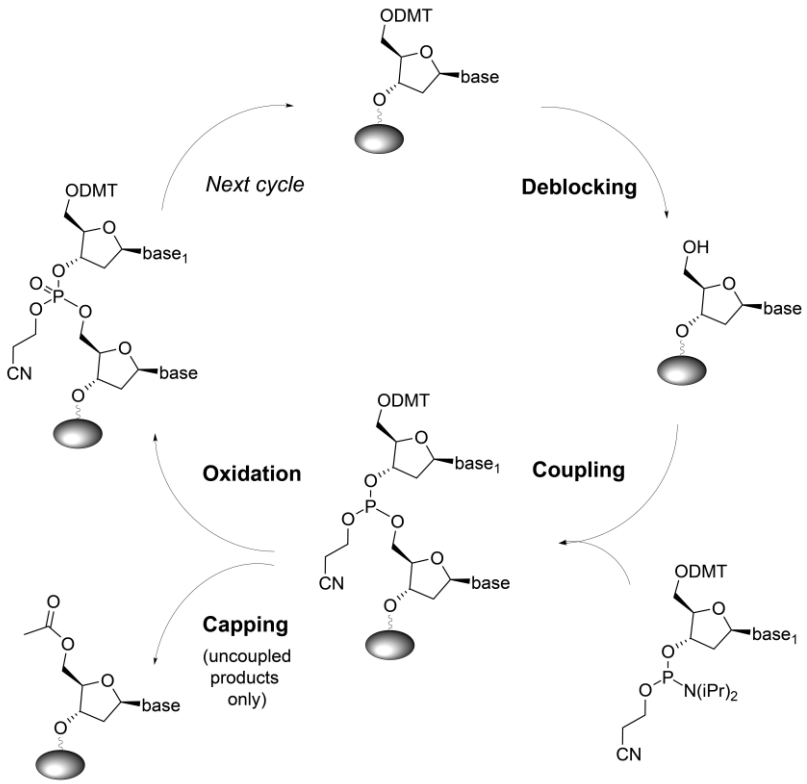

Figure 1.4 Solid-phase DNA synthesis. The four stages of the phosphoramidite method are shown; 1) Deblocking, 2) Coupling, 3) Capping and 4) Oxidation.

It should be pointed out that biologically derived and enzymatically synthesized DNA can also be used in DNA nanotechnology, for example see DNA origami below. It is also worth noting that the reasons for the use of DNA rather than RNA to create nanostructures are mostly practical; RNA is much less stable as a molecule and it is harder to synthesize in high yield. Additionally, RNA is more prone to forming stable secondary structures, which can compete with the desired intermolecular interactions required to

form the target self-assembled structure. However, recently, RNA has also demonstrated versatility as a building block for self-assembled structures.[13]

When constructing any larger object from smaller components there are some basic criteria which must be met. At the simplest level, each building block must be structurally well-defined, and there must be a way of connecting each block together. As DNA hybridization is highly programmable this has allowed a variety of different strategies to be used for the assembly of DNA nanostructures, these approaches are divided and summarized below.

1.4.2 Assembly using branched junctions

While oligonucleotide sequences can be designed so that they recognize a complementary strand and therefore form a double helical structure, the linear nature of the duplex limits structural complexity. To apply DNA as a construction material it would need to be adapted into 2D or 3D motifs. Branched DNA junctions are known to be a crucial part of biological processes, but it was the visionary idea of Seeman to repurpose these for structural applications.[5]

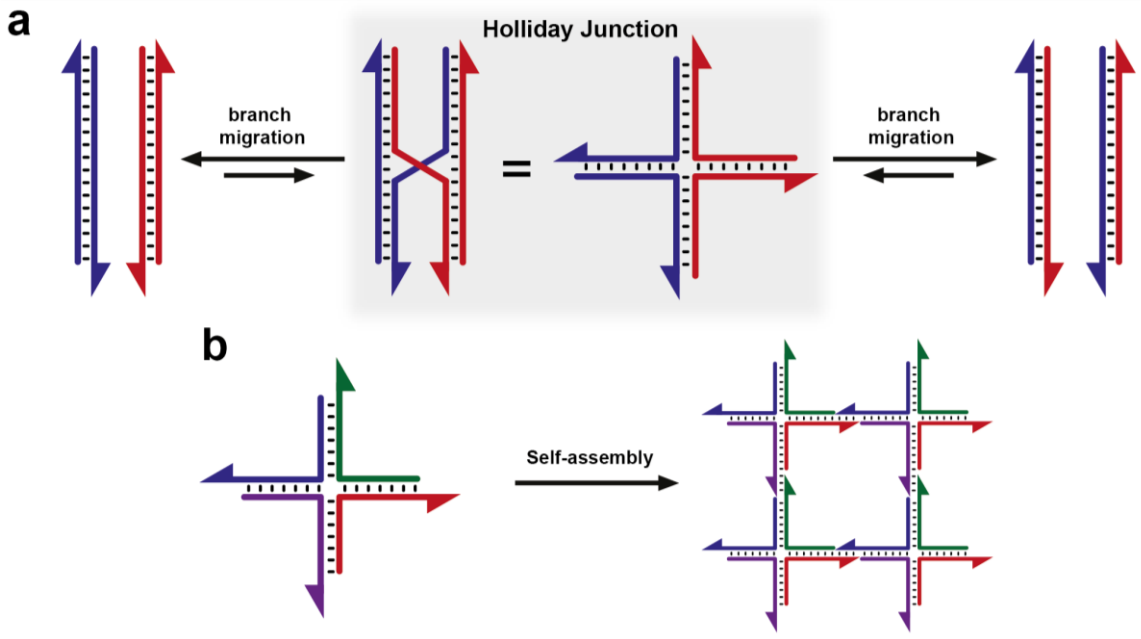

Figure 1.5 – The Holliday junction and asymmetric analogues. a) A mobile Holliday junction is shown which is prone to branch migration. b) An immobile branched junction is created using sequence asymmetry, conceptual self-assembly via sticky end cohesion to produce a periodic 2D network.

Seeman's original idea was that DNA junctions, assembled into a crystalline array, could be used as a scaffold for the organization of macromolecules, such as proteins. For this to be possible it is important that the junctions are stable, i.e. not prone to branch migration as seen in the biologically derived junctions, Figure 1a. This problem was overcome by the introduction of sequence asymmetry to create immobile junctions, described in Figure 1.5b.[14] Sequence asymmetry is an important design concept in DNA nanotechnology, it involves the introduction of unique oligonucleotide sequences to different parts of a structure to prevent dynamic rearrangement and allow site-specific addressability. In the case of the immobile junctions this means a unique sequence is used for each arm, shown as different colors in Figure 1.5b.

To facilitate the further assembly of these 2D building blocks into long-range structures, short single-stranded (ssDNA) overhangs bearing complementary sequences were positioned at the end of each arm, these are referred to as 'sticky ends'. Through base-pairing of the ssDNA sticky ends the building blocks can be expected to align into an infinite 2D network. This experiment laid down a foundational concept for DNA nanotechnology: long-range order can be achieved by using branched junctions and the periodicity of the resultant structure could be manipulated by changes to the junction used. Unfortunately, these structures were not able to form the expected network structures and this was found to be due to intrinsic flexibility and conformational mobility of the junction.[15-17] Pre-assembly into more rigid architectures was later used to create rigid building blocks for network assembly.[18,19] This led to the development of more robust junctions and tile-based DNA assembly, which are discussed in more detail in the next section.

Although flexibility prevents the use of Holliday-type branched junctions as the basic individual components for 2D assembly, this flexibility enabled their application in 3D construction. The first 3D DNA nanostructure, with the connectivity of a cube, was reported by Seeman in 1991, Figure 1.6a.[20] Although synthesized through a series of catenane-like intermediates which were enzymatically ligated, the final structure can be broken down into essentially eight three-way junctions. This strategy was expanded to produce simple structures, a trefoil knot,[21] mechanically interlocked topologies,[22] and larger structures such as a truncated octahedron,[23] and it was proposed that this methodology could be used to produce a wide-range of polyhedra. Expansion of the branched junction toolbox to five- and six-arm,[24] and later eight- and twelve-arm

junctions has also been achieved.[25] The five-arm junction was applied in the construction of large icosahedra which have been used for the encapsulation and controlled release of macromolecular cargo.[26,27] However, the demanding synthetic procedures required to create such structures have resulted in the development of other, simpler and more modular, routes to 3D DNA nanostructures.

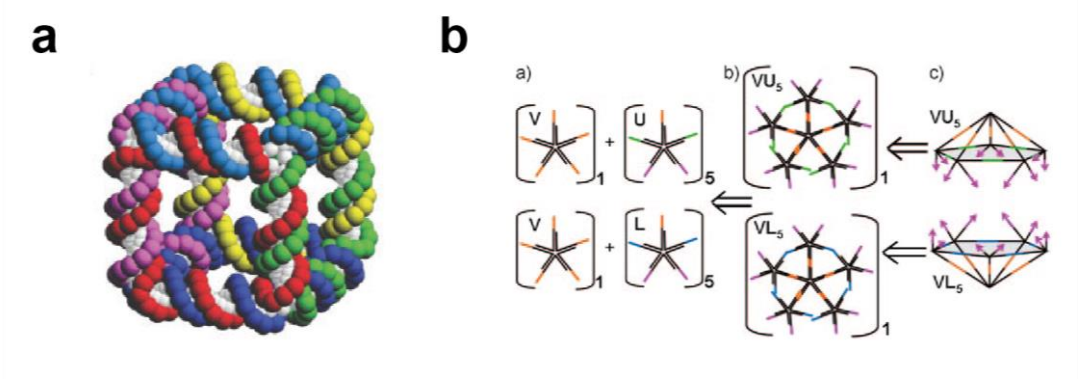

Figure 1.6 - 3D DNA nanostructures. a) A DNA cube, the first 3D DNA nanostructure. Adapted with permission from reference 15 (Nature Publishing Group, 2003) b) Icosahedron produced in a modular fashion from 5-arm branched junctions. Reproduced with permission from reference 21 (Wiley-VCH, 2009)

1.4.3 Tile-based DNA assembly

The need for rigid components, which provide the necessary preorganization to allow the formation of long-range DNA lattices, led to the use of double-crossover (DX) junctions as building blocks.[28,29] DX motifs consist of two Holliday junctions which are connected by helical domains. The helical domains can be parallel (DP) or anti-parallel (DA), anti-parallel versions are commonly used as they are more stable. Another variable is the number of helical half-turns between each crossover point, these can be odd (O) or even (E). Thus, for example a DAE junction is a double-crossover molecule with antiparallel helical domains and an even number of half-turns between each crossover point, see Figure 1.7a. The DAE and DAO junctions were found to form robust 2D networks by treating each DX unit as a programmable tile, using unique sticky ends to drive network formation, Figure 1.7b-c.[30] This use of rigid DNA tiles for the formation of networks was expanded to a variety of crossover junctions/tile designs.[31] With a robust method for 2D crystallization of DNA, the applicability of these networks for the

nanoscale organization of materials was investigated. The first example of periodic organization of macromolecules on a 2D DNA network was the positioning of streptavidin protein, using biotin-labelled DNA as the molecular recognition component.[32] The same DNA structure was used to template the growth of silver nanowires, showing the versatility of 2D networks as scaffolds. To date, controlled arrangement of various proteins and gold nanoparticles have been realized, introducing differing spacing and periodicities by changing the tile design used. These nanoarrays have shown great potential for use in enzyme cascades, biosensing, nanoelectronics and photonics.[31,33]

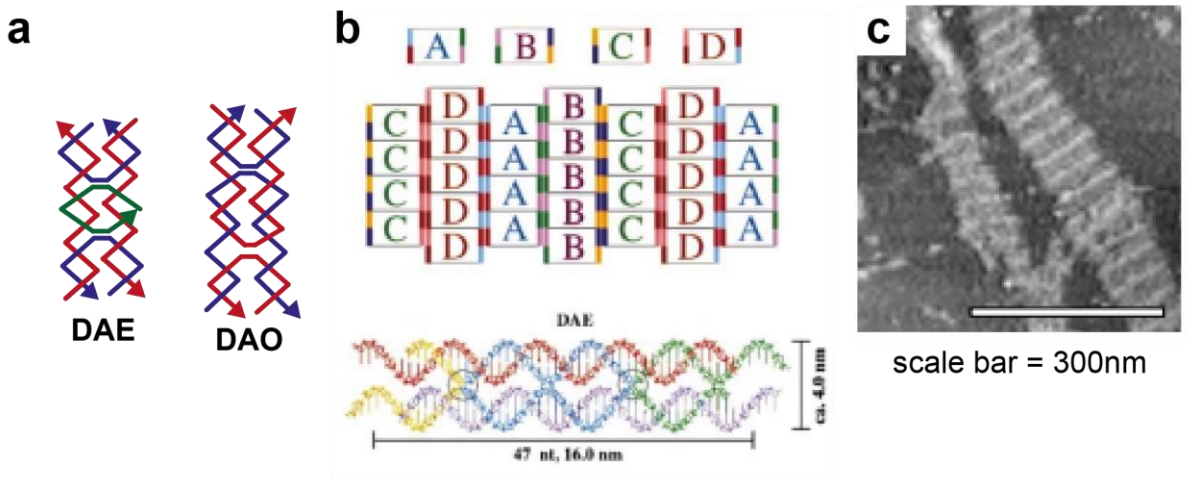

Figure 1.7 – Tile-based DNA assembly. a) Structure of the DX junctions DAE and DAO. b) 2D Network assembly using DAE tiles. c) Atomic Force Microscopy (AFM) image of 2D DNA crystal formed from DAE tiles. Adapted with permission from reference 25 (Nature Publishing Group, 1998)

The applicability of tile-based assembly is not limited to two dimensions. Mao used the intrinsic curvature of three-point star tiles in a modular approach to produce a series of discrete polyhedral Figure 1.8a.[34,35] An important aspect of these assemblies was the use of a sequence symmetric approach; contrary to using unique sequences for the sticky ends, the tile arms were designed to have equivalent and self-complementary ssDNA overhangs. Sequence symmetry simplifies design, reduces costs and can reduce the occurrence of assembly errors.[36] Five-point stars were implemented to produce larger structures, icosahedra, further highlighting the importance of tile flexibility in the production of 3D structures.[37] The expansion of this methodology to produce more complex 3D architectures was recently reported, showing that tile-based assembly is a valuable assembly strategy for the production of complicated structures.[38] These have

been used as model systems to answer fundamental questions about the stereoselectivity of nanostructure assembly.[39]

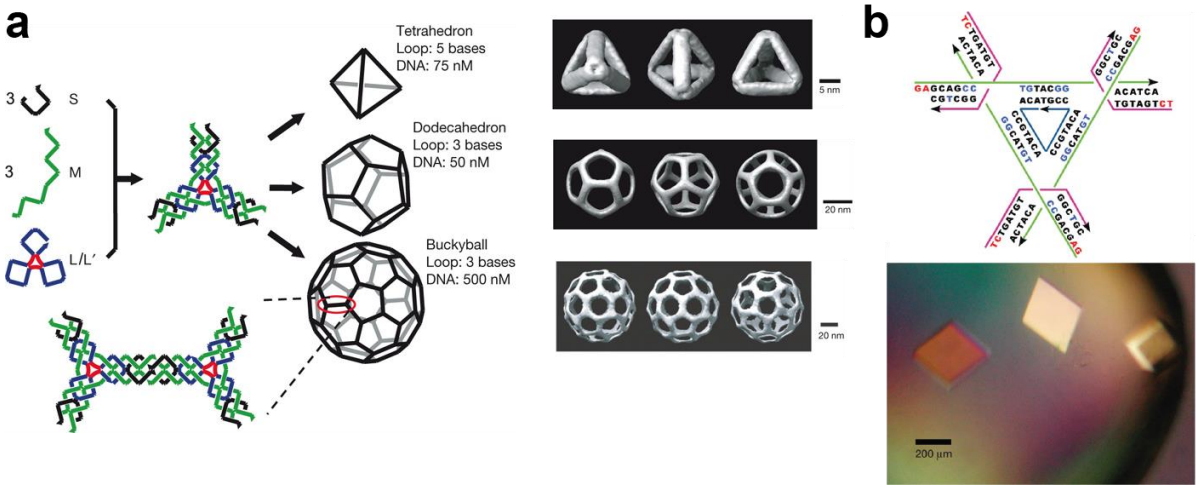

Figure 1.8 – 3D structures from tile-based assembly. a) Self-assembled polyhedral from three point star motif tiles. Adapted with permission from reference 29 (Nature Publishing Group, 2008). b) Tensegrity tile used to create macroscopic 3D DNA crystals. Reproduced with permission from reference 35 (Nature Publishing Group, 2009).

Long-range 3D tile-based assembly was realized by Mao and Seeman, who used rigid 3D tensegrity triangles to produce a macroscopic crystal, Figure 1.8b.[40] The crystal structure was resolved to allow structural characterization of this nanostructured DNA-based material at high resolution. Although not strictly through tile-based assembly, a precursor design which used non-canonical base-pairing to produce a 3D crystal has recently been shown to undergo pH switchability and applied in biocatalysis.[41,42]

An important concept in the design of DNA tiles is the dihedral angle between each unique dsDNA which makes up the complete tile structure. This angle is a consequence of the consistent helical pitch in dsDNA, and can be varied by altering the spacing between crossover points, or branched junctions, that tie the duplexes together. The tiles described so far were designed to have an approximate 180° dihedral between duplexes. However the creation of more rigid, 3D tiles in the form of helix bundles was achieved by reducing the dihedral angles such that the tile folds on itself full circle, see Figure 1.9. The reduction of the dihedral angle is achieved by changing the number of nucleotides between the crossover points, divergence from full or half-turns alters the relative helical pitch of the arms relative to each other. These bundles were shown to form into 1D

nanotubes, with very small radii, which were used to template metallic nanowire synthesis and also to form 2D lattices.[43,44] Additionally, applications in artificial photosynthesis have been demonstrated, using seven-helix bundles as scaffolds to arrange chromophores into an artificial light-harvesting antenna.[45]

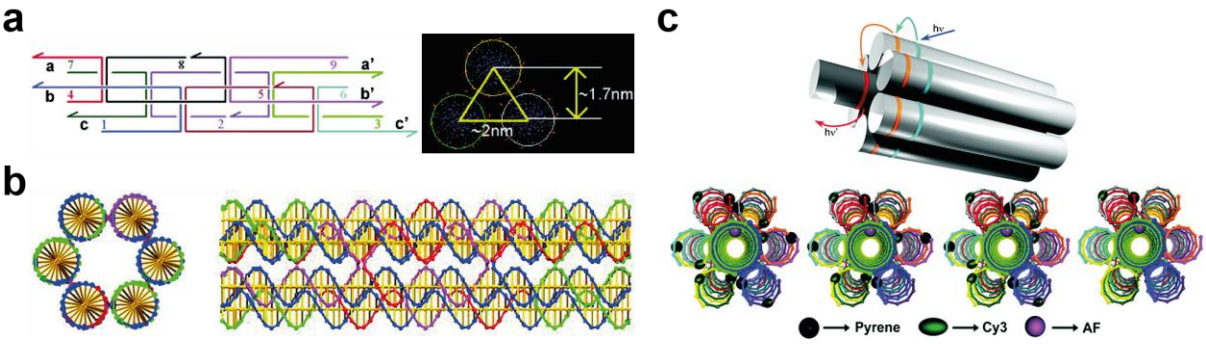

Figure 1.9 – Changing dihedral angles within tiles. a) Three-helix bundles are formed with a 60° angle between helices. Reproduced with permission from reference 39 (American Chemical Society, 2005). B) Six-helix bundles have a 120° angle between helices. Reproduced with permission from reference 38 (American Chemical Society, 2005). C) Positioning of fluorophores on a seven-helix bundle produces an artificial light harvesting antenna. Reproduced with permission from reference 40 (American Chemical Society, 2011)

Another interesting aspect of DNA nanotechnology, especially tile-based assembly, is its application in computer science.[46] From this point of view, each unique unit can be treated as a 'Wang' tile, an abstract mathematical concept which addresses the arrangement of individual building blocks into an infinite 2D network. Wang tiles can be represented as squares with unique edges that can only come together with their proper edge partner. This is analogous to sequence asymmetric DNA tiles which have unique sticky ends which allow specific tile-tile interactions. Assembly of the tiles results in an ordered network which can be periodic or aperiodic in nature, depending on the set of tiles used. When using certain sets of tiles, 'algorithmic self-assembly' is possible,[47] which can be used to carry out logical operations.[48] This relies on the use of different interaction strengths between tiles, which can be achieved by altering the DNA sequence of each sticky end. For example, Winfree used this concept to make a set of tiles which grow into a 2D network with the discrete 'Sierpinski triangle' pattern.[49] In these systems the growth of the crystal depends on the current state of the crystal and can be equated to a series of inputs, added tiles, creating a defined output, the growth pattern. Importantly, this means

that DNA nanostructures can solve any computable problem and are therefore great candidates for use in molecular computing. [50]

The concept of tile-based DNA assembly has recently been reduced to its simplest structural form by equating a single DNA strand to a tile, termed single-stranded tiles (SSTs).[51] The method uses a large number of unique asymmetric units, each SST having a unique sequence, and therefore precise address, in the final structure. This is used to create a large molecular canvas, approximately 60 x 100 nm in size, consisting of individual pixels which can be omitted selectively to create a variety of complex shapes. The SST assembly strategy has more recently been taken into the third dimension by the introduction of a 90° dihedral angle between SSTs upon hybridization, Figure 1.10.[52] Additionally, the introduction of strand displacement mechanisms to SST designs has been shown to allow morphological reconfiguration.[53]

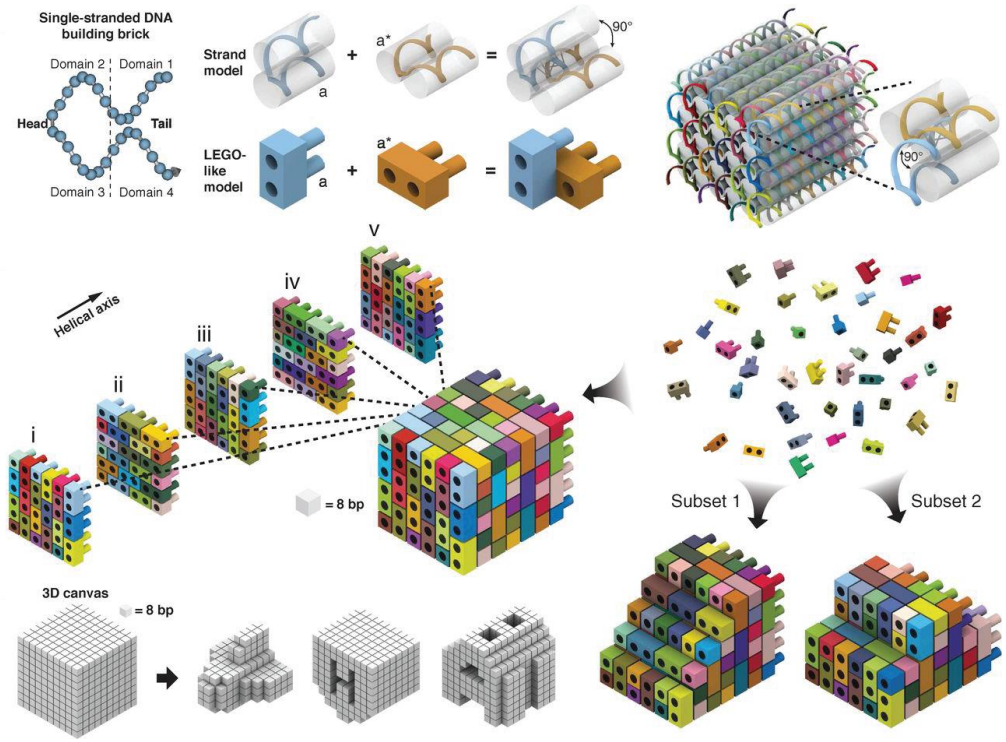

Figure 1.10 – 3D shapes from DNA bricks. a) Assembly of 3D nanostructures from single stranded tiles (SSTs), each SST has a unique position in the final structures represented by different colored bricks. Reproduced with permission from reference 47 (AAAS, 2012).

In summary, tile-based assembly has taken DNA nanotechnology from concept to application. The wide array of tile designs available and the range of structures which can be produced from them is impressive. The use of tile-assembled DNA nanostructures as

scaffolds for the precise organization of other components has also been well established. However, the majority of the 2D assemblies created from tile-based assemblies are periodic structures, the introduction of more complexity is limited by the increasing assembly error rate.[54] For this reason, alternative approaches have emerged for creating robust designer nanomaterials based with DNA.

1.4.4 DNA origami

Rothemund introduced the concept of scaffolded DNA origami to the community in 2006.[55] This work built upon a design strategy introduced by Joyce and co-workers, where a 1700nt single strand of DNA was folded into an octahedron, guided by 40nt chaperones.[56] The origami method makes use of a long scaffold strand, around 7000nt in length, genomic DNA obtained from the M13 bacteriophage. This circular scaffold strand is forced to fold into a specific shape through the introduction of around 250 unique 'staple' strands, less than 100nt, which pinch it together at specific sites. The staple strands are added in a large excess, and need not be highly pure oligonucleotides. The result are large 2D nanostructures, around 100nm across, with arbitrary shapes and a resolution of 6nm, which is defined by the length of the staple strands.

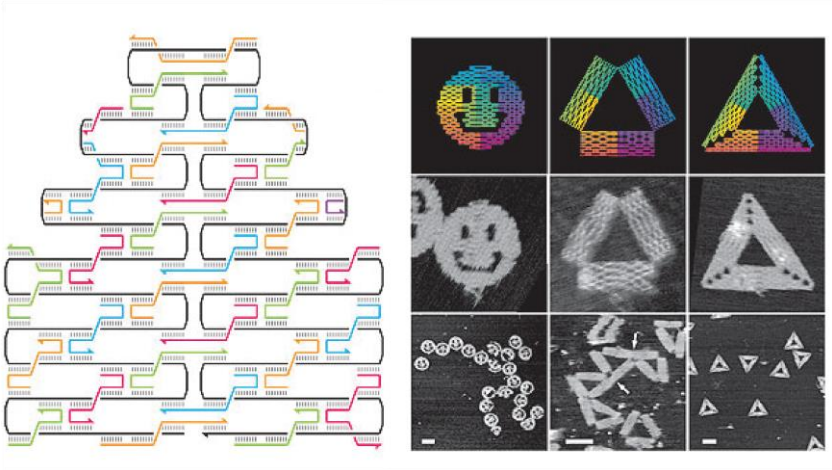

Figure 1.11 – 2D Scaffolded DNA Origami. The long scaffold strand (black) is folded into a 2D shape by the colored staple strands, resulting in the production of arbitrary 2D shapes. Adapted with permission from reference 50 (Nature Publishing Group, 2006).

Conceptually, DNA origami bears a lot of similarities to the SST approach introduced in the previous section, the SST method which appeared later was inspired by the

structural complexity which could be achieved through DNA origami. Like the SST method, the level of structural diversity available comes at the price of a very large sequence pool. Although this makes DNA origami a costly endeavor it has still become widely used by various research groups due its accessibility, high level of control and ease of characterization of the assembled structures.

In 2009, three different strategies to take the origami method into three dimensions were reported. The first involved directing six different regions of the scaffold strand to form the six sides of a large cube, furthermore one side acted as a lid which could be opened in response to a specific DNA input.[57,58] A similar strategy was used by Sugiyama's group to produce hollow prisms folded from multi-armed 2D structures.[59] The second involved the introduction of acute dihedral angles to fold the sheets over on themselves,

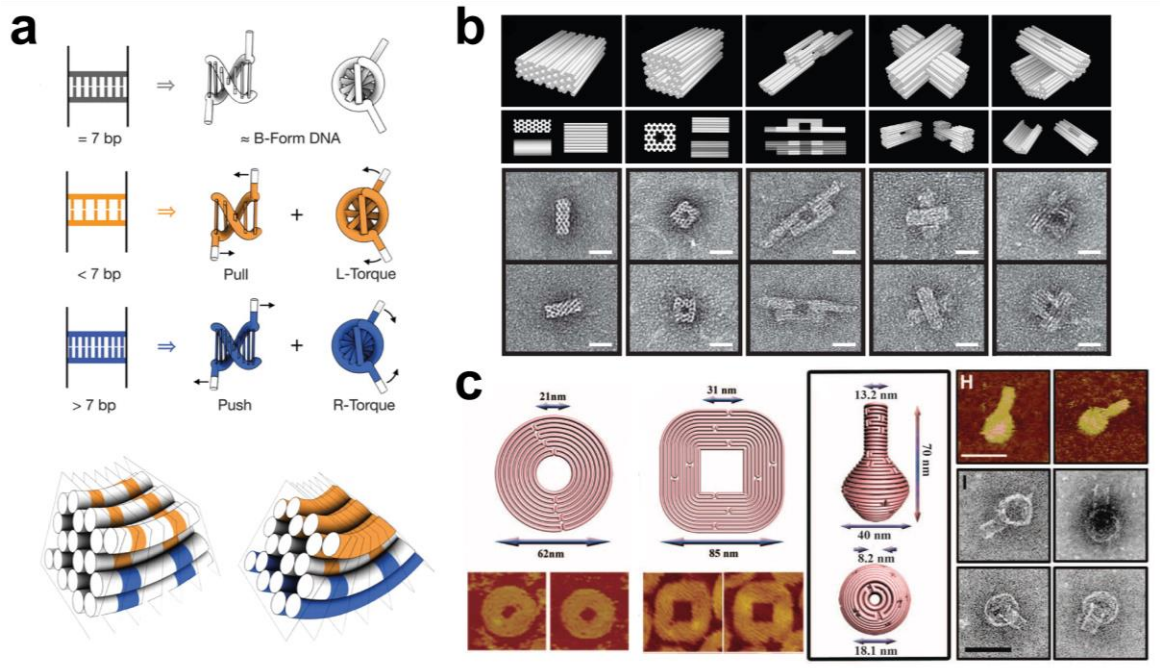

Fig 1.12 – 3D Scaffolded DNA origami. a) Addition (blue) or deletion (orange) of nucleotides caused over and underwinding of the helices to produce curvature in an origami bundle. Adapted with permission from reference 56 (AAAS, 2009) b) Layering of origami sheets to create 3D structures. Reproduced with permission from (Nature Publishing Group, 2009) c) Introduction of curvature across two planes to create complex 3D nanostructures. Adapted with permission from reference 57 (AAAS, 2011).

creating a honeycomb lattice when viewed end-on, Figure 1.12b.[60] The third method described relied on the introduction of curvature though torsional strain caused by under- and over-winding of dsDNA portions, producing curved and twisted constructs, Figure 1.12a.[61] The complexity of curvature was further developed by Yan et al. who

introduced curvature across two planes resulting in structures reminiscent of these produced from a potter's wheel, Figure 1.12c.[62] Another approach for 3D construction was the use of tensegrity, seen in tile-based assembly before, but on a larger scale to produce discrete pre-stressed structures bearing similarities to macroscopic architecture.[63]

Unlike the infinite networks which are, in theory, possible with tile-based DNA assembly, the size of a single origami is limited by the scaffold length of approximately 7000nt. The potential to expand the size was addressed by Rothemund, introducing staple strands along the edges of single-scaffold structures, treating each origami sheet as a tile to allow hierarchical assembly. However the yields were very poor due to the need for careful stoichiometry of staple strands, which has led to other strategies. Sugiyama's group introduced the concept of shape recognition between origami tiles, creating nanoscale 'jigsaw pieces' which fit together with specific orientations like mortise and tenon joints.[64] Yan and co-workers layered origami tiles over each other, in a cross motif, and used them to create a square lattice via sticky end cohesion in a tile-based fashion.[65] Other polymerization methods were investigated, linking tiles into ribbons by using ssDNA to zip up the seams between each single-scaffold structure.[66] A very interesting discovery was that origami tiles could be connected using blunt-ended stacking interactions.[67] This introduction of a different mode of assembly, expanding the palette of interactions represented a step towards multiple, specific molecular recognition events guiding self-assembly. The use of a longer scaffold strand, comprised of more than 51,000 nt, has enabled researchers to produce origami structures seven times larger than the conventional approach.[68] The most recent development was the use of origami DNA tripods by Yin's group, which mimic the three-point star tiles described earlier and come together to produce an array of large polyhedra by changing the angle of each corner origami piece.[69] The dimensions of the structures are 100nm across each edge, these are the largest discrete 3D DNA nanostructures yet created.

Due to its popularity DNA origami has been used to solve problems in various areas of science and technology. A single origami tile has around 250 staple strands which can be individually modified to allow site–specific placement of other materials. DNA Origami can be thought of as a robust molecular pegboard to vary the spacing between functional components. This has been used to create nanoscale rulers for microscopy,[70] plasmonic devices,[71-74] protein arrays,[75,76] and for single-molecule analysis.[77] Three-dimensional

origami structures have been used to create smart drug-delivery devices,[78,79] artificial ion-channels,[80] and used as nanoscale foundries for gold nanoparticle synthesis.[81,82]

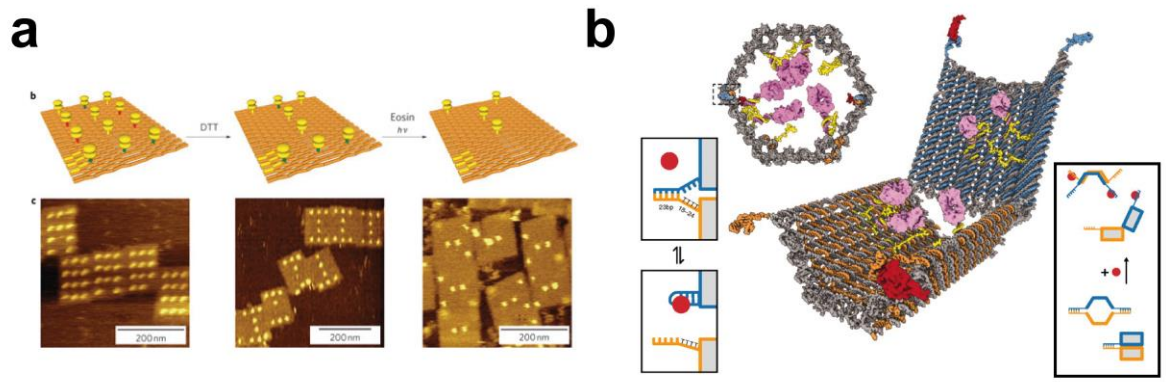

Figure 1.13 – Origami as a tool in nanoscience. a) An example of a 2D DNA origami as a molecular pegboard, the relative positioning proteins is used to study chemical reactions at the single-molecule level. Adapted with permission from reference 70 (Nature Publishing Group, 2010). b) 3D origami structure used to create a stimuli responsive nanocarrier. Adapted with permission from reference 73 (AAAS, 2012).

Overall, DNA origami has rapidly become the most common construction method used in DNA nanotechnology. This is due to the accessibility of the approach, which can be carried out by non-experts, relying on computer-aided design and user-friendly protocols. However, there are limitations to the origami approach, which will become more important as the field develops. Due to the large number of strands needed to fold a single structure and the need to use an excess of the staples, producing waste, the economics may hinder scaling up the technology. Additionally, the yields of origami are not ideal, especially for the more complex structures, and stability (in particular, in vivo stability) can be an issue requiring specific buffer conditions.[83] One final consideration is that although the structure may appear well-formed, certain component strands may be missing. The characterization of such structures is limited to qualitative assessment of the structure, typically by microscopy. While these limitations have not prevented a great deal of important research to be carried out thus far they will need to be addressed in the future.

1.4.5 Supramolecular DNA nanotechnology

The great variety of DNA self-assembly strategies described so far rely solely on Watson-Crick base-pairing to provide structural definition. It is the fact that structural DNA nanotechnology is only based on one type of interaction that has demanded researchers to go to great lengths to increase complexity while retaining fidelity. As alluded to earlier, the introduction of diverse interactions may be a way to increase control over self-assembly, open doors to new structures which were not possible before, while minimizing sequence space and simplifying design rules.

Supramolecular DNA nanotechnology combines the concepts of supramolecular chemistry and DNA self-assembly, with the combining factor often being the chemical modification to DNA strands. However, an overriding theme is that by introducing the toolbox of supramolecular interactions to DNA nanotechnology we will open new horizons of self-assembly. The chemical modification of DNA strands at the synthesis stage can be used to introduce geometric control, create block-copolymer type morphologies, add metal-coordination environments and allow the site-specifc positioning of macromolecules and nanomaterials on a DNA scaffold.

The first instances of supramolecular chemistry being combined with nucleic acid chemistry were the creation of DNA dendrimers.[84] Initially branched RNA structures were synthesized to investigate the role of these unusual structures in mRNA splicing,[85] but the methodology was taken further and successfully produced 3rd generation DNA dendrimers. This is a good example of the modularity of solid-phase oligonucleotide synthesis, the introduction of branching monomers allowing access to unconventional nucleic acids with a global molecular modification that goes beyond primary structure. The development of non-nucleoside branching units gave rise to larger dendrimer structures.[86-88] The potential of these novel nanostructures to modulate the hybridization properties of their oligonucleotide arms was realized,[88,89] creating the supramolecular DNA complexes shown in Figure 1.13.

The application of synthetic insertions to DNA during solid-phase synthesis is not limited to the formation of branched structures. Divalent organic linkers were used to link adenine or thymine tetramers at the 5' end, creating supramolecular polymers through Watson-Crick complementarity when combined.[90] Bergstrom and co-workers introduced rigid synthetic vertices to favour the formation of supramolecular cycles.[91]

Sleiman's group used this strategy to produce a supramolecular DNA hexagon which was used as an organizational scaffold for gold nanoparticles.[92]

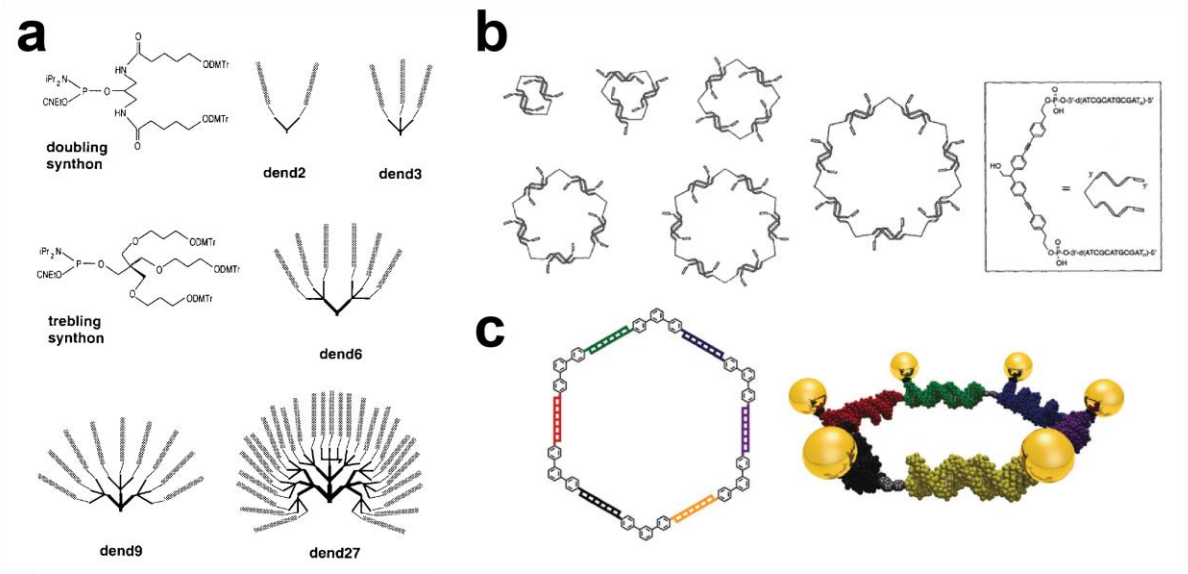

Figure 1.14 – Branched and cyclic DNA structures via synthetic insertions. a) Synthetic branching units enable the synthesis of DNA dendrimers. Adapted with permission from reference 83 (Oxford Journals, 1999) b) Rigid synthetic insertion which produces a variety of cyclic products via DNA hybridization of the symmetric sequences. Adapted with permission from reference 86 (Wiley-VCH, 1997). c) A sequence asymmetric system, with rigid organic vertices is used to produce a single, hexagonal structure, shown here as a scaffold for gold nanoparticles. Adapted with permission from reference 87 (Wiley-VCH, 2006)

The vertex strategy was extended to 3D by firstly ligating cycles into various stable polygons, adding linking strands to align the cycles and rigidifying them with bracing strands to produce stable polyhedra.[93] Importantly, this modular approach represented the first example of an assembly strategy which allowed access to a variety of different 3D DNA nanostructures from a limited set of building. Additionally, the design permitted structural reconfiguration due to the stability of cyclic components. The modularity of this cyclic DNA approach was further highlighted as it was applied to the construction of high aspect-ratio structures, DNA nanotubes.[94] A variety of previous strategies had produced nanotubes that were composed entirely of dsDNA,[95] the possibility of ssDNA regions introduced dynamic capability and a way of tuning mechanical properties, expanding the potential of tubular nanostructures which have wide-ranging applications. This was taken advantage of to allow the capture and release of cargo, in the form of gold

nanoparticles, in response to a specific DNA input.[96] Greschner and Sleiman showed that rigid organic vertices can significantly stabilize DNA hybridization and the structure of the vertex profoundly affects the self-assembly outcome.[97] They also showed that a small DNA-interacting molecule can converge a library of equilibrating DNA structures into a single product,[98] in a process reminiscent of dynamic combinatorial chemistry.[99]

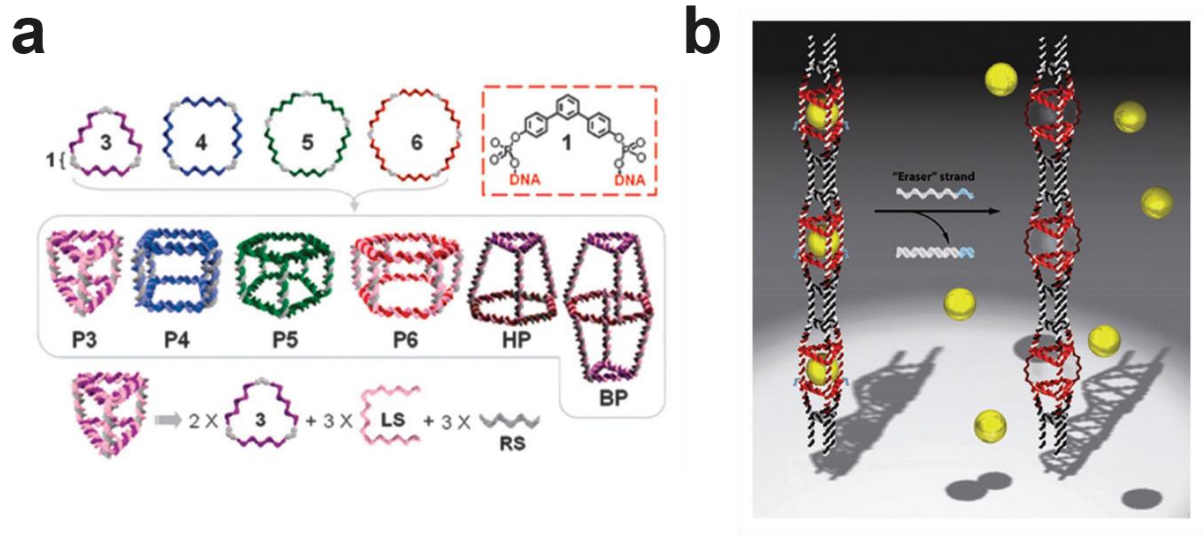

Figure 1.15 – Modular 3D DNA nanostructures. a) The ligation of cycles creates close polygons which can be linked, giving modular access to a range of 3D prisms. Adapted with permission from reference 81 (Americal Chemical Society, 2007). b) Application of this methodology to the production of DNA nanotubes which retain dynamicity due to the presence of single-stranded regions, allowing the loading and release of cargo. Adapted with permission from reference 91 (Nature Publishing Group, 2010).

Replacing 'passive' organic vertices with metal coordinating chelates, such as bipyridine for example, can introduce another supramolecular aspect to DNA assembly. An abundance of remarkable coordination complexes have been self-assembled through the combination of transition metal complexes with rigid, multivalent, organic ligands.[100-109] Considering dsDNA as a rigid linker, analogous complexes could be made, with the advantage of having two orthogonal interactions to drive assembly; metal center geometry and molecular recognition of DNA strands. Kondo et al. attached 2,2-bipyridine (bpy) ligands to the termini of short oligonucleotides, mixing of bpy-A_{20}, bpy-T_{20} and Fe^{2+} coordination resulted in 2D or 3D networks with DNA struts and coordination complex vertices. This strategy was applied to linear arrays, with multiple metal centers linked by different oligonucleotide sequences.[110] This introduces the prospect of using sequence

asymmetry of DNA to create supramolecular complexes where each metal center is not equivalent, i.e. the DNA sequence confers a unique address to each unit. Further development in this area has produced branched structures and closed cycles.[111-114] The modification of individual nucleosides has been use to internally metalate DNA,[115] this was recently used as a method to stabilize three-way branched junctions.[116]

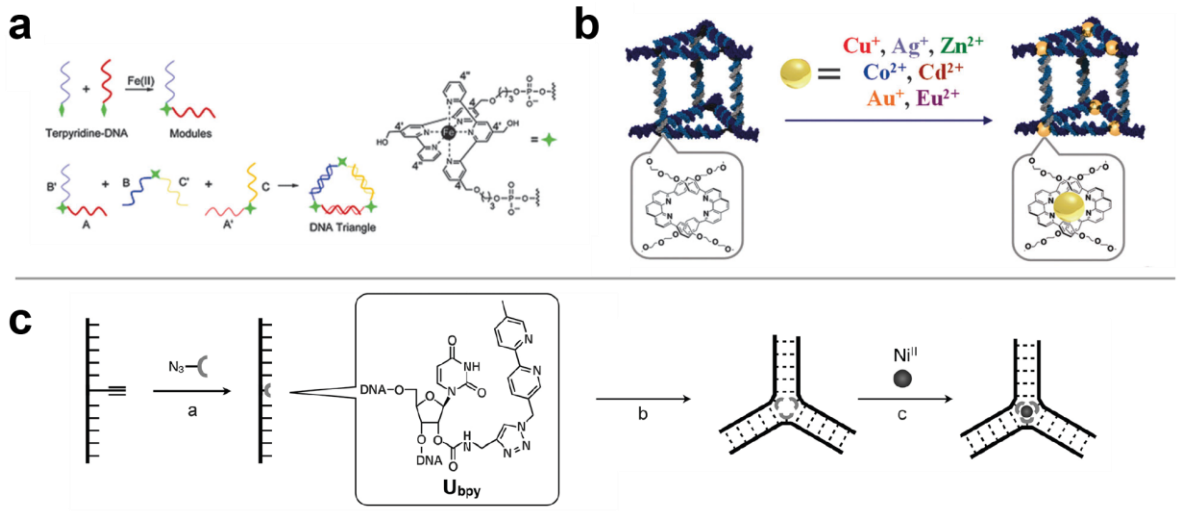

Figure 1.16 – Incorporation of transition metals to DNA nanostructures. a) A supramolecular coordination complex with rigid dsDNA arms. Adapted with permission from reference 108 (American Chemical Society, 2004). b) Incorporation of metal coordination environments to a 3D DNA trigonal prism. Adapted with permission from reference 115 (Nature Publishing Group, 2009). c) Stabilization of a 3-way branched junction by internal metalation. Adapted with permission from reference 111 (Wiley-VCH, 2013).

While metal centers have historically been used as templates for supramolecular chemistry,[117,118] Yang and Sleiman introduced a cyclic metal-DNA structure where the DNA hybridization first oriented (2,9-diphenyl)-1,10-phenanthroline (dpp) ligands, ready for post-assembly metalation with labile metals.[119] Applying this method to a the assembly of a discrete 3D structure created a metal-DNA cage, reminiscent of supramolecular coordination complexes.[120] The introduction of sequence asymmetry provided a chiral four-way junction, used to assemble metal-DNA nanotubes.[121] This strategy was extended to add metal selectivity, using 2,6-bis(2-pyridyl)pyridine (tpy) and bpy to create metal complex terminated duplexes with a large enhancement in stability which exhibited error-checking behavior.[122]

The incorporation of metal centers to DNA provides functionality, which could be due to the unique catalytic, photoactive, electronic or magnetic properties of transitions metals.[123] For example, the discovery of catalytic DNAs,[124] or 'DNAzymes' has exciting implications for the development of novel catalysts by transition metal incorporation to DNA nanostructures. Alternatively, the introduction of metal centers may offer mechanisms for charge transport, with applications in nanoelectronics, artificial photosynthesis and sensing.[125,126]

Another important concept from the world of supramolecular chemistry is that of mechanical interlocking. Mechanically interlocked molecular architectures have shown great potential in molecular devices, the potential to control intramolecular motion allows them to mimic their macroscopic equivalents to produce motors, shuttles, ratchets and switches.[127] These supramolecular structures are interesting as their formation is often guided by weak interactions but the final products are neither covalently bonded or necessarily held together by non-covalent interactions, they are mechanically interlocked. DNA catenanes are important in biology as they are involved in replication of circular DNA.[128-130] In fact, the first 3D DNA nanostructure was a topologically complex catenated structure, albeit held together strongly through hydrogen bonding.[20]

More recently, Willner used ligation to covalently close interlocked DNA macrocycles, producing polycatenanes, which were used to control relative positioning of gold nanoparticles, fluorophores and proteins.[131] Catenation of 3D DNA structures has also been used as a strategy to increase structural stability for biological applications, connecting susceptible nicked regions through ligation.[132] Famulok's group have reported the synthesis of a wide variety of mechanically interlocked DNA structures, creating a toolbox of components for use in nanomechanical devices.[133,134]

Other important non-covalent interactions which can be combined with DNA assembly include aromatic stacking,[135] and hydrophobic interactions.[136] The role of hydrophobic interactions is especially relevant to this thesis and is discussed fully in section 1.5.

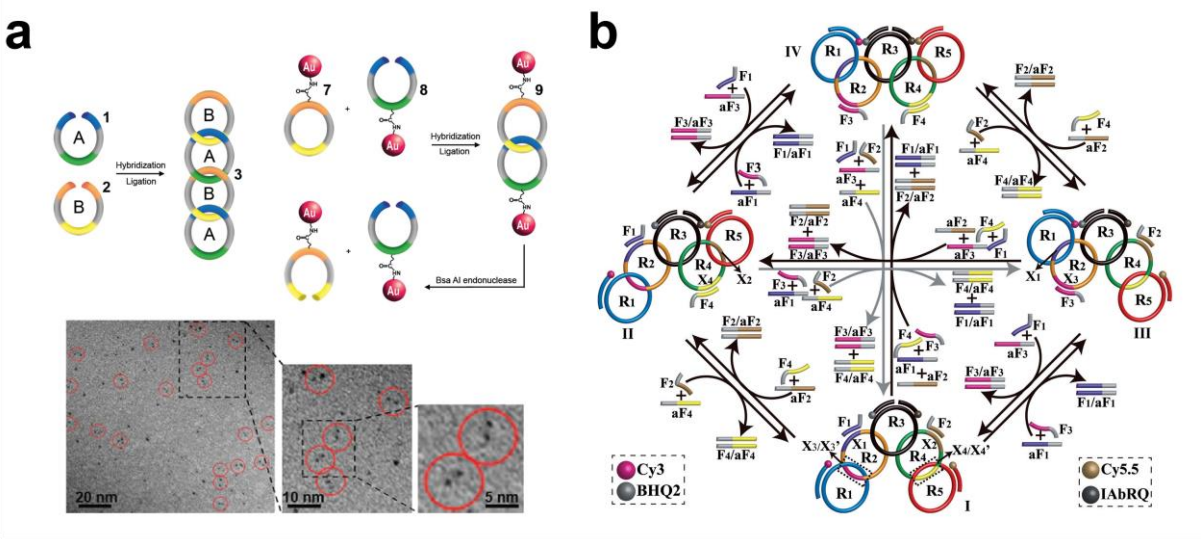

Figure 1.17 – Mechanically interlocked DNA structures. a) DNA polycatenanes are used to position gold nanoparticles. Adapted from reference 126 (National academy of Sciences, 2008). b) Complex reconfigurability within an interlocked DNA olympiadane. Reproduced with permission from reference 129 (Wiley-VCH, 2014).

Overall, supramolecular DNA assembly has capitalized on the molecular tools from decades of supramolecular chemistry to produce DNA nanostructures that would not be accessible through strict DNA hybridization. Additionally, Structural DNA nanotechnology now offers a plethora of different strategies to coax DNA into 2D and 3D architectures, however these constructs, composed purely of DNA lack functionality without the addition of active components. Supramolecular DNA nanotechnology typically introduces new components at specific sites in the structures by chemical modification to the oligonucleotides to produce a 'handle', whether for non-covalent or covalent conjugation to an active unit. Thus, the combination of synthetic chemistry with DNA assembly brings us one-step closer to applying DNA nanostructures in modern technology.

1.4.6 Dynamic DNA nanotechnology

Self-assembled systems which retain dynamic character are the most promising candidates for biomimetic molecular machines. As introduced very briefly earlier in this chapter, DNA nanostructures can exhibit switchable, dynamic and reconfigurable behavior. This has allowed researchers to create programmable molecular machines from DNA nanostructures.

Toehold mediated strand displacement is a critical reaction which enables the actuation of most dynamic DNA devices.[137] The principle of strand displacement is that a thermodynamically equilibrated system can be induced to reconfigure upon addition of a specific DNA strand, Figure 1.18a. To a duplex which contains an ssDNA overhang, referred to as the toehold region, is added an input strand which will bind first to the toehold region and then undergo branch migration. Branch migration is a random walk process which consists of a back-and-forth of pairing and unpairing of nucleobases coming to an end when the most stable complex is reached. Therefore DNA sequences can easily be designed to undergo strand displacement, by introducing overhangs and input strands. Crucially, it is our ability to quantitatively calculate enthalpy contributions from the hybridization of different sequences which makes this possible. The kinetics of the strand displacement process are dependent on the length and GC-content of the toehold region. Winfree has shown that the kinetics can be accurately predicted, with a toehold region of 5nt or more being the optimum length for fast displacement.[138]

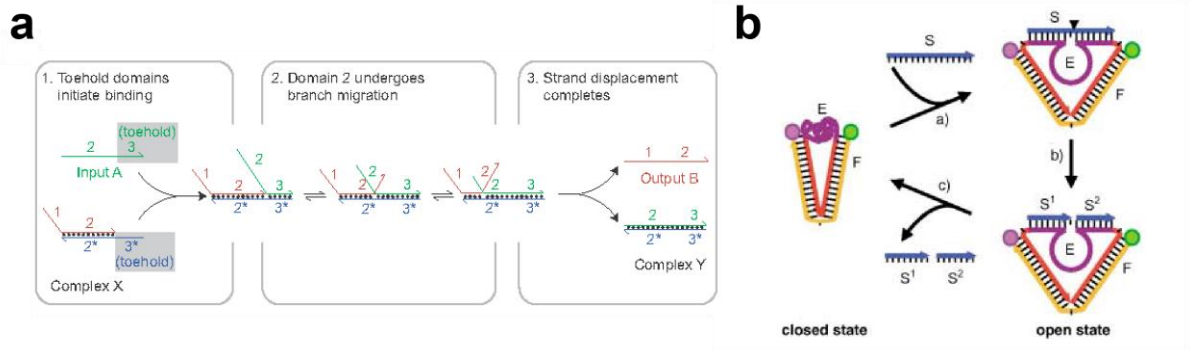

Figure 1.18 – Dynamic DNA nanodevices. a) Schematic of the strand displacement reaction, a key concept in dynamic DNA nanotechnology. Reproduced with permission from reference 132 (Nature Publishing Group, 2011). b) An autonomous DNA motor which is powered by a DNA enzyme (enzyme cleavage site indicated by the black arrowhead). Reproduced with permission from reference 135 (Wiley-VCH, 2004).

The strand displacement concept was first applied in a DNA machine which resembled a pair of tweezers, the input of DNA strands could be used to open and close the device.[139] Since then, ongoing development in this area has produced a variety of structurally switchable DNA nanostructures which can emulate macroscopic machinery such as motors and rotors,[133,140] walkers,[141,142] and even a nanoscale 'assembly line'.[143] Strand displacement has also been used in the structural reconfiguration of 2D and 3D DNA nanostructures,[93,139,144] for example to aid encapsulation and release of cargo.[57,96] The introduction of toehold regions which contain biologically relevant sequences has been used to create stimuli responsive drug-delivery vehicles, which 'unzip' in the presence of a cancer marker RNA sequence.[145]

In summary, the reversible nature of the non-covalent interactions which hold together DNA nanostructures enables the creation of dynamic nanodevices from DNA. The modes of operation are not limited to strand displacement processes. Structural changes in response to environmental factors, such as pH, or to other chemical species, such as metal ions, have also been used to create DNA machines.[146] The resulting dynamic DNA assemblies have applications in sequence responsive drug-delivery, sensing and molecular computing.

1.5 DNA amphiphiles

Block copolymer self-assembly is a useful fabrication method used to create materials for wide-ranging practical applications such as nanolithography, drug-delivery, and catalysis.[147] Amphiphilic block copolymers self-assemble due to microphase separation of two or more conjoined polymer blocks with differing solubilities.[148] Driven by the hydrophobic effect in aqueous media, micelles, rods and lamellae can be produced. Furthermore, the resulting morphologies can be varied by tuning the relative lengths of the constituent polymer blocks and the solvent conditions. Amphiphilic self-assembly can create well-defined nanostructures using a completely different set of interactions than structural DNA nanotechnology, and can introduce the capability of block copolymers for long-range self-assembly.[95,149] For this reason the combination of the two approaches provides a powerful platform with great opportunities for novel, useful and dynamic nanotechnology.

DNA amphiphiles can be thought of as block copolymers; where the hydrophilic block is an oligonucleotide and the hydrophobic block can vary from a simple lipid chain to a high molecular weight synthetic polymer. In this section, the synthesis, self-assembly and application of this relatively new class of materials is described.

1.5.1 Synthetic approaches

A variety of approaches to create DNA amphiphiles have been reported.[136] These can be loosely divided into two classes; pre-synthetic or post-synthetic. Pre-synthetic approaches capitalize on the efficient solid-phase coupling chemistry used for oligonucleotide synthesis, with addition of a hydrophobe to the DNA strand on the solid support. The post-synthetic strategy involves the attachment of the hydrophobe to DNA strands after they are fully deprotected and soluble in aqueous media. This usually involves the addition of a functional group to the DNA strand during synthesis, which can be used as a reactive handle for the subsequent conjugation. The variety of attachment chemistries are shown in Figure 1.19.

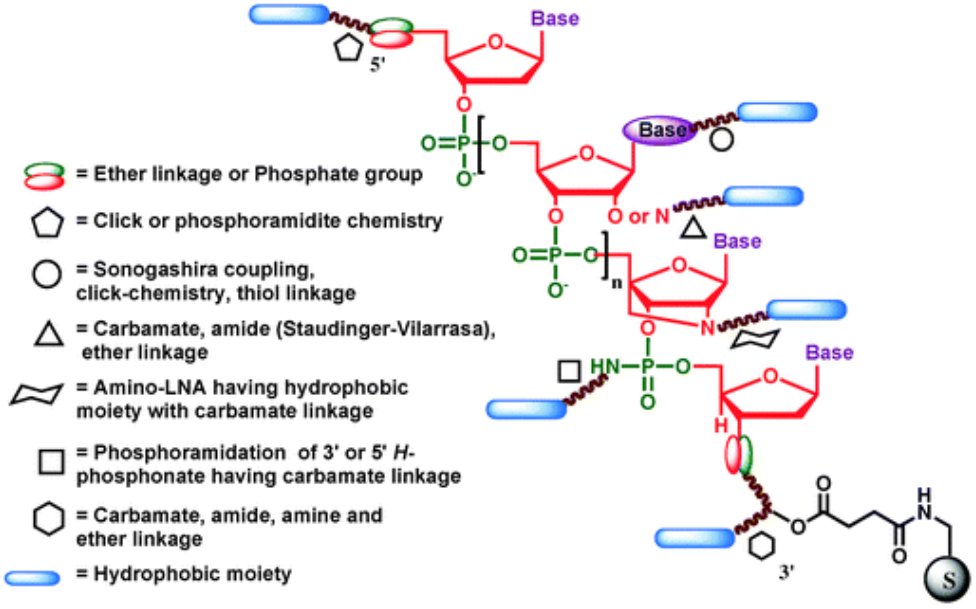

Figure 1.19 – Synthesis of DNA amphiphiles. The various possibilities of attachment chemistry are shown. Reporoduced with permission from reference 130 (Royal Society of Chemistry, 2011).

Considerations for the synthetic strategy will largely depend on the hydrophobic group that is to be attached. Importantly, if the pre-synthetic route is to be used then the hydrophobe must be able to withstand the conditions used in phosphoramidite synthesis

of the DNA strand. The main concerns are the acidic conditions used for deblocking, the oxidation steps and the basic conditions typically used for cleavage from the solid-support and removal of protecting groups. If stability is not a concern it should be noted that the pre-synthetic route is generally the higher yielding and faster alternative. A plethora of hydrophobic phosphoramidites and functionalized solid supports are now commercially available, allowing 3', 5' or internal modification of oligonucleotides. Another important consideration is that while solid-phase phosphoramidite coupling works very well for small molecules it is not as well suited to long polymers. This is due to the small solid support pore-sizes, typically 500-2000Å, and the randomly coil conformation of the polymer which impedes accessibility to the single reactive site. While a post-synthetic method can be used to make DNA-polymer conjugates, solubility is a major drawback demanding a careful balance to solubilize both oligonucleotide and polymer.[150]

1.5.2 DNA amphiphile self-assembly

The morphology of a self-assembled amphiphiles aggregate depends on the ratio of the hydrophilic and hydrophobic components. One advantage of using DNA as an equivalent of a 'polymer' block is that complete control over the length of the DNA is synthetically possible, whereas polymers will always exhibit some degree of polydispersity. This was showcased by Tan's group, who showed that the radius of micelles could be tuned precisely by changing the DNA length, they also showed size-dependent cellular uptake profiles.[151] The introduction of an oligonucleotide component to block copolymer-like assemblies also adds orthogonal molecular recognition, which can be used to turn self-assembled aggregates into smart nanodevices. Dynamic DNA assembly can be used as a tool to modulate these amphiphilic assemblies, with switchable systems designed to respond to stimuli which act on the DNA.

Shape-shifting DNA micelles have been reported that respond to an input DNA sequence by changing morphology. This can be due to changes in the cone-angle upon a ssDNA to dsDNA transition (Figure 1.21a),[152] thermal annealing of duplexes or enzymatic processing of the oligonucleotide portion. Gianneschi's group prepared DNA amphiphiles of brush morphologies through ring-opening metathesis polymerization (ROMP) and showed all three of these processes could in fact change morphology from spherical

micelles to rods and back to spherical micelles.[153] This has been shown for other types of DNA-based micelles, including those made from DNA-polypropylene oxide (PPO) amphiphiles, where cellular uptake profiles were found to be shape-dependent.[154]

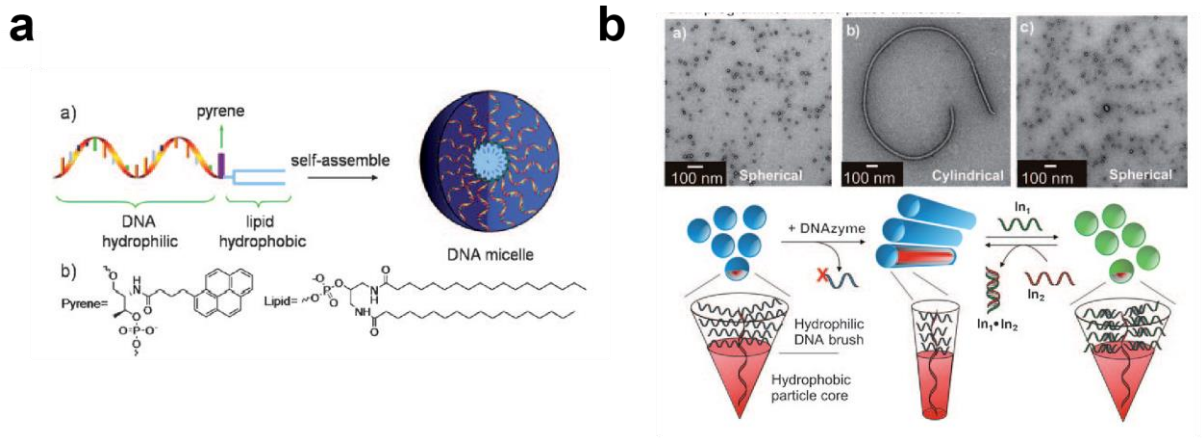

Figure 1.20 – DNA amphiphile self-assembly. a) DNA based micelles self-assemble from lipid-DNA conjugates. Reproduced with permission from reference 146 (Wiley-VCH, 2010). B) Micelles formed from DNA-polymer conjugates undergo stimuli responsive morphological changes. Reproduced with permission from reference 148 (Wiley-VCH, 2010).

Interestingly, in the presence of lipid bilayers some DNA-amphiphiles exhibit a preference to insert into the bilayer, packing with the lipid molecules, rather than self-aggregating. Based on this behavior, lipid-oligonucleotides have been applied as tools for vesicle fusion, mimicking the SNARE protein complex.[155] Insertion into biological membranes is also useful for the delivery of nucleic acid therapeutics. There have been an array of lipid-oligonucleotide conjugates used as to enhance stability and cellular uptake of short interfering RNA (siRNA) or antisense oligonucleotides (ASOs) without the need for toxic transfection agents.[156] From *in vivo* studies the mechanism of uptake was shown to be mediated by insertion of the nucleic acid amphiphiles into endogenous lipoproteins and subsequent receptor-mediated uptake of the nucleic acid-lipoprotein complex.[157]

Additionally, the organization of nucleic acids into unnatural, spherical morphologies has been shown to increase the stability in biological media, due to the dense packing of DNA which prevents access to nucleases. This was initially demonstrated by using spherical gold nanoparticle scaffolds.[158] However, the assembly of DNA amphiphiles created from ROMP polymers into spherical micelles showed that

the same effect can be achieved without the need for inorganic nanoparticles.[159] These micelles have recently been synthesized with locked-nucleic acid (LNA) antisense oligonucleotide coronas, and shown to successfully effect intracellular gene regulation.[160] The cellular uptake and subsequent gene regulation of these nucleic acid containing nanoparticles without the need for transfection, is one of very few examples of such systems.[161,162] This shows the potential of DNA amphiphiles as a solution to important challenges in medicine. As well as delivering nucleic acid therapeutics on their corona, DNA-based micelles can be used to encapsulate small molecule drugs in their cores. For example, Herrmann's group showed encapsulation of doxorubicin in a micelle made from DNA-polypropylene oxide (PPO) amphiphiles.[163] The addition of a complementary DNA strand conjugated to folic acid decorated the corona with a ligand for targeted delivery, showing selective uptake in cancer cells. The nucleic acid portion can itself be transformed into a targeting ligand by introducing an aptamer forming sequence, this was used to produce micelles which displayed aptamers on their corona, exhibiting strong and specific binding to receptors overexpressed on cancer cells.[164]

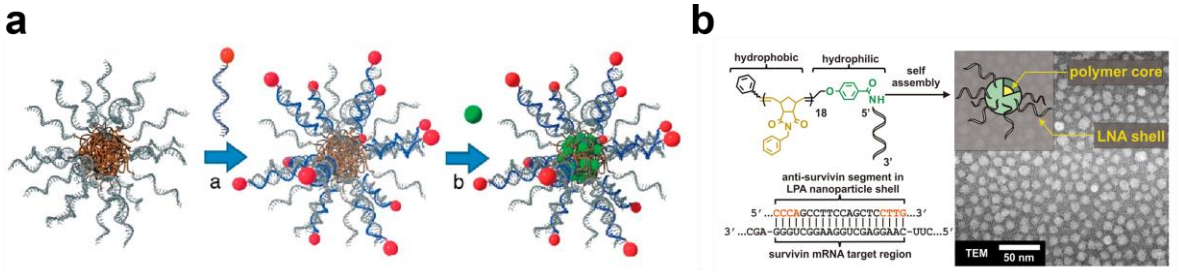

Figure 1.21 – Applications of DNA amphiphiles in nanomedicine. a) DNA-PPO micelles can be functionalized with a targeting ligand (red sphere) and loaded with small molecule drug (green sphere) for targeted drug delivery. Reproduced with permission from reference 158 (Wiley-VCH, 2008b). b) Gene regulating DNA-polymer micelles which bear LNA antisense on their corona. Reproduced with permission from reference 155 (American Chemical Society, 2014).

Looking at the recent progress in the field it is clear that the incorporation of a 'smart' nucleic acid component in amphiphilic self-assembly is advantageous, especially showing promise for diagnostic and therapeutic applications in nanomedicine. Another exciting prospect is the integration of DNA amphiphiles with 2D and 3D DNA nanoscaffolds, creating hybrid structures with novel, synergistic properties.

1.5.3 Integration of amphiphiles with DNA nanostructures

From the point of view of DNA nanotechnology, DNA amphiphiles represent a new way to interface DNA nanostructures with other materials, especially those of biological relevance such as lipid membranes. One challenge in the field is to align DNA nanostructures on surfaces. Historically, structures have been deposited on inorganic surfaces for microscopy analysis, an issue with this is that irreversible surface adsorption nullifies any dynamic character and can disrupt the structures. One solution to this problem is to place DNA nanostructures on a 'soft' surface with some degree of fluidity. This can aid characterization, allowing structures to be studied in a more 'native' state, but is will also be important to create functional devices which are dependent on dynamic assembly. Lipid bilayers have emerged as an excellent candidate for this purpose.

To direct nanostructures to lipid bilayers hydrophobic anchors must be used, these are commonly introduced to the structures by substituting one of the constituent strands with a DNA amphiphile. For example, Albinsson and co-workers used porphyrin-modifed thymidine to introduce a hydrophobic anchor to DNA strands.[165] These were incorporated into a 2D hexagonal DNA nanostructure and the number of anchors needed to stably align the construct to a lipid bilayer was found to be three.[166] This demonstrated that just a relatively small modification to the DNA nanostructure can be used to give a strong interaction with bilayers and that this is tunable, by changing the number of anchors per structure. These structures are currently being explored for applications as artificial photosynthetic systems, taking advantage of the redox activity of the porphyrin moeities.[167]

Taking advantage of the fluidity of lipid membranes mentioned above, the study of assembly processes between nanostructures is possible as they retain dynamicity. High-speed atomic force microscopy (AFM) was used to study the interactions between origami hexagons in real-time. Cholesterol anchors were used to align the hexagonal structures on the bilayer and an azobenzene modification was used to allow DNA hybridization to be 'switched on' or 'off' by irradiation with light.[168] In a similar vein, DNA origami 'barges' were created, also with cholesterol anchors to allow association with a lipid bilayer surface.[169] Single-molecule fluorescence microscopy was used to evaluate the random lateral diffusion of structures on the bilayer surface. The creation of artificial

membrane channels made of DNA has also been explored. Another example, combining DNA amphiphiles with 3D DNA nanostructures was the integration of cholesterol-modified staple strands to a large DNA origami structure was used to create an artificial ion-channel.[80] More recently, a simpler design for DNA-based ion-channels was reported, using porphyrin anchors to facilitate insertion into the bilayer.[170]

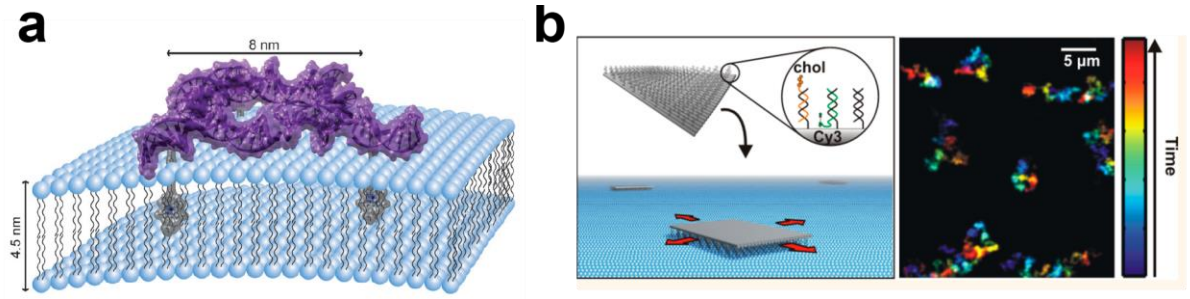

Figure 1.22 - DNA nanostructure on lipid bilayers. a) A DNA hexagon is aligned to the lipid bilayer via three porphyrin anchors. Reproduced with permission from reference 161 (Wiley-VCH, 2011) b) A DNA origami tile functionalized on one side with cholesterol groups can 'explore' bilayers, as visualized with single-molecule fluorescence microscopy. Reproduced with permission from reference 164 (American Chemical Society, 2014)

The application of DNA amphiphiles with DNA nanostructures is not limited to lipid-bilayer anchoring. Sleiman and co-workers have integrated DNA-amphiphiles into 3D structures with applications in membrane biophysics, drug-delivery and fundamental studies of orthogonal assembly modes working together. A critical aspect of the DNA nanostructures used for these studies is the availability of multiple ssDNA regions which can hybridize to DNA-amphiphiles. The use of a cubic DNA scaffold with addressable ssDNA regions was used to position DNA-polyethylene glycol (DNA-PEG) block copolymers generated by ROMP, precisely in 3D.[171] This decoration with PEG chains was found to enhance nuclease resistance of the DNA nanostructure. The extension of this method to long-range assembly was achieved by the use of robust DNA nanotubes with periodically spaced single stranded regions as the scaffold.[172] The nanotubes were used to longitudinally position micellar aggregates of DNA-PEG and DNA-polystyrene (DNA-PS). These hybrid assemblies were stimuli responsive, with introduction of a specific DNA sequence removing the DNA-polymer conjugates by strand displacement. Conway et al. used a modular, DNA minimal scaffold to position varying numbers of cholesterol

modified DNA and fluorophores.[173] Combining dynamic DNA nanotechnology approaches with lipid-bilayer bound nanostructures produced a stimuli responsive platform with promise in artificial signal transduction, controlled protein interactions and surface bound DNA nanodevices in general. Additionally, Simmel's group have used the hydrophobic association of cholesterol modified DNA to drive the folding of a hinged DNA origami structure, like the closing of a book.[174] O'Reilly, Turberfield and co-workers integrated a temperature-responsive polymer-DNA conjugate with a DNA tetrahedron.[150] The structure exhibited surfactant like behavior which could be reversed by temperature control.

1.6 DNA-guided assembly of gold nanoparticles

DNA nanotechnology has produced a variety of scaffolds for the organization of matter on the nanoscale. An important class of nanomaterial which can benefit from the structural control and complexity available through DNA nanotechnology are gold nanoparticles. Gold nanoparticles (AuNPs) have far-reaching potential for practical applications in medicine, energy, photonics, nanoelectronics, catalysis and computation.[175] A full discussion of their physical properties is beyond the scope of this thesis and has been well documented.[176] However, it is important to note that these unique nanomaterials exhibit special optical and electronic properties which are particle size dependent.[177] Additionally, these collective properties are highly dependent on the geometry of nanoparticle assemblies, the precise control of which was previously a challenge. As described briefly before, DNA nanotechnology has presented solutions to this challenge. As such, the focus of this section will be a brief introduction to DNA-mediated assembly of gold nanoparticles, which has developed into a large field in itself.[178,179] The assembly strategies can be divided into two distinct approaches. The method introduced by Mirkin relies on the use of poly-functionalized AuNPs; gold nanoparticles with the highest surface coverage of DNA possible.[180] These are used to create long-range crystalline like assemblies. The alternative approach, pioneered by Alivisatos, is the use of discretely functionalized AuNPs; gold nanoparticles with exactly one or two DNA strands attached.[181] The assembly relies uses DNA scaffold strands to produce small clusters of well-defined numbers of nanoparticles. Both approaches will be discussed.

1.6.1 Conjugation strategies

An important consideration for the creation of DNA-functionalized gold nanoparticles (DNA-AuNPs) is the attachment chemistry. The most common approaches are based on the gold-sulfur bond,[182,183] which requires modification of the DNA strands to introduce a sulfur containing group. The first reported examples used DNA strands modified with alkane thiols. These are typically introduced as a 3' modification using a specialized solid support which introduces the thiol as a disulfide, treatment with a reducing agent activates the modification for conjugation to the gold surface. While these anchors have been used successfully in a wide variety of studies, thermal stability and resistance to reducing agents and salts commonly used in biological buffers is a concern for some applications.

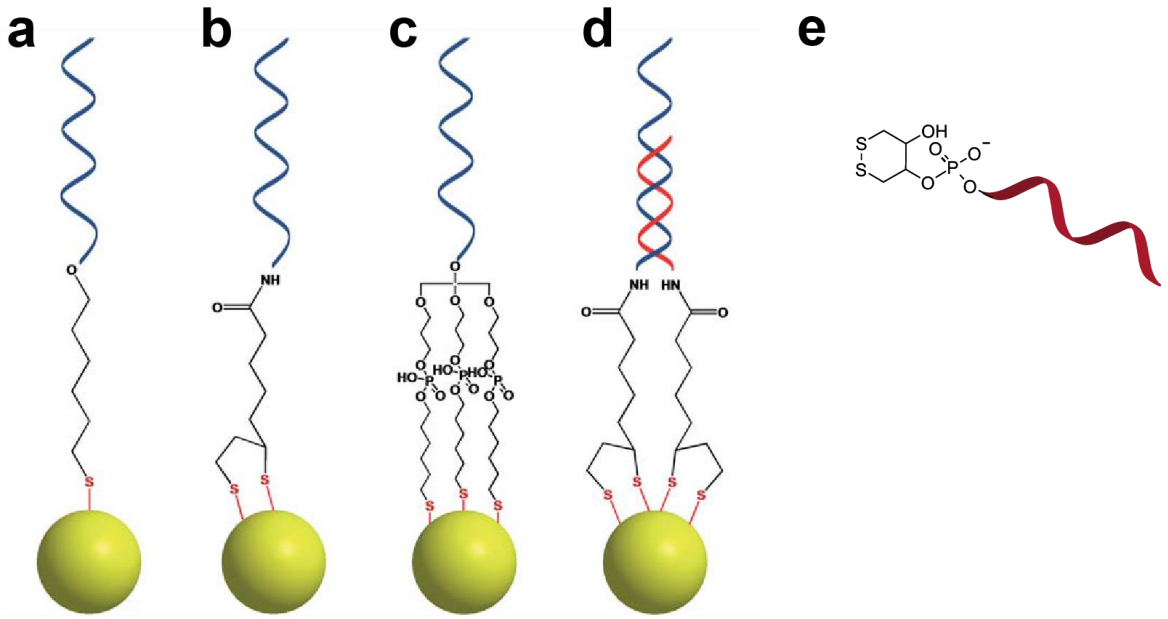

Figure 1.23 – Gold binding moieties. a) Alkane thiol, b) lipoic acid, c) trithiol dendron, d) double stranded strategy using lipoic acid, e) DTPA modification. Adapted with permission[184] (Royal Society of Chemistry, 2011).

The need for more stable DNA-AuNPs has resulted in the development of novel anchoring groups. One approach is the use of cyclic disulfides, which can be introduced to the oligonucleotide post synthesis, such as lipoic acid,[185] or during the synthesis using the common reagent dithiol phosphoramidite (DTPA), Figure 1.23. These modifications

do not require activation and introduce significant stability due to their chelating ability, and in the case of DTPA, multiple anchors can be put on one DNA strand to give very stable nanoparticle conjugates.[186] Multiple thiol groups can also be used, Mirkin and co-workers synthesized a tri-thiol dendron using phosphoramidite chemistry, which exhibited higher stability than cyclic disulfides. Another effective approach is to bring multiple anchors together by hybridizing two DNA strands which are modified, one on the 3' and one on the 5' ends, with cyclic disulfides. This method creates a rigid chelating arm from dsDNA, preorganized for binding to the gold surface.[187-189]

1.6.2 Long-range assemblies

The first examples of DNA-mediated assembly of gold nanoparticles appeared in 1996. Mirkin's group prepared two sets of gold nanoparticles, which were each poly-functionalized with 3' thiol modified DNA strands of unique sequences.[180] A linker was created, with a duplex portion flanked by 8nt ssDNA arms which were complementary to each of the AuNP bound strands. The two populations of AuNPs could be mixed together, existing as separate entities in solution. Upon addition of the linker DNA hybridization occurred, resulting in aggregation of the nanoparticles. This work not only showed that DNA may be used as the mediator for colloidal crystallization but revealed the potential of DNA-AuNPs in biomolecule sensing. The dependence of inter-particle distance on the optical properties of AuNPs results in drastic color changes when the linker DNA strand is added. This was demonstrated soon after the initial discovery, by a slight change in the linking strategy to allow 10fmol of a 30nt ssDNA to be detected colorimetrically.[190] These initial discoveries have led to large efforts to develop DNA-AuNPs for bioanalytics and as diagnostic tools.[191]

DNA nanostructures have also been used as scaffolds for the long-range organization of gold nanoparticles, as described in section 1.4.4. This can be achieved by sticky end cohesion between the DNA-AuNP and an ssDNA overhang positioned at a specific location on the structure or by direct attachment of a component DNA strand to the AuNP. The use of tile-based DNA assembly to create periodic arrays allows the controlled patterning of AuNPs onto surfaces, with tunable spacing.[192-194] Chiral helical structures have also been created using tile-based assembly of nanotubes with AuNPs aligned at specific points along the tubes.[195] The incorporation of single AuNPs into the

monomer unit of a DNA nanotube allowed access to both long-range and discrete structures from a modular platform.[189] As the overall properties of AuNP assemblies are dependent on inter-particle spacing, the ability to tune this rationally is a crucial step in the development of plasmonic devices for applications in sensing, information technology and energy.

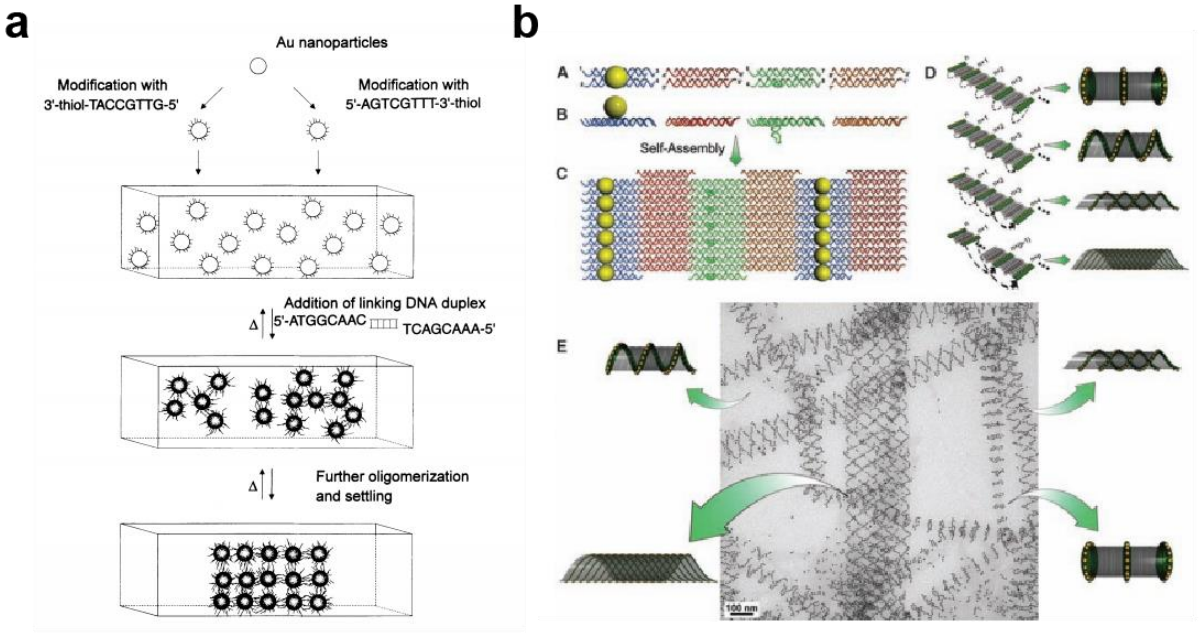

Figure 1.24 – DNA approach to gold nanoparticle assembly. a) Mirkin's original DNA mediated nanoparticle assembly method. Reproduced with permission from reference 175 (Nature Publishing Group, 1996) b) The use of tile-based DNA assemblies to create long ranging, periodic and chiral AuNP arrangements. Reproduced with permission from reference 190 (AAAS, 2009).

1.6.3 Discrete assemblies

There is also considerable interest in the production of discrete clusters of gold nanoparticles. These plasmonic structures are an important class of material that display unique structure dependent optoelectronic properties.[178] There is particular interest in these structures for applications in surface enhanced Raman spectroscopy (SERS).[196] The creation of electromagnetic 'hotspots' between particles produces large field enhancements which can allow single-molecule detection with higher sensitivity than fluorescence microscopy.[197] DNA-mediated assembly represents a powerful strategy for the production of AuNP architectures which exhibit such properties.

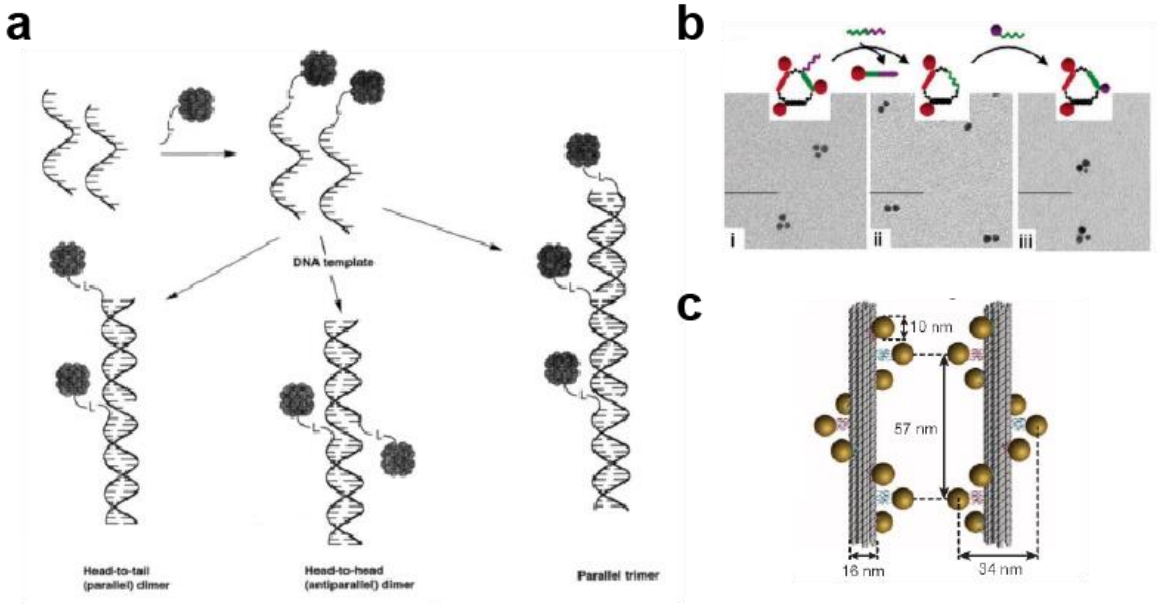

Figure 1.25 – DNA-linked discrete gold nanoparticle clusters. a) The original method for DNA-mediated discrete nanoparticle assemblies introduced by Alivisatos. Reproduced with permission from reference 176 (Nature Publishing Group, 1996). b) Switchable AuNP assemblies through the use of dynamic DNA nanotechnology. Adapted with permission from reference 194 (American Chemical Society, 2007) c) A chiral plasmonic nanoparticle cluster from a DNA origami bundle. Adapted with permission from reference 68 (Nature Publishing Group, 2012).

Alivisatos created the first discrete assembly of gold nanoparticles using DNA as the linker in 1996.[181] The key to the approach was the creation of a DNA-AuNP monoconjugate. This was achieved by using thiol modified DNA and 1.4nm AuNPs which displayed a single maleimide group. These were then organized on a template strand to provide different relative spacings of the nanoparticles. It is important to note that a lot of the early work in this area involved developing techniques for obtaining pure DNA-AuNP monoconjugates, with agarose gel electrophoresis becoming the most commonly used.[198] The introduction of an extension strand strategy to improve resolution of electrophoresis was an important development.[144] The formation of discrete AuNP clusters using DNA has since been expanded to 2D,[92] dynamic,[199] and 3D chiral structures,[73,200] using all manner of DNA design methodologies, examples are shown in Figure 1.25.[201] Importantly, DNA mediated AuNP clusters have been shown to exhibit unprecedented switchable optical properties,[73] create SERS active assemblies,[202] and plasmonic waveguides.[203]

1.6.4 Anisotropic building blocks

The DNA-mediated assembly strategies for gold nanoparticles described so far have involved either one or an isotropic coverage of DNA strands per particle. What this means for the discrete assemblies is that all of the structural information is held by the DNA nanostructures and not the nanoparticles themselves. The ability to program spherical particles with structural information, such as valency and regioselectivity is much sought after. To impart nanoparticles with discrete numbers of DNA strands, and furthermore at specific positions on the nanoparticle surface has been proposed as a way to gain a new level of control over nanoparticle assembly.[204,205] In this respect the nanoparticles would contain the information necessary to be treated like individual DNA tiles, allowing the possibility of algorithmic assembly and self-assembly of complex architectures without the need for an additional scaffold.

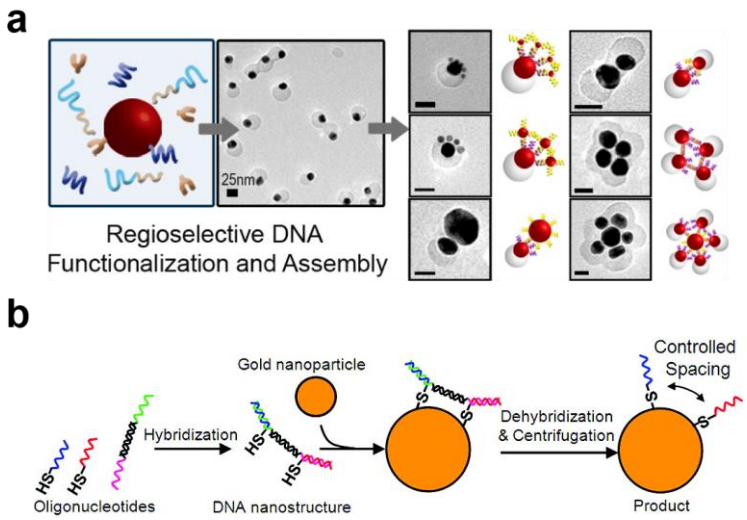

Figure 1.26 – Ansotropic gold nanoparticles. a) A method to introduce regioselectivity to gold nanoparticles using amphiphilic polymers, Reproduced with permission from reference 206 (American Chemical Society, 2013). b) A method to control the spacing between two oligonucleotides on a gold nanoparticle surface. Reproduced with permission from reference 199 (American Chemical Society, 2009).

With this in mind, various strategies to create such particles have been explored. One dimensional DNA nanostructures were used as templates, positioning thiol modified DNA strands to control the spacing between DNA strands on the AuNP surface.[206-208] Another strategy involved immobilizing AuNPs on a surface to create Janus particles with localized patches of DNA strands.[209-211] Deaton's group developed a stepwise solid-phase approach which relies on electrostatic repulsion to produce geometrically defined DNA-

AuNPs with a controlled number of strands.[212] More recently, amphiphilic polymers have been used to allow regioselective DNA functionalization on gold nanoparticles.[213] However, the control of both discrete number, directionality and the introduction of different sequences has not yet been achieved. This topic will be addressed fully in chapter 4.

1.7 Context and scope of this thesis

Theoretically, DNA represents the most reliable, programmable and accessible bottom-up nanofabrication material. However, in reality, the more complex the design the more assembly errors will emerge. In fact, this was seen especially in the algorithmic self-assembly of DNA tiles, where the more complex the algorithm the more error-prone the output. Therefore, to strike a balance between complexity and fidelity has become a major challenge in the field and begs the question – *how much complexity do we really need for functionality?* In this vein, the stripping down of 2D, 3D and dynamic DNA assemblies to minimal structural complexity but maximal functional capability has spawned new approaches to DNA nanotechnology. One of these approaches, which is the concern of this thesis research, is that of supramolecular DNA assembly.

Supramolecular assembly uses the introduction of chemical entities into DNA strands, and their subsequent nanostructures, to provide new structural control and functionality. The research covered in this thesis is specifically focused on the introduction of orthogonal supramolecular interactions to DNA nanostructures and investigation of the properties of the resultant hybrid systems.

In chapter 2, the design and synthesis of novel dendritic DNA amphiphiles and their self-assembly properties are investigated. A DNA-minimal cubic scaffold with ssDNA regions is used to site-specifically position the amphiphiles in 3D. This then used as a platform to answer fundamental questions about the effect of nanoscale organization of hydrophobic 'residues' on their self-assembly behavior. From the standpoint of amphiphilic self-assembly this represents a route around conventional assembly rules, such as critical micelle concentration, by the overwhelming effect of templation. These structures also introduce an orthogonal assembly language which can be programmed to carry out inter- or intra-molecular interactions, bringing together DNA nanostructures

through hydrophobic interactions or creating encapsulation environments for controlled-release of small molecule guests.

Chapter 3 describes the extension of the synthetic methodology used in chapter 2 to produce a range of linear sequence-defined DNA-polymer conjugates. This modular approach to DNA-amphiphile synthesis uses commercially available solid-phase synthesis reagents, is facile and high-yielding. This approach to DNA-polymer conjugate synthesis, the sequential coupling of oligomeric blocks via phosphoramidite chemistry, allows the introduction of sequence definition in the polymer block as well as the oligonucleotide portion. The creation of DNA-polymer conjugates with different patterns of hydrophobic and hydrophilic patches within the polymer chain is used to explore the effect of primary, molecular, structure on the resulting hierarchical self-assembly. The result is a new platform for designing DNA-based micelles with tunable morphologies and properties.

In chapter 4, the concept of organizing DNA-conjugates on the cubic scaffold is expanded to applications in gold nanoparticle assembly. In this instance the DNA conjugates contain highly reactive gold-binding moieties. Through their positioning on the DNA scaffold, the ability to transfer a pattern of DNA strands to gold nanoparticles is realized. This transforms the spherical colloid to an anisotropic building block, with applications in DNA-mediated nanoparticle assembly. Geometric diversity is introduced via a series of different DNA prisms, formed using the same modular 'clip-by-clip' strategy. Sequence asymmetry in the parent scaffold is transferred to the gold nanoparticle, giving rise to anisotropic nanoparticles which have well-defined molecular recognition properties. The fidelity of the pattern transfer is investigated, as well as the self-assembly properties of these unique nanoparticles.

In the appendix, the preliminary investigation into the effect of dendritic DNA amphiphiles on the serum protein interactions of DNA nanostructures is described. Evidence for the DNA amphiphile mediated binding of DNA nanostructures to bovine serum albumin (BSA) is presented. This will have important implications in the development of DNA nanostructures for biomedical applications.

1.8 References

1 Lehn, J. M. 'Supramolecular chemistry: Receptors, catalysts, and carriers'. *Science* **227**, 849-856 (1985).

2 Gust, D., Moore, T. A. & Moore, A. L. 'Mimicking Photosynthetic Solar Energy Transduction'. *Accounts of Chemical Research* **34**, 40-48 (2000).

3 Hannon, G. J. 'RNA interference'. *Nature* **418**, 244-251 (2002).

4 Dill, K. A. & MacCallum, J. L. 'The Protein-Folding Problem, 50 Years On'. *Science* **338**, 1042-1046 (2012).

5 Seeman, N. C. 'Nucleic acid junctions and lattices'. *Journal of Theoretical Biology* **99**, 237-247 (1982).

6 Watson, J. D. & Crick, F. H. C. 'Molecular Structure of Nucleic Acids: A Structure for Deoxyribose Nucleic Acid'. *Nature* **171**, 737-738 (1953).

7 Crick, F. 'Central Dogma of Molecular Biology'. *Nature* **227**, 561-563 (1970).

8 Stofer, E., Chipot, C. & Lavery, R. 'Free Energy Calculations of Watson−Crick Base Pairing in Aqueous Solution'. *Journal of the American Chemical Society* **121**, 9503-9508 (1999).

9 Lu, Y., Weers, B. & Stellwagen, N. C. 'DNA persistence length revisited'. *Biopolymers* **61**, 261-275 (2002).

10 Beaucage, S. L. & Caruthers, M. H. 'Synthetic strategies and parameters involved in the synthesis of oligodeoxyribonucleotides according to the phosphoramidite method'. *Current protocols in nucleic acid chemistry / edited by Serge L. Beaucage ... [et al.]* **Chapter 3**, Unit 3.3 (2001).

11 Beaucage, S. L. & Caruthers, M. H. 'Deoxynucleoside phosphoramidites—A new class of key intermediates for deoxypolynucleotide synthesis'. *Tetrahedron Letters* **22**, 1859-1862 (1981).

12 Caruthers, M. H. *et al.* 'Chemical synthesis of deoxyoligonucleotides by the phosphoramidite method'. *Methods in enzymology* **154**, 287-313 (1987).

13 Grabow, W. W. & Jaeger, L. 'RNA Self-Assembly and RNA Nanotechnology'. *Accounts of Chemical Research* **47**, 1871-1880 (2014).

14 Kallenbach, N. R., Ma, R.-I. & Seeman, N. C. 'An immobile nucleic acid junction constructed from oligonucleotides'. *Nature* **305**, 829-831 (1983).

15 Ma, R. I., Kallenbach, N. R., Sheardy, R. D., Petrillo, M. L. & Seeman, N. C. 'Three-arm nucleic acid junctions are flexible'. *Nucleic Acids Research* **14**, 9745-9753 (1986).

16 Petrillo, M. L. *et al.* 'The ligation and flexibility of four-arm DNA junctions'. *Biopolymers* **27**, 1337-1352 (1988).

17 Yu, J., Ha, T. & Schulten, K. 'Conformational model of the Holliday junction transition deduced from molecular dynamics simulations'. *Nucleic Acids Research* **32**, 6683-6695 (2004).

18 Liu, D., Wang, M., Deng, Z., Walulu, R. & Mao, C. 'Tensegrity: Construction of Rigid DNA Triangles with Flexible Four-Arm DNA Junctions'. *Journal of the American Chemical Society* **126**, 2324-2325 (2004).

19 Mao, C., Sun, W. & Seeman, N. C. 'Designed two-dimensional DNA holliday junction arrays visualized by atomic force microscopy'. *Journal of the American Chemical Society* **121**, 5437-5443 (1999).

20 Chen, J. & Seeman, N. C. 'Synthesis from DNA of a molecule with the connectivity of a cube'. *Nature* **350**, 631-633 (1991).

21 Mueller, J. E., Du, S. M. & Seeman, N. C. 'Design and synthesis of a knot from single-stranded DNA'. *Journal of the American Chemical Society* **113**, 6306-6308 (1991).

22 Mao, C., Sun, W. & Seeman, N. C. 'Assembly of Borromean rings from DNA'. *Nature* **386**, 137-138 (1997).
23 Zhang, Y. & Seeman, N. C. 'Construction of a DNA-truncated octahedron'. *Journal of the American Chemical Society* **116**, 1661-1669 (1994).
24 Wang, Y., Mueller, J. E., Kemper, B. & Seeman, N. C. 'Assembly and characterization of five-arm and six-arm DNA branched junctions'. *Biochemistry* **30**, 5667-5674 (1991).
25 Wang, X. & Seeman, N. C. 'Assembly and Characterization of 8-Arm and 12-Arm DNA Branched Junctions'. *Journal of the American Chemical Society* **129**, 8169-8176 (2007).
26 Bhatia, D. *et al.* 'Icosahedral DNA Nanocapsules by Modular Assembly'. *Angewandte Chemie International Edition* **48**, 4134-4137 (2009).
27 Banerjee, A. *et al.* 'Controlled Release of Encapsulated Cargo from a DNA Icosahedron using a Chemical Trigger'. *Angewandte Chemie International Edition* **52**, 6854-6857 (2013).
28 Fu, T. J. & Seeman, N. C. 'DNA double-crossover molecules'. *Biochemistry* **32**, 3211-3220 (1993).
29 Li, X., Yang, X., Qi, J. & Seeman, N. C. 'Antiparallel DNA Double Crossover Molecules As Components for Nanoconstruction'. *Journal of the American Chemical Society* **118**, 6131-6140 (1996).
30 Winfree, E., Liu, F., Wenzler, L. A. & Seeman, N. C. 'Design and self-assembly of two-dimensional DNA crystals'. *Nature* **394**, 539-544 (1998).
31 Lin, C., Liu, Y., Rinker, S. & Yan, H. 'DNA Tile Based Self-Assembly: Building Complex Nanoarchitectures'. *ChemPhysChem* **7**, 1641-1647 (2006).
32 Yan, H., Park, S. H., Finkelstein, G., Reif, J. H. & LaBean, T. H. 'DNA-Templated Self-Assembly of Protein Arrays and Highly Conductive Nanowires'. *Science* **301**, 1882-1884 (2003).
33 Sharma, J. *et al.* 'DNA-Tile-Directed Self-Assembly of Quantum Dots into Two-Dimensional Nanopatterns'. *Angewandte Chemie International Edition* **47**, 5157-5159 (2008).
34 He, Y. *et al.* 'Hierarchical self-assembly of DNA into symmetric supramolecular polyhedra'. *Nature* **452**, 198-201 (2008).
35 Zhang, C. *et al.* 'Symmetry Controls the Face Geometry of DNA Polyhedra'. *Journal of the American Chemical Society* **131**, 1413-1415 (2009).
36 He, Y. *et al.* 'Sequence Symmetry as a Tool for Designing DNA Nanostructures'. *Angewandte Chemie International Edition* **44**, 6694-6696 (2005).
37 Zhang, C. *et al.* 'Conformational flexibility facilitates self-assembly of complex DNA nanostructures'. *Proceedings of the National Academy of Sciences* **105**, 10665-10669 (2008).
38 Tian, C. *et al.* 'Directed self-assembly of DNA tiles into complex nanocages'. *Angewandte Chemie - International Edition* **53**, 8041-8044 (2014).
39 He, Y. *et al.* 'On the Chirality of Self-Assembled DNA Octahedra'. *Angewandte Chemie International Edition* **49**, 748-751 (2010).
40 Zheng, J. *et al.* 'From molecular to macroscopic via the rational design of a self-assembled 3D DNA crystal'. *Nature* **461**, 74-77 (2009).
41 Muser, S. E. & Paukstelis, P. J. 'Three-Dimensional DNA Crystals with pH-Responsive Noncanonical Junctions'. *Journal of the American Chemical Society* **134**, 12557-12564 (2012).

42 Geng, C. & Paukstelis, P. J. 'DNA Crystals as Vehicles for Biocatalysis'. *Journal of the American Chemical Society* **136**, 7817-7820 (2014).
43 Mathieu, F. *et al.* 'Six-Helix Bundles Designed from DNA'. *Nano Letters* **5**, 661-665 (2005).
44 Park, S. H. *et al.* 'Three-Helix Bundle DNA Tiles Self-Assemble into 2D Lattice or 1D Templates for Silver Nanowires'. *Nano Letters* **5**, 693-696 (2005).
45 Dutta, P. K. *et al.* 'DNA-Directed Artificial Light-Harvesting Antenna'. *Journal of the American Chemical Society* **133**, 11985-11993 (2011).
46 Stojanovic, M. N., Stefanovic, D., Labean, T. & Yan, H. in *Bioelectronics: From Theory to Applications* 427-455 (2005).
47 Winfree, E. *Algorithmic Self-Assembly of DNA*, Caltech, (1998).
48 Mao, C., LaBean, T. H., Reif, J. H. & Seeman, N. C. 'Logical computation using algorithmic self-assembly of DNA triple-crossover molecules'. *Nature* **407**, 493-496 (2000).
49 Rothemund, P. W. K., Papadakis, N. & Winfree, E. 'Algorithmic Self-Assembly of DNA Sierpinski Triangles'. *PLoS Biol* **2**, e424 (2004).
50 Winfree, E. 'Algorithmic self-assembly of DNA: Theoretical motivations and 2D assembly experiments'. *Journal of Biomolecular Structure and Dynamics* **17**, 263-270 (2000).
51 Wei, B., Dai, M. & Yin, P. 'Complex shapes self-assembled from single-stranded DNA tiles'. *Nature* **485**, 623-626 (2012).
52 Ke, Y., Ong, L. L., Shih, W. M. & Yin, P. 'Three-Dimensional Structures Self-Assembled from DNA Bricks'. *Science* **338**, 1177-1183 (2012).
53 Wei, B., Ong, L. L., Chen, J., Jaffe, A. S. & Yin, P. 'Complex reconfiguration of DNA nanostructures'. *Angewandte Chemie - International Edition* **53**, 7475-7479 (2014).
54 Evans, C. & Winfree, E. in *DNA Computing and Molecular Programming* Vol. 8141 *Lecture Notes in Computer Science* (eds David Soloveichik & Bernard Yurke) Ch. 5, 61-75 (Springer International Publishing, 2013).
55 Rothemund, P. W. K. 'Folding DNA to create nanoscale shapes and patterns'. *Nature* **440**, 297-302 (2006).
56 Shih, W. M., Quispe, J. D. & Joyce, G. F. 'A 1.7-kilobase single-stranded DNA that folds into a nanoscale octahedron'. *Nature* **427**, 618-621 (2004).
57 Andersen, E. S. *et al.* 'Self-assembly of a nanoscale DNA box with a controllable lid'. *Nature* **459**, 73-76 (2009).
58 Kuzuya, A. & Komiyama, M. 'Design and construction of a box-shaped 3D-DNA origami'. *Chemical Communications*, 4182-4184 (2009).
59 Endo, M., Hidaka, K., Kato, T., Namba, K. & Sugiyama, H. 'DNA Prism Structures Constructed by Folding of Multiple Rectangular Arms'. *Journal of the American Chemical Society* **131**, 15570-15571 (2009).
60 Douglas, S. M. *et al.* 'Self-assembly of DNA into nanoscale three-dimensional shapes'. *Nature* **459**, 414-418 (2009).
61 Dietz, H., Douglas, S. M. & Shih, W. M. 'Folding DNA into Twisted and Curved Nanoscale Shapes'. *Science* **325**, 725-730 (2009).
62 Han, D. *et al.* 'DNA Origami with Complex Curvatures in Three-Dimensional Space'. *Science* **332**, 342-346 (2011).
63 Liedl, T., Hogberg, B., Tytell, J., Ingber, D. E. & Shih, W. M. 'Self-assembly of three-dimensional prestressed tensegrity structures from DNA'. *Nat Nano* **5**, 520-524 (2010).

64 Rajendran, A., Endo, M., Katsuda, Y., Hidaka, K. & Sugiyama, H. 'Programmed Two-Dimensional Self-Assembly of Multiple DNA Origami Jigsaw Pieces'. *ACS Nano* **5**, 665-671 (2010).
65 Ke, Y. *et al.* 'Multilayer DNA origami packed on a square lattice'. *Journal of the American Chemical Society* **131**, 15903-15908 (2009).
66 Jungmann, R. *et al.* 'DNA origami-based nanoribbons: assembly, length distribution, and twist'. *Nanotechnology* **22**, 275301 (2011).
67 Woo, S. & Rothemund, P. W. K. 'Programmable molecular recognition based on the geometry of DNA nanostructures'. *Nat Chem* **3**, 620-627 (2011).
68 Marchi, A. N., Saaem, I., Vogen, B. N., Brown, S. & LaBean, T. H. 'Toward Larger DNA Origami'. *Nano Letters* **14**, 5740-5747 (2014).
69 Iinuma, R. *et al.* 'Polyhedra Self-Assembled from DNA Tripods and Characterized with 3D DNA-PAINT'. *Science* **344**, 65-69 (2014).
70 Steinhauer, C., Jungmann, R., Sobey, T. L., Simmel, F. C. & Tinnefeld, P. 'DNA Origami as a Nanoscopic Ruler for Super-Resolution Microscopy'. *Angewandte Chemie International Edition* **48**, 8870-8873 (2009).
71 Hung, A. M. *et al.* 'Large-area spatially ordered arrays of gold nanoparticles directed by lithographically confined DNA origami'. *Nat Nano* **5**, 121-126 (2010).
72 Pal, S. *et al.* 'DNA Directed Self-Assembly of Anisotropic Plasmonic Nanostructures'. *Journal of the American Chemical Society* **133**, 17606-17609 (2011).
73 Kuzyk, A. *et al.* 'DNA-based self-assembly of chiral plasmonic nanostructures with tailored optical response'. *Nature* **483**, 311-314 (2012).
74 Dai, G. *et al.* 'DNA Origami-Directed, Discrete Three-Dimensional Plasmonic Tetrahedron Nanoarchitectures with Tailored Optical Chirality'. *ACS Applied Materials & Interfaces* **6**, 5388-5392 (2014).
75 Voigt, N. V. *et al.* 'Single-molecule chemical reactions on DNA origami'. *Nat Nano* **5**, 200-203 (2010).
76 Fu, J., Liu, M., Liu, Y., Woodbury, N. W. & Yan, H. 'Interenzyme Substrate Diffusion for an Enzyme Cascade Organized on Spatially Addressable DNA Nanostructures'. *Journal of the American Chemical Society* **134**, 5516-5519 (2012).
77 Rajendran, A., Endo, M. & Sugiyama, H. 'Single-Molecule Analysis Using DNA Origami'. *Angewandte Chemie International Edition* **51**, 874-890 (2012).
78 Douglas, S. M., Bachelet, I. & Church, G. M. 'A Logic-Gated Nanorobot for Targeted Transport of Molecular Payloads'. *Science* **335**, 831-834 (2012).
79 Takenaka, T. *et al.* 'Photoresponsive DNA Nanocapsule Having an Open/Close System for Capture and Release of Nanomaterials'. *Chemistry – A European Journal* **20**, 14951-14954 (2014).
80 Langecker, M. *et al.* 'Synthetic Lipid Membrane Channels Formed by Designed DNA Nanostructures'. *Science* **338**, 932-936 (2012).
81 Sun, W. *et al.* 'Casting inorganic structures with DNA molds'. *Science* **346** (2014).
82 Helmi, S., Ziegler, C., Kauert, D. J. & Seidel, R. 'Shape-Controlled Synthesis of Gold Nanostructures Using DNA Origami Molds'. *Nano Letters* (2014).
83 Hahn, J., Wickham, S. F. J., Shih, W. M. & Perrault, S. D. 'Addressing the Instability of DNA Nanostructures in Tissue Culture'. *ACS Nano* **8**, 8765-8775 (2014).
84 Hudson, R. H. E. & Damha, M. J. 'Nucleic acid dendrimers: novel biopolymer structures'. *Journal of the American Chemical Society* **115**, 2119-2124 (1993).

85 Damha, M. J., Ganeshan, K., Hudson, R. H. E. & Zabarylo, S. V. 'Solid-phase synthesis of branched oligoribonucleotides related to messenger RNA splicing intermediates'. *Nucleic Acids Research* **20**, 6565-6573 (1992).
86 Teigelkamp, S., Ebel, S., Will, D. W., Brown, T. & Beggs, J. D. 'Branched poly-labelled oligonucleotides: enhanced specificity of fork-shaped biotinylated oligoribonucleotides for antisense affinity selection'. *Nucleic Acids Research* **21**, 4651-4652 (1993).
87 Shchepinov, M. S., Udalova, I. A., Bridgman, A. J. & Southern, E. M. 'Oligonucleotide dendrimers: Synthesis and use as polylabelled DNA probes'. *Nucleic Acids Research* **25**, 4447-4454 (1997).
88 Shchepinov, M. S., Mir, K. U., Elder, J. K., Frank-Kamenetskii, M. D. & Southern, E. M. 'Oligonucleotide dendrimers: stable nano-structures'. *Nucleic Acids Research* **27**, 3035-3041 (1999).
89 Scheffler, M., Dorenbeck, A., Jordan, S., Wüstefeld, M. & von Kiedrowski, G. 'Self-Assembly of Trisoligonucleotidyls: The Case for Nano-Acetylene and Nano-Cyclobutadiene'. *Angewandte Chemie International Edition* **38**, 3311-3315 (1999).
90 Ohya, Y., Noro, H., Komatsu, M. & Ouchi, T. 'Synthesis of Symmetric Oligo-DNA Dimers and Their Formation of Polymeric Supramolecular Assembly'. *Chemistry Letters* **25**, 447-448 (1996).
91 Shi, J. & Bergstrom, D. E. 'Assembly of Novel DNA Cycles with Rigid Tetrahedral Linkers'. *Angewandte Chemie International Edition in English* **36**, 111-113 (1997).
92 Aldaye, F. A. & Sleiman, H. F. 'Sequential self-assembly of a DNA hexagon as a template for the organization of gold nanoparticles'. *Angewandte Chemie - International Edition* **45**, 2204-2209 (2006).
93 Aldaye, F. A. & Sleiman, H. F. 'Modular access to structurally switchable 3D discrete DNA assemblies'. *Journal of the American Chemical Society* **129**, 13376-13377 (2007).
94 Aldaye, F. A. *et al.* 'Modular construction of DNA nanotubes of tunable geometry and single- or double-stranded character'. *Nature Nanotechnology* **4**, 349-352 (2009).
95 Carneiro, K. M. M., Avakyan, N. & Sleiman, H. F. 'Long-range assembly of DNA into nanofibers and highly ordered networks'. *Wiley Interdisciplinary Reviews: Nanomedicine and Nanobiotechnology* **5**, 266-285 (2013).
96 Lo, P. K. *et al.* 'Loading and selective release of cargo in DNA nanotubes with longitudinal variation'. *Nat Chem* **2**, 319-328 (2010).
97 Greschner, A. A., Toader, V. & Sleiman, H. F. 'The role of organic linkers in directing DNA self-assembly and significantly stabilizing DNA duplexes'. *Journal of the American Chemical Society* **134**, 14382-14389 (2012).
98 Greschner, A. A., Bujold, K. E. & Sleiman, H. F. 'Intercalators as Molecular Chaperones in DNA Self-Assembly'. *Journal of the American Chemical Society* **135**, 11283-11288 (2013).
99 Aldaye, F. A. & Sleiman, H. F. 'Guest-mediated access to a single DNA nanostructure from a library of multiple assemblies'. *Journal of the American Chemical Society* **129**, 10070-10071 (2007).
100 Fujita, M. *et al.* 'Self assembly of ten molecules into nanometre-sized organic host frameworks'. *Nature* **378**, 469-471 (1995).
101 Conn, M. M. & Rebek Jr, J. 'Self-assembling capsules'. *Chemical Reviews* **97**, 1647-1668 (1997).

102 Fujita, M. 'Self-assembly of [2]catenanes containing metals in their backbones'. *Accounts of Chemical Research* **32**, 53-61 (1999).
103 Takeda, N., Umemoto, K., Yamaguchi, K. & Fujita, M. 'A nanometre-sized hexahedral coordination capsule assembled from 24 components'. *Nature* **398**, 794-796 (1999).
104 Leininger, S., Olenyuk, B. & Stang, P. J. 'Self-Assembly of Discrete Cyclic Nanostructures Mediated by Transition Metals'. *Chemical Reviews* **100**, 853-907 (2000).
105 Eddaoudi, M. *et al.* 'Modular chemistry: Secondary building units as a basis for the design of highly porous and robust metal-organic carboxylate frameworks'. *Accounts of Chemical Research* **34**, 319-330 (2001).
106 Seidel, S. R. & Stang, P. J. 'High-symmetry coordination cages via self-assembly'. *Accounts of Chemical Research* **35**, 972-983 (2002).
107 Kitagawa, S., Kitaura, R. & Noro, S. I. 'Functional porous coordination polymers'. *Angewandte Chemie - International Edition* **43**, 2334-2375 (2004).
108 Gianneschi, N. C., Masar, M. S. & Mirkin, C. A. 'Development of a Coordination Chemistry-Based Approach for Functional Supramolecular Structures'. *Accounts of Chemical Research* **38**, 825-837 (2005).
109 Fujita, M., Tominaga, M., Hori, A. & Therrien, B. 'Coordination assemblies from a Pd(II)-cornered square complex'. *Accounts of Chemical Research* **38**, 369-378 (2005).
110 Waybright, S. M., Singleton, C. P., Wachter, K., Murphy, C. J. & Bunz, U. H. F. 'Oligonucleotide-Directed Assembly of Materials: Defined Oligomers'. *Journal of the American Chemical Society* **123**, 1828-1833 (2001).
111 Gothelf, K. V., Thomsen, A., Nielsen, M., Cló, E. & Brown, R. S. 'Modular DNA-Programmed Assembly of Linear and Branched Conjugated Nanostructures'. *Journal of the American Chemical Society* **126**, 1044-1046 (2004).
112 Stewart, K. M. & McLaughlin, L. W. 'Four-Arm Oligonucleotide Ni(II)−Cyclam-Centered Complexes as Precursors for the Generation of Supramolecular Periodic Assemblies'. *Journal of the American Chemical Society* **126**, 2050-2057 (2004).
113 Choi, J. S. *et al.* 'Synthesis of DNA triangles with vertexes of Bis(terpyridine)iron(II) complexes'. *Journal of the American Chemical Society* **126**, 8606-8607 (2004).
114 Mitra, D., Di Cesare, N. & Sleiman, H. F. 'Self-assembly of cyclic metal-DNA nanostructures using ruthenium tris(bipyridine)-branched oligonucleotides'. *Angewandte Chemie - International Edition* **43**, 5804-5808 (2004).
115 Tanaka, K., Tengeiji, A., Kato, T., Toyama, N. & Shionoya, M. 'A Discrete Self-Assembled Metal Array in Artificial DNA'. *Science* **299**, 1212-1213 (2003).
116 Duprey, J. L. H. A., Takezawa, Y. & Shionoya, M. 'Metal-locked DNA three-way junction'. *Angewandte Chemie - International Edition* **52**, 1212-1216 (2013).
117 Dietrich-Buchecker, C. O., Sauvage, J. P. & Kintzinger, J. P. 'Une nouvelle famille de molecules : les metallo-catenanes'. *Tetrahedron Letters* **24**, 5095-5098 (1983).
118 Beves, J. E., Blight, B. A., Campbell, C. J., Leigh, D. A. & McBurney, R. T. 'Strategies and tactics for the metal-directed synthesis of rotaxanes, knots, catenanes, and higher order links'. *Angewandte Chemie - International Edition* **50**, 9260-9327 (2011).
119 Yang, H. & Sleiman, H. F. 'Templated synthesis of highly stable, electroactive, and dynamic metal-DNA branched junctions'. *Angewandte Chemie - International Edition* **47**, 2443-2446 (2008).
120 Yang, H. *et al.* 'Metal–nucleic acid cages'. *Nat Chem* **1**, 390-396 (2009).

121 Yang, H. *et al.* 'Chiral metal-DNA four-arm junctions and metalated nanotubular structures'. *Angewandte Chemie - International Edition* **50**, 4620-4623 (2011).
122 Yang, H., Rys, A. Z., McLaughlin, C. K. & Sleiman, H. F. 'Templated ligand environments for the selective incorporation of different metals into DNA'. *Angewandte Chemie - International Edition* **48**, 9919-9923+9769 (2009).
123 McLaughlin, C. K., Hamblin, G. D. & Sleiman, H. F. 'Supramolecular DNA assembly'. *Chemical Society Reviews* **40**, 5647-5656 (2011).
124 Breaker, R. R. & Joyce, G. F. 'A DNA enzyme that cleaves RNA'. *Chemistry & Biology* **1**, 223-229.
125 Yang, H., Metera, K. L. & Sleiman, H. F. 'DNA modified with metal complexes: Applications in the construction of higher order metal-DNA nanostructures'. *Coordination Chemistry Reviews* **254**, 2403-2415 (2010).
126 Morgan, J. R., Nguyen, D. V. X., Frohman, A. R., Rybka, S. R. & Zebala, J. A. 'Reversible metal-dependent destabilization and stabilization of a stem-chelate-loop probe binding to an unmodified DNA target'. *Bioconjugate chemistry* **23**, 2020-2024 (2012).
127 Kay, E. R., Leigh, D. A. & Zerbetto, F. 'Synthetic Molecular Motors and Mechanical Machines'. *Angewandte Chemie International Edition* **46**, 72-191 (2007).
128 Clayton, D. A. & Vinograd, J. 'Circular dimer and catenate forms of mitochondrial DNA in human leukaemic leucocytes'. *Nature* **216**, 652-657 (1967).
129 Hudson, B. & Vinograd, J. 'Catenated circular DNA molecules in heLa cell mitochondria'. *Nature* **216**, 647-652 (1967).
130 Wang, J. C. & Schwartz, H. 'Noncomplementarity in base sequences between the cohesive ends of coliphages 186 and λ and the formation of interlocked rings between the two DNA's'. *Biopolymers* **5**, 953-966 (1967).
131 Weizmann, Y., Braunschweig, A. B., Wilner, O. I., Cheglakov, Z. & Willner, I. 'A polycatenated DNA scaffold for the one-step assembly of hierarchical nanostructures'. *Proceedings of the National Academy of Sciences* **105**, 5289-5294 (2008).
132 Conway, J. W., McLaughlin, C. K., Castor, K. J. & Sleiman, H. 'DNA nanostructure serum stability: Greater than the sum of its parts'. *Chemical Communications* **49**, 1172-1174 (2013).
133 Jester, S.-S. & Famulok, M. 'Mechanically Interlocked DNA nanostructures for Functional Devices'. *Accounts of Chemical Research* **47**, 1700-1709 (2014).
134 Lu, C. H. *et al.* 'Switchable reconfiguration of an interlocked DNA olympiadane nanostructure'. *Angewandte Chemie - International Edition* **53**, 7499-7503 (2014).
135 Wang, W., Wan, W., Zhou, H.-H., Niu, S. & Li, A. D. Q. 'Alternating DNA and π-Conjugated Sequences. Thermophilic Foldable Polymers'. *Journal of the American Chemical Society* **125**, 5248-5249 (2003).
136 Patwa, A., Gissot, A., Bestel, I. & Barthélémy, P. 'Hybrid lipid oligonucleotide conjugates: Synthesis, self-assemblies and biomedical applications'. *Chemical Society Reviews* **40**, 5844-5854 (2011).
137 Zhang, D. Y. & Seelig, G. 'Dynamic DNA nanotechnology using strand-displacement reactions'. *Nat Chem* **3**, 103-113 (2011).
138 Zhang, D. Y. & Winfree, E. 'Control of DNA Strand Displacement Kinetics Using Toehold Exchange'. *Journal of the American Chemical Society* **131**, 17303-17314 (2009).
139 Yurke, B., Turberfield, A. J., Mills, A. P., Simmel, F. C. & Neumann, J. L. 'A DNA-fuelled molecular machine made of DNA'. *Nature* **406**, 605-608 (2000).

140 Chen, Y., Wang, M. & Mao, C. 'An Autonomous DNA Nanomotor Powered by a DNA Enzyme'. *Angewandte Chemie International Edition* **43**, 3554-3557 (2004).
141 Wickham, S. F. J. *et al.* 'A DNA-based molecular motor that can navigate a network of tracks'. *Nat Nano* **7**, 169-173 (2012).
142 Shin, J.-S. & Pierce, N. A. 'A Synthetic DNA Walker for Molecular Transport'. *Journal of the American Chemical Society* **126**, 10834-10835 (2004).
143 Gu, H., Chao, J., Xiao, S.-J. & Seeman, N. C. 'A proximity-based programmable DNA nanoscale assembly line'. *Nature* **465**, 202-205 (2010).
144 Aldaye, F. A. & Sleiman, H. F.
145 Bujold, K. E. *et al.* 'Sequence-Responsive Unzipping DNA Cubes with Tunable Cellular Uptake Profiles'. *Chemical Science* (2014).
146 Teller, C. & Willner, I. 'Functional nucleic acid nanostructures and DNA machines'. *Current Opinion in Biotechnology* **21**, 376-391 (2010).
147 Alexandridis, P. L., B. *Amphiphilic Block Copolymers: Self-Assembly and Applications*. (Elsevier, 2000).
148 Mai, Y. & Eisenberg, A. 'Self-assembly of block copolymers'. *Chemical Society Reviews* **41**, 5969-5985 (2012).
149 Carneiro, K. M. M., Aldaye, F. A. & Sleiman, H. F. 'Long-Range Assembly of DNA into Nanofibers and Highly Ordered Networks Using a Block Copolymer Approach'. *Journal of the American Chemical Society* **132**, 679-685 (2009).
150 Wilks, T. R. *et al.* '"Giant Surfactants" Created by the Fast and Efficient Functionalization of a DNA Tetrahedron with a Temperature-Responsive Polymer'. *ACS Nano* **7**, 8561-8572 (2013).
151 Liu, H. *et al.* 'DNA-Based Micelles: Synthesis, Micellar Properties and Size-Dependent Cell Permeability'. *Chemistry – A European Journal* **16**, 3791-3797 (2010).
152 Thompson, M. P., Chien, M.-P., Ku, T.-H., Rush, A. M. & Gianneschi, N. C. 'Smart Lipids for Programmable Nanomaterials'. *Nano Letters* **10**, 2690-2693 (2010).
153 Chien, M.-P., Rush, A. M., Thompson, M. P. & Gianneschi, N. C. 'Programmable Shape-Shifting Micelles'. *Angewandte Chemie International Edition* **49**, 5076-5080 (2010).
154 Alemdaroglu, F. E., Alemdaroglu, N. C., Langguth, P. & Herrmann, A. 'Cellular Uptake of DNA Block Copolymer Micelles with Different Shapes'. *Macromolecular rapid communications* **29**, 326-329 (2008).
155 Chan, Y. H., van Lengerich, B. & Boxer, S. G. 'Lipid-anchored DNA mediates vesicle fusion as observed by lipid and content mixing'. *Biointerphases* **3**, Fa17 (2008).
156 Raouane, M., Desmaële, D., Urbinati, G., Massaad-Massade, L. & Couvreur, P. 'Lipid Conjugated Oligonucleotides: A Useful Strategy for Delivery'. *Bioconjugate Chemistry* (2012).
157 Wolfrum, C. *et al.* 'Mechanisms and optimization of in vivo delivery of lipophilic siRNAs'. *Nat Biotech* **25**, 1149-1157 (2007).
158 Seferos, D. S., Prigodich, A. E., Giljohann, D. A., Patel, P. C. & Mirkin, C. A. 'Polyvalent DNA Nanoparticle Conjugates Stabilize Nucleic Acids'. *Nano Letters* **9**, 308-311 (2008).
159 Rush, A. M., Thompson, M. P., Tatro, E. T. & Gianneschi, N. C. 'Nuclease-Resistant DNA via High-Density Packing in Polymeric Micellar Nanoparticle Coronas'. *ACS Nano* **7**, 1379-1387 (2013).

160 Rush, A. M. *et al.* 'Intracellular mRNA Regulation with Self-Assembled Locked Nucleic Acid Polymer Nanoparticles'. *Journal of the American Chemical Society* **136**, 7615-7618 (2014).
161 Rosi, N. L. *et al.* 'Oligonucleotide-modified gold nanoparticles for infracellular gene regulation'. *Science* **312**, 1027-1030 (2006).
162 Chen, T. *et al.* 'DNA Micelle Flares for Intracellular mRNA Imaging and Gene Therapy'. *Angewandte Chemie International Edition* **52**, 2012-2016 (2013).
163 Alemdaroglu, F. E., Alemdaroglu, N. C., Langguth, P. & Herrmann, A. 'DNA Block Copolymer Micelles – A Combinatorial Tool for Cancer Nanotechnology'. *Advanced Materials* **20**, 899-902 (2008).
164 Wu, Y., Sefah, K., Liu, H., Wang, R. & Tan, W. 'DNA aptamer–micelle as an efficient detection/delivery vehicle toward cancer cells'. *Proceedings of the National Academy of Sciences* **107**, 5-10 (2010).
165 Woller, J. G., Börjesson, K., Svedhem, S. & Albinsson, B. 'Reversible hybridization of DNA anchored to a lipid membrane via porphyrin'. *Langmuir : the ACS journal of surfaces and colloids* **28**, 1944-1953 (2012).
166 Börjesson, K., Lundberg, E. P., Woller, J. G., Nordén, B. & Albinsson, B. 'Soft-surface DNA nanotechnology: DNA constructs anchored and aligned to lipid membrane'. *Angewandte Chemie - International Edition* **50**, 8312-8315 (2011).
167 Albinsson, B., Hannestad, J. K. & Börjesson, K. 'Functionalized DNA nanostructures for light harvesting and charge separation'. *Coordination Chemistry Reviews* (2012).
168 Suzuki, Y., Endo, M., Yang, Y. & Sugiyama, H. 'Dynamic Assembly/Disassembly Processes of Photoresponsive DNA Origami Nanostructures Directly Visualized on a Lipid Membrane Surface'. *Journal of the American Chemical Society* **136**, 1714-1717 (2014).
169 Johnson-Buck, A., Jiang, S., Yan, H. & Walter, N. G. 'DNA–Cholesterol Barges as Programmable Membrane-Exploring Agents'. *ACS Nano* **8**, 5641-5649 (2014).
170 Burns, J. R. *et al.* 'Lipid-Bilayer-Spanning DNA Nanopores with a Bifunctional Porphyrin Anchor'. *Angewandte Chemie International Edition* **52**, 12069-12072 (2013).
171 McLaughlin, C. K. *et al.* 'Three-dimensional organization of block copolymers on "DNA- minimal" scaffolds'. *Journal of the American Chemical Society* **134**, 4280-4286 (2012).
172 Carneiro, K. M. M. *et al.* 'Stimuli-responsive organization of block copolymers on DNA nanotubes'. *Chemical Science* **3**, 1980-1986 (2012).
173 Conway, J. W. *et al.* 'Dynamic Behavior of DNA Cages Anchored on Spherically Supported Lipid Bilayers'. *Journal of the American Chemical Society* **136**, 12987-12997 (2014).
174 List, J., Weber, M. & Simmel, F. C. 'Hydrophobic Actuation of a DNA Origami Bilayer Structure'. *Angewandte Chemie International Edition* **53**, 4236-4239 (2014).
175 Boisselier, E. & Astruc, D. 'Gold nanoparticles in nanomedicine: preparations, imaging, diagnostics, therapies and toxicity'. *Chem Soc Rev* **38**, 1759-1782 (2009).
176 Eustis, S. & el-Sayed, M. A. 'Why gold nanoparticles are more precious than pretty gold: noble metal surface plasmon resonance and its enhancement of the radiative and nonradiative properties of nanocrystals of different shapes'. *Chem Soc Rev* **35**, 209-217 (2006).

177 Kelly, K. L., Coronado, E., Zhao, L. L. & Schatz, G. C. 'The Optical Properties of Metal Nanoparticles: The Influence of Size, Shape, and Dielectric Environment'. *The Journal of Physical Chemistry B* **107**, 668-677 (2002).
178 Tan, S. J., Campolongo, M. J., Luo, D. & Cheng, W. 'Building plasmonic nanostructures with DNA'. *Nat Nano* **6**, 268-276 (2011).
179 Barrow, S. J., Funston, A. M., Wei, X. & Mulvaney, P. 'DNA-directed self-assembly and optical properties of discrete 1D, 2D and 3D plasmonic structures'. *Nano Today* **8**, 138-167 (2013).
180 Mirkin, C. A., Letsinger, R. L., Mucic, R. C. & Storhoff, J. J. 'A DNA-based method for rationally assembling nanoparticles into macroscopic materials'. *Nature* **382**, 607-609 (1996).
181 Alivisatos, A. P. *et al.* 'Organization of 'nanocrystal molecules' using DNA'. *Nature* **382**, 609-611 (1996).
182 Rodriguez, J. A. *et al.* 'Coverage Effects and the Nature of the Metal−Sulfur Bond in S/Au(111): High-Resolution Photoemission and Density-Functional Studies'. *Journal of the American Chemical Society* **125**, 276-285 (2002).
183 Hakkinen, H. 'The gold-sulfur interface at the nanoscale'. *Nat Chem* **4**, 443-455 (2012).
184 Zhang, T., Yang, Z. & Liu, D. 'DNA discrete modified gold nanoparticles'. *Nanoscale* **3**, 4015-4021 (2011).
185 Sharma, J. *et al.* 'Toward reliable gold nanoparticle patterning on self-assembled DNA nanoscaffold'. *Journal of the American Chemical Society* **130**, 7820-7821 (2008).
186 Lee, J.-S., Lytton-Jean, A. K. R., Hurst, S. J. & Mirkin, C. A. 'Silver Nanoparticle−Oligonucleotide Conjugates Based on DNA with Triple Cyclic Disulfide Moieties'. *Nano Letters* **7**, 2112-2115 (2007).
187 Zhang, T. *et al.* 'A new strategy improves assembly efficiency of DNA mono-modified gold nanoparticles'. *Chemical Communications* **47**, 5774-5776 (2011).
188 Li, F., Zhang, H., Dever, B., Li, X.-F. & Le, X. C. 'Thermal Stability of DNA Functionalized Gold Nanoparticles'. *Bioconjugate Chemistry* **24**, 1790-1797 (2013).
189 Lau, K. L., Hamblin, G. D. & Sleiman, H. F. 'Gold nanoparticle 3D-DNA building blocks: High purity preparation and use for modular access to nanoparticle assemblies'. *Small* **10**, 660-666 (2014).
190 Elghanian, R., Storhoff, J. J., Mucic, R. C., Letsinger, R. L. & Mirkin, C. A. 'Selective Colorimetric Detection of Polynucleotides Based on the Distance-Dependent Optical Properties of Gold Nanoparticles'. *Science* **277**, 1078-1081 (1997).
191 Giljohann, D. A. *et al.* 'Gold Nanoparticles for Biology and Medicine'. *Angewandte Chemie International Edition* **49**, 3280-3294 (2010).
192 Li, H., Park, S. H., Reif, J. H., LaBean, T. H. & Yan, H. 'DNA-Templated Self-Assembly of Protein and Nanoparticle Linear Arrays'. *Journal of the American Chemical Society* **126**, 418-419 (2003).
193 Zhang, J., Liu, Y., Ke, Y. & Yan, H. 'Periodic Square-Like Gold Nanoparticle Arrays Templated by Self-Assembled 2D DNA Nanogrids on a Surface'. *Nano Letters* **6**, 248-251 (2006).
194 Le, J. D. *et al.* 'DNA-Templated Self-Assembly of Metallic Nanocomponent Arrays on a Surface'. *Nano Letters* **4**, 2343-2347 (2004).
195 Sharma, J. *et al.* 'Control of Self-Assembly of DNA Tubules Through Integration of Gold Nanoparticles'. *Science* **323**, 112-116 (2009).

196 Guerrini, L. & Graham, D. 'Molecularly-mediated assemblies of plasmonic nanoparticles for Surface-Enhanced Raman Spectroscopy applications'. *Chemical Society Reviews* **41**, 7085-7107 (2012).
197 Nie, S. & Emory, S. R. 'Probing Single Molecules and Single Nanoparticles by Surface-Enhanced Raman Scattering'. *Science* **275**, 1102-1106 (1997).
198 Zanchet, D., Micheel, C. M., Parak, W. J., Gerion, D. & Alivisatos, A. P. 'Electrophoretic Isolation of Discrete Au Nanocrystal/DNA Conjugates'. *Nano Letters* **1**, 32-35 (2000).
199 Aldaye, F. A. & Sleiman, H. F. 'Dynamic DNA templates for discrete gold nanoparticle assemblies: Control of geometry, modularity, write/erase and structural switching'. *Journal of the American Chemical Society* **129**, 4130-4131 (2007).
200 Mastroianni, A., Claridge, S. & Alivisatos, A. P. 'Pyramidal and Chiral Groupings of Gold Nanocrystals Assembled Using DNA Scaffolds'. *Journal of the American Chemical Society* **131**, 8455-8459 (2009).
201 Kuzuya, A. 'DNA nanostructures as scaffolds for metal nanoparticles'. *Polym J* (2012).
202 Thacker, V. V. *et al.* 'DNA origami based assembly of gold nanoparticle dimers for surface-enhanced Raman scattering'. *Nat Commun* **5** (2014).
203 Klein, W. P. *et al.* 'Multiscaffold DNA Origami Nanoparticle Waveguides'. *Nano Letters* **13**, 3850-3856 (2013).
204 Kim, J.-W. & Deaton, R. 'Molecular Self-Assembly of Multifunctional Nanoparticle Composites with Arbitrary Shapes and Functions: Challenges and Strategies'. *Particle & Particle Systems Characterization* **30**, 117-132 (2013).
205 Halverson, J. D. & Tkachenko, A. V. 'DNA-programmed mesoscopic architecture'. *Physical Review E - Statistical, Nonlinear, and Soft Matter Physics* **87** (2013).
206 Suzuki, K., Hosokawa, K. & Maeda, M. 'Controlling the Number and Positions of Oligonucleotides on Gold Nanoparticle Surfaces'. *Journal of the American Chemical Society* **131**, 7518-7519 (2009).
207 Zhang, T. *et al.* 'DNA Bimodified Gold Nanoparticles'. *Langmuir : the ACS journal of surfaces and colloids* **28**, 1966-1970 (2011).
208 Zhang, C., Ma, J., Yang, J., Liu, S. & Xu, J. 'Binding Assistance Triggering Attachments of Hairpin DNA onto Gold Nanoparticles'. *Analytical Chemistry* **85**, 11973-11978 (2013).
209 Xu, X., Rosi, N. L., Wang, Y., Huo, F. & Mirkin, C. A. 'Asymmetric Functionalization of Gold Nanoparticles with Oligonucleotides'. *Journal of the American Chemical Society* **128**, 9286-9287 (2006).
210 Maye, M. M., Nykypanchuk, D., Cuisinier, M., van der Lelie, D. & Gang, O. 'Stepwise surface encoding for high-throughput assembly of nanoclusters'. *Nature materials* **8**, 388-391 (2009).
211 Xing, H. *et al.* 'DNA-Directed Assembly of Asymmetric Nanoclusters Using Janus Nanoparticles'. *ACS Nano* **6**, 802-809 (2011).
212 Kim, J.-W., Kim, J.-H. & Deaton, R. 'DNA-Linked Nanoparticle Building Blocks for Programmable Matter'. *Angewandte Chemie International Edition* **50**, 9185-9190 (2011).
213 Tan, L. H., Xing, H., Chen, H. & Lu, Y. 'Facile and Efficient Preparation of Anisotropic DNA-Functionalized Gold Nanoparticles and Their Regioselective Assembly'. *Journal of the American Chemical Society* **135**, 17675-17678 (2013).

2 Site-specific positioning of dendritic alkyl chains on DNA cages enables their geometry-dependent self-assembly

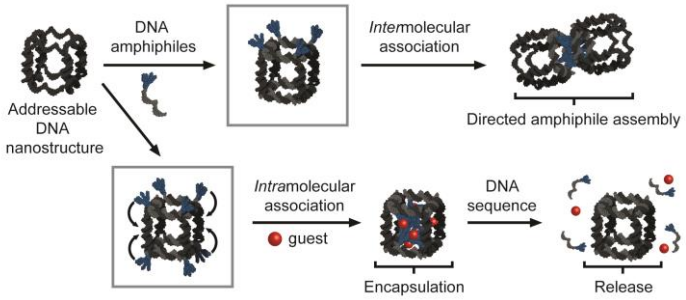

This chapter is composed mainly of work published as "Site-specific positioning of dendritic alkyl chains on DNA cages enables their geometry-dependent self-assembly", Edwardson, T. G. W.; Carneiro, K. M. M.; McLaughlin, C. K.; Serpell, C. J. and Sleiman, H. F. *Nature Chem.*, **2013**, 5, 868-875.

2.1 Abstract

The selective association of hydrophobic side-chains is a strong determinant of protein structure. In this chapter, the discovery of a similar form of self-assembly within 3D DNA nanostructures is described. This was achieved by using small, DNA minimal nanostructures as scaffolds for site-specific positioning of hydrophobic groups. Dendritic DNA amphiphiles (**D-DNA**) were synthesized, containing an addressable oligonucleotide portion and a hydrophobic alkyl dendron at the 5' terminus. Two variations of **D-DNA** were hybridized to the single-stranded edges of a DNA cube. It was found that anisotropic organization of these hydrophobic domains on the 3D scaffold results in a new set of assembly rules that are dependent on spatial orientation, number and chemical identity of the **D-DNA** on the cubic structure. When four amphiphiles are organized on one cube face, the hydrophobic residues engage in an intermolecular "handshake" between two

cubes, resulting in a dimer. When eight amphiphiles are organized on the top and bottom faces of the cube, they engage in a "handshake" inside the cube. This produces a monodisperse micellar core within the DNA nanostructure, which can encapsulate small molecules and release them in the presence of a specific DNA sequence.

2.2 Introduction

Nature uses a combination of non-covalent interactions to create a hierarchy of complex systems from simple building blocks. The relationship between individual recognition motifs and resulting macromolecular assemblies is simplified when limited to a smaller set of assembly rules, and DNA nanotechnology has used this concept to create a wide variety of self-assembled structures with high fidelity.[1-5] However, pure DNA nanotechnology that relies on Watson-Crick base-pairing is limited by this very simplicity, and ongoing efforts in this area have been focused on creating increased complexity without introducing self-assembly defects.[6-12]

To this end, a range of orthogonal chemical interactions have been introduced into DNA nanotechnology over the last few years.[13-16] Of particular interest is the combination of hydrophobic interactions with DNA self-assembly.[17-19] Lipid-DNA conjugates can confer unique stability and self-assembly properties.[20] Their use as a membrane anchor has been studied in the context of biophysical measurements on lipid-bilayers,[21-23] as well as a platform for DNA based light harvesting devices[24] and a synthetic membrane channel.[25] Alkyl modification of oligonucleotides is also used to increase serum stability and cell permeability for nucleic acid therapeutics.[26] Recent reports of DNA amphiphiles have showed that they are capable of both integration into lipid nanoparticles, and base pair-mediated DNA strand recognition.[27,28]

While the importance of the hydrophobic effect in determination of precisely defined discrete protein structures is well documented,[29-31] to date it has not been put to use so precisely in DNA nanostructures. Amphiphilic DNA assembly has been used to produce micellar systems in which the DNA block forms a corona in aqueous media while hydrophobic sections form bulk-like non-polar phases.[32-34] The resultant structures have been based around isotropic radial geometries, and display some degree of polydispersity. Elsewhere in supramolecular chemistry, the hydrophobic effect has been used in the formation of some well-defined and monodisperse local structure such as an

organic trefoil knot,[35] cyclodextrin inclusion complexes[36] and the selectivity of host systems for ions.[37] However, very few studies have examined the positioning of hydrophobic moieties in an anisotropic manner on a non-peptidic supramolecular scaffold and its effect on self-assembly.[25]

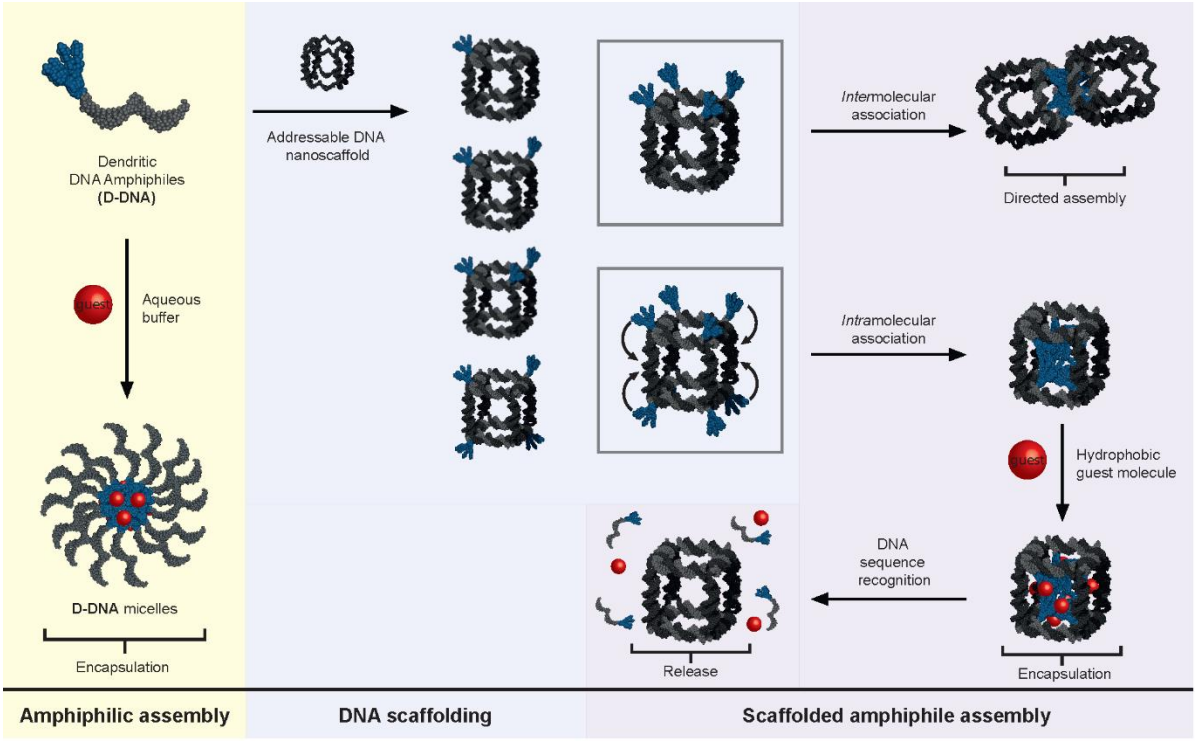

Figure 2.1 – The different modes of D-DNA assembly. **D-DNA** amphiphiles can spontaneously form micelles in aqueous solution and encapsulate guest molecules in their core (left). Organization on a 3D DNA scaffold below their critical micelle concentration allows access to a library of DNA nanostructures with different number and orientation of hydrophobic **D-DNA** domains (middle). Particular numbers or geometric arrangements allow access to further assembly mediated by **D-DNA**; *inter*molecular hydrophobic assembly between DNA cubes with four **D-DNA** units on one cube face, or *intra*molecular assembly to form scaffolded micelles within the DNA cage, which are capable of encapsulating small molecules and releasing them in the presence of a specific DNA sequence (right)

In this chapter, the anisotropic integration of a new class of dendritic alkyl chain-based DNA amphiphiles (**D-DNA**) within a 3D DNA nanostructure is described. It is found that by combining the highly specific recognition of the oligonucleotide sequence with the orthogonal association of hydrophobic moieties, a hybrid system is created which can be induced to associate through its hydrophobic domains either inter- or intramolecularly. The spatial orientation, number and chemical identity of these

amphiphiles on the scaffold can drastically affect the resulting self-assembly; with the positioning of four amphiphiles on one face of the cube a highly specific intermolecular "handshake" of alkyl chains is observed forming stable dimers, while the decoration of the cubic scaffold with eight amphiphiles results in an intramolecular collapse of hydrophobic moieties within the cavity of the DNA cage. This forms a monodisperse micelle which encapsulates small molecules and releases them specifically with an added DNA strand.

2.3 Results and Discussion

2.3.1 Synthetic approach for alkyl D-DNA

An important consideration in the approach is to create DNA conjugates with a distinct hydrophobic domain, while still retaining the ability of the DNA strands to efficiently hybridize with their complementary partner. This can be complicated with conventional lipid-DNAs as they aggregate at nanomolar concentrations.[38] With this in mind, a new class of DNA amphiphiles, **D-DNA**, were synthesized, which are less prone to spontaneous micelle formation in solution.

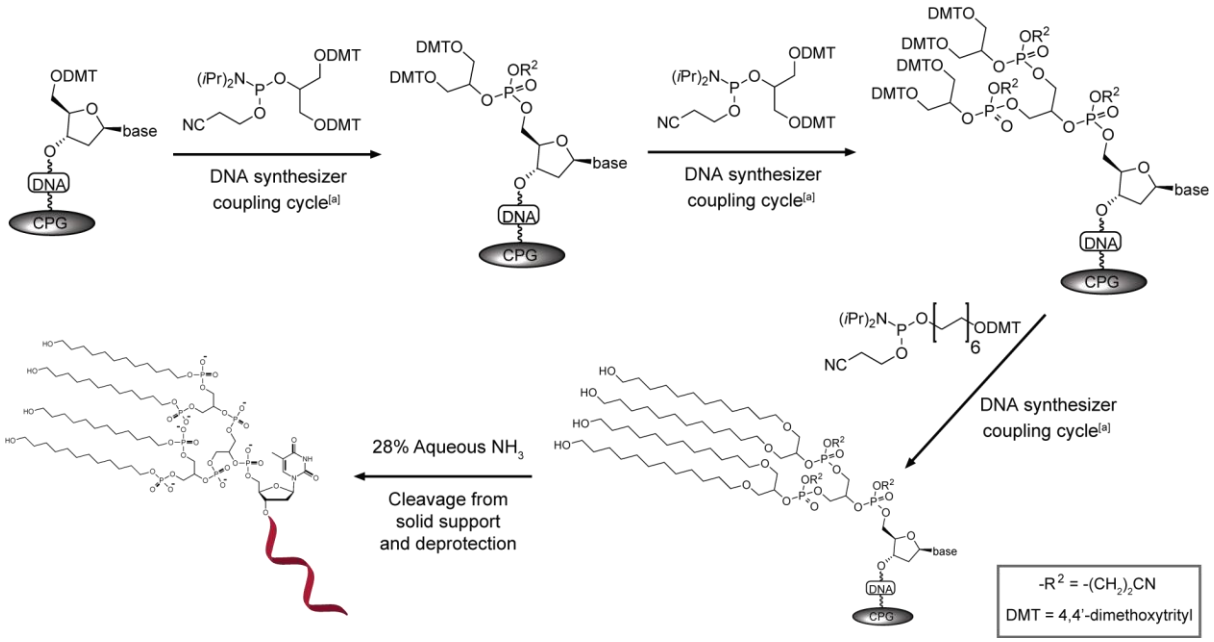

Figure 2.2 – Synthetic scheme for D-DNA synthesis. Here **D-DNA-1** (**D1**) is given as an example. Two stepwise additions of symmetrical branching phosphoramidite, followed by dodecane-diol phosphoramidite after the oligonucleotide couplings produce the 5' alkyl dendron modification. Cleavage and removal of nucleobase and phosphate protecting groups under basic conditions results in the DNA amphiphile. ([a] see *Experimental Section 2.5.3*)

This was achieved by extending the charged phosphodiester backbone from the oligonucleotide portion into the hydrophobic modification. This also simplifies the synthesis greatly as solid-phase DNA protocols can be used for the entire procedure, thus opening the opportunity for automated, and high-yielding synthesis on a DNA synthesizer. A divergent synthetic strategy was employed, in which branching units are introduced at the 5'-end of the DNA strand twice, such that four C12-based carbon chains can be attached at the DNA end, Figure 2.2.

This produces two dendritic DNA amphiphiles **D-DNA-1** (**D1**) and **D-DNA-2** (**D2**), Figure 2.3, in good yield. The advantage of this approach is the modular and facile synthesis from commercially available starting materials. By capitalizing on the efficiency of automated synthesis and using phosphoramidite building blocks the limit of structural diversity lies with the operator's imagination. This is in contrast to the majority of DNA amphiphile synthetic strategies which can require significant synthetic expertise to obtain a single target structure.[20]

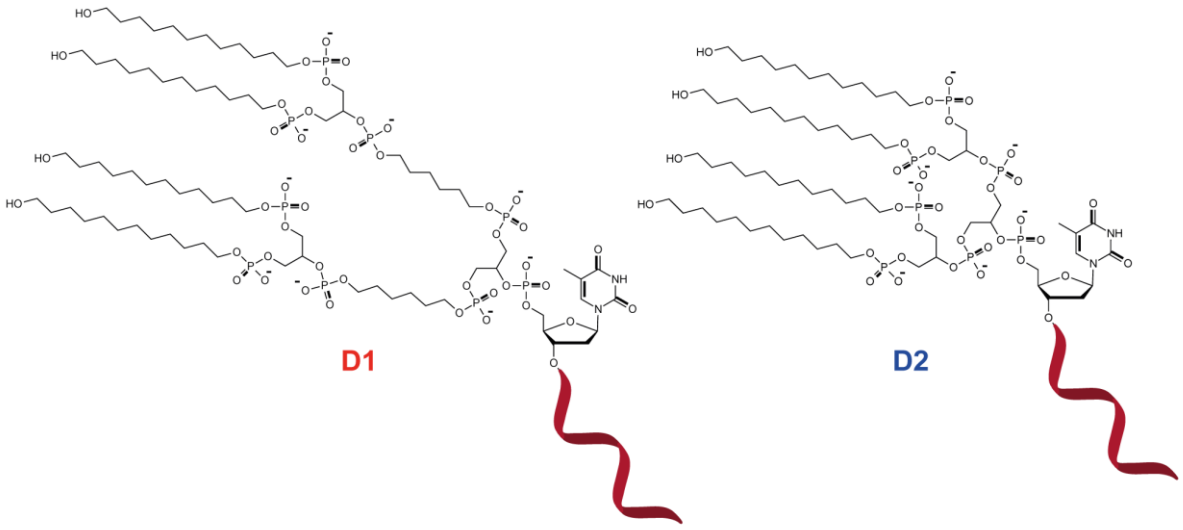

Figure 2.3 – Chemical structure of D-DNA modifications. The structure of dendritic DNA amphiphiles **D1** and **D2** is shown, in each molecule the oligonucleotide portion is 19 bases long. **D1** differs from **D2** only in the addition of two hexanediol spacers between symmetric branch units.

D1 and **D2** both contain four hydroxyl terminated dodecane (C12) chains as the hydrophobic portion. **D2** has no spacer between the first and the second branch points, however **D1** has additional 6-carbon spacers (1,6-hexanediol) between these branching units, which introduce two more phosphodiester linkages. The amphiphiles can be easily separated from the unmodified DNA by reverse phase HPLC. HPLC analysis shows that the smaller **D2** behaves like a more hydrophobic entity than **D1** (Figure 2.4), and this is corroborated by the studies below. It is possible that the four neighboring C12 chains in **D2** behave like a dense hydrophobic unit, while the additional hexanediol units in **D1**, which are flanked by phosphodiester linkages, act as a flexible spacer and allow for a greater distance between the four C12 chains.

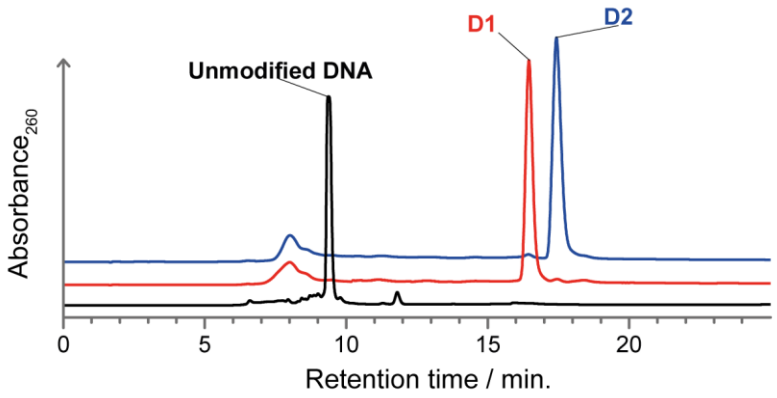

Figure 2.4 – HPLC traces of purified D-DNA. Reverse phase HPLC traces of the **D-DNA** products highlight the difference in hydrophobicity of **D1** and **D2** (broad peak at 8 minutes due to buffer, based on controls). Additional details can be found in *Experimental Section 2.5.4*.

2.3.2 Self-assembly properties of D-DNA

As a starting point it was important to understand the amphiphilic self-assembly properties of **D1** and **D2** in solution as this would play an important role when the DNA cube is introduced. Specifically, to address (i) whether the **D-DNA** structures spontaneously form aggregates in solution, (ii) whether the oligonucleotide portion retains its hybridization ability and (iii) whether **D1** and **D2** display a difference in their aggregation properties, due to structural variation of the 5' modification.

The critical micelle concentration (CMC) of both **D1** and **D2** was investigated using fluorescence emission of a hydrophobic dye, Nile Red. This molecule is nearly non-emissive in bulk aqueous media, but its inclusion in a non-polar microenvironment such

as the core of a micellar structure results in an intense fluorescence signal.[39] To determine the CMC of each conjugate, fluorescence spectra of 2.5μM Nile Red in a tris-acetate-magnesium (1xTAMg, [Mg^{2+}] = 12.5mM) buffer were measured in the presence of increasing concentrations of **D1** and **D2.**

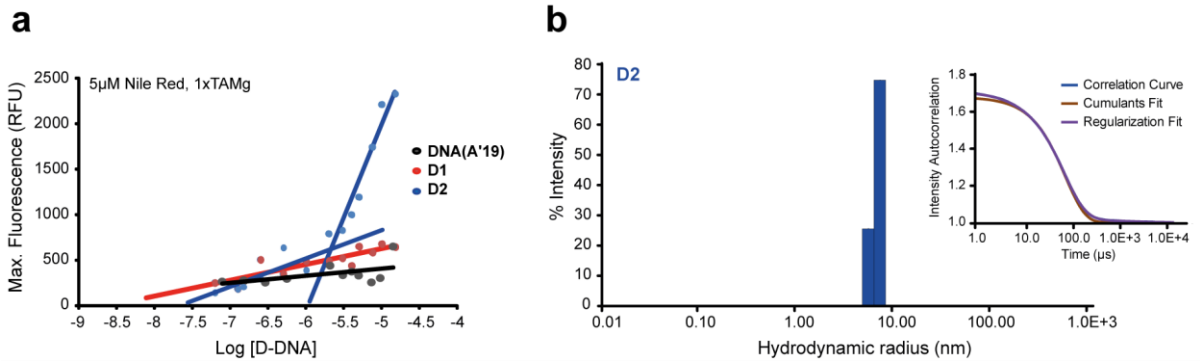

Figure 2.5 – Self-assembly of D-DNA. a) Plot of maximum fluorescence at 640 nm versus Log concentration for each conjugate; the intersection of the two gradients represents the critical micelle concentration. The critical micelle concentration of **D2** was determined to be 1.8 ± 0.4 μM after multiple measurements (see *Experimental Section 2.5.8*). **D1** behaves as unmodified DNA with no apparent critical micelle concentration in the range 10 nM-15 μM. d) The dynamic light scattering (DLS) histogram of **D2** micelles at 10 μM **D2** in 1xTAMg buffer at 25 °C, the measured hydrodynamic radius was 7.4 nm ± 0.4 nm. The inset shows the intensity correlation curve which is fitted to the raw data (see *Experimental Section 2.5.9*).

D1 showed little change in emission intensity with increasing concentration, similar to the unmodified DNA control, consistent with little aggregation in the concentration range of interest (10nM to 15μM). However in the case of **D2** an increase in fluorescence intensity was observed with increasing concentration. This, accompanied with a spectral blue shift of the fluorescence emission, is indicative of inclusion of Nile Red into a hydrophobic environment.[40] Specifically, it was found that **D2** aggregates with an associated CMC of 1.8 ± 0.4μM in the presence of 12.5mM Mg^{2+} (Figure 2.5). Dynamic light scattering (DLS) was used to investigate the size of the **D2** micelles in solution. An unmodified DNA control and **D1** displayed no significant scattering in solution (*Experimental Section*, Figure 2.23). However **D2** displayed scattering above the determined CMC with an associated hydrodynamic radius of 7.4nm ± 0.2nm and low polydispersity (Figure 2.5b).

Additionally, when the same fluorescence and DLS experiments were carried out in pure water (*Experimental Section*, Figure 2.22f) without Mg^{2+} present, no evidence of aggregation was observed for either **D1** or **D2**. This highlights the need for counter ions in solution to shield the charge repulsion between negatively charged phosphate moieties, in both the core which contains the phosphodiester linked alkyl dendron and the corona consisting of the oligonucleotide portion, to allow the intermolecular aggregation to take place.

To determine if the ability of the **D-DNA** conjugates to hybridize to a complementary DNA sequence was hindered by the 5' modification, gel mobility assays and thermal denaturation studies were carried out. These experiments indicated that the addition of the hydrophobic moieties to the 5' terminus did not hinder duplex formation of the oligonucleotide with its complementary partner, shown in Figure 2.6.

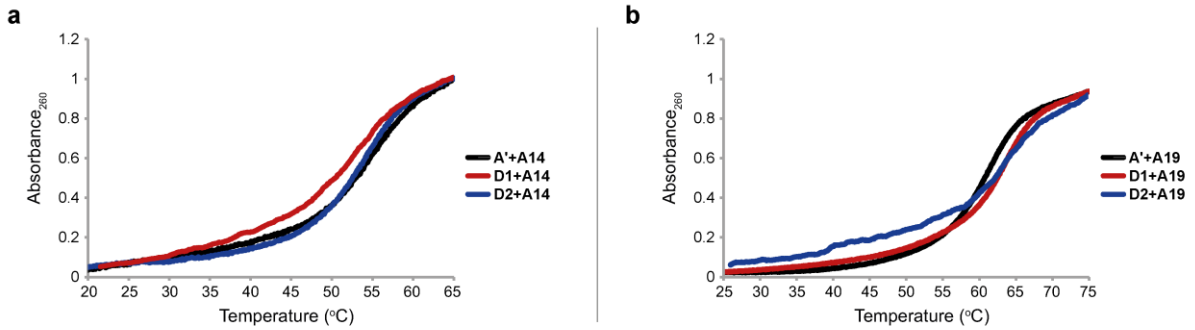

Figure 2.6 – **Melting curves of D-DNA**. a) Typical sigmoidal melting curves are seen for the hybridization of the 14 base region which is used to bind the amphiphiles to the cube. b) Melting curves for the full 19 base complement to the amphiphiles. In both cases there is little change in the melting temperature (T_m) from the DNA control, showing that the 5' **D-DNA** modifications do not disrupt the duplex formation of the appended oligonucleotide (Full details in *Experimental Section 2.5.7*)

2.3.3 Decoration of DNA scaffold with D-DNA

With the self-assembly properties of the individual **D-DNA** conjugates in solution established the next section focuses on their organization on a DNA scaffold, and the resulting characteristics of these DNA nanostructure-amphiphile hybrids. The approach uses a DNA cage to precisely position the hydrophobic moieties in three dimensions, and this requires that the scaffold meets certain criteria: multiple single-stranded regions

available on each structure and the capacity to address each single-stranded region specifically through the introduction of sequence asymmetry.

DNA nanostructures which meet these criteria have been developed previously by the Sleiman group.[41] One such example is the DNA cube formed by a clip-by-clip methodology shown in Figure 2.7. To assemble this cubic cage, four DNA strands ('clips') are designed, such that the ends of each clip are brought together by hybridization with the back edge of the next clip, cyclizing these strands into one face of the 3D-structure. To close the cube, the ends of the fourth clip close on the back edge of the first clip (Figure 2.7). These 20 nt duplexes which form the structure are termed 'clipping-regions' herein.

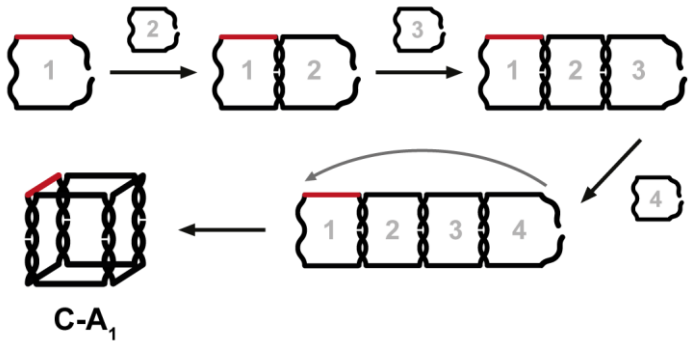

Figure 2.7 – **Clip-by-clip assembly method**. The DNA cube **C-A$_1$** is assembled in a one-pot thermal anneal from four 80 nt ssDNA clip strands. This example has one '*A*' binding site for binding of a complementary **D-DNA**.

Using this method, cubes (**C-A$_x$**) assemble in a one-pot annealing protocol in quantitative yield. A fundamental property of this architecture is that it contains eight single-stranded 20 base regions which can be addressed individually by making each of their sequences unique. DNA cubes, **C-A$_x$**, were synthesized with different numbers of ssDNA sites that are complementary to **D1**/**D2**. For example, in Figure 2.7 the cube **C-A$_1$** contains one **A** binding site, shown as a red line, and can hybridize to a maximum of one strand with the complementary sequence **A'**.

As a starting point, the ability of these ssDNA regions to bind to their complementary sequence was confirmed by gel electrophoresis. The unmodified DNA strand **A'** is a 19nt oligonucleotide which hybridizes only to the 14 central bases of the cube edge with a five thymine (5T) overhang. The addition of appropriate molar

equivalents of **A'** to the cubes **C-A1**, **C-A2**, **C-A3** and **C-A4** produces a series of cubic structures with increasing number of double-stranded regions and consequently reduced electrophoretic mobility (Figure 2.8).

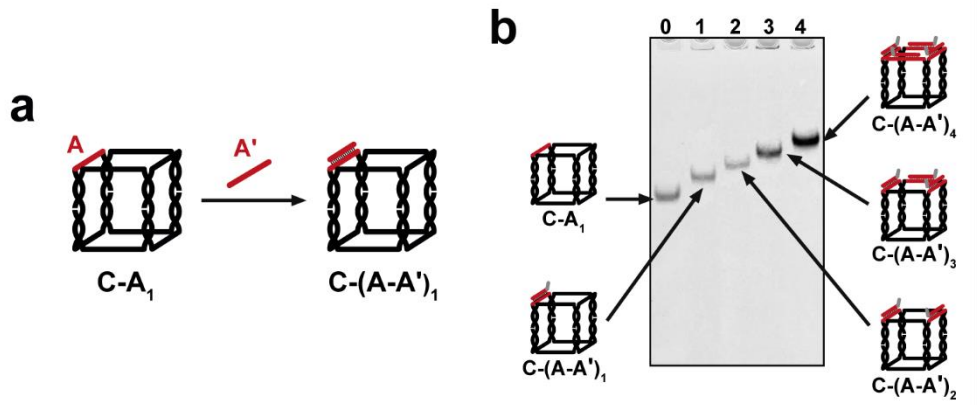

Figure 2.8 – **Site-specific addressability of DNA cube**. Each single-stranded site on the cube structure can be addressed individually by introduction of sequence asymmetry. c) Native 6 % Polyacrylamide Gel Electrophoresis (PAGE) analysis of unmodified DNA sequence **A'** addition to the cube scaffold: Lane 0, **C-A1**; Lane 1, **C-(A-A')1**; Lane 2, **C-(A-A')2**; Lane 3, **C-(A-A')3**; Lane 4, **C-(A-A')4** (The concentration of each structure is between 500 nM and 1.25 μM depending on the number of appended **A'**).

To promote efficient binding of the amphiphiles **D1**/**D2** to the DNA scaffold, only the central 14 bases of each cube edge were used for hybridization, and a five 5T spacer was added to orient the alkyl dendrons away from the crowded corners of the cubic structure and introduce flexibility (Figure 2.9a). Using this design, the addition of **D1** to the cubic structure was carried out by annealing cubes **C-A1** to **C-A4** with appropriate molar equivalents of **D1** to give a final concentration of each structure between 500 nM and 1.25 μM. The resulting single band species as seen by native PAGE (Figure 2.9b) mirror those seen for the unmodified DNA control **A'**. This was expected as **D1** does not exhibit any amphiphilic aggregation in this concentration range, and we see that this behaviour persists when organized on the scaffold. These alkyl functionalized DNA cages could be especially useful for biological applications, as they may be able to interact with lipid bilayers and improve the membrane permeability of the DNA structure, thus increasing cellular uptake.[26,42] Each structure also retains four ssDNA sites available for hybridization on the face opposite from the **D-DNA**.

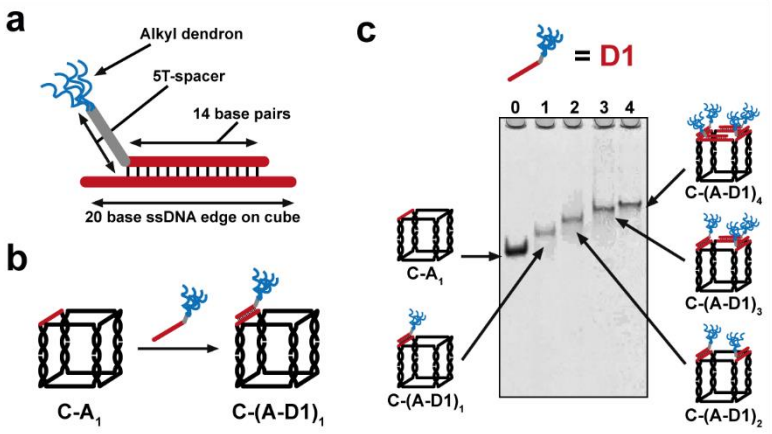

Figure 2.9 – Organization of D1 on cubic scaffold. a) Binding motif for the hybridization of **D-DNA** to the cubic scaffold. b) Site-specific placement of the D-DNA on the cubic scaffold. c) Native 6 % PAGE analysis of **D1** addition to the cube scaffold: Lane 0, **C-A$_1$**; Lane 1, **C-(A-D1)$_1$**; Lane 2, **C-(A-D1)$_2$**; Lane 3, **C-(A-D1)$_3$**; Lane 4, **C-(A-D1)$_4$.**

With the previous observation that **D2** undergoes spontaneous micelle formation around 1.8 µM, the decoration of the cube with **D2** was carried out at reduced concentration, between 147 nM and 435 nM of assembled structure (*i.e.* below the CMC of **D2**). The same annealing procedure used for **D1** was performed and the assembly followed by native PAGE. Figure 2.10a shows the addition of one to three **D2** strands to the cube giving a ladder of decreasing mobility analogous to the results for **D1**.

However with the addition of four **D2** to one face of the cube, a striking change in assembly is observed: a single band with mobility corresponding to a much larger entity is obtained (Figure 2.10b, lane 3). The experiments described in the next section are all consistent with the identity of the structure as cube dimer **1** (Figure 2.10c), brought together by the intermolecular hydrophobic association of amphiphiles between the faces of two distinct cubes.

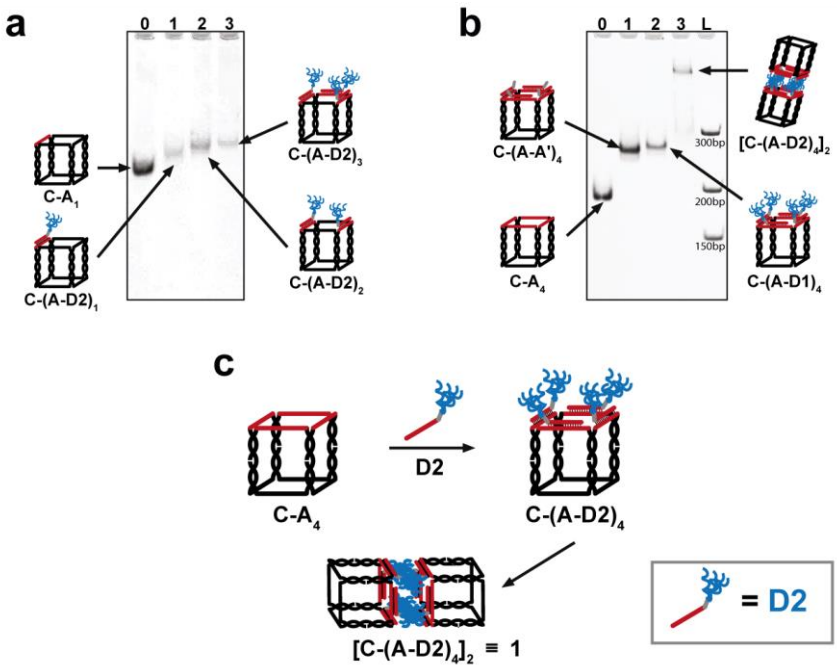

Figure 2.10 – Organization of D2 on cubic scaffold. a) Native 6 % PAGE showing addition of varying number of **D2** to the cube scaffold: Lane 0, **C-A$_1$**; Lane 1, **C-(A-D2)$_1$**; Lane 2, **C-(A-D2)$_2$**; Lane 3, **C-(A-D2)$_3$** (The concentration of each assembled structure is between 189 nM and 435 nM before loading on gel). b) Comparison of DNA cube **C-A$_1$** (Lane 0) with the quadruple decorated cubes, Native 6 % PAGE: Lane 1, **C-(A-A')$_4$**; Lane 2, **C-(A-D1)$_4$**; Lane 3, **C-(A-D2)$_4$** on native PAGE (25 °C, assembled structure concentration of 147 nM) shows the marked difference in mobility of the **C-(A-D2)$_4$** species. c) Schematic showing proposed assembly process for [**C-(A-D2)$_4$**] $_2$; the arrangement of four **D2** on one face of the cube creates a large hydrophobic group which can aggregate specifically producing a 'cube-dimer' (see below for characterization)

2.3.4 Intermolecular assembly mediated by D-DNA

Upon discovery of higher-order association for the cube **C-(A-D2)$_4$**, a number of control experiments were designed to confirm the identity of the structure and nature of the assembly. Firstly, a model cube dimer was designed and synthesized, using a simple linking strategy to assemble two cubes. This used the linker strand **LA** which contained two identical 20 base sequences that are complementary to the cube edge, separated by a 20 nt of random sequence as an ssDNA spacer, Figure 2.11. Comparison of the electrophoretic mobility of this model dimer with the **C-(A-D2)$_4$** species revealed that the mobility observed was consistent with the proposed dimer structure, **1**.

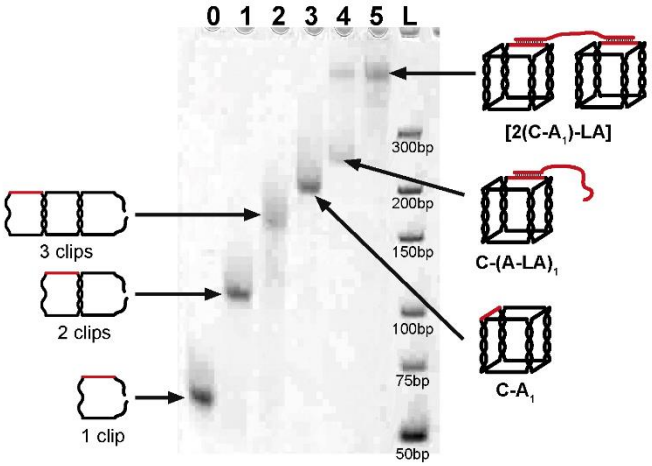

Figure 2.11 – Cube-dimer control sample. The intermediate assemblies containing between one and three clips are shown as a precursor to the fully formed cube, **C-A$_1$**. The addition of a symmetrical linking strand (**LA**), which has two binding sites with sequence **A'** connected by a 20 base linker, produces linked cubes when correct stoichiometry is used. This was used as a reference for the mobility of the dimer structure Native 6% PAGE: **[C-(A-D2)$_4$]$_2$**. Lane 0- **Clip1-AB**, Lane 1 – **(Clip1-AB, Clip2-T14)**, Lane 2 – **(Clip1-AB, Clip2-T14, Clip3-T14)**, Lane 3 – **C-A$_1$**, Lane 4 - **C-(A-LA)$_1$** (1:1 stoichiometry), Lane 5 – **[2(C-A$_1$)-LA]** (2:1 stoichiometry), Lane L - **Ladder**.

It was found that the dimer **1** is surprisingly robust; stable at 25°C under electrophoretic conditions, Figure 2.10b. DLS was employed to further characterize this novel hybrid structure, and scattering correlating to an R_h of 9.3nm ± 0.3nm was observed, consistent with an estimated R_h of 9.2nm for **1** (Figure 2.12a). Additional characterization was achieved by AFM, Figure 2.12b. Although surface drying effects and shear forces could be expected to disassemble the dimeric structures, a number of dimers with a 2:1 aspect ratio remained after deposition on mica.

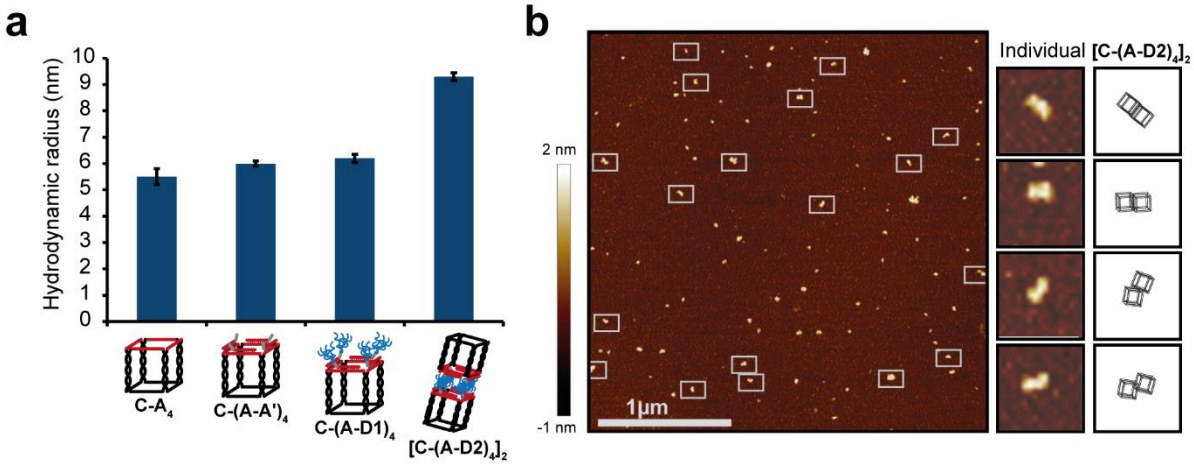

Figure 2.12 – Cube-dimer characterization. a) DLS measurements produce R_h which is consistent with a two cube assembly in comparison with controls. b) AFM height images reveal that a population of dimeric structures still persist after surface adsorption and drying.

Finally, in order to establish that this dimer self-assembly is mediated by hydrophobic collapse of the alkyl chains across two intact cubes, four equivalents of eraser strands (**E_A**) were added to **1**, which are fully complementary to the cube edges. This resulted in strand displacement of the **D2** amphiphiles from the cube and restored the band for monomeric cube **C-A_4**, Figure 2.13.

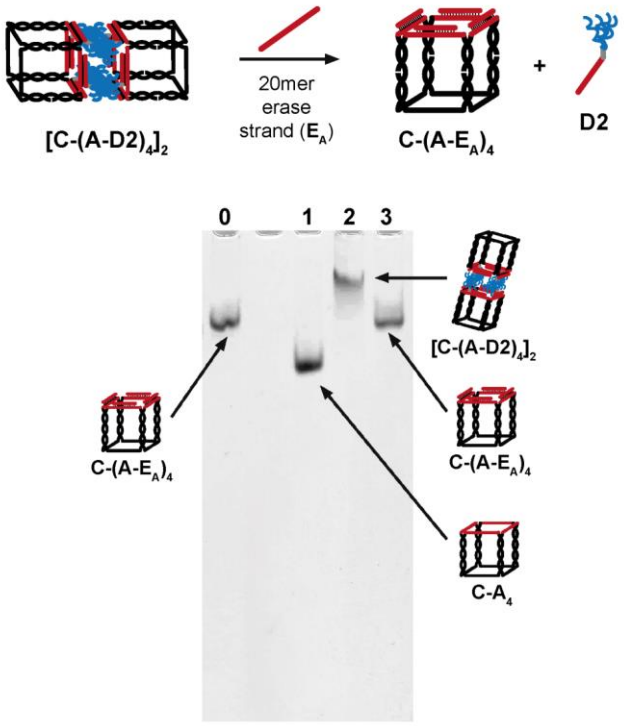

Figure 2.13 - Erasing D-DNA-2 to disassemble cube-dimer. The addition of a full complementary 20nt $\mathbf{E_A}$ to the cube-dimer removes the **D2** amphiphiles by strand displacement, causing disassembly of the cube dimer and returning the discrete cubes with four $\mathbf{E_A}$ attached. The concentration of each assembled structure is 147nM before loading on the gel. Lane 0- **C-A$_4$-E$_A$** reference, Lane 1 – **C-A$_4$**, Lane 2 – **[C-(A-D2)$_4$]$_2$**, Lane 3 – **[C-(A-D2)$_4$]$_2$ + E$_A$** (8% Native PAGE, 7°C).

The dimer structure **1** represents a unique type of programmed self-assembly. By orienting four **D-DNA** conjugates, corresponding to sixteen C12 alkyl chains, on one face of the cube we confer amphiphilic character to an entire domain of the DNA nanostructure. Furthermore, due to the templating effect of the DNA scaffold we obtain a single monodisperse structure in very good yield. Similarly, shape transitions of DNA-polymer conjugate assemblies have been observed before in response to DNA templation and enzymatic treatment.[43,44] This hybrid structure highlights two points: amphiphiles can be programmed to selectively give a desired arrangement using a 3D DNA scaffold, and DNA nanostructures can be bound together selectively using hydrophobic collapse of their residues in an analogous manner to proteins (*e.g.*, a coiled coil motif). This phenomenon occurs below the critical micelle concentration of the DNA amphiphiles.

Based on the discovery of the dimer **1**, it was hypothesized that decoration of two opposite faces of the cube with **D2** may produce an extended one-dimensional track of cubes. This would require hybridizing the **D1** or **D2** conjugates to all eight binding sites of cube **C-A$_4$B$_4$** (Figure 2.14a). Interestingly, the formation of large aggregated assemblies was not observed. In fact both alkyl-modified cubes **2** and **3** exhibited higher gel mobility than the unmodified cubes themselves, seen in Figure 2.14b.

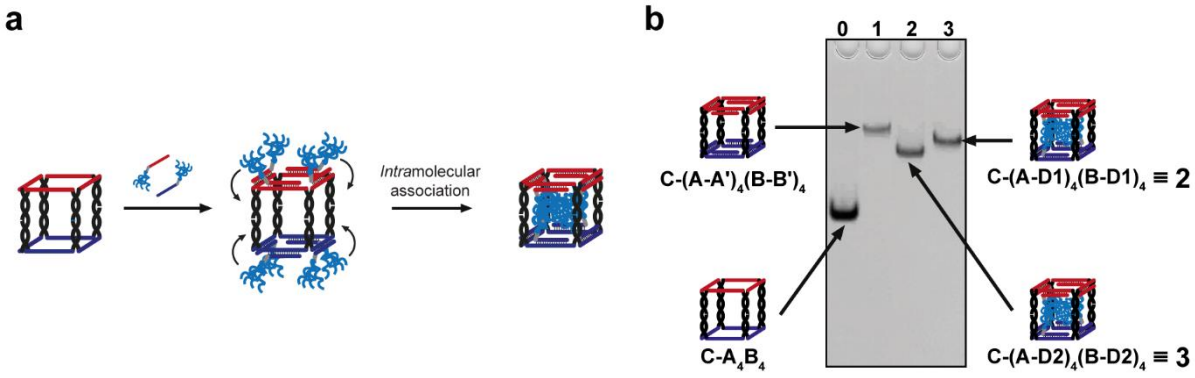

Figure 2.14 – Assembly of core-shell structures. a) Assembly scheme for the organization of eight D-DNA on the cubic scaffold, which results in spontaneous intramolecular assembly. b) Native 6 %PAGE analysis of fully decorated cubes: Lane 0, **C-A$_4$B$_4$**; Lane 1, **C-(A-A')$_4$(B-B')$_4$'**; Lane 2, **2**; Lane 3, **3**(The concentration of each decorated cube is 250 nM).

DLS shows these structures to possess smaller hydrodynamic radii, 6.3nm ± 0.2nm and 6.4nm ± 0.2nm for **2** and **3** respectively, and lower polydispersity compared to the all-DNA cube control, **C-(A-A')$_4$(B-B')$_4$**; 7.7nm ± 0.2nm. This is despite the fact that the amphiphile-decorated cubes each have 32 additional alkyl chains, as compared to the control cube. This is consistent with the hypothesis that these 32 alkyl chains have collapsed *inside the cube*, resulting in contraction of the scaffold. The similarity in size between **2** and **3** also suggests that the scaffold itself is the limiting factor packing the lipidic chains into the central cavity.

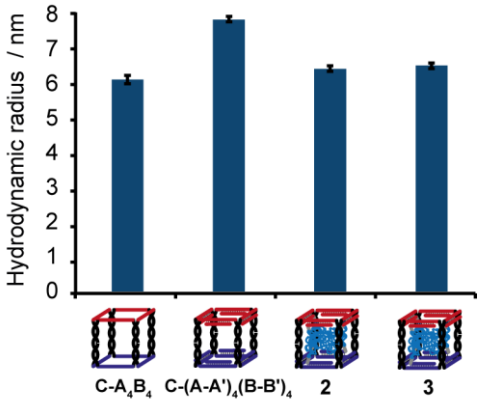

Figure 2.15 – Summary of DLS data for cube-core structure. Cube-core structures have smaller R_h than double stranded cube, suggesting compaction due to internal **D-DNA** collapse. Full details can be found in *Experimental Section 2.5.9*.

AFM studies of the cube-core structures **2** and **3** showed no dimers, but discrete well-defined cube structures that are stable to surface adsorption (Figure 2.16), with heights and radii in range with cube controls, see *Experimental Section*, Figure 2.32.

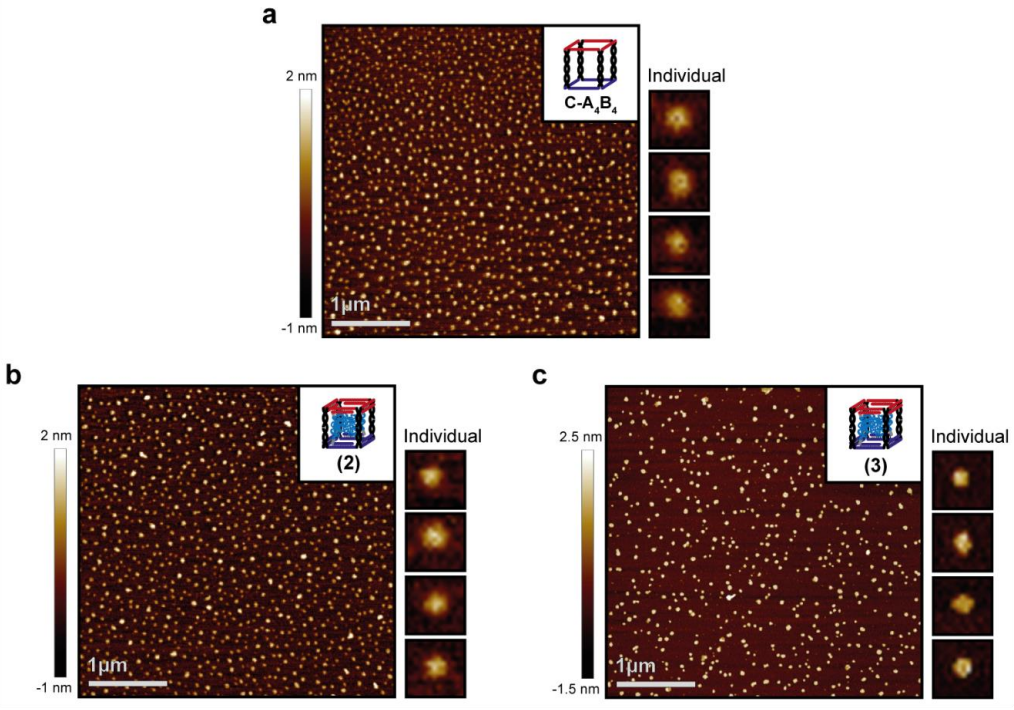

Figure 2.16 – AFM analysis of cube-core structures. AFM height images show populations of discrete cube structures for the cube control a) **C-A4B4**, and the fully decorated cubes; b) **2** and c) **3**. The contraction of the individual cubes is particularly evident for **3** consistent with the solution based techniques (see *Experimental Section 2.5.15* for additional AFM images).

These results suggest that by organizing eight **D-DNA** on a DNA cage, the amphiphiles can assemble together and produce a micellar environment within the cage, and that this occurs below the CMC of these amphiphiles. These structures differ from standard micelles in that they are fully monodisperse and stabilized by the encapsulating DNA cage.

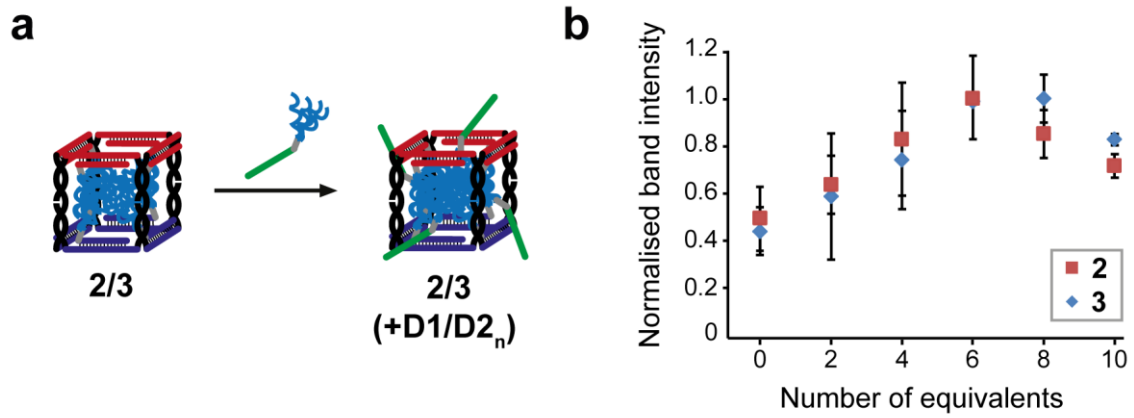

Figure 2.17 – Additional D-DNA loading in cube-core structures. a) Loading of additional **D-DNA** amphiphiles with non-complementary sequence (green) into the hydrophobic core of **2 and 3.** b) Plot of normalized PAGE band intensity for **2 and 3** vs. number of equivalents of additional non-complementary **D-DNA**. Both structures show an increase in intensity, consistent with inclusion of these D-DNA amphiphiles. Beyond the addition of six amphiphiles, the loss in band intensity is due to aggregation caused by excessive loading of material onto the gel. For further details see *Experimental Section 2.5.16*.

To further support the collapse of the alkyl chains into a hydrophobic core structure within the cube, the potential to load additional amphiphiles into this core was first examined. This was carried out using amphiphiles that have the same hydrophobic portion as **D1** or **D2** but with non-complementary sequences to the cube, Figure 2.17a. Addition of these cargo amphiphiles to the preformed structures **2** and **3** was followed by native PAGE (*Experimental Section 2.5.16*). This revealed an increase in intensity of the band corresponding to the cube core-shell structure, consistent with their incorporation within the cube, Figure 2.17b. In contrast, addition of these non-complementary amphiphiles to the naked cube does not result in their incorporation, and they remain as separate entities in the gel. Both core-shell structures, **2** and **3** showed this loading of additional amphiphiles to a similar extent.

Finally, the potential of these structures to load small molecule cargo into their hydrophobic cavity was examined, Figure 2.18. DNA nanotubes have been previously shown to encapsulate gold nanoparticles, and DNA cages were conjugated to proteins within their cavities.[45,46] They have also been shown to bind DNA intercalators directly on their duplexes.[47] However, because of their relatively large pore sizes, DNA cages have not been previously demonstrated to encapsulate small molecules.

For loading and release, Nile Red was used as the guest molecule and monitored the fluorescence intensity upon titration with the cube-core micelle structures. Both structures **2** and **3** caused significant fluorescence enhancement, consistent with their ability to encapsulate Nile Red in their hydrophobic core, Figure 2.18b. In contrast, the unmodified DNA cube, in its single or double-stranded form, did not enhance fluorescence under the same conditions (see *Experimental Section*, Figure 2.37). Next, the ability of these scaffolded micelles to selectively release the small molecule guest was investigated.

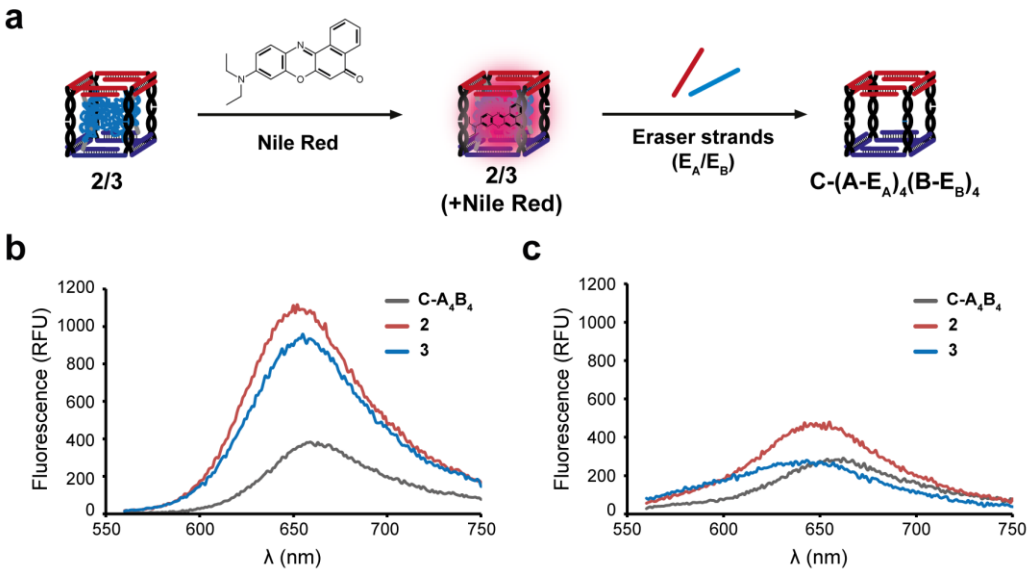

Figure 2.18 – Loading and release of Nile Red in cube-core structures. a) Loading of the hydrophobic dye Nile Red which is highly fluorescent upon inclusion in a non-polar microenvironment such as the core of the scaffolded micelle. The release mechanism is through strand displacement of the D-DNA by the 20nt eraser strands $\mathbf{E_A/E_B}$ disassembling the hydrophobic core. b) Fluorescence emission spectra of Nile Red in the presence of cubes **C-A_4B_4, 2 and 3**. c) Fluorescence emission spectra of Nile Red in the presence of cubes **C-A_4B_4, 2 and 3** after removal of the **D-DNA** by strand displacement (measured 30 minutes after addition of eraser strands $\mathbf{E_A/E_B}$). Both cube-core structures show a drop in fluorescence, the remaining low fluorescence signal of the **D1** sample is due to residual hydrophobic interactions. (see *Experimental Section 2.5.17*).

Each edge in the cage is 20 bases long, but the eight DNA amphiphiles are only complementary to 14 edge bases. To the cube-core micelles **2** and **3,** we added DNA strands that are fully complementary to the cube edges, $\mathbf{E_A}$ and $\mathbf{E_B}$. This should result in hybridization of these strands to the cube edges and displacement of the eight DNA amphiphiles from the cube, and this result was confirmed by gel electrophoresis (see *Experimental Section*, Figure 2.37). Monitoring this process by fluorescence spectroscopy showed loss in the emission intensity of Nile Red, to the same range as the unmodified cube, consistent with the release of this small molecule from the capsule, Figure 2.18c.

These experiments are consistent with encapsulation of small molecule guests within the hydrophobic core of the DNA cube, and their release by de-aggregation of this micellar core. It is of note that this phenomenon occurs below the critical micelle concentration of the DNA amphiphiles.

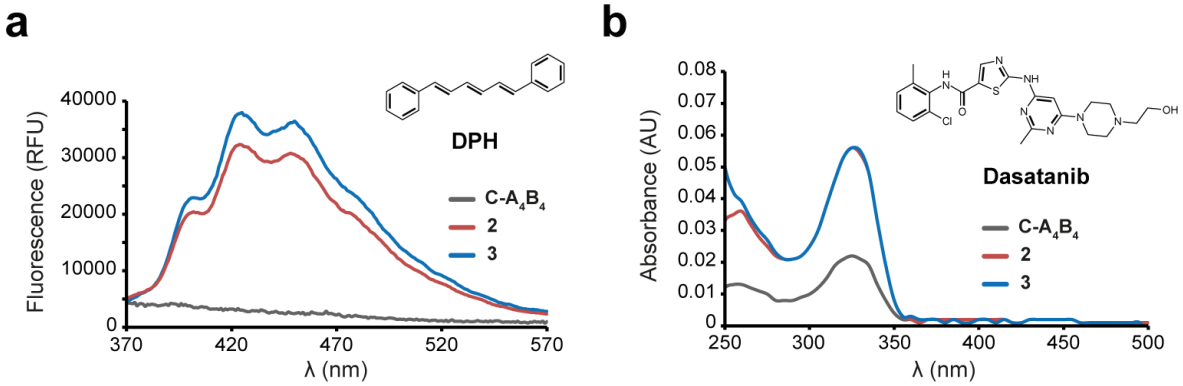

Figure 2.19 – Encapsulation of small molecules in cube-core structures. a) Fluorescence emission of 1,6-Diphenyl-1,3,5-hexatriene (DPH) in the presence of cubes **C-A$_4$B$_4$**, **2 and 3** after removal of unencapsulated dye by centrifugation. b) Absorbance spectra of Dasatanib (λ_{max}=325nm) in the presence of **C-A$_4$B$_4$**, **2** and **3** after loading with Dasatanib and removal of excess by centrifugation. (see *Experimental Section 2.5.19*)

With the loading and release potential of **2** and **3** determined, the loading capacity of the hydrophobic cores was studied. Loading capacities of 5 (±1.4) molecules Nile Red per **2** and 9 (±1.2) molecules per **3** were determined using fluorescence techniques (see *Experimental Section 2.5.18*, Figure 2.38). These numbers compare very favourably with those previously reported for larger amphiphilic assemblies.[48] Additionally, the loading capacity was investigated using another fluorescent probe, DPH (Fig 2.19a), which gave

similar values of 7 (±0.6) molecules DPH per **2** and 10 (±0.8) molecules per **3** calculated from the experimental data (*Experimental Section 2.5.18*, Figure 2.39).

The loading and release mechanism for hydrophobic cargo within a DNA nanostructure should be applicable to other molecules as the host-guest recognition is based on hydrophobic effect. It is expected to make DNA cages useful for drug delivery applications, but also fundamentally as molecular hosts that confine their guest in hydrophobic environments made up of a small, well-defined number of lipid-like chains.

As these structures have obvious potential in the loading and selective release of a cargo for drug delivery applications the ability of the structures **2** and **3** to encapsulate a more drug-like molecule was investigated. The tyrosine kinase inhibitor Dasatanib (DAS), used to treat chronic myelogenous leukemia, was chosen as a model drug for encapsulation as it is poorly soluble in aqueous media and could therefore benefit from transport in a delivery vehicle.[49] The encapsulation of DAS in cube-core micelles **2** and **3** was determined by absorbance spectroscopy, Figure 2.19b. It was found that both structures **2** and **3** retained elevated amounts of DAS compared to controls (see *Experimental Section 2.5.19*).

2.4 Conclusions

In summary, this chapter has revealed that the anisotropic positioning of hydrophobic side-chains on a DNA scaffold can lead to unanticipated modes of orthogonal association. Four amphiphiles gathered together on a DNA cube face can selectively associate intermolecularly to dimerize two cubes. Eight amphiphiles come together intramolecularly to form a micellar environment within the DNA cage. These structures differ from standard micelles in that they are monodisperse and stabilized by the encapsulating DNA cage, below the CMC of the amphiphiles. These scaffolded micelles allow for encapsulation and release of hydrophobic small molecule cargo, as the core forming units can be erased from the scaffold by strand displacement. They are potentially useful for targeted drug delivery applications, as well as for the examination of new reactivity in this confined space.

The simplified and modular synthetic scheme reported here can lead to a variety of structures with diverse applications such as membrane anchoring, cell uptake, encapsulation and release and directed hydrophobic assembly. As there are a total of

eight potential binding sites on the cube, there are as many as 26 different structural isomers for each amphiphile. Here only those which best exemplify the effect of the orientation on the final product were discussed. This is done without changing the scaffold structurally, however the scaffold is also a modular assembly and the size, shape, flexibility and number of binding sites can be changed with ease. It is apparent that a number of possible assemblies could be synthesized with differing properties. These can augment the field of DNA nanotechnology with orthogonal interactions working together, without increasing the DNA sequence space.

2.5 Experimental Section

2.5.1 General

Magnesium acetate, Stains-All®, acetic acid, tris(hydroxymethyl)-aminomethane (Tris), formamide, urea, Nile Red and 1,6-Diphenyl-1,3,5-hexatriene were used as purchased from Aldrich. Acetic acid and boric acid were purchased from Fisher Scientific and used without further purification. Acetone ACS reagent grade was purchased from Fisher. Ammonium citrate dibasic and 3-hydroxypicolinic acid were purchased from Aldrich. Acrylamide/Bis-acrylamide (40% 19:1 solution) and TEMED were obtained from Bioshop Canada Inc. and used as supplied. Derivatized (dA, dC, dG and T nucleoside)1000Å LCAA-CPG supports with loading densities of 25-40 μmol/g and standard reagents used for automated DNA synthesis were purchased through Bioautomation. Sephadex G-25 (super fine, DNA grade) was purchased from Glen Research. 1xTBE buffer is composed of 90mM Tris and Boric acid and 2 mM EDTA with pH 8.3. 1xTAMg buffer is composed of 45 mM Tris and 12.5 mM $Mg(OAc)_2 \cdot 6H_2O$ with pH adjusted to 7.8 using glacial acetic acid.

2.5.2 Instrumentation

Standard automated oligonucleotide solid-phase synthesis was performed on a Mermade MM6 synthesizer from Bioautomation. UV-Vis quantification measurements were performed with a BioTek Synergy HT microplate reader. A Varian Cary 300 Bio spectrophotometer was used for melting temperature experiments. Gel electrophoresis experiments were carried out on an acrylamide 20 X 20 cm vertical Hoefer 600 electrophoresis unit. Thermal annealing of all DNA structures was conducted using an

Eppendorf Mastercycler® 96 well thermocycler. Mass determination was carried out using Matrix-Assisted Laser Desorption/Ionization Time-Of-Flight Mass Spectrometry (MALDI-TOF-MS) on a Bruker Autoflex™ III MALDI-TOF mass spectrometer.

2.5.3 D-DNA synthesis

The **D-DNA** synthesis was adapted from a previously reported protocol.[50] DNA synthesis was performed on a 1 µmole scale, starting from the required nucleotide modified 1000Å LCAA-CPG solid-support. Derivatized (dA, dC, dG and T nucleoside) 1000Å LCAA-CPG supports with loading densities of 25-40µmol/g and standard reagents used for automated DNA synthesis were purchased through Bioautomation. Symmetrical branching (cat.# CLP-5215), DMT-hexane-diol (cat.# CLP-1120) and DMT-dodecane-diol (cat.# CLP-1114) spacer phosphoramidites were purchased from Chemgenes. For symmetrical branching, DMT-hexane-diol and DMT-dodecane-diol (0.07-0.1M, anhydrous acetonitrile) extended coupling times of 5, 10 and 15 minutes were used respectively. Removal of the DMT protecting group was carried out using 3% v/v TCA in dichloromethane. Completed sequences were deprotected in 28% aqueous ammonium hydroxide solution for 16-18 hours at 60°C. The crude deprotected solution was separated from the solid support and concentrated under reduced pressure at 60°C. This crude solid was re-suspended in 0.5mL Millipore water and filtered through a 0.45µm syringe filter for reverse-phase HPLC purification.

Table 2.1 - Sequences used for DNA amphiphiles. Red T and A refer to non-complementary 5 base spacers between cube complement and hydrophobic portion. Nonstandard amidite codes: (***D***=DMT-dodecane-diol), (***X***=DMT-hexane-diol), (***S***=Symmetrical branching).

Name	Sequence (5'-xx-3')
A'	TTTTTCAGTTGACCATATA
B'	TTTTACCATCTGGTATTAC
C'	TTTTTCTCGCAGTCGCGGT
D1-A	***DSXS***TTTTTCAGTTGACCATATA
D2-A	***DSS***TTTTTCAGTTGACCATATA
D1-B	***DSXS***TTTTACCATCTGGTATTAC
D2-B	***DSS***TTTTACCATCTGGTATTAC

D1-C	***DSXS***TTTTTCTCGCAGTCGCGGT
D2-C	***DSS***TTTTTCTCGCAGTCGCGGT
A14	TATATGGTCAACTG
A19	TATATGGTCAACTGAAAAA
A20	TCCTATATGGTCAACTGCTC
E_A	GAGCAGTTGACCATATAGGA
E_B	ACTCCATCTGGTATTACTAC

2.5.4 HPLC Purification

Solvents (0.22µm filtered): 50mM Triethylammonium acetate (TEAA) buffer (pH 7.8) and HPLC grade acetonitrile. Elution gradient: 0-50% acetonitrile over 20 minutes. Column: Hamilton PRP-1 5 µm 100 Å 2.1 x 150 mm. For each separation approximately 1 OD_{260} of crude DNA was injected as a 100µL solution in 1:1 Millipore water:TEAA. Typical retention times for the products are 16.5 minutes and 17.5 minutes for **D1** and **D2** respectively. The unmodified 19 nt DNA has a retention time of 9.5 minutes.

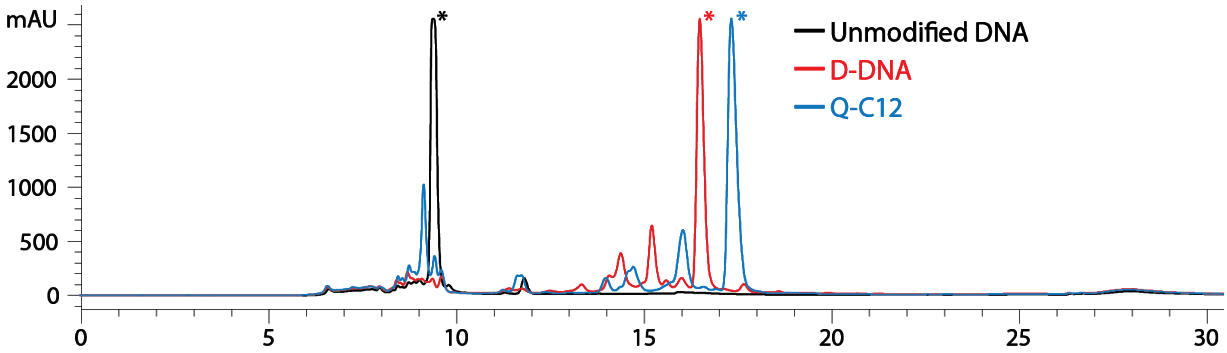

Figure 2.20 - HPLC traces of crude D-DNA syntheses. HPLC traces of crude product mixtures from **D-DNA** synthesis (red and blue traces) in reference to the unmodified 19 nt, **A'** (black trace). The prominent n-1 peaks from the **D-DNA** correspond to failure of the last coupling, four dodecane-diol chains. Peak area integration estimates yields of 55% and 50% for **D1** and **D2** respectively using automated synthesis with manufacturers recommended protocols. An optimized synthesis using the 'syringe technique' gave improved yields of 61% and 59% for **D1** and **D2** respectively.

2.5.5 MALDI-TOF-MS characterization

The matrix used was comprised 0.7M 3-hydroxypicolinic acid and 0.07M ammonium citrate in acetonitrile:water 50:50 v/v. solution.[51] In each case 2μL of a 50-100μM solution of HPLC purified DNA in Millipore water was mixed with 8μL of matrix solution. Between 1-3μL of this final solution was spotted on an AnchorChip™ and solvents removed by air drying prior to mass determination. In each case, the masses observed for the **D-DNA** and DNA controls matched well with the calculated values.

Table 2.2 - MALDI-TOF-MS Table Calculated and experimental m/z values for all DNA amphiphiles synthesized including the unmodified oligonucleotide controls.

Name	Calculated m/z ($[M-H]^-$ ion)	Measured m/z
A'	5766.8	5798.3
B'	5742.8	5718.2
C'	5775.8	5761.1
D1-A	7646.5	7650.7
D2-A	7286.2	7294.9
D1-B	7622.5	7754.8
D2-B	7262.2	7228.2
D1-C	7655.5	7787.4
D2-C	7295.2	7264.6

2.5.6 PAGE analysis of D-DNA hybridization

Native 12% PAGE analysis was carried out at 7°C for 2.5 hours at a constant voltage of 250V. Sample loading was 0.02-0.04 OD_{260} DNA per lane. Complementary strands were annealed at 25°C for 1 hour to give 2.5μM of the duplex in 1xTAMg. The DNA bands were visualized by incubation with Stains-All®. Both **D1** and **D2** show decreased mobility relative to the DNA control as expected. The small difference in mobility between **D1** and **D2** can be attributed to the number of charged phosphate groups associated with each structure.

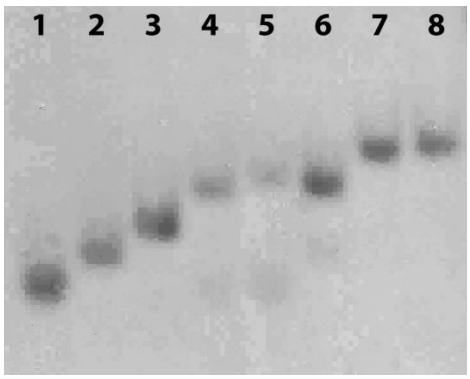

Figure 2.21 - D-DNA hybridization to complement strands. Native 6% PAGE**:** Lane 1- **A14,** Lane 2- **A20**, Lane 3- **A14+A'**, Lane 4**- A14+D1**, Lane 5- **A14+D2**, Lane 6- **A20+A'**, Lane 7- **A20+D1**, Lane 3- **A20+D2**. (12% Native PAGE, 7°C)

2.5.7 Melting temperatures

The hybridization of the DNA amphiphiles to their complement strands was also confirmed by measurement of the thermal denaturation of the duplexes by UV absorption. For each experiment equimolar amounts of DNA amphiphile and complement strand were combined in 1xTAMg buffer to give a final volume of 150μL with a duplex concentration of 2.5μM. Samples were annealed for 1 hour at 25°C before transfer to a quartz cuvette. Absorbance at 260nm was monitored over the appropriate temperature range.

2.5.8 D-DNA CMC determination

A stock solution of Nile Red 0.1mM in acetone was used for all experiments. Series dilutions of DNA sample (in the range 15μM to 0.75nM) were made up to a final volume of 150μL, with a concentration of 2.5μM Nile Red in 1xTAMg in a 96-well top-read microplate. The samples were left to incubate at room temperature for 3-16 hours. The plate was read using a Biotek Synergy well-plate fluorimeter. Excitation was at 535nm with a slit width of 9nm and emission was monitored between 560nm and 750nm.

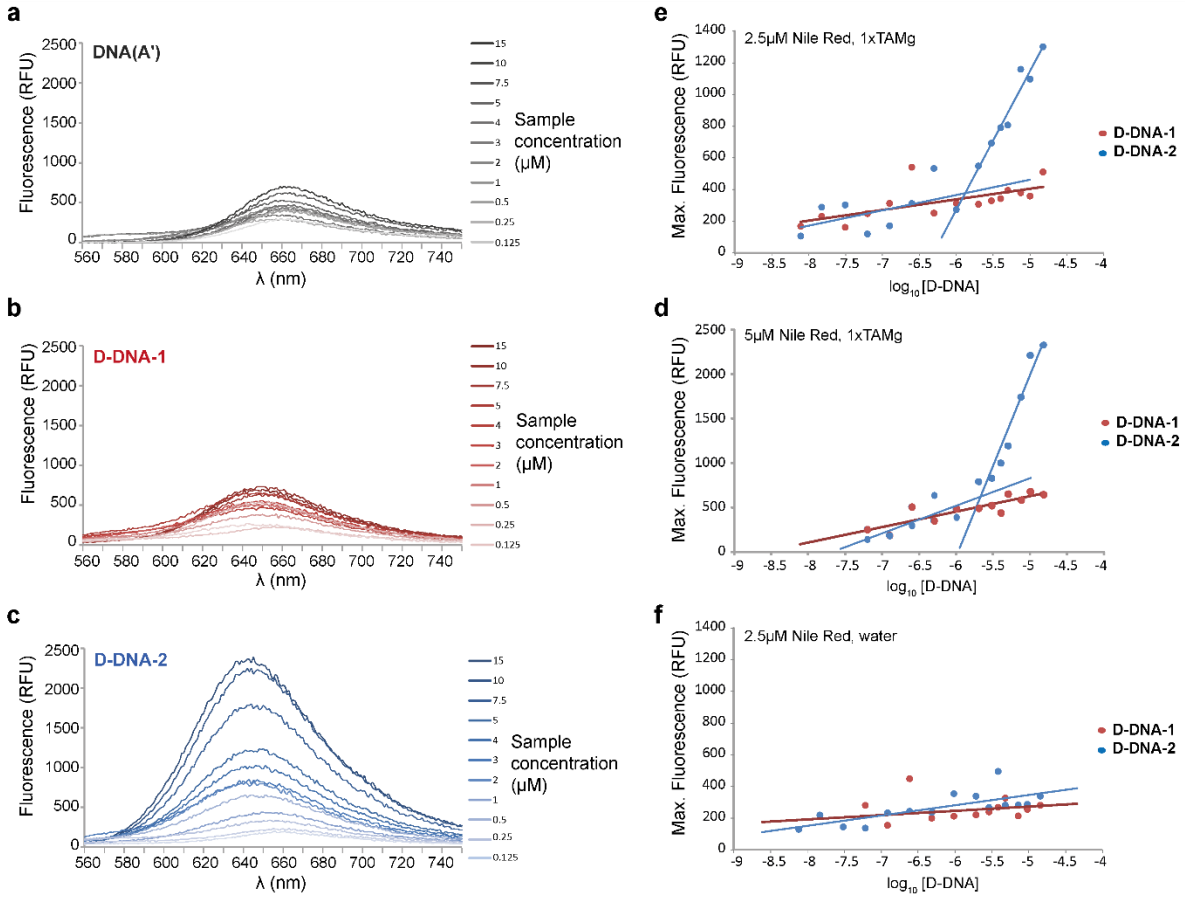

Figure 2.22 - Fluorescence spectra for Nile Red encapsulation. Fluorescence spectra of Nile Red with varying concentration of a) DNA control **A'**, b) **D1** and c) **D2** d) Plot of Log_{10}[D-DNA] against maximal fluorescence intensity for **D-DNA** in the presence of 5 μM Nile Red. CMC behavior is only exhibited by **D-DNA-2**. e) Same plot for **D-DNA** in the presence of 2.5 μM Nile Red. The CMC was calculated from the intersection of the two linear fits shown on the graph. Triplicate measurements in the presence of both 2.5 μM and 5 μM Nile Red revealed no effect of Nile Red concentration on the estimated CMC for **D2**. f) Both **D-DNA** amphiphiles showed no self-assembly behavior when the same experiment was carried out in pure water. This reflects the highly anionic character of the phosphodiester backbone which requires Mg^{2+} for charge compensation.

2.5.9 Dynamic Light Scattering

DLS experiments were carried out using a DynaPro™ Instrument from Wyatt Technology. Dynamic Light scattering was used to confirm the presence and determine the size of the **D2** aggregates above the CMC. Sterile water and 1xTAMg buffer were filtered using a 0.45µm nylon syringe filter before use in DLS sample preparation. All measurements were carried out at 25°C.

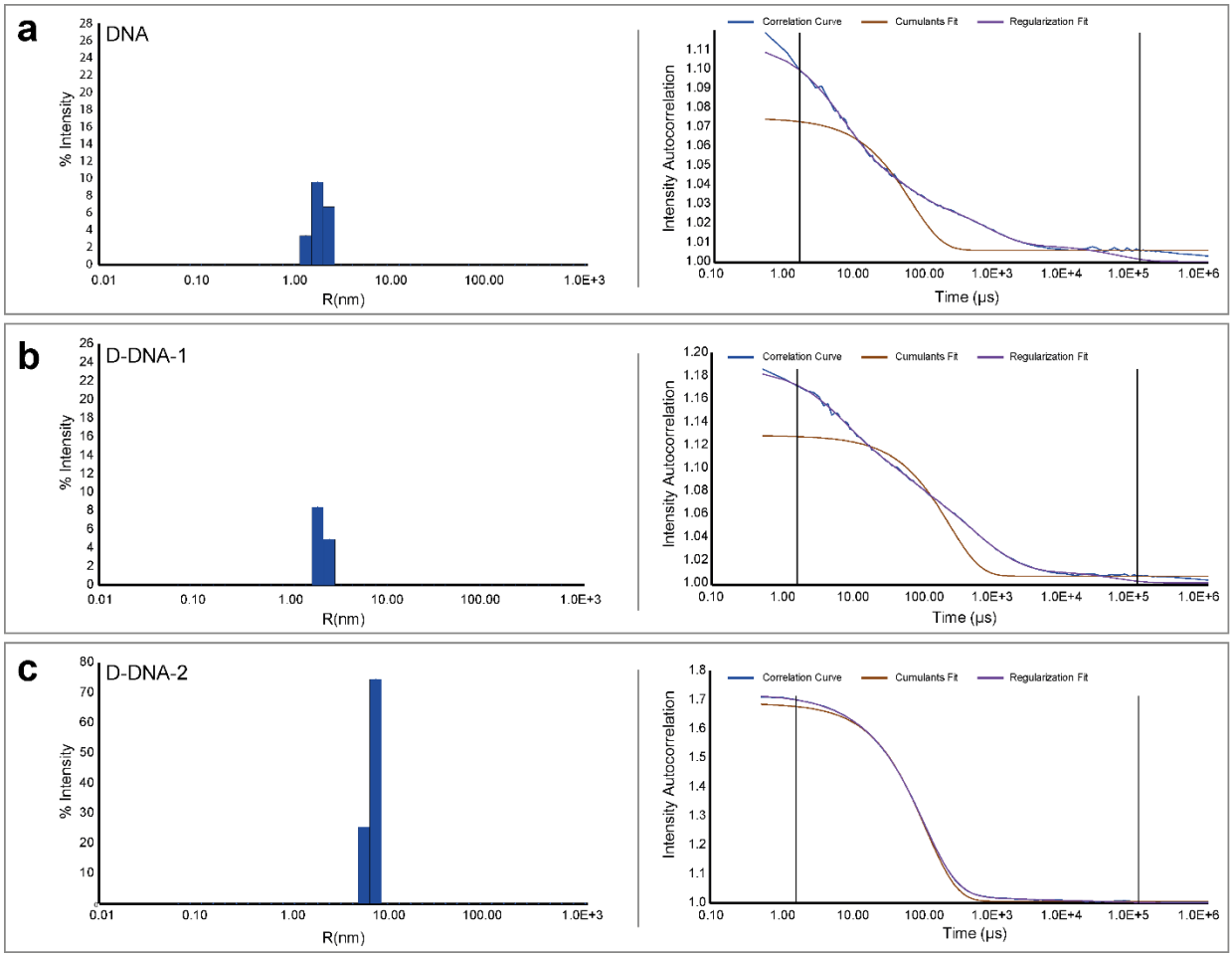

Figure 2.23 - Dynamic light scattering on DNA amphiphiles. DLS regularization distribution histograms and associated correlation functions for 10 µM solutions of a) DNA control **A'**, b) **D1** and c) **D2**. The poor intensity and correlation functions measured for **A'** and **D1** are representative of little aggregation, only individual strands in solution. In contrast the data for **D2** reveals excellent correlation and higher scattering intensity due to the presence of micelles. In each histogram the residual buffer peaks have been removed for clarity.

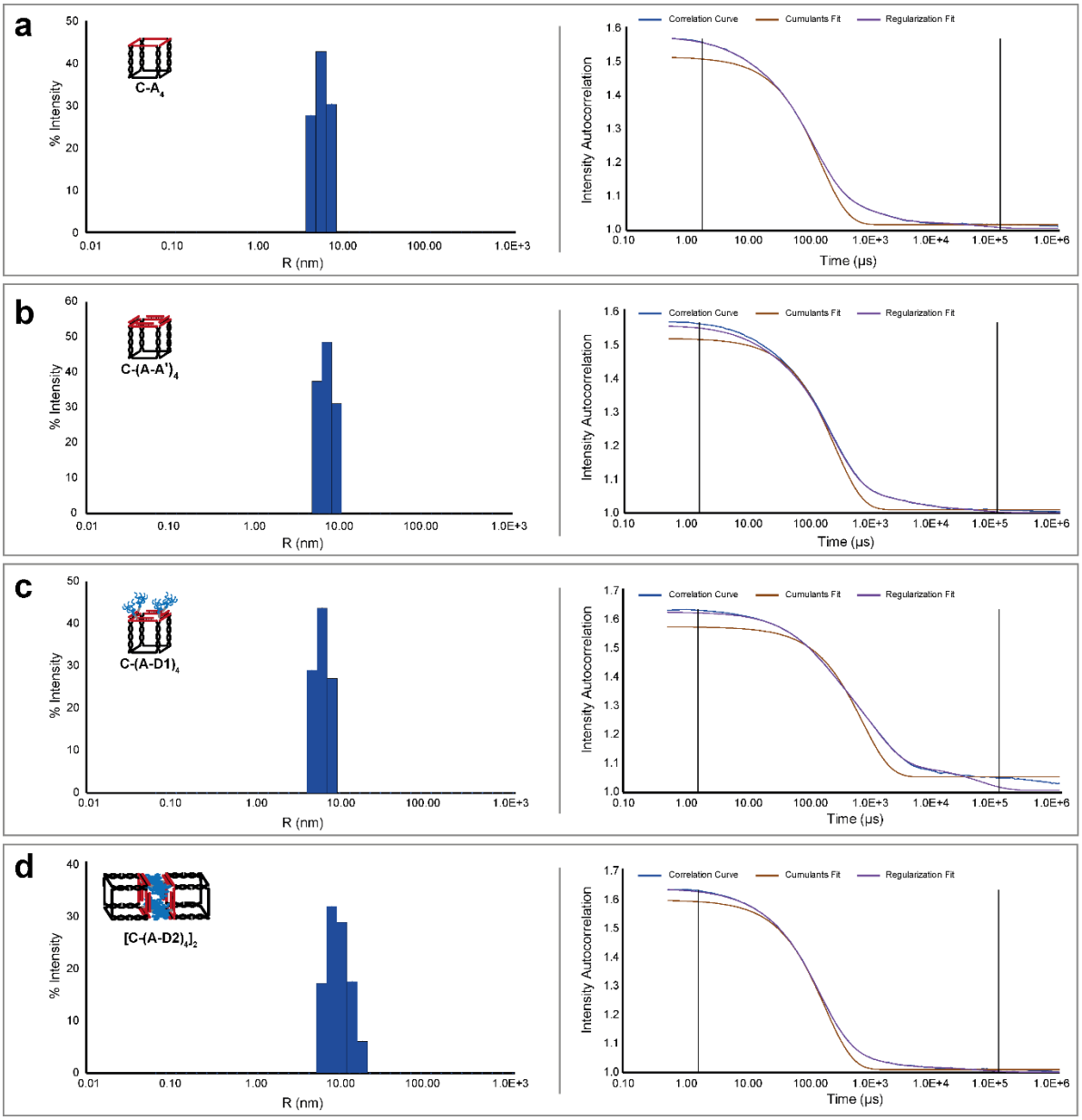

Figure 2.24 - DLS measurements of quadruple decorated cubes DLS regularization distribution histograms and associated correlation functions are shown for a) **C-A4**, b) **C-(A-A')4**, c) **C-(A-D1)4** and d) **[C-(A-D2)4]2**. It is possible that the slight contraction in size for **C-(A-D1)4** compared to the DNA control **C-(A-A')4** is due to a partial collapse of the alkyl chains across the face of the cube rather than extending into the aqueous medium. Each sample was studied at 625 nM of assembled structure in 1xTAMg buffer. The clear jump in hydrodynamic radius for the dimeric **[C-(A-D2)4]2** structure mirrors the electrophoresis results. The broader size distribution for the cube-dimer is consistent with the aspect ratio which deviates from a spherical shape, and possibly the dynamic character of the hydrophobic intermolecular association between the two cubes.

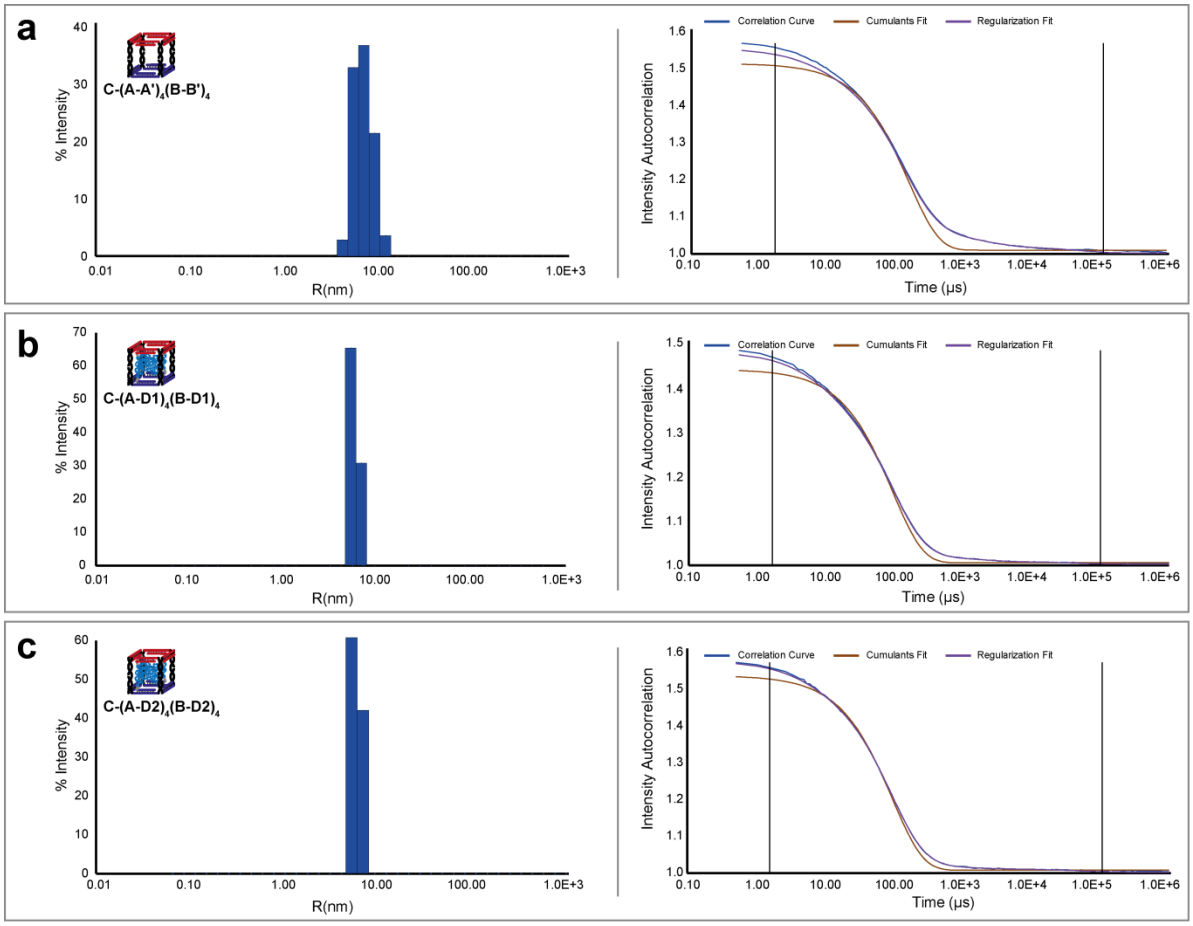

Figure 2.25 - DLS measurements of cube core structures DLS regularization distribution histograms and associated correlation functions are shown for a) **C-(A-A')$_4$(B-B')$_4$**, b) **C-(A-D1)$_4$(B-D1)$_4$** and c) **C-(A-D2)$_4$(B-D2)$_4$**. Samples were studied at 420 nM of assembled structure in 1xTAMg buffer.

Table 2.3 - Summary of all D-DNA decorated cube DLS measurements. All samples were measured in at least triplicate and the mean value for hydrodynamic radii and polydispersity of each sample are shown below. Error margins were derived from the standard deviation of the multiple measurements.

Sample	Mean hydrodynamic radius (nm)	Mean polydispersity (%)
C-A$_4$	6.0 ± 0.2	24.8 ± 3.4
C-(A-A')$_4$	7.0 ± 0.4	22.4 ± 6.0
C-(A-D1)$_4$	6.1 ± 0.3	23.1 ± 2.9
[C-(A-D2)$_4$]$_2$	9.3 ± 0.3	23.6 ± 6.2
C-(A-A')$_4$(B-B')$_4$	7.7 ± 0.2	22.55 ± 3.7
C-(A-D1)$_4$(B-D1)$_4$	6.3 ± 0.2	14.2 ± 6.4
C-(A-D2)$_4$(B-D2)$_4$	6.4 ± 0.2	16.1 ± 3.6

2.5.10 Synthesis of clip strands

DNA synthesis was performed on a 1μmole scale, starting from the required nucleotide modified 1000Å LCAA-CPG solid-support. Coupling efficiency was monitored after removal of the dimethoxytrityl (DMT) 5′-OH protecting groups. DMT-hexaethyloxy-Glycol phosphoramidite (cat# CLP-9765) was purchased from Chemgenes. Removal of the DMT protecting group was carried out using 3% DCA in dichloromethane. Completed sequences were deprotected in 28% ammonium hydroxide solution for 16-18 hours at 60°C.

Table 2.4 - Sequences used for cube clips. Nonstandard amidite codes: (**H**= (-CH_2CH_2-O-)$_6$-OP(O_2)O-)). The hexaethyloxy-Glycol spacers are used as flexible junctions to allow the cube structure to form. The T14 tracks are inserted in the single-stranded regions to act as non-binding sequences.

Name	Sequence (5'-xx-3')
Clip1-AB	TCGCTGAGTA**H**TCCTATATGGTCAACTGCTC**H**GCAAGTGTGGGCACGCACA C**H**GTAGTAATACCAGATGGAGT**H**CACAAATCTG
Clip2-AB	CTATCGGTAG**H**TCCTATATGGTCAACTGCTC**H**TACTCAGCGACAGATTTGTG **H**GTAGTAATACCAGATGGAGT**H**CAACTAGCGG
Clip3-AB	CACTGGTCAG**H**TCCTATATGGTCAACTGCTC**H**CTACCGATAGCCGCTAGTTG **H**GTAGTAATACCAGATGGAGT**H**GGTTTGCTGA
Clip4-AB	CCACACTTGC**H**TCCTATATGGTCAACTGCTC**H**CTGACCAGTGTCAGCAAACC **H**GTAGTAATACCAGATGGAGT**H**GTGTGCGTGC
Clip1-C	TCGCTGAGTA**H**GCCTGGCCTTGGTCCATTTG**H**GCAAGTGTGGGCACGCACA C**H**CGCACCGCGACTGCGAGGAC**H**CACAAATCTG
Clip3-C	CACTGGTCAG**H**AAAACTCTGCCGTAAGAGGA**H**CTACCGATAGCCGCTAGTT G**H**CGCACCGCGACTGCGAGGAC**H**GGTTTGCTGA
Clip1-T14	TCGCTGAGTA**H**TCCTTTTTTTTTTTTTTCTC**H**GCAAGTGTGGGCACGCACAC **H**GTATTTTTTTTTTTTTTAGT**H**CACAAATCTG
Clip2-T14	CTATCGGTAG**H**TCCTTTTTTTTTTTTTTCTC**H**TACTCAGCGACAGATTTGTG **H**GTATTTTTTTTTTTTTTAGT**H**CAACTAGCGG
Clip3-T14	CACTGGTCAG**H**TCCTTTTTTTTTTTTTTCTC**H**CTACCGATAGCCGCTAGTTG **H**GTATTTTTTTTTTTTTTAGT**H**GGTTTGCTGA
Clip4-T14	CCACACTTGC**H**TCCTTTTTTTTTTTTTTCTC**H**CTGACCAGTGTCAGCAAACC **H**GTATTTTTTTTTTTTTTGAGT**H**GTGTGCGTGC
LA	GAGCAGTTGACCATATAGGAAGCCACCGTCGTGACGTGTAGAGCAGTTGAC CATATAGGA

2.5.11 Purification of clip strands

Cube sequences were purified on 8% polyacrylamide/8M urea polyacrylamide gel (PAGE; up to 20 OD_{260} of crude DNA per gel) at constant current of 30mA for 1.5 hour (30 min at 250V followed by 1hr at 500V), using the 1x TBE buffer. Following electrophoresis, the plates were wrapped in plastic and placed on a fluorescent TLC plate and illuminated with a UV lamp (254nm). The bands were quickly excised, and the gel pieces were crushed and incubated in 12mL of sterile water at 60 ^{o}C for 12-16 hours. Samples were then dried to ca. 1.5 mL, desalted using size exclusion chromatography (Sephadex G-25), and carefully quantified (OD_{260}) using UV-Vis spectroscopy.

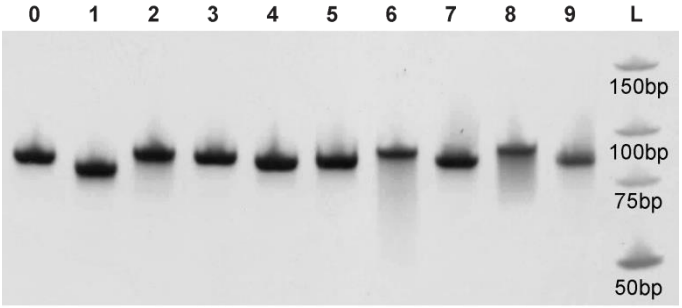

Figure 2.26 - Analytical denaturing PAGE on cube clips. 8% polyacrylamide/8M urea analytical PAGE. Run at constant current of 30 mA for 1.5 hour (30 min at 250 V followed by 1 hr at 500 V). In each lane between 0.02-0.03 OD_{260} of DNA has been loaded. Lane 1-**Clip1-AB**, Lane 2- **Clip2-AB**, Lane 3- **Clip3-AB**, Lane 4- **Clip4-AB**, Lane 5- **Clip1-C**, Lane 6- **Clip3-C**, Lane 7- **Clip1-T14**, Lane 3- **Clip2-T14**, Lane 9- **Clip3-T14**, Lane 10 – **Clip4-T14**. (8% denaturing PAGE, >25^{o}C)

2.5.12 Preparation of 3D structures

In each case, equimolar amounts of Clip1, Clip2, Clip3 and Clip4 were combined in 1xTAMg buffer with a total DNA concentration of 5μM (giving a final cube concentration of 1.25μM). Samples were annealed with the following protocol: held at 95^{o}C for 5 minutes then 80^{o}C for 3 minutes, cooled to 60^{o}C (2min/^{o}C) and finally slowly cooled to 4^{o}C (3min/^{o}C).[41] For the different symmetrical variants reported in the manuscript various different combinations of the clip strands were used as shown in Table 2.5.

Table 2.5 - Sequence symmetrical cube variants. In each case the designation Clip#-X can be substituted with its equivalent which differs only in the single stranded regions (e.g Clip1-AB can be replaced with Clip1-C and the resulting structure will differ only in the sequence of the single stranded portion). The complete cube structures are shown in open form for clarity.

Name	Component strands	Structure
C-A_1	Clip1-AB, Clip2-T14, Clip3-T14, Clip4-T14	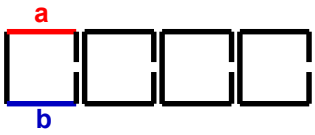
C-A_2	Clip1-AB, Clip2-T14, Clip3-AB, Clip4-T14	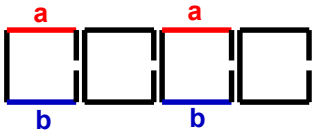
C-A_3	Clip1-AB, Clip2-AB, Clip3-AB, Clip4-T14	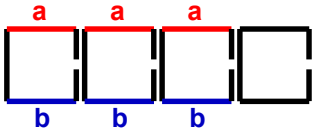
C-A_4B_4(=C-A_4)	Clip1-AB, Clip2-AB, Clip3-AB, Clip4-AB	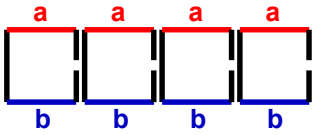
C-A_2C_2	Clip1-C, Clip2-AB, Clip3-C, Clip4-AB	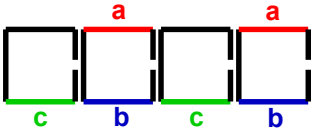

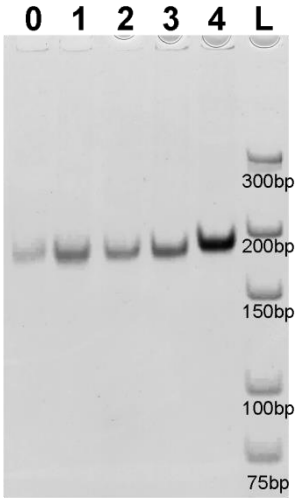

Figure 2.27 - Assembled cubes with differing sequence symmetries. Lane 0- **C-A_4B_4**, Lane 1 - **C-A_3**, Lane 2 - **C-A_2**, Lane 3 **- C-A_1**, Lane 4 - **C-A_2C_2**, Lane L - **Ladder**. (6% Native PAGE, 7°C)

2.5.13 Preparation of D-DNA decorated cubic scaffolds

Appropriate equivalents of required **D-DNA** (at concentrations between 1μM - 5μM) are mixed with a pre-assembled cube (2μL, 1.25μM [cube]) in a tris (40 mM) acetic acid (18 mM) $Mg(OAc)_2$ (12.5 mM) buffer (1xTAMg buffer, pH 8) to give a final concentration of the DNA structure (**C-(A-D#)$_x$(B-D#)$_x$**) between 147nM and 1μM. The **D-DNA** was then annealed with the cube for 30-45 mins at 37^{o}C and cooled to room temperature over 15 mins. Alternatively the four cube clip strands and appropriate equivalents of D-DNA were combined and annealed together: held at 95^{o}C for 5 minutes then 80^{o}C for 3 minutes, cooled to 60^{o}C (2 min/^{o}C) and finally slowly cooled to 4^{o}C (3min/^{o}C). The assembled products were analyzed in reference to the cube control or GeneRuler™ Ultra Low Range DNA Ladder (Fermentas Inc.) on native PAGE (6–8%, 250V, 70mA, 2–3h, 7-25^{o}C) in 1xTAMg buffer and gel bands visualized with Stains-All®. Samples were then characterized by gel mobility in reference to the cube structure which has been previously characterized.[2]

2.5.14 Gel mobility shift assays

A number of electrophoresis experiments were carried out on the D-DNA decorated cubes with variation in stoichiometry, concentration, annealing protocol and DNA sequences. In each case native PAGE was carried out at 7^{o}C or 25^{o}C for 2.5 hours at a constant voltage of 250V. Sample loading is approximately 2.5 picomoles of assembled construct per lane. The optical density of one mole of each specific construct is dependent on the number of bases present in the structure; this varies with addition of the varying numbers of D-DNA. The DNA bands were visualized by incubation with Stains-All®. This section contains additional PAGE experiments carried out to aid characterization of the D-DNA decorated cubic scaffolds.

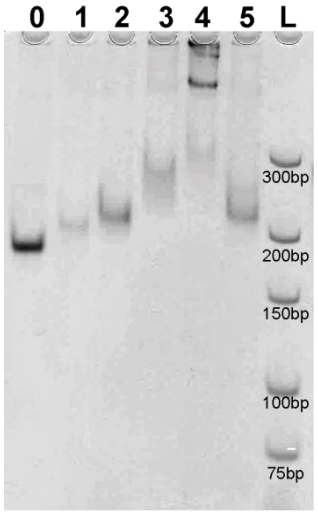

Figure 2.28 - Decoration of cubes with D-DNA-2 above the CMC. The addition of one **D2** to cube **C-A$_1$** (Lane 1), or two equivalents of **D2** to cube **C-A$_2$** (Lane 2) results in single band species. The concentration of each assembled structure is between 500nM and 1.25μM. Addition of three equivalents of **D2** to cube **C-A$_3$** (Lane 3), or four equivalents of **D2** to cube **C-A$_4$** at results in smeared bands showing a mixture of aggregated products, including the cube-dimer. Lane 0- **C-A$_1$**, Lane 1 – **C-(A-D2)$_1$**, Lane 2 – **C-(A-D2)$_2$**, Lane 3 – **C-(A-D2)$_3$**, Lane 4 - **C-(A-D2)$_4$,** Lane 5 – **C-(A-D2)$_2$**, Lane L - **Ladder**. (6% Native PAGE, 7^{o}C)

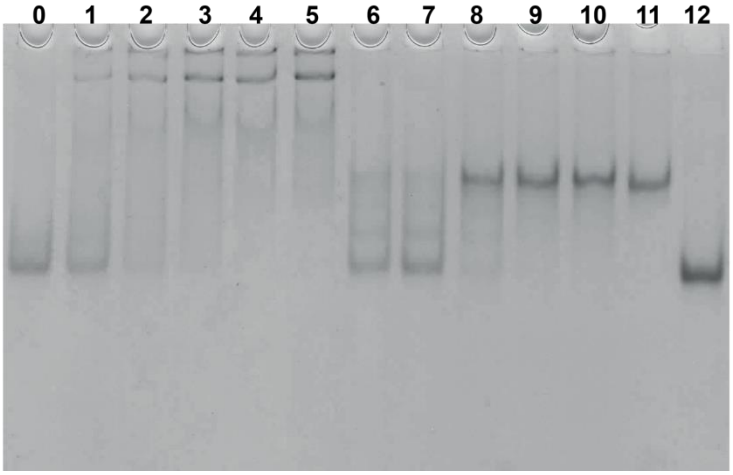

Figure 2.29 - Titration of cube C-A$_4$ containing four available identical binding sites, with D-DNA molecules above the CMC. a) The addition of increasing equivalents of **D2** (Lanes 0-5) and **D1** (Lanes 6-11) to the cube **C-A$_4$** at 2.5μM of the **D-DNA**. The concentration of each assembled structure is 500nM. The major product for **D2** is the cube-dimer, (Lanes 0-5) however additional bands attributed to the competing assembly modes of micelle formation of individual **D2** conjugates and hybridization to the cubic scaffold are observed. For the addition of **D1** (Lanes 6-11) conversion to a single monomeric product, **C-(A-D1)$_4$**, is observed. Lanes 0-5 - **C-A$_4$** + **D2** (0.7, 1, 2, 2.7, 3.3, 4 equiv.), Lanes 6-11 – **C-A$_4$** + **D1** (1, 2, 3, 4, 5, 6 equiv.) Lane 12 - **C-A$_4$** (6% Native PAGE, 7^{o}C)

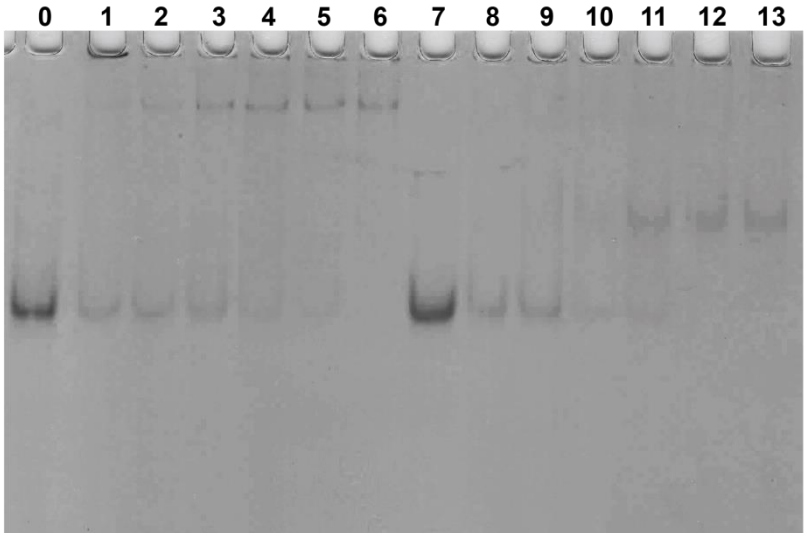

Figure 2.30 - Titration of cube C-A_4 containing four available identical binding sites, with D-DNA molecules below the CMC. a) The addition of increasing equivalents of **D2** (Lanes 0-6) and **D1** (Lanes 7-13) to the cube **C-A_4** at 800nM of the **D-DNA**. The concentration of each assembled structure is 147nM. The major product for **D2** is the cube-dimer, (Lanes 0-6) and at this concentration no other products are observed. For the addition of **D1** (Lanes 7-13) conversion to the single monomeric product, **C-(A-D1)$_4$**, is observed as before. Lane 0 - **C-A_4**, Lanes 1-5 - **C-A_4** + **D2** (0.7, 1, 2, 2.7, 3.3, 4 equiv.), Lane 7 - **C-A_4**, Lanes 8-11 – **C-A_4** + **D1** (0.5, 1, 2, 2.7, 3.3, 4) (6% Native PAGE, 25^{o}C)

2.5.15 Atomic force microscopy

AFM was carried out using a MultiMode8™ SPM connected to a Nanoscope™ V controller from Veeco. All images were obtained using ScanAsyst mode in air with ScanAsyst cantilevers (Nominal values: Tip radius – 2nm, Resonant frequency – 70kHz, Spring constant – 0.4N/m) from Bruker. Samples were diluted to between 25nM and 50nM of assembled structure in 1xTAMg buffer and 5µL of this solution was deposited on a freshly cleaved mica surface and allowed to adsorb for 1 minute. Then 50µL of 0.22µm filtered Millipore water was dropped on the surface and the excess aqueous solution removed with filter paper after 1 minute. Samples were dried under vacuum overnight and transferred to a desiccator 4 hours prior to imaging.

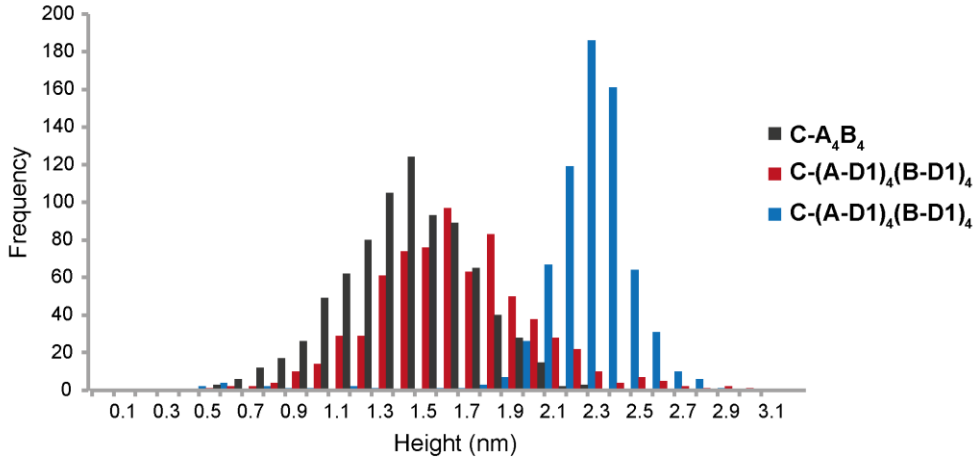

Figure 2.31 - Statistical analysis of AFM images. Height histogram for the analysis of over 500 individual particles is shown. Noticeably all samples exhibit reduced heights due to the strong surface adsorption of the polyanionic molecules in the presence of Mg^{2+}. The cube control **C-A$_4$B$_4$** has an average height of 1.4±0.3 nm. The average heights of **C-(A-D1)$_4$(B-D1)$_4$** and **C-(A-D2) $_4$(B-D2)$_4$** are 1.7±0.4 nm and 2.3±0.2 nm respectively. The large increase in average height for the **C-(A-D2) $_4$(B-D2)$_4$** sample can be attributed to the presence of some aggregates which are likely mediated by the hydrophobic D2 chains as the surface concentration increases with drying. However, overall both structures show a population of discrete objects further indicating that the alkyl chains are packed into the central cavity of each structure. For this reason it should be noted that the solution based results (Figure 2.23) are more representative as the structures are in their native environment.

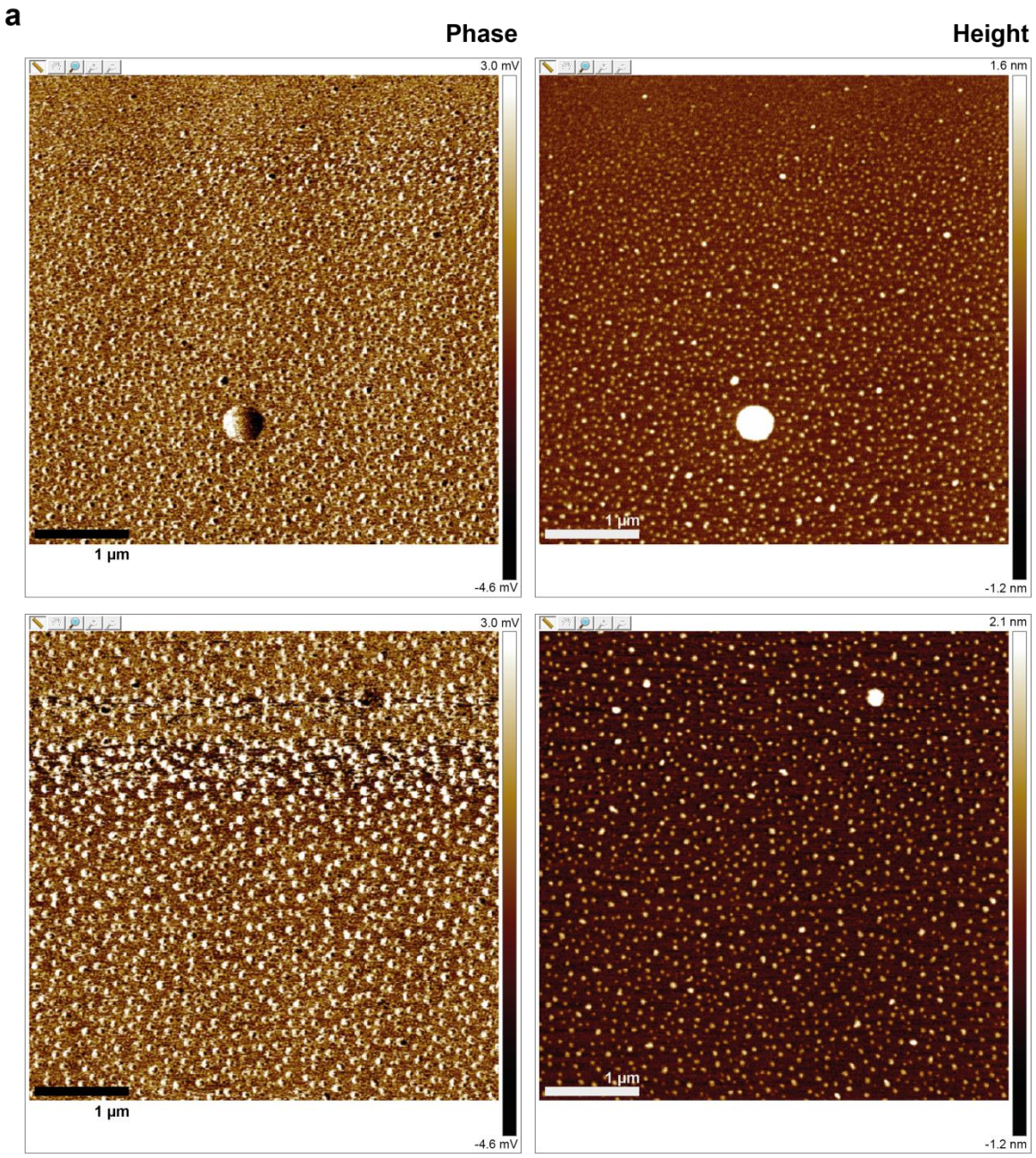

Figure 2.32 - Additional AFM images I. Additional height and phase images of the cube-core structure **C-(A-D1)$_4$(B-D1)$_4$ (=2).**

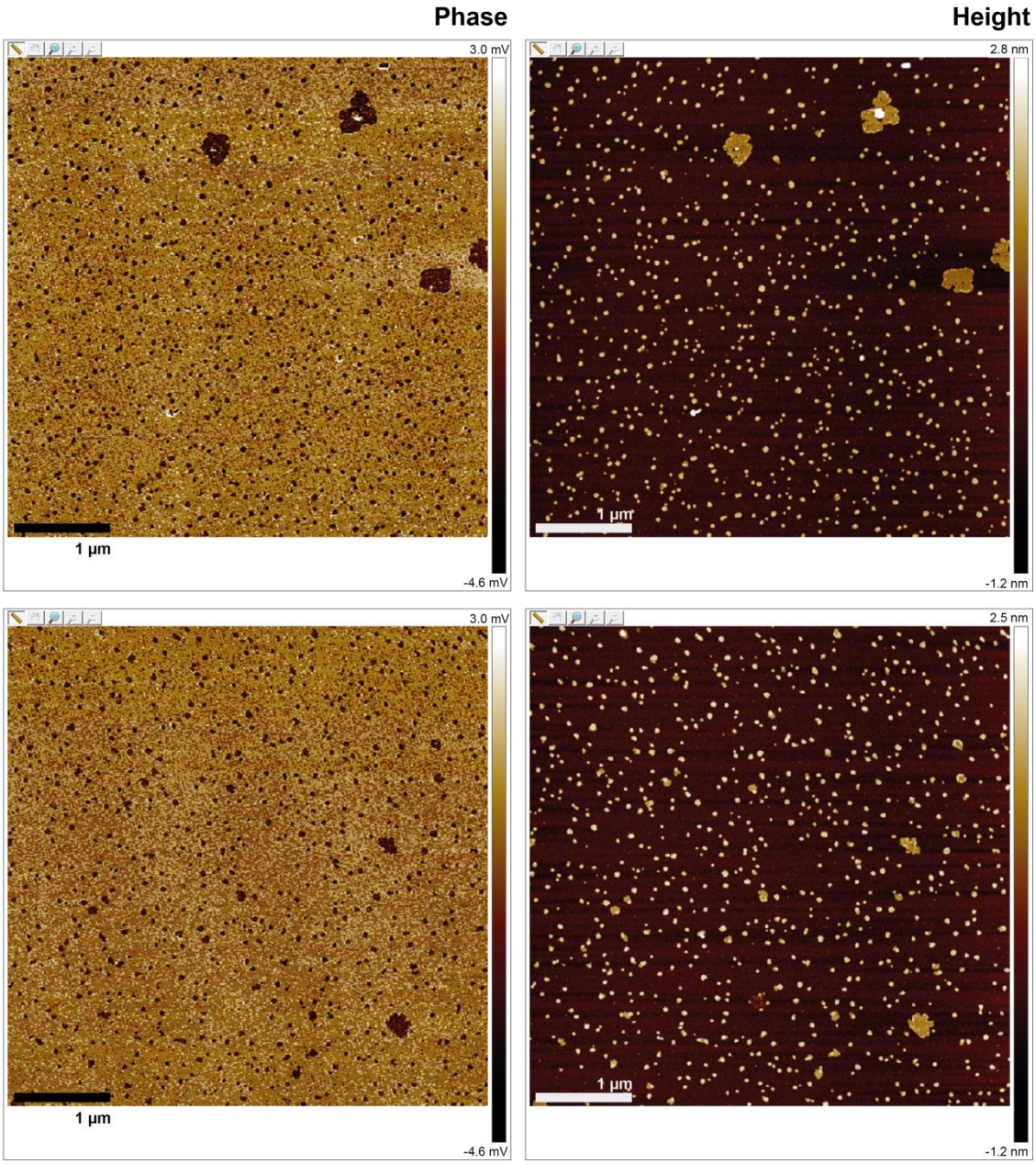

Figure 2.33 - Additional AFM images II. Additional height and phase images of the cube-core structure **C-(A-D2)$_4$(B-D2)$_4$ (=3).** Some aggregation is visible and is reflected in the height statistics (see Figure 2.31).

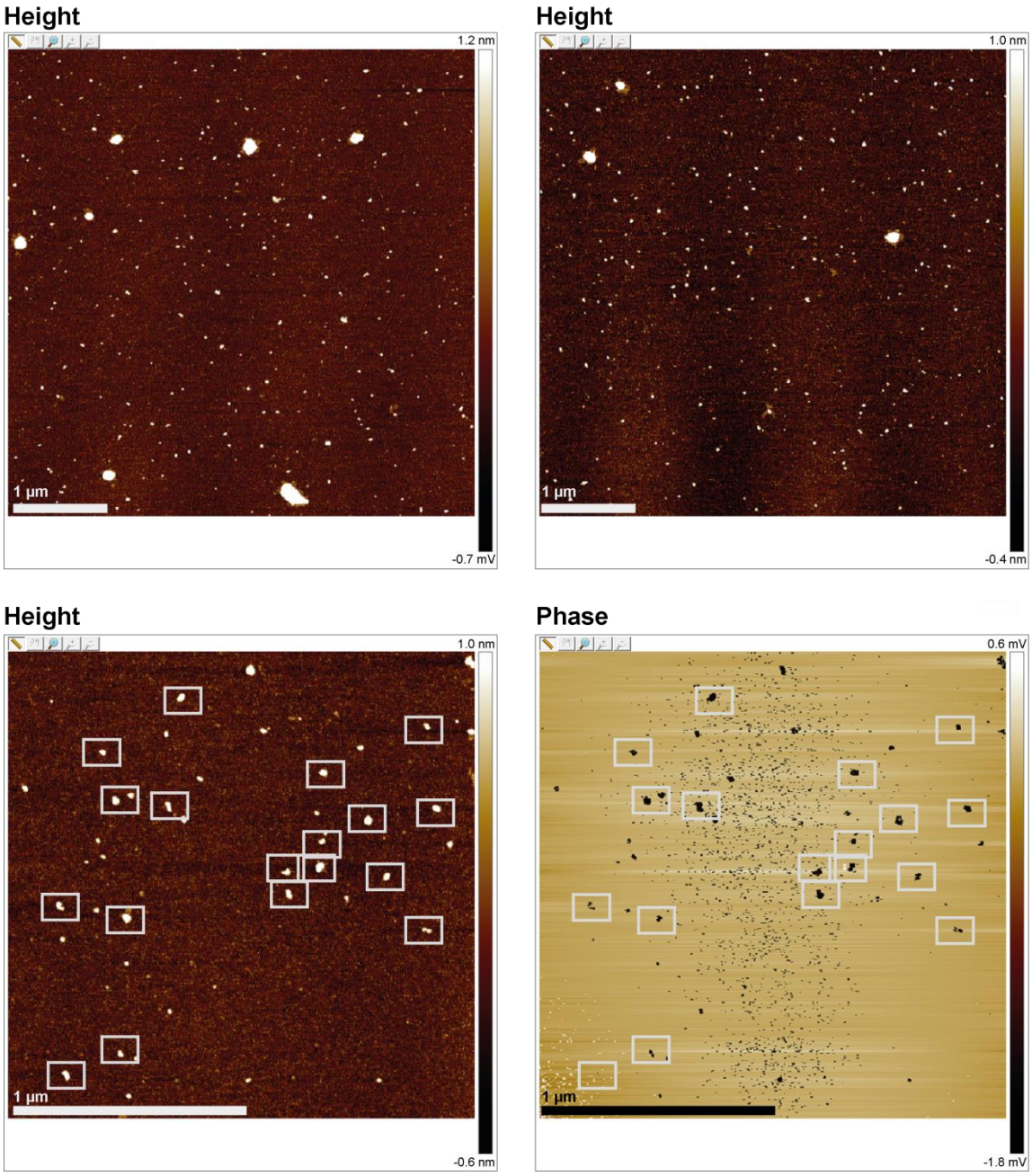

Figure 2.34 - Additional AFM images III. Additional height and phase images of the cube-dimer structure **[C-(A-D2)$_4$]$_2$**. The wider field of view (top) shows a dispersion of small particles. The lower images reveal the presence of small aggregate particles which correspond to two cubes, either in diameter or aspect ratio as well as individual cubes. A preliminary examination of the non-monomeric particles shows an aspect ratio of approximately 1.9, however it should be noted that under the conditions of drying and surface adsorption on mica in the presence of divalent cations the intermolecular hydrophobic association is expected to be mostly disrupted.

2.5.16 Incorporation of additional amphiphiles

The fully D-DNA decorated cubes **C-(A-D1)$_4$(B-D1)$_4$**, **C-(A-D2) $_4$(B-D2)$_4$** and the DNA control **C-A$_4$B$_4$** were assembled in 1xTAMg at a concentration of 313nM. To 3μL aliquots of these solutions were added between 0.7 and 6 equivalents of **D1/D2-C** which have the same **D-DNA** alkyl dendron but non-complementary sequence to the DNA cube. The samples were incubated at room temperature for 1 hour before loading on native PAGE for analysis. The DNA bands were visualized with Stains-All® and the band intensity was analyzed using ImageJ software on the raw scanned images of the gels.

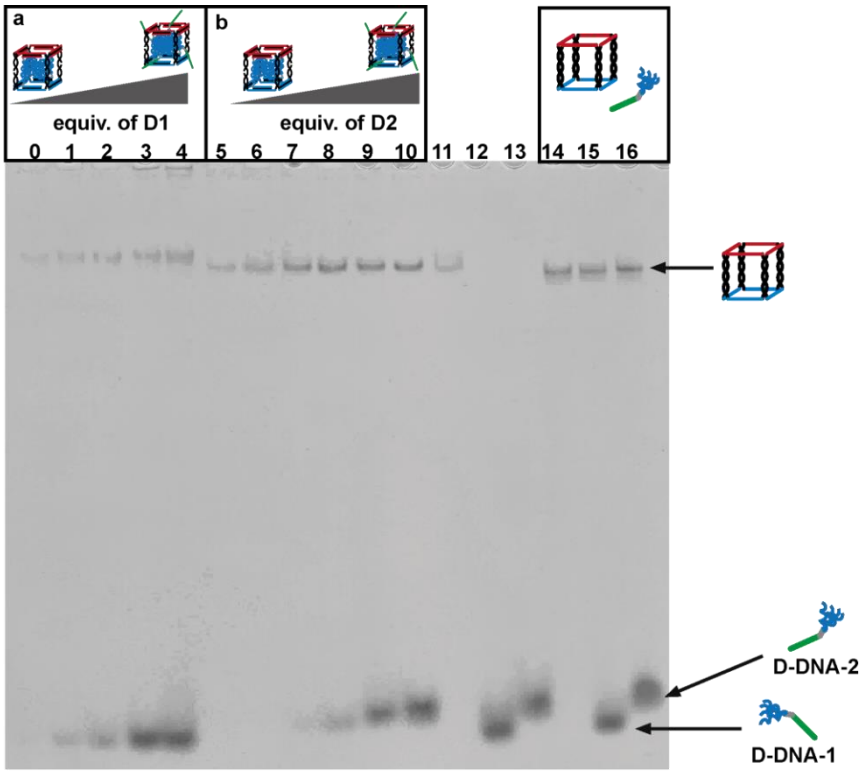

Figure 2.35 - Representative native PAGE of additional amphiphile loading. The addition of increasing equivalents of non-complementary **D-DNA** (green) to the cube-core structures a) **C-(A-D1)$_4$(B-D1)$_4$** (Lanes 0-4) and b) **C-(A-D2) $_4$(B-D2)$_4$** (Lanes 6-10). The increase in intensity of the bands corresponding to the cube-core structures indicates the presence of more DNA and the lack of change in mobility suggests that the additional amphiphiles pack into the hydrophobic micellar core of the DNA cage. The individual D-DNA conjugates are shown in lanes 12 and 13. Lanes 14-16 show the addition of an excess of the non-complementary D-DNA to the naked cube structure **C-A$_4$B$_4$** and lack of interaction, thus demonstrating that the interaction between the additional D-DNA and the cube-core structures is mediated by the hydrophobic interaction. Additionally Lane 11 contains a mixture of **C-(A-D1)$_4$(B-D1)$_4$** and **C-(A-D2) $_4$(B-D2)$_4$** showing there is no crossover between these stable structures. (6% Native PAGE, 7°C)

2.5.17 Loading and release of Nile Red

For the measurement of fluorescence intensity of Nile Red in the presence of the DNA cube, **C-A$_4$B$_4$**, and cube-core assemblies, **C-(A-D1)$_4$(B-D1)$_4$** and **C-(A-D2) $_4$(B-D2)$_4$,** the following protocol was used. To a 97.5µL solution of DNA in 1xTAMg was added 2.5µL of Nile Red solution (0.1mM in acetone) in a sterile black 96-well top-read MicroWell™ Plate. The resulting concentration of Nile Red is 5µM and the concentration of the DNA structures was **C-A$_4$B$_4$** (313 nM), **C-(A-D1)$_4$(B-D1)$_4$** and **C-(A-D2) $_4$(B-D2)$_4$** (250 nM). The sample solutions were gently shaken at room temperature overnight before the fluorescence was read using a Biotek® Synergy well-plate fluorimeter. For removal of the **D-DNA** by strand displacement concentrated solutions of 20nt eraser ssDNAs **E$_A$** and **E$_B$** were prepared (120µM) to reduce the effect of dilution on the experiment and 1µL of each was added to the 100µL samples of Nile Red encapsulating D-DNA cubes, after a 30 minute incubation the fluorescence emission was measured.

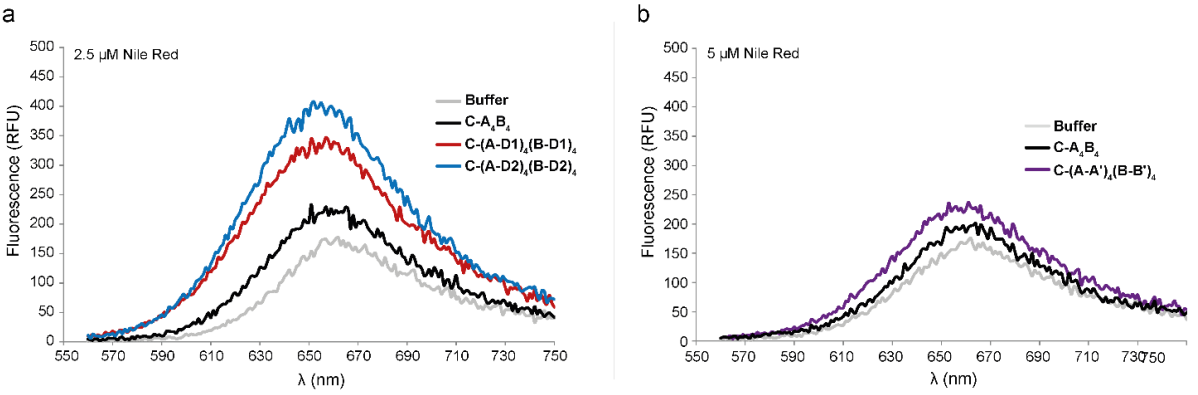

Figure 2.36 - Additional fluorescence emission spectra of cube-core structures. The fluorescence intensity of Nile Red was measured in the presence of a low concentration of the cube-core structures **C-(A-D1)$_4$(B-D1)$_4$** and **C-(A-D2) $_4$(B-D2)$_4$**, control cube **C-A$_4$B$_4$** and 1xTAMg buffer alone. a) In each sample the total concentration of Nile Red is 2.5 µM, the concentration of the structures **C-(A-D1)$_4$(B-D1)$_4$** and **C-(A-D2) $_4$(B-D2)$_4$** is 125 nM and the cube **C-A$_4$B$_4$** is 600 nM. Even at this low concentration the cube-core structures give elevated fluorescence of the Nile Red, signaling its inclusion into the non-polar core. The naked cube shows baseline fluorescence close to that of the buffer alone. b) Control experiment to verify the effect of increased number of double stranded regions on the cube on the observed fluorescence in the presence of 5 µM Nile Red. The concentration of the cube structures **C-A$_4$B$_4$** and **C-(A-A')$_4$(B-B')$_4$** are 250 nM. It is apparent that the fully double stranded cube **C-(A-A')$_4$(B-B')$_4$** does not exhibit significantly elevated fluorescence and remains close to the naked cube and buffer control.

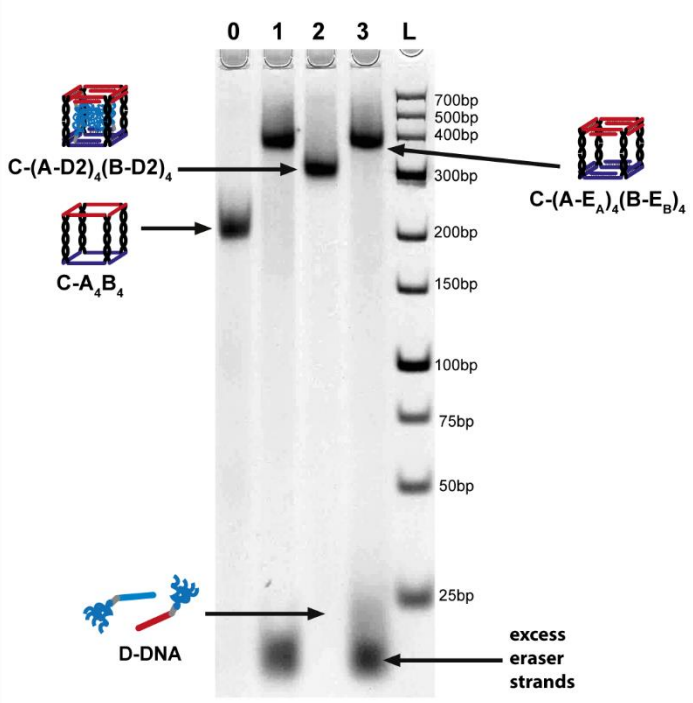

Figure 2.37 - Removal of D-DNA by strand displacement, PAGE analysis. The removal of the D-DNA from the structure **C-(A-D2)$_4$(B-D2)$_4$** is shown by native PAGE. Lane 0- **C-A$_4$B$_4$**, Lane 1 - **C-(A-E$_A$)$_4$(B-E$_B$)$_4$**, Lane 2 – **C-(A-D2)$_4$(B-D2)$_4$**, Lane 3 - **C-(A-D2)$_4$(B-D2)$_4$ (-D2),** Lane L – **Ladder** (6% Native PAGE, 7°C). The conversion of **C-(A-D2)$_4$(B-D2)$_4$** to **C-(A-E$_A$)$_4$(B-E$_B$)$_4$** is marked by decrease in electrophoretic mobility as the contracting effect of the hydrophobic core is no longer present and the resulting structure is a fully double stranded cube (Lanes 3 and 4). The remainder **D-DNA** is also visible at high mobility, corresponding to individual strands in solution after disassembly of the micellar core. The presence of multiple bands for the D-DNA is due to the different sequences (A and B), and the presence of excess eraser strands.

2.5.18 Determination of Loading capacity

To determine the loading capacity of the cube-core structures **C-(A-D1)$_4$(B-D1)$_4$** and **C-(A-D2)$_4$(B-D2)$_4$** the hydrophobic dyes Nile Red and 1,6-Diphenyl-1,3,5-hexatriene (DPH) were used as guest molecules. Optimal loading of the structures **2** and **3** was obtained by one-pot thermal annealing of the DNA structure (125-250nM) in the presence of a large excess of cargo molecule (250-500μM) using the standard protocol (SI-VIa). Removal of un-encapsulated dye was achieved by preparative centrifugation (15,000 x *g*, 4°C, 20min.) carried out between 2-5 times.[48] The supernatant was removed and an aliquot of each sample was loaded on 12% denaturing PAGE along with samples of known concentration to quantify the isolated yield of dye-loaded cubes. Additionally, in each case a small aliquot of the purified cargo containing cube-micelles were loaded on native 6% PAGE to confirm the fidelity of the assemblies, in every case the structures remain intact. Fluorescence emission spectra of each sample were collected in triplicate by mixing a 18.75μL aliquot of sample with 56.25μL of acetone and recording the emission spectra (Nile Red: exc. 535nm, DPH: exc. 350nm) of the sample in a 75μL quartz cuvette. A standard curve for [dye] versus maximal fluorescence intensity was used to calculate the [dye] present in each sample. The ratio of dye to cube structure was used to calculate the loading capacity as a mole fraction.

Similar loading values for the two different dyes strongly suggest a similar host guest recognition which is due to the hydrophobic alkyl dendrons within the core of the cube-micelle structure. It is possible that the difference in loading capacity between the **D1** and **D2** cube-micelles is due to the difference in packing/organization of the alkyl chains within the core. The smaller size of **C-(A-D2)$_4$(B-D2)$_4$** suggests a more tightly packed core which may be more similar in structure to the D2 micelles which are also capable of encapsulation. The larger/looser **D1** core may not be as organized for encapsulation.

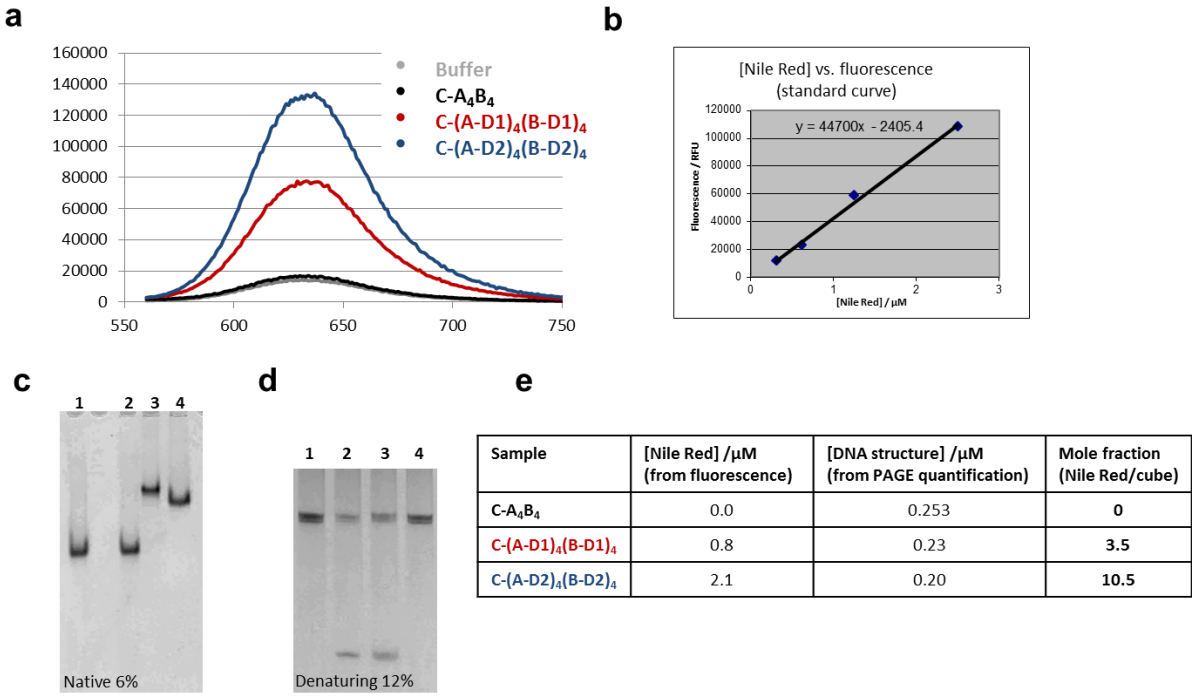

Sample	[Nile Red] /µM (from fluorescence)	[DNA structure] /µM (from PAGE quantification)	Mole fraction (Nile Red/cube)
C-A_4B_4	0.0	0.253	**0**
C-(A-D1)$_4$(B-D1)$_4$	0.8	0.23	**3.5**
C-(A-D2)$_4$(B-D2)$_4$	2.1	0.20	**10.5**

Figure 2.38 - Exemplary data set for Nile Red loading capacity. a) Uncorrected emission spectra of samples after centrifugation to remove excess Nile Red. B) Standard curve used for [Nile Red] calculation. c) 6% Native PAGE showing intact samples after centrifugation; Lane 1 – reference cube, Lane 2 – **C-A_4B_4**, Lane 3 – **C-(A-D1)$_4$(B-D1)$_4$**, Lane 4 – **C-(A-D2)$_4$(B-D2)$_4$**, d) 12% Denaturing PAGE analysis of the samples used for DNA quantification; Lane 1 - **C-A_4B_4**, Lane 2 – **C-(A-D1)$_4$(B-D1)$_4$**, Lane 3 – **C-(A-D2)$_4$(B-D2)$_4$**, Lane 4 – quantification standard (**C-A_4B_4**). e) Table showing quantification results from this data set.

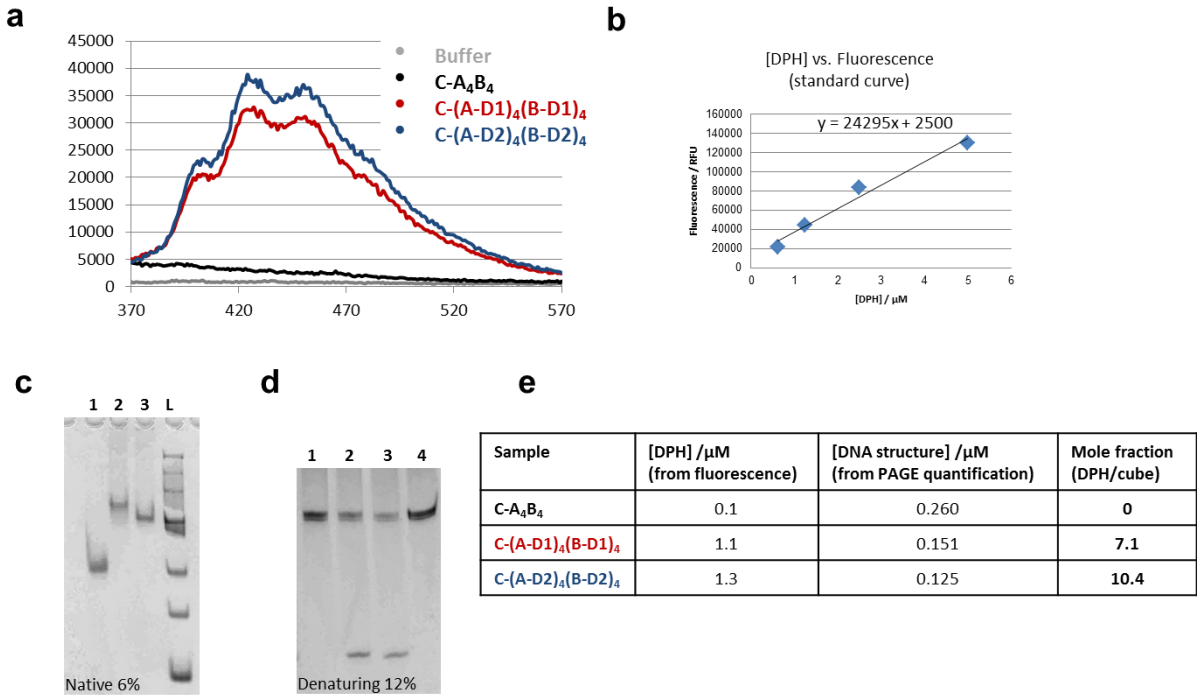

Sample	[DPH] /µM (from fluorescence)	[DNA structure] /µM (from PAGE quantification)	Mole fraction (DPH/cube)
C-A_4B_4	0.1	0.260	**0**
C-$(A\text{-}D1)_4(B\text{-}D1)_4$	1.1	0.151	**7.1**
C-$(A\text{-}D2)_4(B\text{-}D2)_4$	1.3	0.125	**10.4**

Figure 2.39 - Exemplary data set for DPH loading capacity. a) Uncorrected emission spectra of samples after centrifugation to remove excess DPH. B) Standard curve used for [DPH] calculation. c) 6% Native PAGE showing intact samples after centrifugation; Lane 1 - **C-A_4B_4**, Lane 3 – **C-$(A\text{-}D1)_4(B\text{-}D1)_4$**, Lane 4 – **C-$(A\text{-}D2)_4(B\text{-}D2)_4$**, Lane L – DNA Ladder (100-700bp). d) 12% Denaturing PAGE analysis of the samples used for DNA quantification; Lane 1 – quantification standard (**C-A_4B_4**), Lane 2 - **C-A_4B_4**, Lane 3 – **C-$(A\text{-}D1)_4(B\text{-}D1)_4$**, Lane 4 – **C-$(A\text{-}D2)_4(B\text{-}D2)_4$**. e) Table showing quantification results from this data set.

2.5.19 Encapsulation of Dasatanib

The Dasatanib (Kind gift from Dr. Panasci) was prepared as a working solution of 10mM in DMSO for experiments. Loading of the structures **C-(A-D1)$_4$(B-D1)$_4$** and **C-(A-D2) $_4$(B-D2)$_4$** was obtained by one-pot thermal annealing of the DNA structure (125-250nM) in the presence of an excess of Dasatanib (250μM) using the standard protocol (SI-VIa), the final solution was 200μL with 2.5% DMSO in 1xTAMg buffer. Removal of the free drug was achieved by preparative centrifugation (15,000 x g, 4°C, 20 min.) between 3-6 times. For determination of the Dasatanib loading a 25μL of the supernatant was mixed with 50μL of DMSO and the absorbance (200-500nm) was measured. The presence of Dasatanib was monitored by the absorbance at 325nm using a Biotek Synergy HT well-plate spectrometer.

2.5.20 Purification of cargo-loaded cubes

Several methods of purification were tested for the purification of cargo-loaded cubes from the un-encapsulated cargo including: centrifugation, centrifugal filtration, dialysis, size exclusion chromatography, submicron filtration and agarose gel electrophoresis. In summary, it was found that preparative centrifugation (15,000 x *g*, 4°C, 20 min.) was best for the dyes Nile Red and DPH as these molecules precipitate in the 1xTAMg buffer. In the case of more soluble guest molecules size-exclusion chromatography using Illustra MicroSpin G-25 Columns (GE Healthcare) or similar device is very effective at removing small molecules, although the recovery of DNA nanostructures is not high using the manufacturer's protocols.

2.6 References

1 Seeman, N. C. 'DNA in a material world'. *Nature* **421**, 427-431 (2003).

2 Lin, C., Liu, Y. & Yan, H. 'Designer DNA Nanoarchitectures'. *Biochemistry* **48**, 1663-1674 (2009).

3 Deng, Z., Lee, S. H. & Mao, C. 'DNA as nanoscale building blocks'. *Journal of Nanoscience and Nanotechnology* **5**, 1954-1963 (2005).

4 Goodman, R. P. *et al.* 'Rapid Chiral Assembly of Rigid DNA Building Blocks for Molecular Nanofabrication'. *Science* **310**, 1661-1665 (2005).

5 Rothemund, P. W. K. 'Folding DNA to create nanoscale shapes and patterns'. *Nature* **440**, 297-302 (2006).

6 Woo, S. & Rothemund, P. W. K. 'Programmable molecular recognition based on the geometry of DNA nanostructures'. *Nat Chem* **3**, 620-627 (2011).
7 Douglas, S. M. *et al.* 'Self-assembly of DNA into nanoscale three-dimensional shapes'. *Nature* **459**, 414-418 (2009).
8 Han, D. *et al.* 'DNA Origami with Complex Curvatures in Three-Dimensional Space'. *Science* **332**, 342-346 (2011).
9 Andersen, E. S. *et al.* 'Self-assembly of a nanoscale DNA box with a controllable lid'. *Nature* **459**, 73-76 (2009).
10 Schulman, R., Yurke, B. & Winfree, E. 'Robust self-replication of combinatorial information via crystal growth and scission'. *Proceedings of the National Academy of Sciences* **109**, 6405-6410 (2012).
11 Rajendran, A., Endo, M., Katsuda, Y., Hidaka, K. & Sugiyama, H. 'Programmed Two-Dimensional Self-Assembly of Multiple DNA Origami Jigsaw Pieces'. *ACS Nano* **5**, 665-671 (2010).
12 Ke, Y., Ong, L. L., Shih, W. M. & Yin, P. 'Three-Dimensional Structures Self-Assembled from DNA Bricks'. *Science* **338**, 1177-1183 (2012).
13 Yang, H. *et al.* 'Metal–nucleic acid cages'. *Nat Chem* **1**, 390-396 (2009).
14 Wang, W., Wan, W., Zhou, H.-H., Niu, S. & Li, A. D. Q. 'Alternating DNA and π-Conjugated Sequences. Thermophilic Foldable Polymers'. *Journal of the American Chemical Society* **125**, 5248-5249 (2003).
15 Carneiro, K. M. M. *et al.* 'Stimuli-responsive organization of block copolymers on DNA nanotubes'. *Chemical Science* **3**, 1980-1986 (2012).
16 Milnes, P. J. *et al.* 'Sequence-specific synthesis of macromolecules using DNA-templated chemistry'. *Chemical Communications* **48**, 5614-5616 (2012).
17 Kwak, M. & Herrmann, A. 'Nucleic acid amphiphiles: Synthesis and self-assembled nanostructures'. *Chemical Society Reviews* **40**, 5745-5755 (2011).
18 Neelakandan, P. P. *et al.* 'Hydrophobic Self-Assembly of a Perylenediimide-Linked DNA Dumbbell into Supramolecular Polymers'. *Journal of the American Chemical Society* **132**, 15808-15813 (2010).
19 Eryazici, I., Yildirim, I., Schatz, G. C. & Nguyen, S. T. 'Enhancing the Melting Properties of Small Molecule-DNA Hybrids through Designed Hydrophobic Interactions: An Experimental-Computational Study'. *Journal of the American Chemical Society* **134**, 7450-7458 (2012).
20 Patwa, A., Gissot, A., Bestel, I. & Barthélémy, P. 'Hybrid lipid oligonucleotide conjugates: Synthesis, self-assemblies and biomedical applications'. *Chemical Society Reviews* **40**, 5844-5854 (2011).
21 Chan, Y. H., Lenz, P. & Boxer, S. G. 'Kinetics of DNA-mediated docking reactions between vesicles tethered to supported lipid bilayers'. *Proceedings of the National Academy of Sciences of the United States of America* **104**, 18913-18918 (2007).
22 Woller, J. G., Börjesson, K., Svedhem, S. & Albinsson, B. 'Reversible hybridization of DNA anchored to a lipid membrane via porphyrin'. *Langmuir : the ACS journal of surfaces and colloids* **28**, 1944-1953 (2012).
23 Benkoskr, J. J. & Höök, F. 'Lateral mobility of tethered vesicle-DNA assemblies'. *Journal of Physical Chemistry B* **109**, 9773-9779 (2005).
24 Albinsson, B., Hannestad, J. K. & Börjesson, K. 'Functionalized DNA nanostructures for light harvesting and charge separation'. *Coordination Chemistry Reviews* (2012).
25 Langecker, M. *et al.* 'Synthetic Lipid Membrane Channels Formed by Designed DNA Nanostructures'. *Science* **338**, 932-936 (2012).

26 Raouane, M., Desmaële, D., Urbinati, G., Massaad-Massade, L. & Couvreur, P. 'Lipid Conjugated Oligonucleotides: A Useful Strategy for Delivery'. *Bioconjugate Chemistry* (2012).
27 Thompson, M. P., Chien, M.-P., Ku, T.-H., Rush, A. M. & Gianneschi, N. C. 'Smart Lipids for Programmable Nanomaterials'. *Nano Letters* **10**, 2690-2693 (2010).
28 Kurz, A. *et al.* 'Lipid-Anchored Oligonucleotides for Stable Double-Helix Formation in Distinct Membrane Domains'. *Angewandte Chemie International Edition* **45**, 4440-4444 (2006).
29 O'Shea, E. K., Klemm, J. D., Kim, P. S. & Alber, T. 'X-ray structure of the GCN4 leucine zipper, a two-stranded, parallel coiled coil'. *Science* **254**, 539-544 (1991).
30 Koga, N. *et al.* 'Principles for designing ideal protein structures'. *Nature* **491**, 222-227 (2012).
31 Boyle, A. L. *et al.* 'Squaring the circle in peptide assembly: From fibers to discrete nanostructures by de novo design'. *Journal of the American Chemical Society* **134**, 15457-15467 (2012).
32 Schnitzler, T. & Herrmann, A. 'DNA Block Copolymers: Functional Materials for Nanoscience and Biomedicine'. *Accounts of Chemical Research* **45**, 1419-1430 (2012).
33 Wu, Y., Sefah, K., Liu, H., Wang, R. & Tan, W. 'DNA aptamer–micelle as an efficient detection/delivery vehicle toward cancer cells'. *Proceedings of the National Academy of Sciences* **107**, 5-10 (2010).
34 Wang, L. *et al.* 'Reversibly controlled morphology transformation of an amphiphilic DNA-dendron hybrid'. *Chemical Communications* **48**, 3715-3717 (2012).
35 Ponnuswamy, N., Cougnon, F. B. L., Clough, J. M., Pantoş, G. D. & Sanders, J. K. M. 'Discovery of an organic trefoil knot'. *Science* **338**, 783-785 (2012).
36 Wenz, G., Han, B.-H. & Müller, A. 'Cyclodextrin Rotaxanes and Polyrotaxanes'. *Chemical Reviews* **106**, 782-817 (2006).
37 Kilah, N. L. *et al.* 'Enhancement of Anion Recognition Exhibited by a Halogen-Bonding Rotaxane Host System'. *J. Am. Chem. Soc.* **132**, 11893-11895 (2010).
38 Liu, H. *et al.* 'DNA-Based Micelles: Synthesis, Micellar Properties and Size-Dependent Cell Permeability'. *Chemistry – A European Journal* **16**, 3791-3797 (2010).
39 Greenspan, P., Mayer, E. P. & Fowler, S. D. 'Nile red: a selective fluorescent stain for intracellular lipid droplets'. *The Journal of Cell Biology* **100**, 965-973 (1985).
40 Greenspan, P. & Fowler, S. D. 'Spectrofluorometric studies of the lipid probe, nile red'. *Journal of Lipid Research* **26**, 781-789 (1985).
41 McLaughlin, C. K. *et al.* 'Three-dimensional organization of block copolymers on "DNA- minimal" scaffolds'. *Journal of the American Chemical Society* **134**, 4280-4286 (2012).
42 Borjesson, K., Lundberg, E. P., Woller, J. G., Norden, B. & Albinsson, B. 'Soft-Surface DNA Nanotechnology: DNA Constructs Anchored and Aligned to Lipid Membrane'. *Angew Chem Int Ed Engl* (2011).
43 Ding, K., Alemdaroglu, F. E., Börsch, M., Berger, R. & Herrmann, A. 'Engineering the Structural Properties of DNA Block Copolymer Micelles by Molecular Recognition'. *Angewandte Chemie International Edition* **46**, 1172-1175 (2007).
44 Chien, M.-P., Rush, A. M., Thompson, M. P. & Gianneschi, N. C. 'Programmable Shape-Shifting Micelles'. *Angewandte Chemie International Edition* **49**, 5076-5080 (2010).

45 Lo, P. K. *et al.* 'Loading and selective release of cargo in DNA nanotubes with longitudinal variation'. *Nat Chem* **2**, 319-328 (2010).
46 Erben, C. M., Goodman, R. P. & Turberfield, A. J. 'Single-Molecule Protein Encapsulation in a Rigid DNA Cage'. *Angewandte Chemie International Edition* **45**, 7414-7417 (2006).
47 Jiang, Q. *et al.* 'DNA Origami as a Carrier for Circumvention of Drug Resistance'. *Journal of the American Chemical Society* **134**, 13396-13403 (2012).
48 Lim, Y.-b., Lee, E. & Lee, M. 'Controlled Bioactive Nanostructures from Self-Assembly of Peptide Building Blocks'. *Angewandte Chemie International Edition* **46**, 9011-9014 (2007).
49 Cao, P. & Bae, Y. 'Polymer nanoparticulate drug delivery and combination cancer therapy'. *Future Oncol* **8**, 1471-1480 (2012).
50 Carneiro, K. M. M., Aldaye, F. A. & Sleiman, H. F. 'Long-Range Assembly of DNA into Nanofibers and Highly Ordered Networks Using a Block Copolymer Approach'. *Journal of the American Chemical Society* **132**, 679-685 (2009).
51 Wu, K. J., Steding, A. & Becker, C. H. 'Matrix-assisted laser desorption time-of-flight mass spectrometry of oligonucleotides using 3-hydroxypicolinic acid as an ultraviolet-sensitive matrix'. *Rapid communications in mass spectrometry : RCM* **7**, 142-146 (1993).

2.7 Introduction to chapter 3

In chapter 2, the site-specific positioning of hydrophobic residues precisely, in 3D, on a nanoscaffold was shown to give geometry dependent *inter*- or *intra*molecular self-assembly. The self-assembly studies carried out were made possible by synthesis of a new type of DNA-amphiphile; **D-DNA**. Crucially, these molecules contained both the information necessary to allow selective binding to a specific address on the DNA cube structure, and a dendritic hydrophobic moiety capable of self-association in aqueous media. As alluded to earlier, the modular synthetic strategy employed to produce **D-DNA** could be used to produce a large library of similar DNA-amphiphiles. Furthermore, the effect of small structure changes to the molecules on the resulting self-assembly properties suggested that a range of molecules with tuneable self-assembly properties could be accessed easily using this synthetic approach.

In chapter 3, the extension of this synthetic methodology to produce linear DNA-polymer like conjugates and sequence controlled polymers attached to DNA is described.

3 | An efficient and modular route to sequence-defined polymers appended to DNA

This chapter is composed mainly of work published as "An Efficient and Modular Route to Sequence-Defined Polymers Appended to DNA", Edwardson, T. G. W.; Carneiro, K. M. M.; Serpell, C. J. and Sleiman, H. F. *Angew. Chem.*, **2014**, 126, 4655–4659. (Wiley-VCH, 2014)

3.1 Abstract

Inspired by biological polymers, sequence-controlled synthetic polymers are highly promising materials that integrate the robustness of synthetic systems with the information-derived activity of biological counterparts. Polymer–biopolymer conjugates are often targeted to achieve this union; however, their synthesis remains challenging. This chapter describes a stepwise solid-phase approach for the generation of completely monodisperse and sequence-defined DNA–polymer conjugates using readily available reagents. These polymeric modifications to DNA display self-assembly and encapsulation behavior, as evidenced by HPLC, dynamic light scattering, and fluorescence studies which is highly dependent on sequence order. The method is general and has the potential to make DNA–polymer conjugates and sequence-defined polymers widely available.

3.2 Introduction

The control of monomer sequence in synthetic polymers is a major challenge for modern polymer chemistry. The key processes in molecular biology are executed by proteins and nucleic acids – natural sequenced polymers capable of storing data, and generating complex structure and function. Synthetic sequence-controlled polymers may find applications in the fields of data storage and biomedicine, and in the creation of materials with precisely tunable bulk properties and function.[1] To date, a number of strategies have been proposed for the synthesis of sequence-defined polymers,[2-5] ranging from solid-phase sequential addition of monomers via peptide or other coupling reactions,[6,7] to biomolecule-templated polymerization,[8,9] to controlling the polymerization mechanism such that addition of a one or few monomers to a growing polymer chain is possible.[10,11] Solid-phase synthesis is especially powerful, as it allows for the introduction of a variety of residues at specific positions on a polymer chain.[12]

An alternative method to introduce molecular recognition into synthetic polymers is through biomolecule-polymer conjugation,[13] where a conventional synthetic polymer and an information-rich DNA or peptide/protein portion are covalently attached.[14] DNA amphiphiles in particular are especially attractive, because they can self-assemble into a variety of morphologies through microphase separation while retaining the 'smart' and addressable biomolecule component,[15-19] and can result in attractive platforms for functional nucleic acids such as aptamers and silencing RNA,[20,21] and as membrane

anchoring and functionalization tools.[22-24] However, the synthesis of amphiphilic DNA polymer conjugates is fundamentally challenging, as it requires the end-to-end coupling of a highly charged DNA strand with a hydrophobic polymer chain. Polymers can be attached to DNA via solid phase synthesis, however the yields are suboptimal as these methods and materials are designed for small molecule attachment.

In this chapter, a simple and versatile method for the synthesis of sequence-defined polymers attached to oligonucleotides is described. The approach involves the sequential coupling of short, well-defined oligomers to a DNA strand on a solid support. This strategy allows the synthesis of monodisperse DNA-polymer conjugates with hydrophilic and hydrophobic units attached to a DNA strand in high yields, and with complete control over the length and sequence of the monomer units in the final structure.

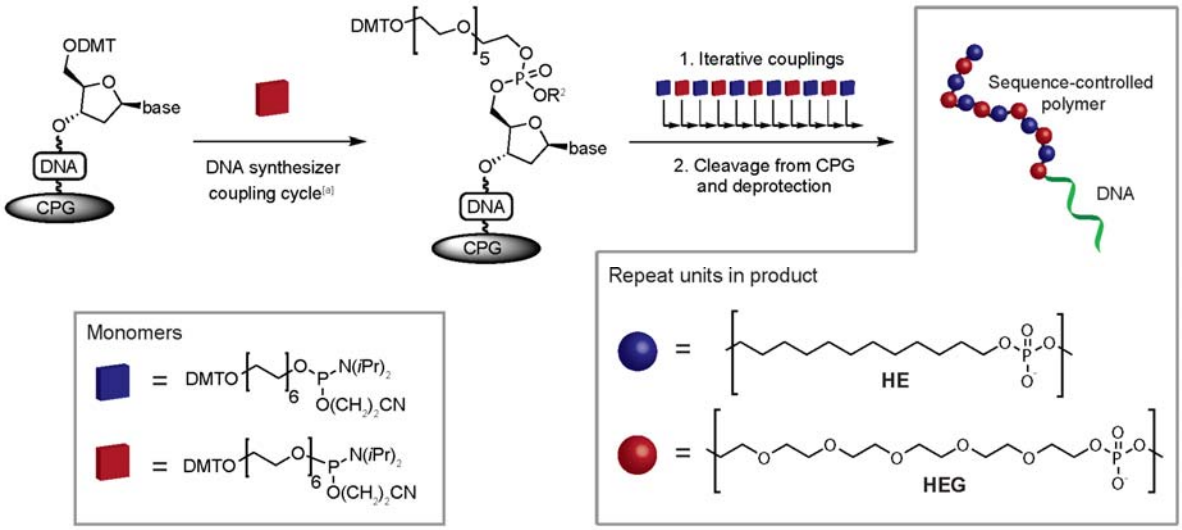

Figure 3.1 - Synthetic methodology for DNA-polymer conjugates. Monomer phosphoramidites (blue and red squares) are coupled to the 5' end of the oligonucleotide on the controlled-pore glass support (CPG) in a stepwise fashion. This produces sequence-defined products with repeat units **HE** and **HEG** (blue and red spheres). (Synthetic details can be found in the *Experimental Section 3.5.3*)

3.3 Results and Discussion

3.3.1 Synthesis and characterization of HE_x-DNA

Figure 3.1 illustrates the general synthetic route for DNA-polymer conjugates using phosphoramidite chemistry.[25] In each case, an oligonucleotide of mixed sequence, comprising of 19 nucleotides, was first synthesized on the solid support using standard automated procedures (*Experimental Section, 3.5.3*). Next, short oligomers of well-known polymers were appended to the oligonucleotide chain, using the same automated phosphoramidite chemistry.

Initially, commercially available dimethoxytrityl (DMT) protected dodecane-diol phosphoramidite was used, which corresponds to a hexameric section of poly(ethylene) – here labelled **HE**, hexaethylene – for the subsequent coupling steps. The resulting DNA-polymer conjugate would therefore consist of a DNA portion functionalised at its 5' terminus with a series of **HE** units punctuated by phosphates. To probe the synthetic limit of the length of these polymeric modifications to the 5' terminus of the DNA strand, molecules with 1 to 12 successive additions of **HE** units were first synthesized.

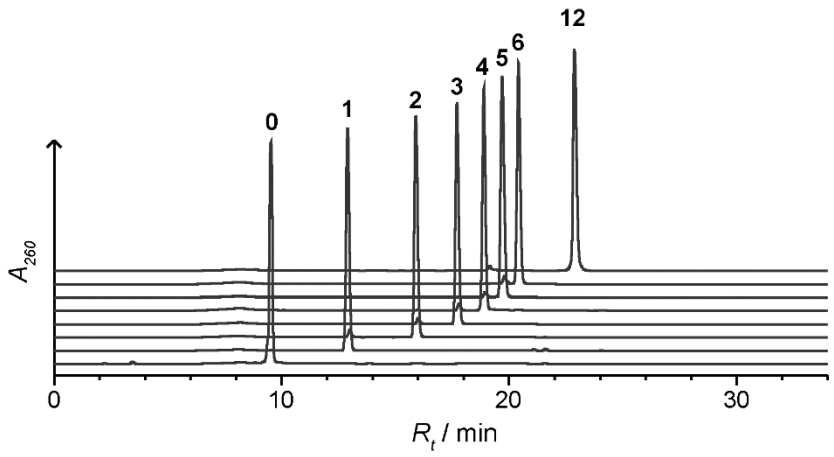

Figure 3.2 - Reverse-phase HPLC traces of purified HE_x-DNA conjugates. Bold numbers above each peak refer to the number of **HE** units appended to the 5' terminus of the oligonucleotide. The relationship between number of **HE** units and retention time is logarithmic. (Crude traces can be found in the Experimental section 3.5.5).

Since the coupling efficiency remains excellent (>97%), it is surely possible to generate much longer polymers, however this initial study was limited to twelve units,

due to the ease of division into blocks for sequence definition (vide infra). The synthesized DNA block copolymers were cleaved from the solid support and the protecting groups were removed under basic conditions (28% ammonia solution, room temperature, overnight). Analysis of the crude mixtures by reverse-phase HPLC (*Experimental Section, 3.5.4*) revealed a narrow product distribution where the target molecule constituted 74-89% of the isolated DNA, a much greater yield than generally found in couplings of full-length polymers to DNA strands. Reverse-phase HPLC analysis of the products (Figure 3.2) revealed increasing retention time with number of **HE** blocks, consistent with an increase in hydrophobicity with each addition of **HE** blocks to the 5' terminus of the oligonucleotide. The identity of the modified oligonucleotides was confirmed by electrospray mass spectrometry (ESI-MS), Table 1, and matrix-assisted laser desorption ionisation mass spectrometry (MALDI-MS) (*Experimental Section, 3.5.6*).

Table 3.1 - ESI-MS characterization and percent yields of HE-DNA conjugates. [a] Attached to the 5' terminus of DNA sequence TTTTTCAGTTGACCATATA [b] Percentage fraction of total DNA isolated (see Experimental section, 3.5.4 for further details)

Conjugate[a]	Product distribution [%][b]	Calculated mass [Da]	Mass found [Da]
HE_1	89	6029.14	6029.13
HE_2	85	6293.29	6293.29
HE_3	86	6557.44	6557.45
HE_4	84	6821.59	6821.61
HE_5	83	7085.74	7085.69
HE_6	83	7349.88	7349.83
HE_{12}	74	8934.78	8934.68

3.3.2 Self-assembly of HE_x-DNA

With the **HE_x-DNA** molecules characterized, the self-assembly behavior of these block copolymer-like DNA amphiphiles was investigated, to confirm whether the phosphate-punctuated **HE** section would behave as a hydrophobic polymer. To probe the self-assembly in solution, DLS was used to determine the presence, and hydrodynamic radius, of micellar aggregates.

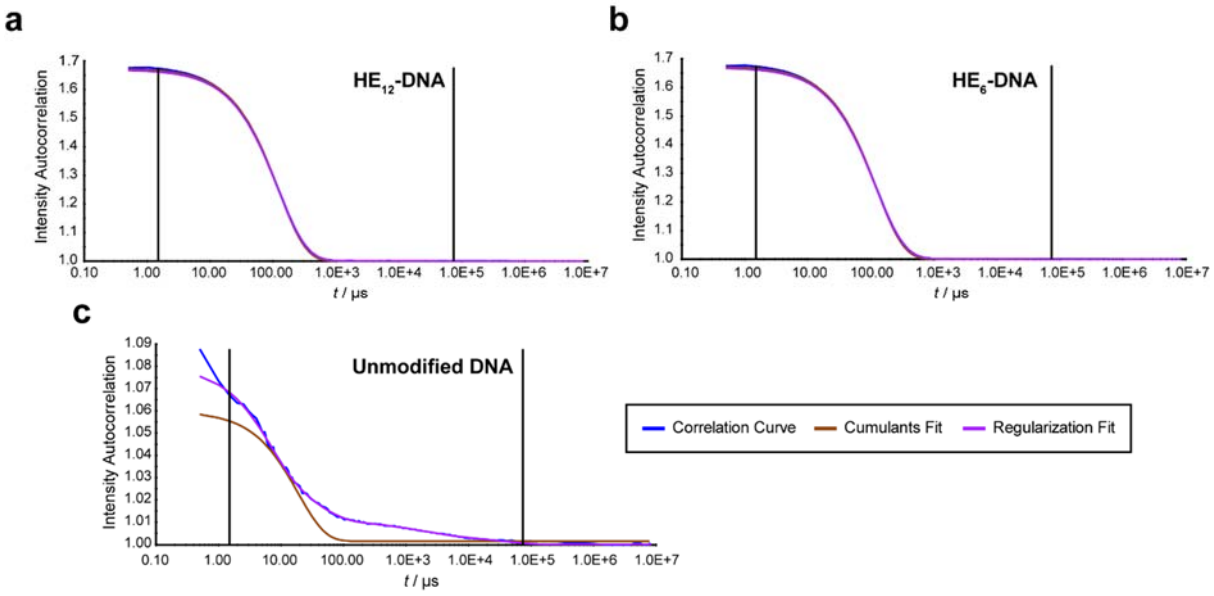

Figure 3.3 - Dynamic light scattering analysis of HE_x-DNA. Representative DLS intensity correlation functions for 10µM solutions of, a) **HE_{12}-DNA** micelles and b) **HE_6-DNA** micelles in comparison to c) unmodified **DNA** control. The low scattering intensity and poor correlation functions measured for **DNA** is characteristic of individual molecules in solution. In contrast the data for **HE_{12}-DNA** and **HE_6-DNA** reveals excellent correlation and higher scattering intensity due to the presence of aggregates.

It was found that the **HE_x-DNA** containing five or less **HE** units existed as discrete molecules at 10 µM in magnesium containing buffer, indicated by poor scattering intensities (Figure 3.3). However, for **HE_6-DNA** scattering correlating to a sphere with an R_h of 6.5 ± 0.4 nm was observed, Table 3.2. This size correlates with DNA-based spherical micelles and is consistent with the tight packing of the **HE** chains in a hydrophobic core with a charged corona made up of DNA.[19] Assuming a linear DNA geometry (6.1 nm), this result suggests that the **HE_6** chain (1.9 nm/unit if stretched) is folded on itself multiple times, potentially adopting a 'concertina' structure analogous to that of phospholipid bilayers. **HE_{12}-DNA** under the same conditions revealed an R_h

of 11.3 ± 0.1 nm, implying that the **HE$_{12}$** chain is more extended. Spherical morphology, monodispersity, and relative size of micelles was confirmed by AFM, shown in Figure 3.4. Thermal and electrophoretic hybridization studies (*Experimental sections, 3.5.8-9*) concluded that all of the **HE$_x$-DNA** molecules retained their ability to hybridize to a complementary DNA strand, highlighting the orthogonal nature of these modes of intermolecular self-assembly.

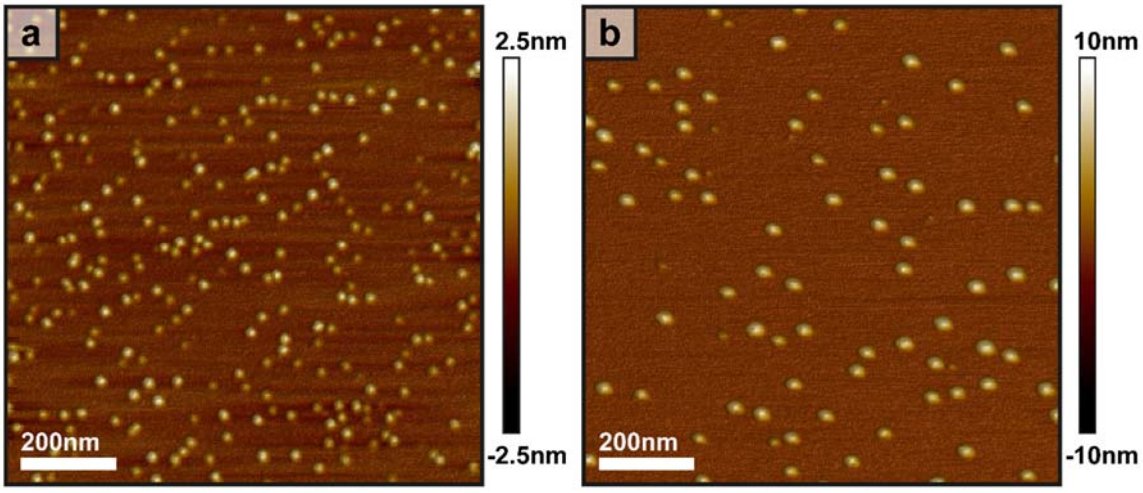

Figure 3.4 - Atomic force microscopy of DNA-polymer micelles. Shown are a) **HE$_6$-DNA** micelles and b) **HE$_{12}$-DNA** micelles in air (Additional images can be found in the Experimental Section).

To further show that the behavior of the conjugates was in line with block copolymer assembly, encapsulation of guest molecules within the hydrophobic core of the micelles was performed using Nile Red, a fluorescent dye which displays significant fluorescence in hydrophobic media, but negligible emission in aqueous solution.[26] An increase in fluorescence was observed with increasing number of **HE** units in a 10μM aqueous solution of the DNA conjugates, showing the expected dependence of the self-assembled macromolecular structure on the component molecular structure.

It was therefore concluded that through phosphoramidite coupling, DNA-poly(ethylene) conjugate mimics were produced in good yields with total control over the degree of polymerization (up to 72 units), leading to molecularly monodisperse products. The presence of phosphate moieties in the polymer backbone does not hinder

the hydrophobic properties of the polymer section, producing spherical micelles capable of encapsulating guests.

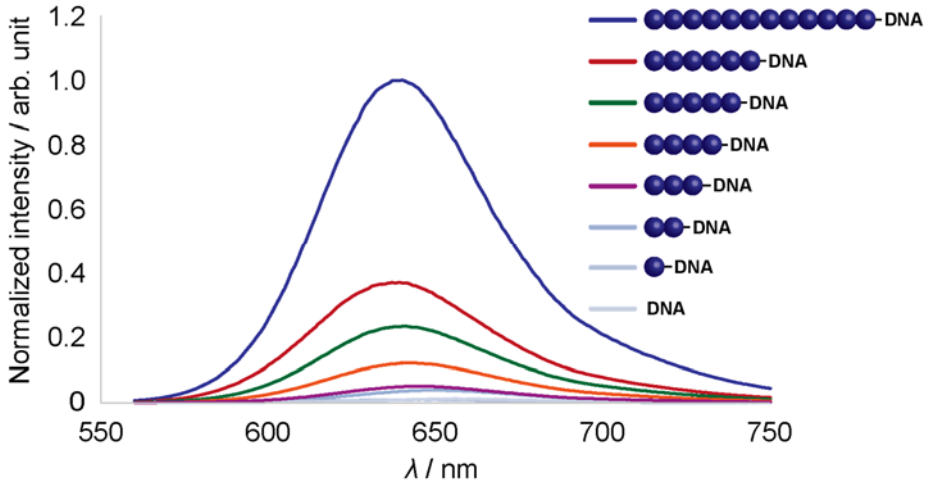

Figure 3.5 – Nile Red encapsulation assay for HE_x-DNA. Fluorescence of Nile Red in the presence of 10μM **HE_x-DNA**. Blue spheres are **HE** blocks; fluorescence increases with the number of blocks.

3.3.3 Synthesis and characterization of HE/HEG series

Since the stepwise synthetic protocol is inherently sequential, it was decided to explore whether a mixed system of hydrophobic **HE** blocks and hydrophilic hexaethylene glycol (**HEG**, also available as a commercial DMT-protected phosphoramidite reagent) blocks could be synthesized, and what self-assembly properties the resultant sequenced polymers might exhibit. Five different modified oligonucleotides, each containing a 5' modification of 12 units in length (six **HE**, six **HEG**) were successfully synthesized. Each of these DNA strands differs in the pattern of the **HE** and **HEG** units, being grouped into blocks of one, two, three, and six oligomers. For the blocks of six, the position with respect to the DNA was also varied, producing two triblock architectures, **HEG_6-HE_6-DNA** and **HE_6-HEG_6-DNA**.

Table 3.2 - ESI-MS characterization and percent yields of HE/HEG-DNA conjugates. [a] Attached to the 5' terminus of DNA sequence TTTTTCAGTTGACCATATA [b] Percentage fraction of total DNA isolated (see Expoerimental section for further details)

Conjugate[a]	Product distribution [%][b]	Calculated mass [Da]	Mass found [Da]
$(HE\text{-}HEG)_6$	51	9414.63	9414.60
$(HE_2\text{-}HEG_2)_3$	62	9414.63	9414.58
$(HE_3\text{-}HEG_3)_2$	56	9414.63	9414.58
$HE_6\text{-}HEG_6$	67	9414.63	9414.58
$HEG_6\text{-}HE_6$	78	9414.63	9414.60

These modifications were synthesized under the same automated conditions as described for the **HE_x-DNA** versions and reverse-phase HPLC ascertained that one major product was obtained for all sequences, in contrast to a non-sequenced control, shown here in Figure 3.6.

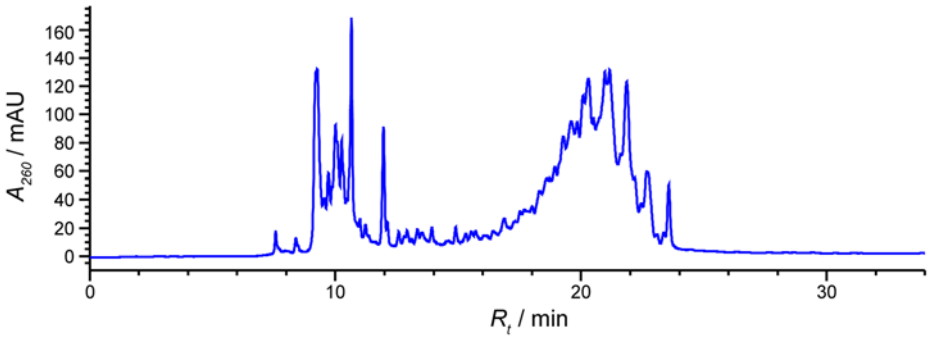

Figure 3.6 – Reverse-phase HPLC on random sequence control. This statistical copolymer modification was made by performing 12 couplings at the 5' terminus of the 19mer oligonucleotide using a 1:1 (w/w) mixture of DMT-hexaethyloxy glycol and DMT-dodecane-diol amidites. The DMT^+ response revealed high coupling efficiency of all 12 random units. The HPLC trace above shows a major distribution of products centered on the retention times seen for the 12 unit sequenced products shown in Figure 3.7.

Typically, the best coupling efficiency occurs when the added monomer is the same as the one before. It is anticipated that coupling protocols for monomer crossover can be optimized through longer coupling times, increased monomer concentration, or

solvent choice. A gradual increase in retention time on the HPLC column was observed as block size increased from one in **(HE-HEG)$_6$** to six in **HE$_6$-HEG$_6$** (Figure 3.7a), indicating a gradual increase in overall hydrophobicity. This may be due to the fact that a minimal number of adjacent **HE** are needed to create a hydrophobic pocket that is available for interaction with the stationary phase, whereas hydrophilic groups flanking each **HE$_x$** block may diminish strong interactions with the stationary phase.

Another variable in the block pattern that affects the hydrophobic behavior is the position of the **HE** and **HEG** blocks with respect to the hydrophilic oligonucleotide; this is evident when comparing the molecules **HE$_6$-HEG$_6$-DNA** and **HEG$_6$-HE$_6$-DNA** (Figure 3.7b). In terms of the amphiphilicity of the different block patterns, **HE$_6$-HEG$_6$-DNA** is a typical amphiphile with a distinct hydrophilic **DNA-HEG** block and a hydrophobic **HE** terminus. The bola-amphiphilic **HEG$_6$-HE$_6$-DNA** may adopt a structure in which the oligonucleotide and the **HEG** blocks are more capable of shielding the **HE** portion from the aqueous medium.

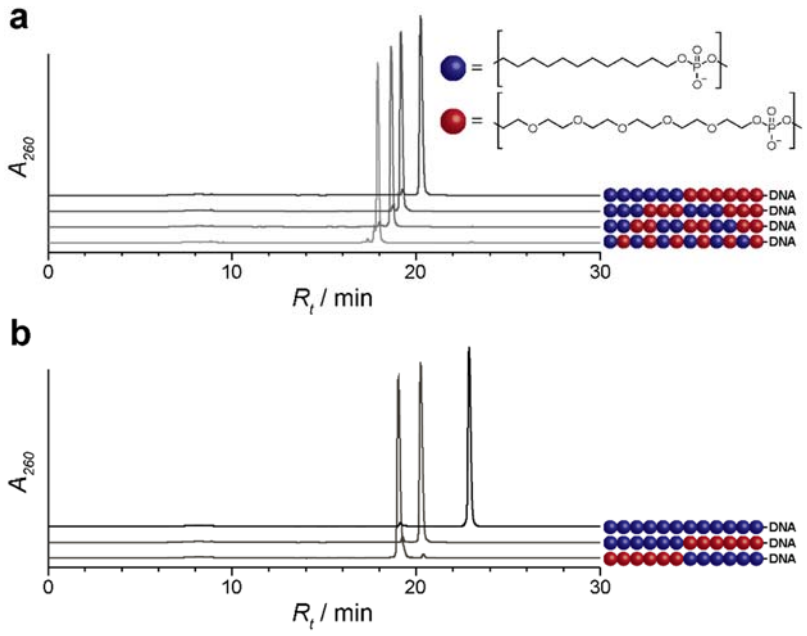

Figure 3.7 –Reverse-phase HPLC traces of sequence defined HE-HEG polymers. a) **HE/HEG** block sizes from 1 to 6. b) **HE/HEG** block positions for **HE$_6$-HEG$_6$-DNA** and **HEG$_6$-HE$_6$-DNA** with respect to the DNA portion (Crude traces are available in the Experimental Section 3.5.5)

To investigate the effect of block pattern on the amphiphilic self-assembly in solution, DLS measurements were carried out for the **HE/HEG** series, revealing that the trends in hydrophobicity observed by HPLC were amplified under self-assembly conditions. The strands with polymer sequences **(HE-HEG)$_6$**, **(HE$_2$-HEG$_2$)$_3$**, and **(HE$_3$-HEG$_3$)$_2$** did not exhibit self-assembly at this concentration. However strong scattering was seen for **HE$_6$-HEG$_6$-DNA** with an associated R_h of 9.7 ± 0.9 nm, although not for **HEG$_6$-HE$_6$-DNA**. It should be noted that AFM characterization was also attempted for **HE$_6$-HEG$_6$-DNA** but was less conclusive than for the **HE** system, this is likely due to different surface adsorption properties which may be mediated by the addition of **HEG** blocks (*Experimental section 3.5.13-14*).

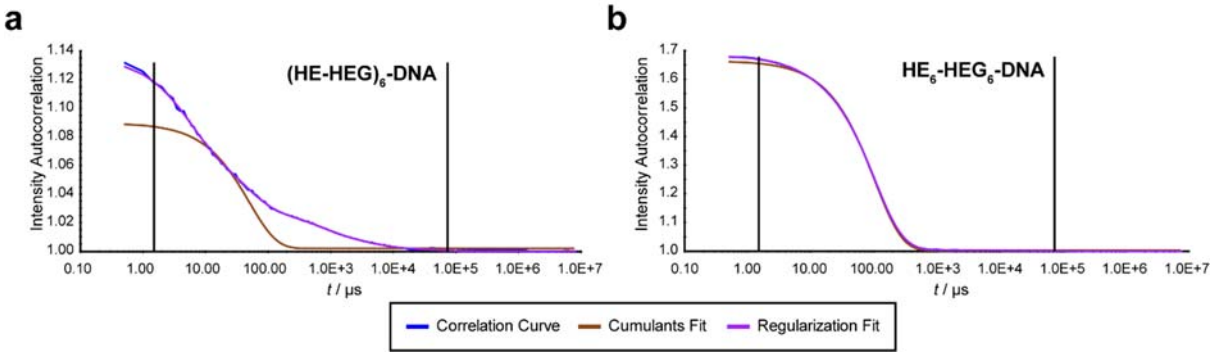

Figure 3.8 - Dynamic light scattering analysis of HE/HEG series. Representative DLS intensity correlation functions for 10µM solutions of, a) non-aggregating **(HE-HEG)$_6$-DNA** and b) **HE$_6$-HEG$_6$-DNA** micelles. The low scattering intensity and poor correlation functions measured for **(HE-HEG)$_6$-DNA** is characteristic of individual molecules in solution. In contrast, **HE$_6$-HEG$_6$-DNA** reveals excellent correlation and higher scattering intensity due to the presence of micelles.

Firstly, the DLS observations lend further weight to the hypothesis that a minimum block size of **HE$_6$** is required to exhibit significant hydrophobic character. Furthermore, the effect of the positioning of the blocks with respect to the oligonucleotide portion is also a major factor in the self-assembly: the terminal **HE$_6$** results in micellization, whereas a central **HE$_6$** block prevents aggregation. Again, thermal and electrophoretic hybridization experiments confirmed the availability of the DNA (Experimental section).

The sequence-specific self-assembly was also assessed using encapsulation of Nile Red (Figure 3.9). In this case a small increase in fluorescence was seen as the block size

increased from one to three **HE** units, consistent with a degree of intramolecular collapse of adjacent **HE** units, generating progressively larger hydrophobic domains as the block size increases, akin to beads on a string. At a block size of six, both of the DNA-sequence

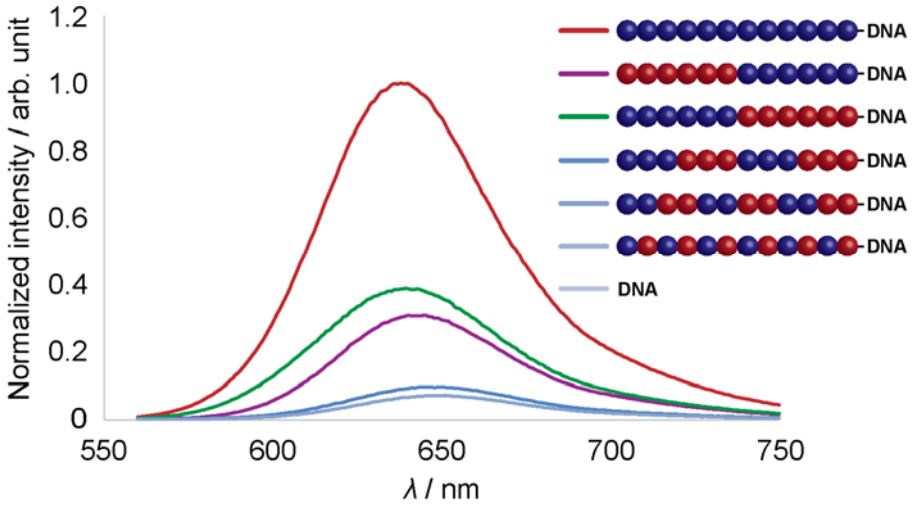

Figure 3.9 – Nile Red encapsulation assay for HE/HEG series. Fluorescence of Nile Red in the presence of 10μM **HE/HEG** sequenced modifications. Increasing intensity is observed with increasing block size. Blue spheres; hydrophobic **HE**, red spheres; hydrophilic **HEG**.

polymers displayed a similar level of Nile Red fluorescence, although that of **HEG$_6$-HE$_6$-DNA** was slightly lower. A small, but reproducible, red shift of the maximum emission from the bola-amphiphile (640 nm) with respect to the linear amphiphile (645 nm) was also observed, which is indicative of Nile Red in a more polar environment.[27] This is consistent with an intermolecular spherical micelle formed by **HE$_6$-HEG$_6$-DNA**, and an intramolecular hydrophobic domain being formed in **HEG$_6$-HE$_6$-DNA**, resulting in a lower volume-to-surface area ratio, and more exposure of the dye to the solvent.

Finally, the reversibility of the self-assembly process was investigated using DLS, Figure 3.10. It was found that the presence of Mg^{2+} was required for micelle formation and could be used to 'switch on' and 'off' the aggregation. Upon addition of Mg^{2+} to a solution of discrete **HE$_6$-DNA**, **HE$_{12}$-DNA** or **HE$_6$-HEG$_6$-DNA** strands, assembly was observed by DLS within 45 seconds. Furthermore, addition of EDTA to sequester Mg^{2+}

was found to cause de-aggregation over the course of 30 seconds. In both cases, non-assembling sequence **HEG$_6$-HE$_6$-DNA** showed no change.

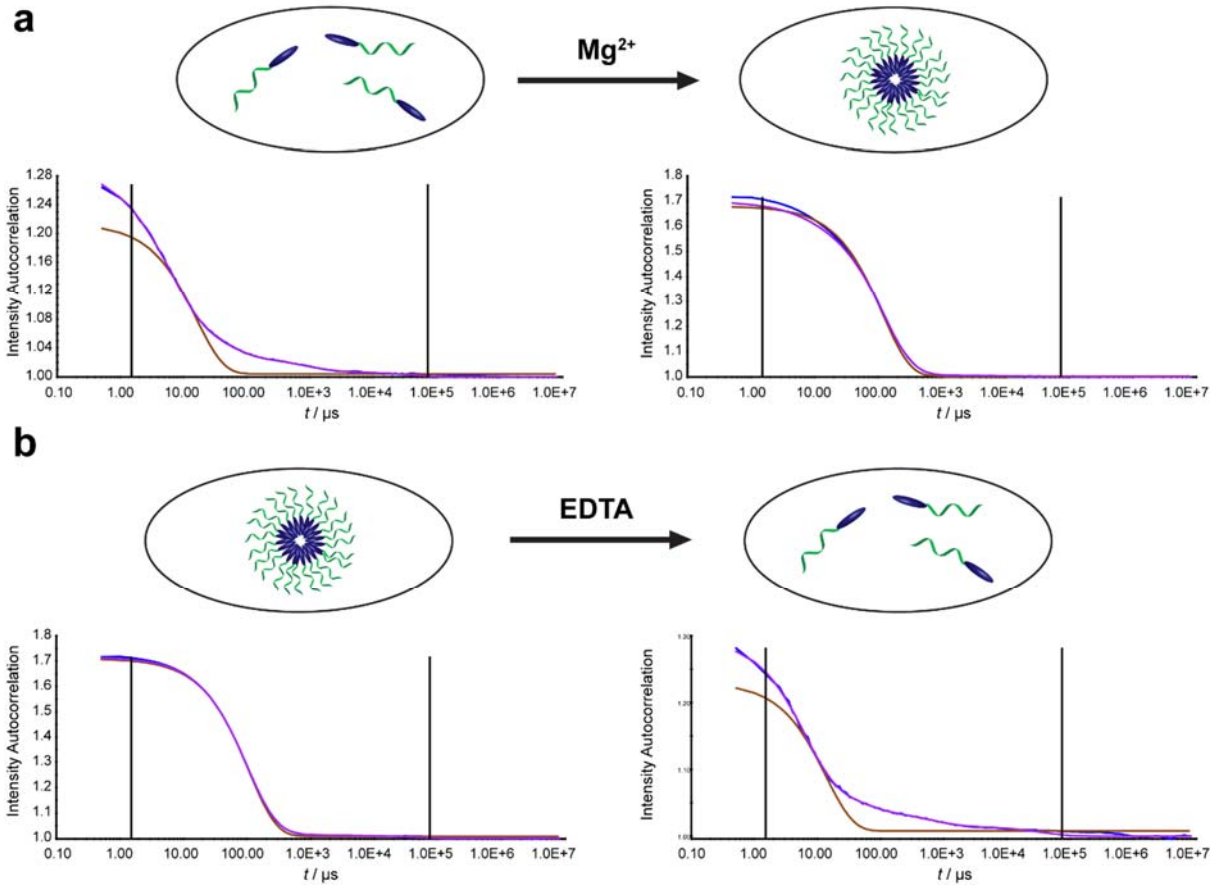

Figure 3.10 – Micellization and de-aggregation of HE$_{12}$-DNA. a) DLS intensity correlation functions for a 10µM solution of **HE$_{12}$-DNA** before and after addition of Mg^{2+} which induces micellization. B) The reverse process is shown, using EDTA to sequester Mg^{2+} ions and denature pre-formed micelles which require Mg^{2+} for assembly due to electrostatic repulsion of the negativity charge phosphates groups. The same experiment on other samples and additional details can be found in the Experimental section 3.5.12.

3.4 Conclusions

In conclusion, this chapter describes a facile and high-yielding procedure for the production of monodisperse amphiphilic DNA block copolymers using standard automated techniques and commercially available materials. Such materials have been previously extremely difficult to obtain in good purity, yield, and with reliable characterization. Secondly, it has been shown that the same procedure can easily be

used to create synthetic sequence-defined polymers, and that the variation in the overall hydrophobicity, self-assembly, and encapsulation properties can be logically altered by variation of the sequence. Control of sequence-specific hydrophobic intra- or intermolecular aggregation within a polymer is an important result: the same process is a major determinant of protein folding, and by mirroring that assembly here, the stage is set for synthetic mimics of the complex structures and functions exhibited by biological sequenced polymers.[28,29] The methods reported are accessible to any researcher with the capacity for oligonucleotide synthesis, and in principle the scope extends far beyond the **HE** and **HEG** components used here – other diols can be converted into a DMT-phosphoramidite reagent and used similarly. Importantly, many functional groups, such as amides, aryl halides, ethers, disulfides, maleimides, alkenes, alkynes and protected amines are compatible with phosphoramidite coupling, Oligonucleotide strands of up to 100 additions can typically be produced with standard equipment, and since the coupling efficiency is excellent, the same maximum lengths can be expected. This synthetic method has the potential to produce new oligonucleotide conjugates for use in therapeutics, as supramolecular foldamers or simple protein mimics for the study of complex self-assembly mediated by hydrophobic, and other supramolecular interactions.

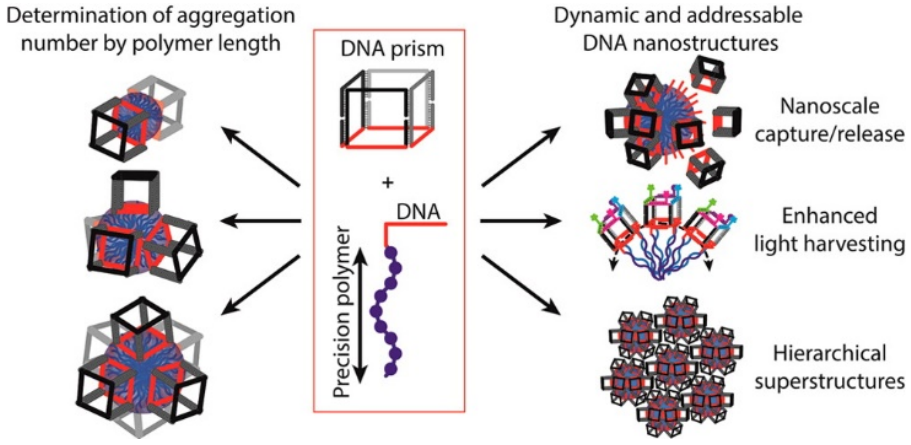

Figure 3.11 – Combination of the approaches described in chapters 2 and 3. The varying length **HE$_x$-DNA** described in this chapter have been applied to create a hierarchy of 3D-DNA nanostructure/polymer hybrids. (American Chemical Society, 2014)

Additionally, the organization of the polymer-DNA conjugates described in this chapter on 3D structures was explored in a similar manner to the **D-DNA** in chapter 2.[30]

This involved the combination of three modular approaches; 1) A selection of prismatic 3D DNA scaffolds with different geometries, 2) Site-specific organization of different number of DNA-polymers on each of the prisms, and 3) Control over the exact length of that DNA-polymer (e.g. **HE$_1$-HE$_{12}$**) and therefore the self-assembly properties. This appraoch gave access to hierarchical family of nanostructures which are shown in summary in Figure 3.11. These were shown to allow controlled capture and release of individual nanostructures and act as scaffolds for efficient light harvesting antennae. This work was published as "Precision Polymers and 3D DNA Nanostructures: Emergent Assemblies from New Parameter Space." Serpell, C. J., Edwardson, T. G. W., Chidchob, P., Carneiro, K. M. M. & Sleiman, H. F. *J. Am. Chem. Soc.* **2014**, 136, 15767-15774.

Author contributions are stated here for clarity as this publication is not a major inclusion in this thesis.

Christopher J. Serpell helped develop the project and primarily contributed to the production of experimental data and writing of the paper. **Thomas G.W. Edwardson** designed and synthesized DNA-polymer conjugates, clip strands and prism linking strands. **Pongphak Chidchob** carried out AFM analysis and helped write the paper. **Karina M.M. Carneiro** assisted in DNA-polymer conjugate synthesis. **Hanadi F. Sleiman** designed the project, guided interpretation of data, discussion of results and concepts and co-wrote the paper.

3.5 Experimental

3.5.1 General

Magnesium acetate, acetic acid, tris(hydroxymethyl)-aminomethane (Tris), formamide, urea and Nile Red were used as purchased from Sigma-Aldrich. Acetic acid and boric acid were purchased from Fisher Scientific and used without further purification. GelRed™ nucleic acid stain was purchased from Biotium Inc. Acetone ACS reagent grade was purchased from Fisher. Ammonium citrate dibasic and 3-hydroxypicolinic acid were purchased from Aldrich. Acrylamide/Bis-acrylamide (40% 19:1 solution) and TEMED were obtained from Bioshop Canada Inc. and used as supplied. 1 μmol Universal 1000Å LCAA-CPG supports and standard reagents used for automated DNA synthesis were purchased through Bioautomation. Sephadex G-25 (super fine, DNA grade) was purchased from Glen Research. 1xTAMg buffer is composed of 45 mM Tris and 12.5 mM $Mg(OAc)_2 \cdot 6H_2O$ with pH adjusted to 8.0 using glacial acetic acid. TBE buffer is 90mM Tris, 90mM boric acid and 1.1mM EDTA with a pH of 8.0.

3.5.2 Instrumentation

Standard automated oligonucleotide solid-phase synthesis was performed on a Mermade MM6 synthesizer from Bioautomation. HPLC purification was carried out on an Agilent Infinity 1260. DNA quantification measurements were performed by UV absorbance with a NanoDrop Lite spectrophotometer from Thermo Scientific. A Varian Cary 300 Bio spectrophotometer was used for melting temperature studies. Gel electrophoresis experiments were carried out on a 20 X 20 cm vertical Hoefer 600 electrophoresis unit. Gel images were captured using a ChemiDoc™ MP System from Bio-Rad Laboratories. Thermal annealing of all DNA structures was conducted using an Eppendorf Mastercycler® 96 well thermocycler. Mass determination was carried out using Matrix-Assisted Laser Desorption/Ionization Time-Of-Flight Mass Spectrometry (MALDI-TOF-MS) on a Bruker Autoflex™ III MALDI-TOF mass spectrometer. Liquid Chromatography Electrospray Ionization Mass Spectrometry (LC-ESI-MS) was carried out using Dionex Ultimate 3000 coupled to a Bruker MaXis Impact™ QTOF. Fluorescence emission spectra were obtained using an Agilent Cary Eclipse Fluorescence Spectrophotometer.

3.5.3 Oligonucleotide synthesis

DNA synthesis was performed on a 1 μmole scale, starting from a universal 1000 Å LCAA-CPG solid-support. Coupling efficiency was monitored after removal of the dimethoxytrityl (DMT) 5′-OH protecting groups. DMT-dodecane-diol (cat.# CLP-1114) and DMT-hexaethyloxy glycol (cat.# CLP-9765) phosphoramidites were purchased from Chemgenes. DMT-hexaethyloxy glycol and DMT-dodecane-diol amidites were dissolved in the appropriate solvent under a nitrogen atmosphere in a glove box (<0.04 ppm oxygen and <0.5 ppm trace moisture). For DMT-hexaethyloxy glycol (0.1M, anhydrous acetonitrile) and DMT-dodecane-diol (0.1M, anhydrous dichloromethane) amidites extended coupling times of 5 minutes were used respectively using 0.25M 5-(ethylthio)tetrazole in anhydrous acetonitrile. Removal of the DMT protecting group was carried out using 3% dichloroacetic acid in dichloromethane on the DNA synthesizer. Completed syntheses were cleaved from the solid support and deprotected in 28% aqueous ammonium hydroxide solution for 16-18 hours at room temperature. The crude product solution was separated from the solid support and concentrated under reduced pressure at 60^{o}C. This crude solid was re-suspended in 1mL Millipore water. Sephadex G-25 column and 0.22μm centrifugal filter were then performed prior to HPLC purification. The resulting solution was quantified by absorbance at 260nm.

Table 3.3 - Sequences used for DNA amphiphiles. Atypical amidite codes: (**D**= dodecane-diol), (**H**= hexaethyloxy glycol).

Molecule	Sequence (5'-xx-3')
DNA	TTTTTCAGTTGACCATATA
HE$_1$-DNA	**D**TTTTTCAGTTGACCATATA
HE$_2$-DNA	**DD**TTTTTCAGTTGACCATATA
HE$_3$-DNA	**DDD**TTTTTCAGTTGACCATATA
HE$_4$-DNA	**DDDD**TTTTTCAGTTGACCATATA
HE$_5$-DNA	**DDDDD**TTTTTCAGTTGACCATATA
HE$_6$-DNA	**DDDDDD**TTTTTCAGTTGACCATATA
HE$_{12}$-DNA	**DDDDDDDDDDDD**TTTTTCAGTTGACCATATA
(HE-HEG)$_6$-DNA	**DHDHDHDHDHDH**TTTTTCAGTTGACCATATA

$(HE_2\text{-}HEG_2)_3$-DNA	**DDHHDDHHDDHH**TTTTTCAGTTGACCATATA
$(HE_3\text{-}HEG_3)_2$-DNA	**DDDHHHDDDHHH**TTTTTCAGTTGACCATATA
$HE_6\text{-}HEG_6$-DNA	**DDDDDDHHHHHH**TTTTTCAGTTGACCATATA
$HEG_6\text{-}HE_6$-DNA	**HHHHHHDDDDDD**TTTTTCAGTTGACCATATA
Acomp	TATATGGTCAACTG

3.5.4 HPLC purification

Solvents (0.22µm filtered): 50mM triethylammonium acetate (TEAA) buffer (pH 8.0) and HPLC grade acetonitrile. Elution gradient: 3-70% acetonitrile over 30 minutes at 60ºC. Column: Hamilton PRP-C18 5µm 100 Å 2.1 x 150mm. For each analytical separation approximately 0.5 OD_{260} of crude DNA was injected as a 20-50µL solution in Millipore water. Detection was carried out using a diode-array detector, monitoring absorbance at 260nm. Retention times and yields (obtained from peak area integration) for the products are summarized in Table 3.4.

Table 3.4 - HPLC data summary for all compounds. The product distribution presented is the percentage of desired product with reference to the total DNA cleaved from the solid support (capped failure sequences). This was determined by peak area integration of the HPLC traces. For this reason the unmodified DNA is not stated as the RP-HPLC did not distinguish clearly between n-1 of natural nucleosides. The isolated yield presented represents the total isolated OD_{260} from each 1µmol scale synthesis of DNA based on a 98% coupling efficiency.

Molecule	Product distribution / %	Retention time / min.	Isolated Yield / %
DNA	n/a	~ 9.5	31
HE_1-DNA	89	13.0	33
HE_2-DNA	85	16.0	31
HE_3-DNA	86	17.7	32
HE_4-DNA	84	18.9	31
HE_5-DNA	83	19.7	31
HE_6-DNA	83	20.5	31
HE_{12}-DNA	74	22.9	27
$(HE\text{-}HEG)_6$-DNA	51	18.6	19
$(HE_2\text{-}HEG_2)_3$-DNA	62	19.4	23
$(HE_3\text{-}HEG_3)_2$-DNA	56	19.9	21

HE_6-HEG_6-DNA	67	21.0	25
HEG_6-HE_6-DNA	78	19.8	29

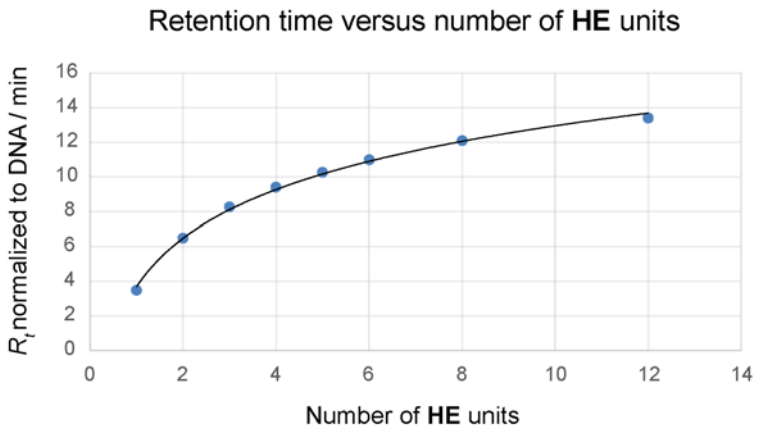

Figure 3.12 - Relationship between C12 blocks and hydrophobicity. For the homopolymeric **HE** modifications (1-12) a plot of number of units versus the retention time shows a logarithmic trend (R^2 = 0.9974). This is expected as the longer the modification the less influence each additional block has on the overall hydrophobicity.

3.5.5 Crude HPLC traces

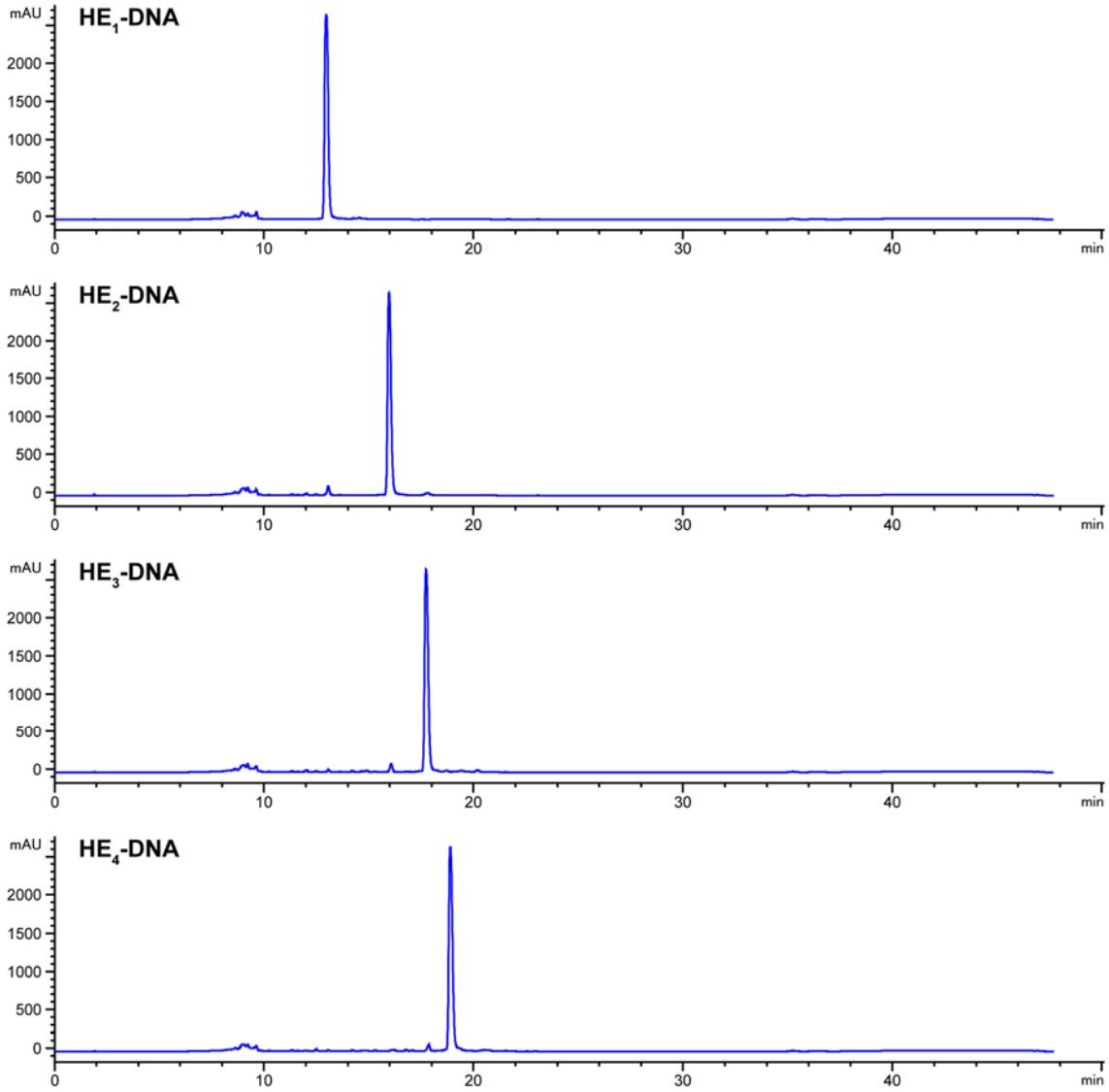

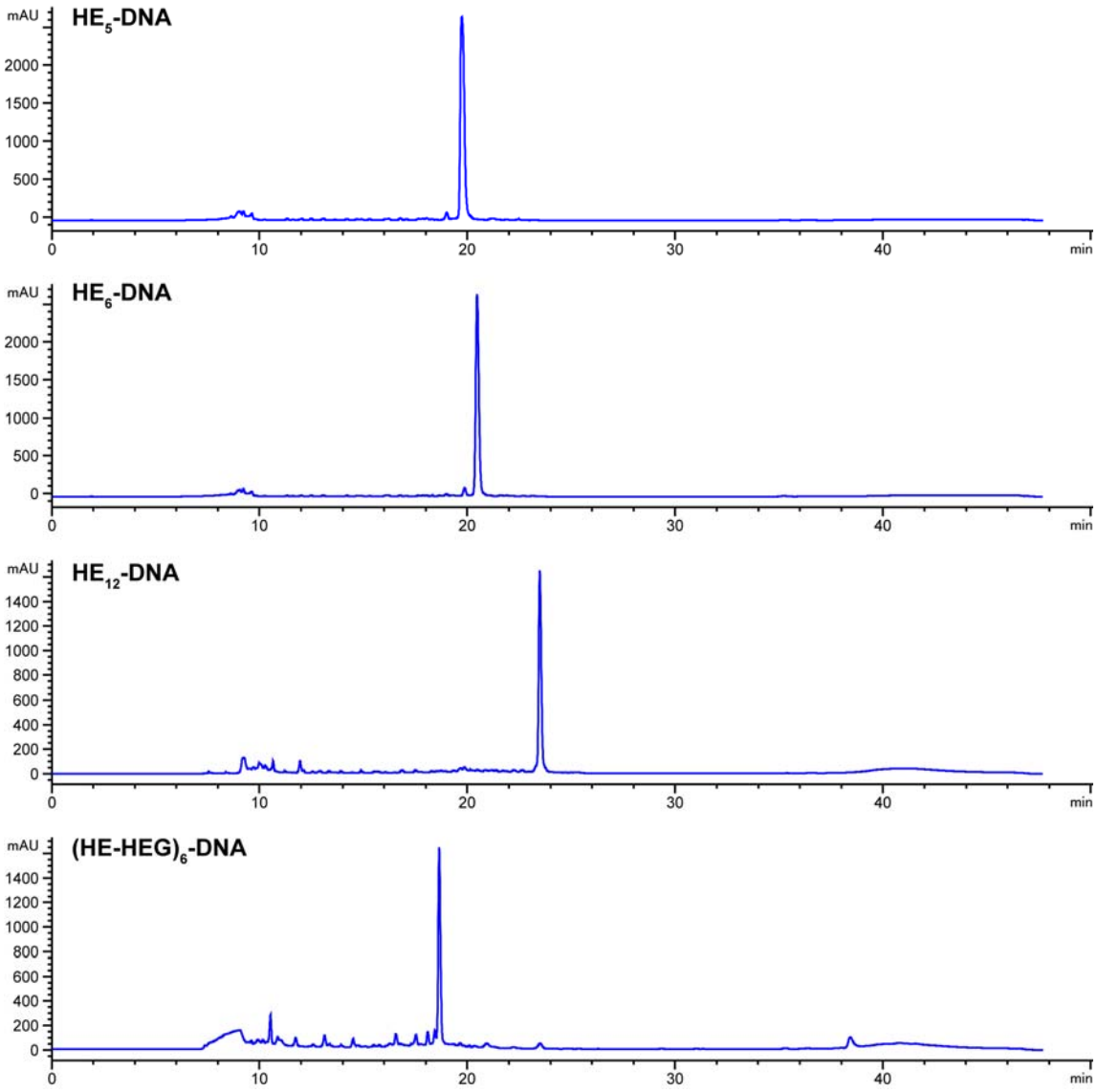
mAU
HE5-DNA
2000
1500
1000
500
0
0
10
20
30
40
min
mAU
HE6-DNA
2000
1500
1000
500
0
0
10
20
30
40
min
mAU
HE12-DNA
1400
1200
1000
800
600
400
200
0
0
10
20
30
40
min
mAU
(HE-HEG)6-DNA
1400
1200
1000
800
600
400
200
0
0
10
20
30
40
min

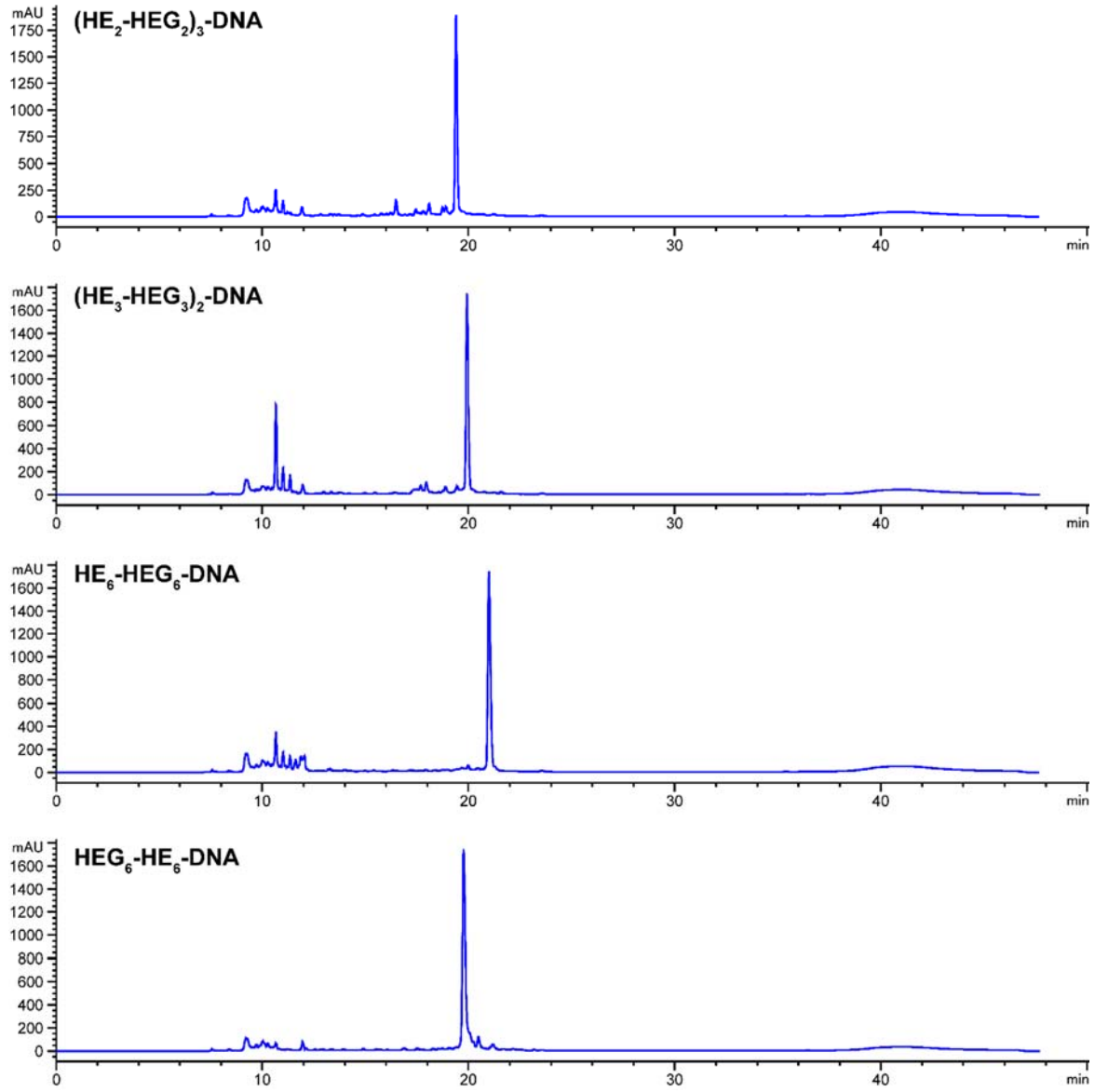
(HE2-HEG2)3-DNA
mAU
1750
1500
1250
1000
750
500
250
0
0
10
20
30
40
min
(HE3-HEG3)2-DNA
mAU
1600
1400
1200
1000
800
600
400
200
0
0
10
20
30
40
min
HE6-HEG6-DNA
mAU
1600
1400
1200
1000
800
600
400
200
0
0
10
20
30
40
min
HEG6-HE6-DNA
mAU
1600
1400
1200
1000
800
600
400
200
0
0
10
20
30
40
min

3.5.6 MALDI-MS characterization

The matrix solution was comprised of a 1:1 mixture of ammonium citrate solution (50mM, water) and 2,4,6-trihydroxyacetophenone solution (sat., MeCN) solution. In each case 1µL of a 50-100µM solution of HPLC purified DNA in Millipore water was mixed with 1µL of matrix solution. Between 0.5-1µL of this final solution was spotted on an AnchorChip™ and solvents were removed by air drying prior to mass determination. Analysis was carried out in linear negative mode. In each case, the masses observed for the DNA conjugates matched well with the calculated values.

Table 3.5 - MALDI-MS Table Calculated and experimental m/z values for all DNA conjugates synthesized.

Molecule	Calculated m/z ($[M-H]^-$)	Found m/z ($[M-H]^-$)
HE_1-DNA	6027.13	6024.84
HE_2-DNA	6292.28	6288.06
HE_3-DNA	6556.43	6551.91
HE_4-DNA	6820.58	6815.98
HE_5-DNA	7084.73	7080.73
HE_6-DNA	7348.87	7344.72
HE_{12}-DNA	8933.77	8931.10
$(HE\text{-}HEG)_6$-DNA	9413.62	9408.68
$(HE_2\text{-}HEG_2)_3$-DNA	9413.62	9410.85
$(HE_3\text{-}HEG_3)_2$-DNA	9413.62	9412.72
$HE_6\text{-}HEG_6$-DNA	9413.62	9412.00
$HEG_6\text{-}HE_6$-DNA	9413.62	9410.99

3.5.7 LC-ESI-MS characterization and data

The oligonucleotides were analyzed by LC-ESI-MS in negative ESI mode. Samples were run through an Acclaim RSLC 120 C18 column (2.2µM 120Å 2.1 x 50mm) using a gradient of 98% mobile phase A (100mM 1,1,1,3,3,3-hexafluoro-2-propanol and 5mM triethylamine in water) and 2 % mobile phase B (Methanol) to 40 % mobile phase A and 60% mobile phase B in 8 minutes. The data was processed and deconvoluted using the Bruker DataAnalysis software version 4.1.

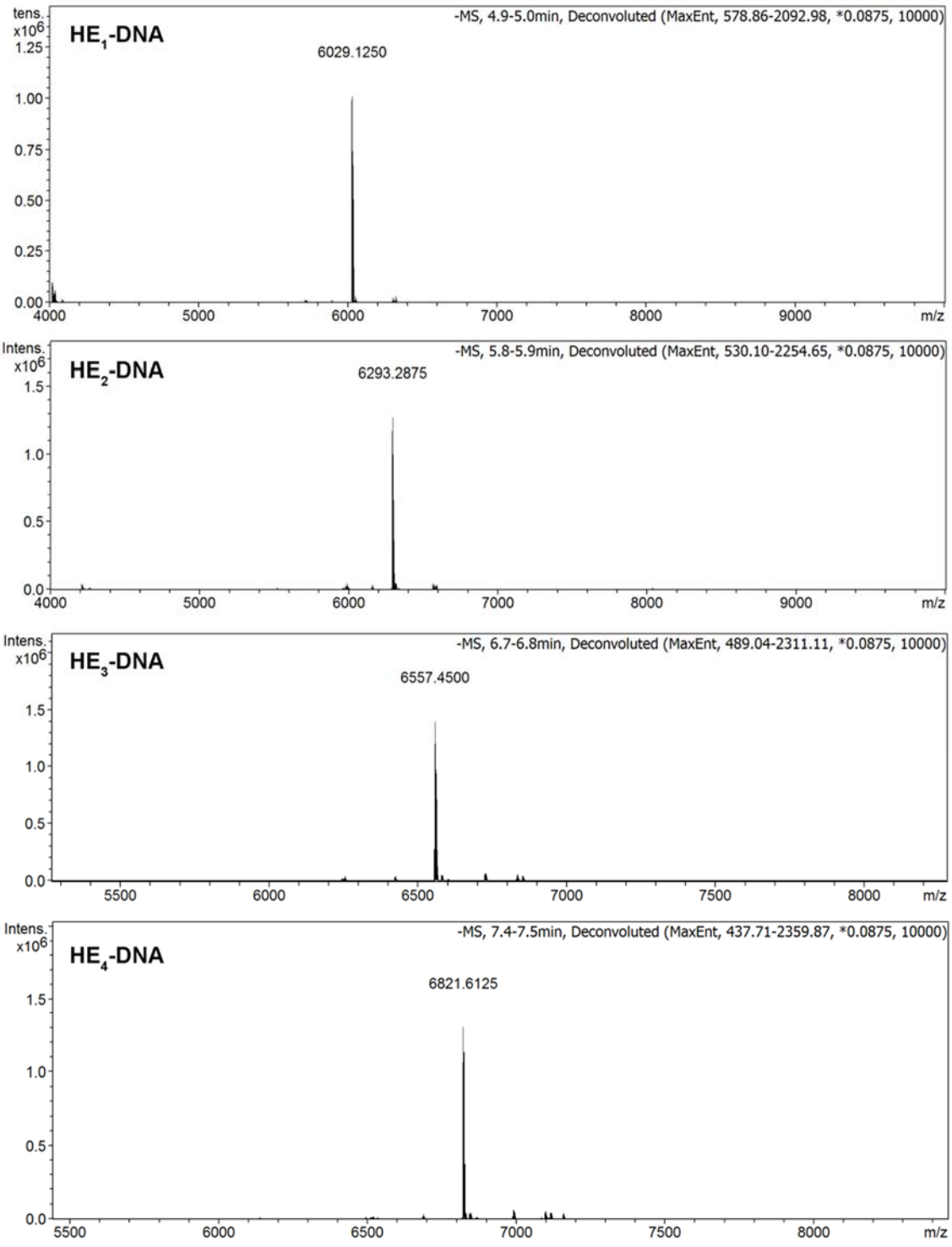
tens.
x10^6
HE1-DNA
-MS, 4.9-5.0min, Deconvoluted (MaxEnt, 578.86-2092.98, *0.0875, 10000)
6029.1250
1.25
1.00
0.75
0.50
0.25
0.00
4000
5000
6000
7000
8000
9000
m/z
Intens.
x10^6
HE2-DNA
-MS, 5.8-5.9min, Deconvoluted (MaxEnt, 530.10-2254.65, *0.0875, 10000)
6293.2875
1.5
1.0
0.5
0.0
4000
5000
6000
7000
8000
9000
m/z
Intens.
x10^6
HE3-DNA
-MS, 6.7-6.8min, Deconvoluted (MaxEnt, 489.04-2311.11, *0.0875, 10000)
6557.4500
1.5
1.0
0.5
0.0
5500
6000
6500
7000
7500
8000
m/z
Intens.
x10^6
HE4-DNA
-MS, 7.4-7.5min, Deconvoluted (MaxEnt, 437.71-2359.87, *0.0875, 10000)
6821.6125
1.5
1.0
0.5
0.0
5500
6000
6500
7000
7500
8000
m/z

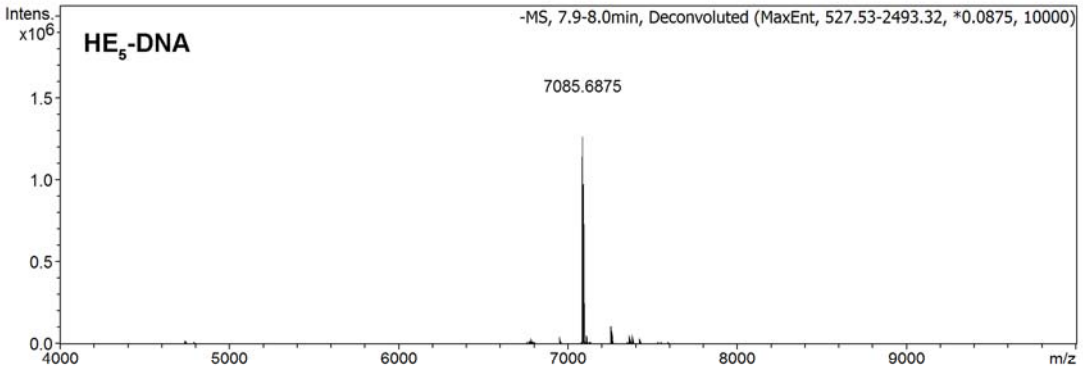
Intens.
x10^6
-MS, 7.9-8.0min, Deconvoluted (MaxEnt, 527.53-2493.32, *0.0875, 10000)
HE5-DNA
7085.6875
1.5
1.0
0.5
0.0
4000
5000
6000
7000
8000
9000
m/z

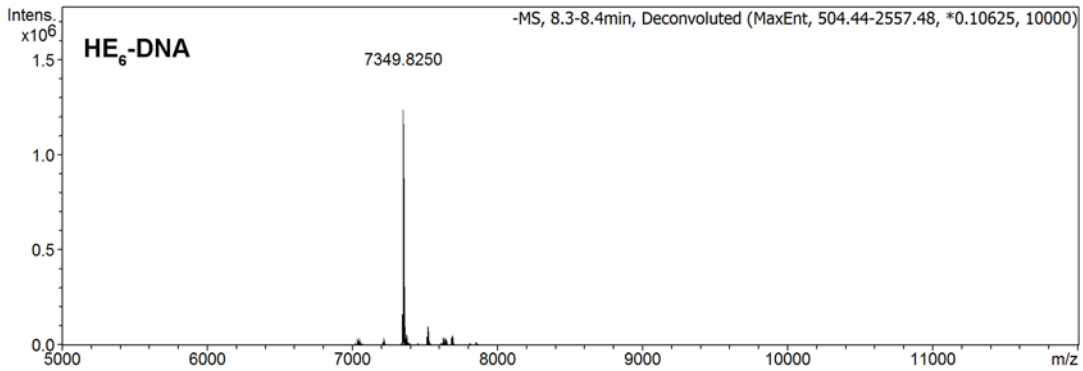
Intens.
x10^6
-MS, 8.3-8.4min, Deconvoluted (MaxEnt, 504.44-2557.48, *0.10625, 10000)
HE6-DNA
7349.8250
1.5
1.0
0.5
0.0
5000
6000
7000
8000
9000
10000
11000
m/z

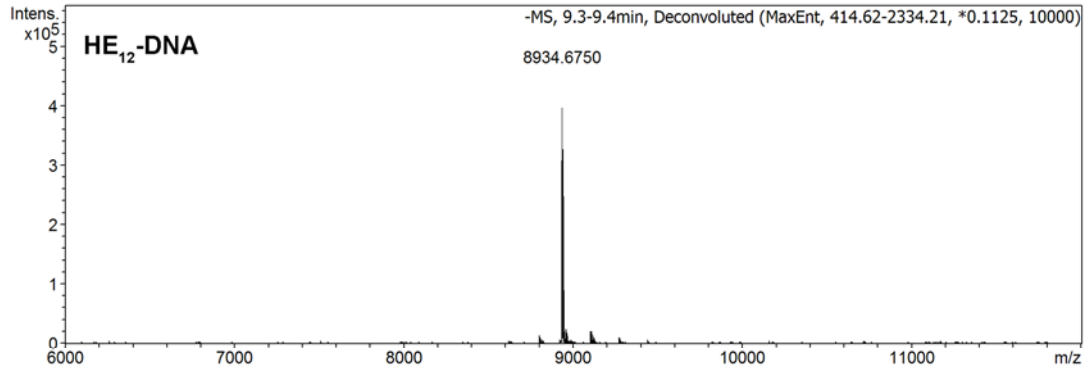
Intens.
x10^5
-MS, 9.3-9.4min, Deconvoluted (MaxEnt, 414.62-2334.21, *0.1125, 10000)
HE12-DNA
8934.6750
5
4
3
2
1
0
6000
7000
8000
9000
10000
11000
m/z

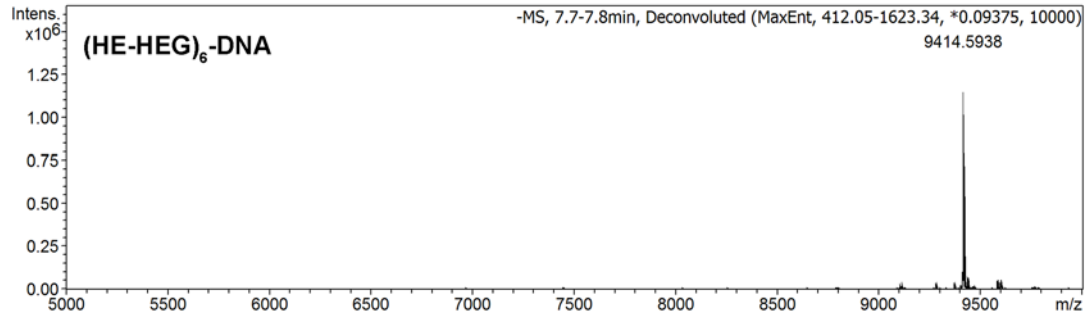
Intens.
x10^6
-MS, 7.7-7.8min, Deconvoluted (MaxEnt, 412.05-1623.34, *0.09375, 10000)
(HE-HEG)6-DNA
9414.5938
1.25
1.00
0.75
0.50
0.25
0.00
5000
5500
6000
6500
7000
7500
8000
8500
9000
9500
m/z

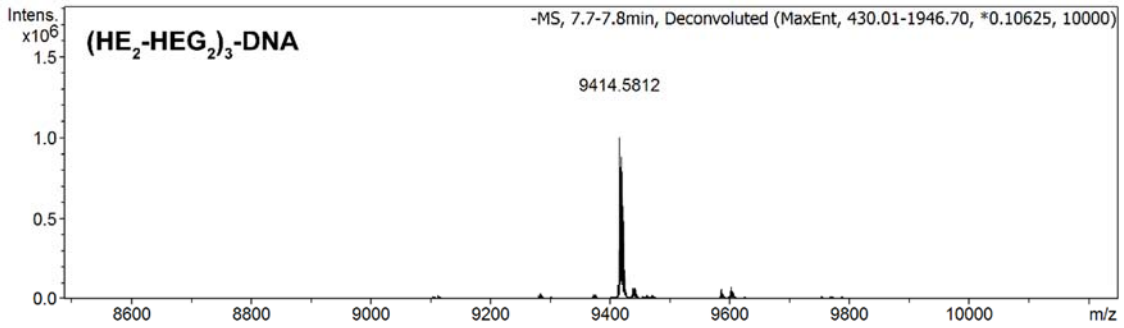
Intens.
x10^6
1.5
1.0
0.5
0.0
(HE2-HEG2)3-DNA
-MS, 7.7-7.8min, Deconvoluted (MaxEnt, 430.01-1946.70, *0.10625, 10000)
9414.5812
8600
8800
9000
9200
9400
9600
9800
10000
m/z

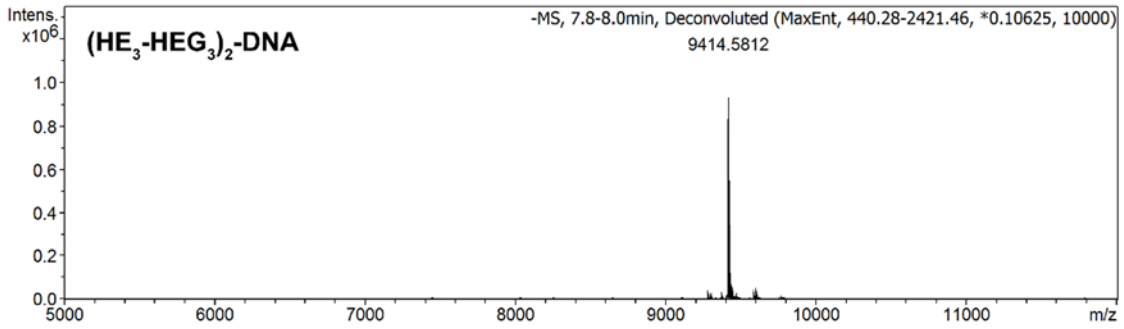
Intens.
x10^6
1.0
0.8
0.6
0.4
0.2
0.0
(HE3-HEG3)2-DNA
-MS, 7.8-8.0min, Deconvoluted (MaxEnt, 440.28-2421.46, *0.10625, 10000)
9414.5812
5000
6000
7000
8000
9000
10000
11000
m/z

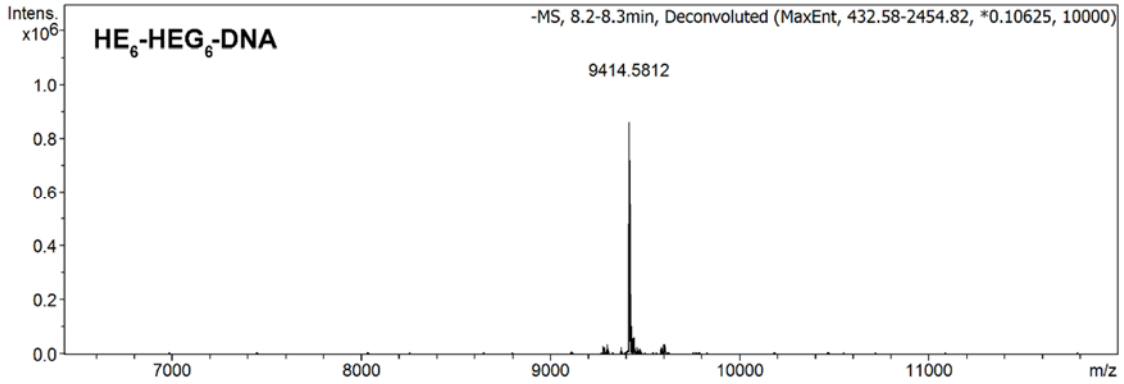
Intens.
x10^6
1.0
0.8
0.6
0.4
0.2
0.0
HE6-HEG6-DNA
-MS, 8.2-8.3min, Deconvoluted (MaxEnt, 432.58-2454.82, *0.10625, 10000)
9414.5812
7000
8000
9000
10000
11000
m/z

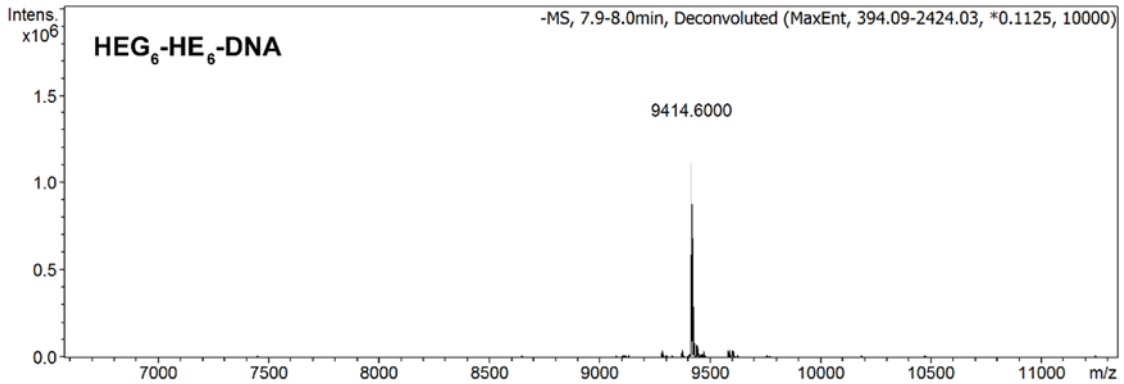
Intens.
x10^6
1.5
1.0
0.5
0.0
HEG6-HE6-DNA
-MS, 7.9-8.0min, Deconvoluted (MaxEnt, 394.09-2424.03, *0.1125, 10000)
9414.6000
7000
7500
8000
8500
9000
9500
10000
10500
11000
m/z

3.5.8 Melting temperatures

The hybridization of the DNA amphiphiles to their complement strands was confirmed by measurement of the thermal denaturation of the duplexes by UV absorption. For each experiment equimolar amounts of DNA amphiphile and complement strand (**Acomp**, see Table 3.3) were combined in 1xTAMg buffer to give a final volume of 150µL with a duplex concentration of 2.5µM. Samples were thermally annealed (95 to 4˚C, 4 hours) before transfer to a quartz cuvette. Absorbance at 260nm was monitored over the appropriate temperature range.

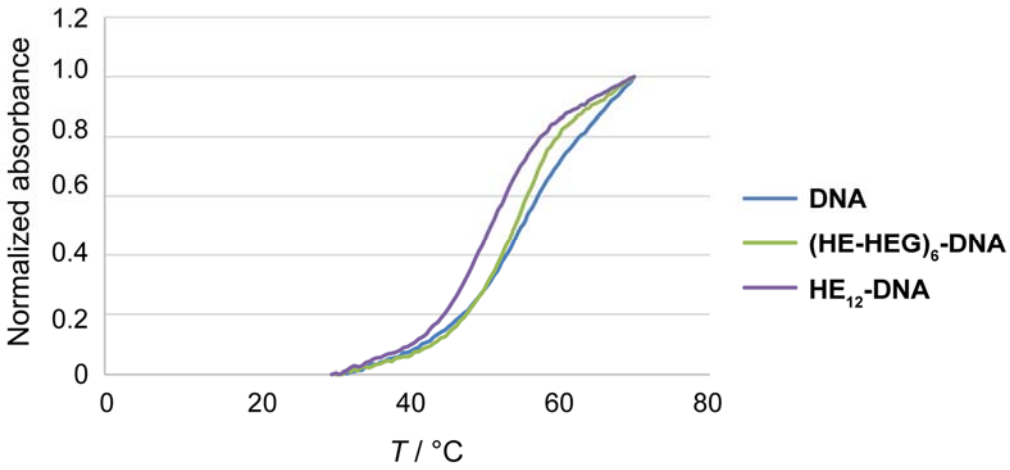

Figure 3.13 - Melting curves of DNA amphiphiles compared to unmodified DNA. Typical sigmoidal melting curves are seen for the hybridization of the complementary strand **Acomp** to **DNA** control, discrete **(HE-HEG)$_6$-DNA** and **HE$_{12}$-DNA** micelles. This shows that in both the case of discrete molecules and self-assembled aggregates the oligonucleotide section is still available for hybridization, with little change in melting temperature (3˚C, between **DNA** and **HE$_{12}$-DNA**).

3.5.9 Electrophoretic mobility assays

Denaturing Polyacrylamide Gel Electrophoresis (PAGE) was carried out at room temperature for 30 minutes at 250V followed by 1 hour at 500V. TBE buffer was used and the concentration of urea in the gel was 8M. For each lane 3µL of annealed sample (10µM, 95 to 4°C, 4 hours) in 1xTAMg was added to 7uL of 8M urea. Native PAGE was carried out at room temperature for 2 hours at a constant voltage of 250V. Sample loading was 0.01 OD_{260} DNA per lane. Single-stranded samples were annealed (95 to 4°C,

4 hours) prior to loading on the gel to promote uniform assembly. Double-stranded samples were similarly annealed (with **Acomp**, see Table 3.3) to provide 25µL of 10µM duplex in 1xTAMg. The DNA bands for all gels were visualized by incubation with GelRed™.ybridization of the DNA amphiphiles to their complement strands was confirmed by measurement of the thermal denaturation

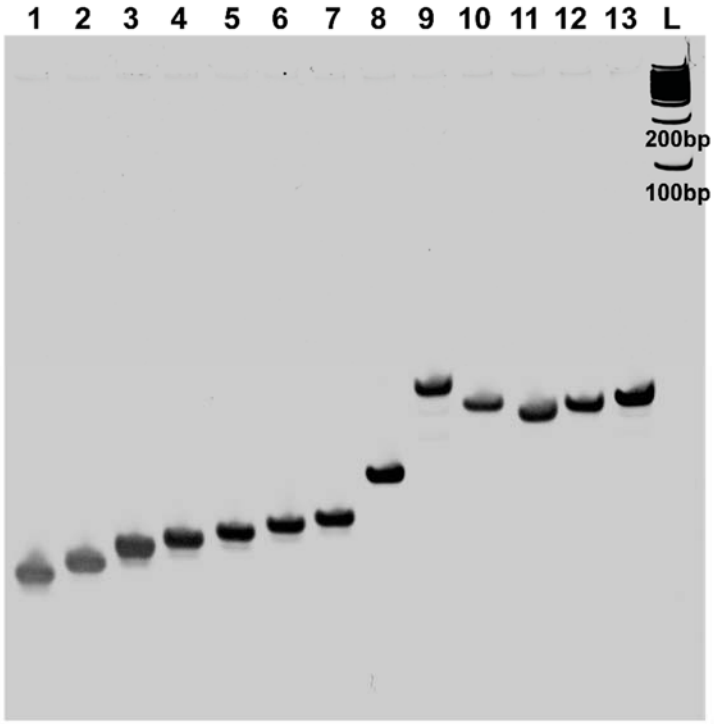

Figure 3.14 - Denaturing PAGE of DNA conjugates. Due to the lack of Mg^{2+} and denaturing conditions no aggregation is observed. A correlation between length of the 5' modification and gel mobility is seen. Lane 1-**DNA**, Lane 2- **HE_1-DNA**, Lane 3- **HE_2-DNA**, Lane 4**- HE_3-DNA**, Lane 5- **HE_4-DNA**, Lane 6- **HE_5-DNA**, Lane 7- **HE_6-DNA**, Lane 8- **HE_{12}-DNA**, Lane 9- **$(HE\text{-}HEG)_6$-DNA**, Lane 10- **$(HE_2\text{-}HEG_2)_3$-DNA**, Lane 11- **$(HE_3\text{-}HEG_3)_2$-DNA**, Lane 12- **$HE_6\text{-}HEG_6$-DNA**, Lane 13- **$HEG_6\text{-}HE_6$-DNA**, Lane L- 100bp DNA ladder (Axygen). (15% Denaturing PAGE)

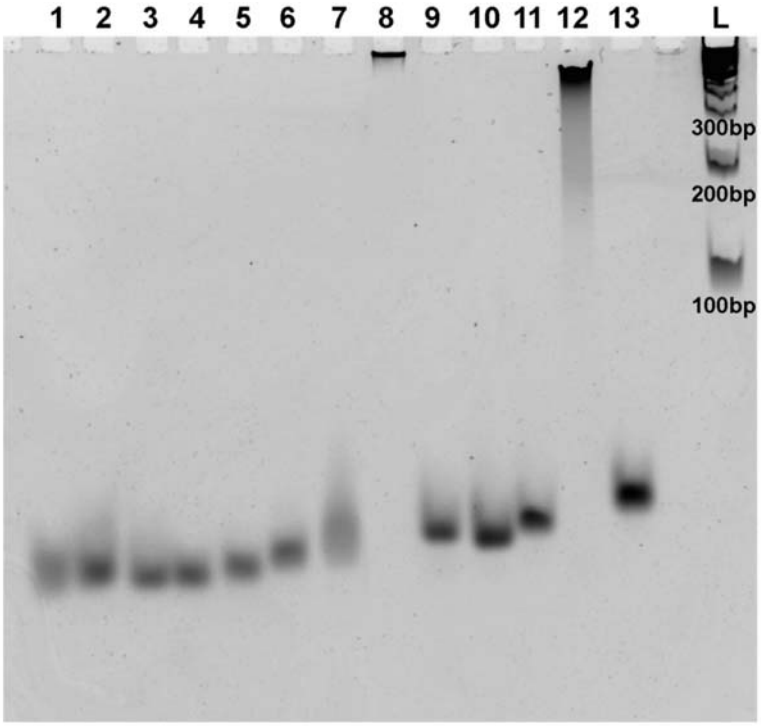

Figure 3.15 - Native PAGE of single-stranded DNA conjugates. The micelles formed by **HE_6-DNA** (Lane 7) appear to collapse to a certain extent under the electrophoretic conditions, while **HE_{12}-DNA** and **HE_6-HEG_6-DNA** (Lanes 8 and 12) micelles remain intact exhibiting substantially reduced mobility. Lane 1- **DNA**, Lane 2- **HE_1-DNA**, Lane 3- **HE_2-DNA**, Lane 4- **HE_3-DNA**, Lane 5- **HE_4-DNA**, Lane 6- **HE_5-DNA**, Lane 7- **HE_6-DNA**, Lane 8- **HE_{12}-DNA**, Lane 9- **$(HE\text{-}HEG)_6$-DNA**, Lane 10- **$(HE_2\text{-}HEG_2)_3$-DNA**, Lane 11- **$(HE_3\text{-}HEG_3)_2$-DNA**, Lane 12- **HE_6-HEG_6-DNA**, Lane 13- **HEG_6-HE_6-DNA**, Lane L- 100bp DNA ladder (Axygen). (6% Native PAGE, room temperature)

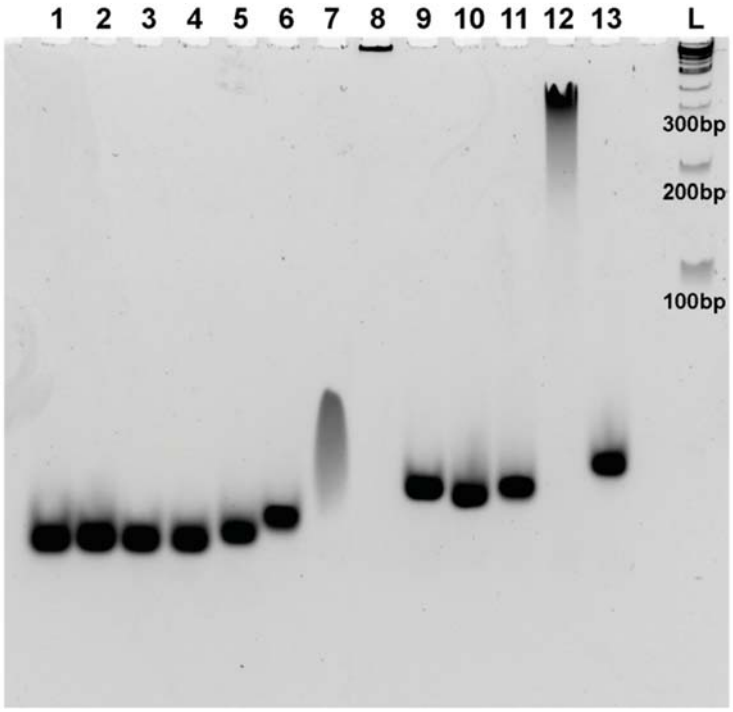

Figure 3.16 - Native PAGE of double-stranded DNA conjugates. In each lane the conjugate is duplexed with the 14 base complement, **Acomp**. The mobility of the micelles formed by **HE_6-DNA**, **HE_{12}-DNA** and **HE_6-HEG_6-DNA** (Lanes 7, 8 and 12 respectively) correspond well with the hydrodynamic radii determined by DLS. Lane 1-**DNA**, Lane 2- **HE_1-DNA**, Lane 3- **HE_2-DNA**, Lane 4**-** **HE_3-DNA**, Lane 5- **HE_4-DNA**, Lane 6- **HE_5-DNA**, Lane 7- **HE_6-DNA**, Lane 8- **HE_{12}-DNA**, Lane 9- **$(HE\text{-}HEG)_6$-DNA**, Lane 10- **$(HE_2\text{-}HEG_2)_3$-DNA**, Lane 11- **$(HE_3\text{-}HEG_3)_2$-DNA**, Lane 12- **HE_6-HEG_6-DNA**, Lane 13- **HEG_6-HE_6-DNA**, Lane L- 100bp DNA ladder (Axygen). (6% Native PAGE, room temperature)

3.5.10 Dynamic Light Scattering

DLS experiments were carried out using a DynaPro™ Instrument from Wyatt Technology. A cumulants fit model was used to confirm the presence and determine the size of a monomodal population of micellar aggregates. Sterile water and TAMg buffers were filtered using a 0.45μm nylon syringe filter before use for DLS sample preparation. All measurements were carried out at 25°C.

Table 3.6 - Summary of hydrodynamic radii data. All samples were measured in at least triplicate and the mean values for hydrodynamic radii are shown below. Error margins were derived from the standard deviation of the multiple measurements.

	Mean hydrodyamic radius (nm)	
Sample	**Single-stranded**	**Double-stranded**
HE_6-DNA	6.5 ± 0.4	5.6 ± 0.1
HE_{12}-DNA	11.3 ± 0.7	11.3 ± 0.1
HE_6-HEG_6-DNA	9.7 ± 0.1	10.0 ± 0.2

Supporting Table ST5| Summary of raw scattering data. All samples were measured in at least triplicate and the mean values for scattering intensity (counts per second) are given below. Numbers in bold correspond to good correlation and the presence of self-assembled aggregates.

	Scattering intensity (KCnt/s)	
Sample	**Single-stranded**	**Double-stranded**
DNA	95	104
HE_1-DNA	105	117
HE_2-DNA	93	112
HE_3-DNA	88	147
HE_4-DNA	89	169
HE_5-DNA	139	156
HE_6-DNA	372	350
HE_{12}-DNA	1550	2000
$(HE\text{-}HEG)_6$-DNA	122	156
$(HE_2\text{-}HEG_2)_3$-DNA	118	145
$(HE_3\text{-}HEG_3)_2$-DNA	110	132
HE_6-HEG_6-DNA	516	741
HEG_6-HE_6-DNA	87	124

3.5.11 Fluorescence of encapsulated Nile Red

DNA-conjugates (10μM) in TAMg buffer (60μL) were thermally annealed (95 to 4ºC, 4 hours). The samples were transferred to glass vials and 1.5μL of Nile Red solution (0.1M, acetone) was added, to give a final Nile Red concentration of 2.5μM. The samples were vortexed briefly, sealed and incubated overnight at room temperature in the absence of light. Fluorescence spectra were recorded at room temperature in a 50μL quartz cuvette using an excitation wavelength of 535nm, and monitoring emission between 560 and 750nm, with excitation and emission slit widths both set at 10nm.

3.5.12 Reversibility of micelle formation

To investigate the reversibility of micelle formation and dependence on Mg^{2+} concentration additional DLS experiments were carried out. Samples of 10μM **HE_6-DNA**, **HE_{12}-DNA**, **HE_6-HEG_6-DNA** and **HEG_6-HE_6-DNA** were prepared in TBE buffer and thermally annealed. DLS measurements were obtained at 25°C for each 20μL sample, then 2.22μL of 10xTAMg was added to raise the Mg^{2+} concentration and the sample scattering measured again. The reverse experiment was carried out by annealing samples (20μL) in TAMg to form micelles and introducing 2.22μL of EDTA solution (125mM EDTA, pH adjusted to 8.0 using Tris) to observe de-aggregation. The data are shown on the next three pages.

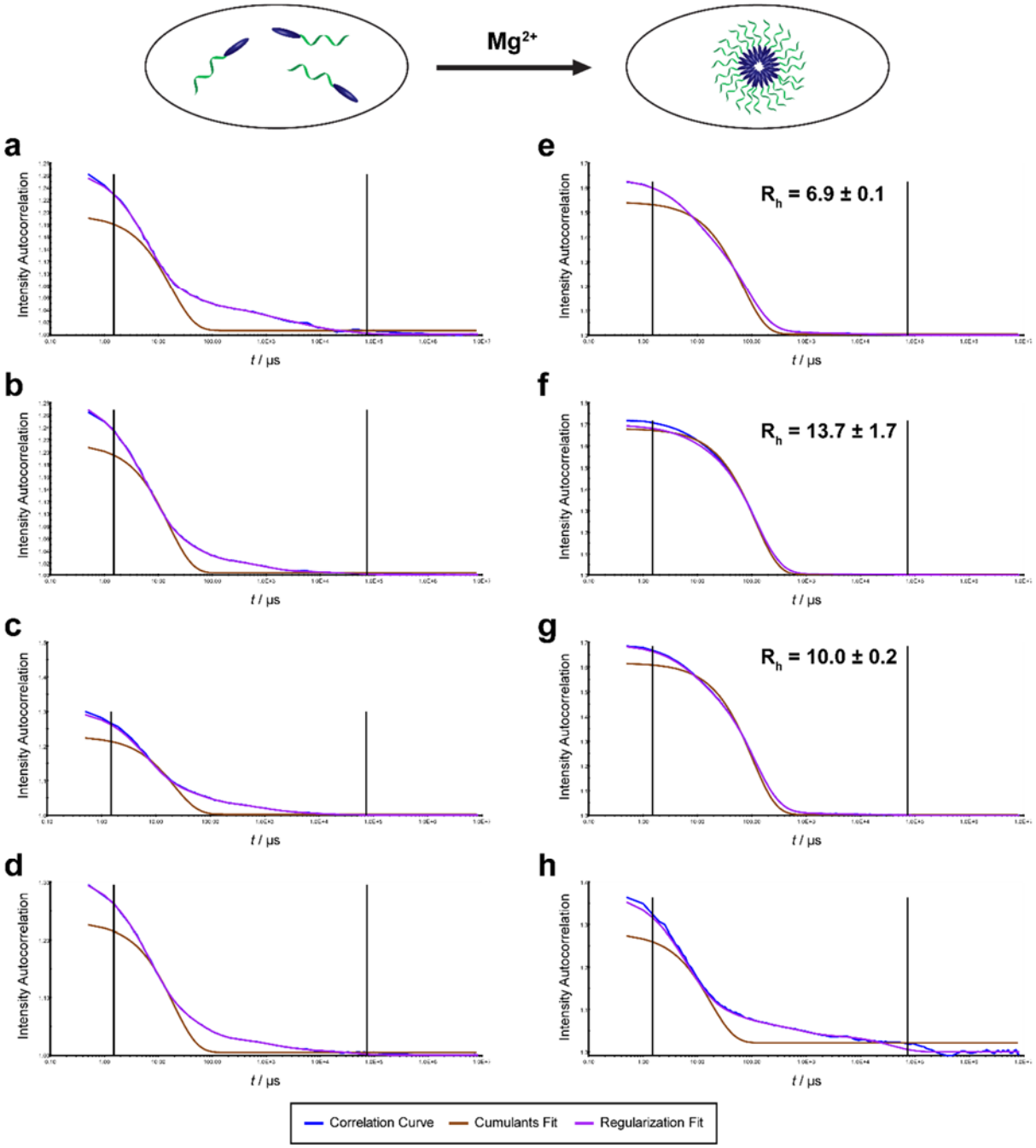

Figure 3.17 - DLS on Mg^{2+} induced aggregation. DLS intensity correlation functions for 10 µM solutions of a) **HE_6-DNA**, b) **HE_{12}-DNA**, c) **HE_6-HEG_6-DNA** and d) **HEG_6-HE_6-DNA** in 1xTBE buffer. The low scattering intensity and poor correlation functions measured for all samples represent individual molecules in solution. Upon addition of Mg^{2+} buffer a rapid change is seen for micelle forming samples e) **HE_6-DNA**, f) **HE_{12}-DNA**, g) **HE_6-HEG_6-DNA** giving good correlation and higher scattering intensity due to the presence of aggregates**.** The control sample h) **HEG_6-HE_6-DNA** shows negligible change as it does not form micellar aggregates. The hydrodynamic radii observed here (nm) are slightly larger than the thermally annealed samples, which is to be expected as different products will be favored.

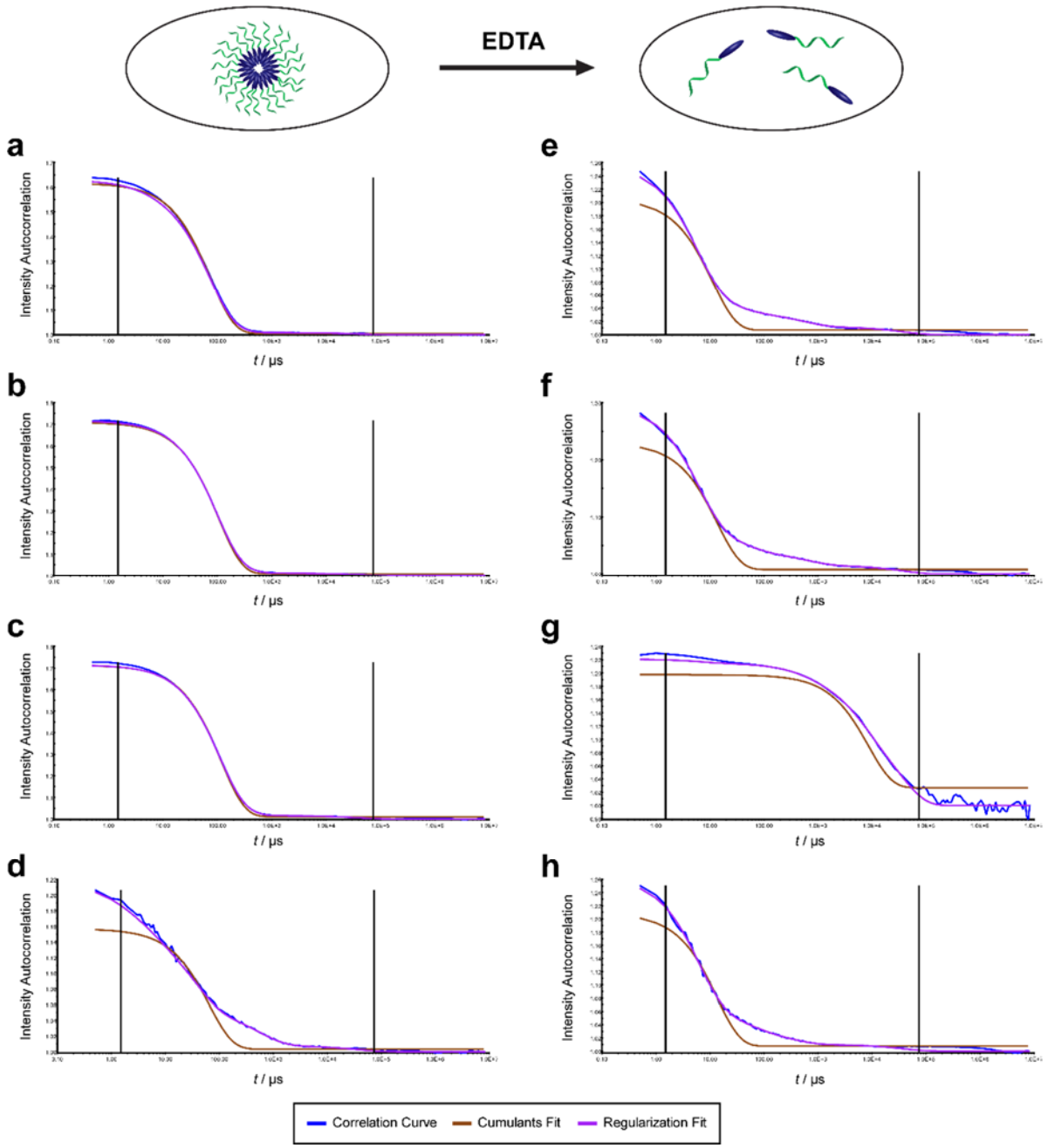

Figure 3.18 - DLS on EDTA induced de-aggregation. DLS intensity correlation functions for 10µM solutions of a) **HE$_6$-DNA**, b) **HE$_{12}$-DNA**, c) **HE$_6$-HEG$_6$-DNA** and d) **HEG$_6$-HE$_6$-DNA** in TAMg. Good correlation is seen for the micelle containing samples **HE$_6$-DNA**, **HE$_{12}$-DNA**, **HE$_6$-HEG$_6$-DNA** but not the control **HEG$_6$-HE$_6$-DNA** (hydrodynamic radii were consistent with the values stated in Table **ST4**). Upon addition of EDTA scattering intensity reduces and autocorrelation is lost for the micelle forming samples e) **HE$_6$-DNA**, f) **HE$_{12}$-DNA**, g) **HE$_6$-HEG$_6$-DNA** indicating de-aggregation**.** The control sample h) **HEG$_6$-HE$_6$-DNA** shows little change as it remains a discrete molecule in solution.

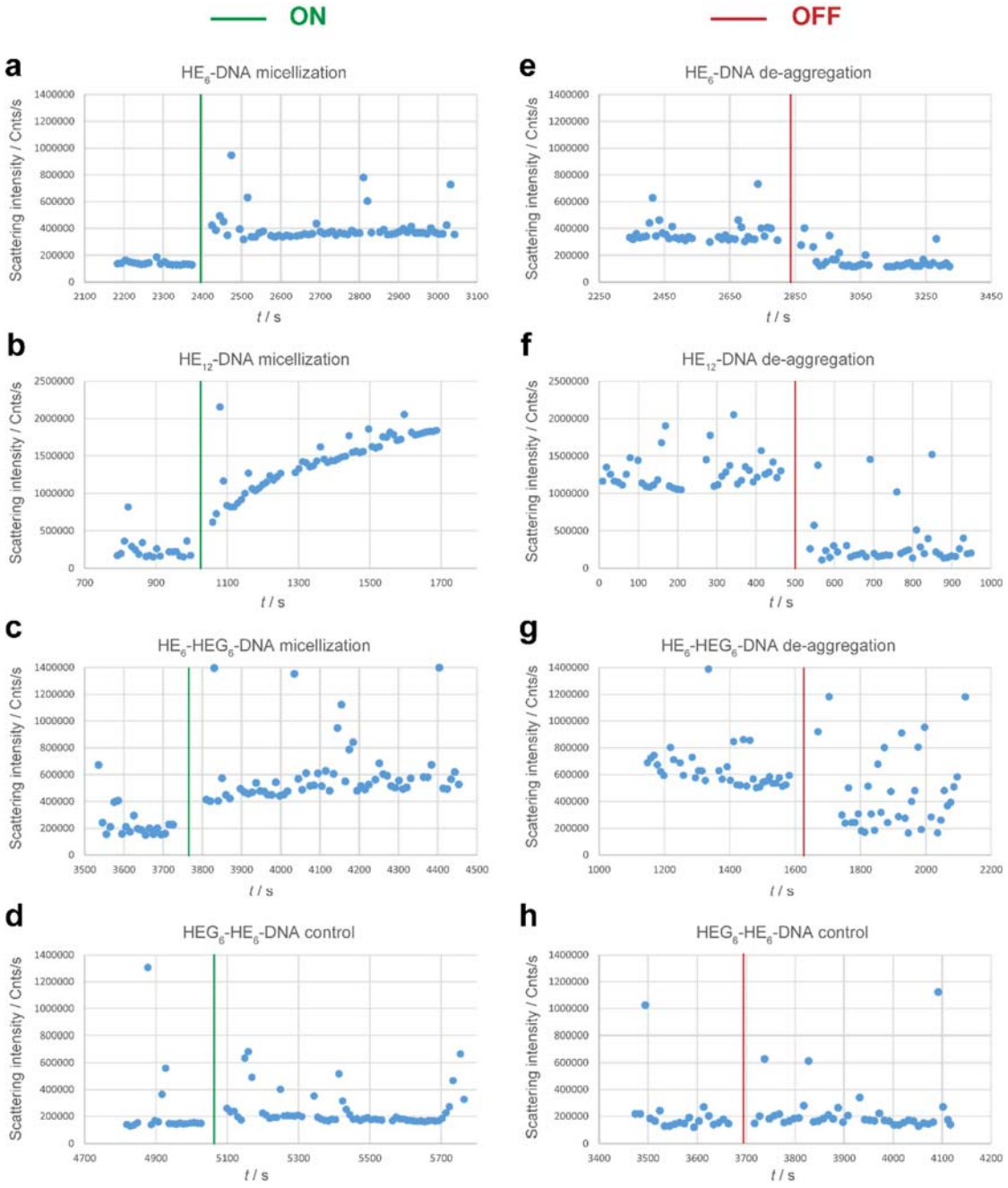

Figure 3.19 - Raw scattering data for micellization and de-aggregation. Scattering intensity over time for 10μM solutions of a) **HE_6-DNA**, b) **HE_{12}-DNA**, c) **HE_6-HEG_6-DNA** and d) **HEG_6-HE_6-DNA** in TBE. The green line represents the addition of Mg^{2+} to the solution. An increase in scattering is seen for the micelle forming samples **HE_6-DNA**, **HE_{12}-DNA**, **HE_6-HEG_6-DNA** but not the control **HEG_6-HE_6-DNA**. The **HE_{12}-DNA** shows a gradual increase, possibly due to cumulative recruitment of more molecules into these larger micelles. Upon addition of EDTA (red line) scattering intensity reduces and for the micelle samples (10μM in 1xTAMg) **HE_6-DNA**, f) **HE_{12}-DNA**, g) **HE_6-HEG_6-DNA** indicating de-aggregation**.** The control sample h) **HEG_6-HE_6-DNA** shows no change as it does not aggregate under these conditions.

3.5.13 Atomic force microscopy in the dry state

Dry AFM was carried out using a MultiMode3™ SPM connected to a Nanoscope™ IIIa. controller from Veeco. All images were obtained using tapping mode in air with AC160TS cantilevers (Nominal values: Tip radius – 9nm, Resonant frequency – 300kHz, Spring constant – 42N/m) from Asylum Research. Samples were diluted to 1μM in TAMg buffer and 4μL of this solution was deposited on a freshly cleaved mica surface (ca. 7 x 7mm) and allowed to adsorb for 1-2 seconds. Then 50μL of 0.22μm filtered Millipore water was dropped on the surface and instantly removed with filter paper. The surface was then washed with a further 200μL of water and the excess removed with a strong flow of nitrogen. Samples were dried under vacuum for 15-30 minutes prior to imaging.

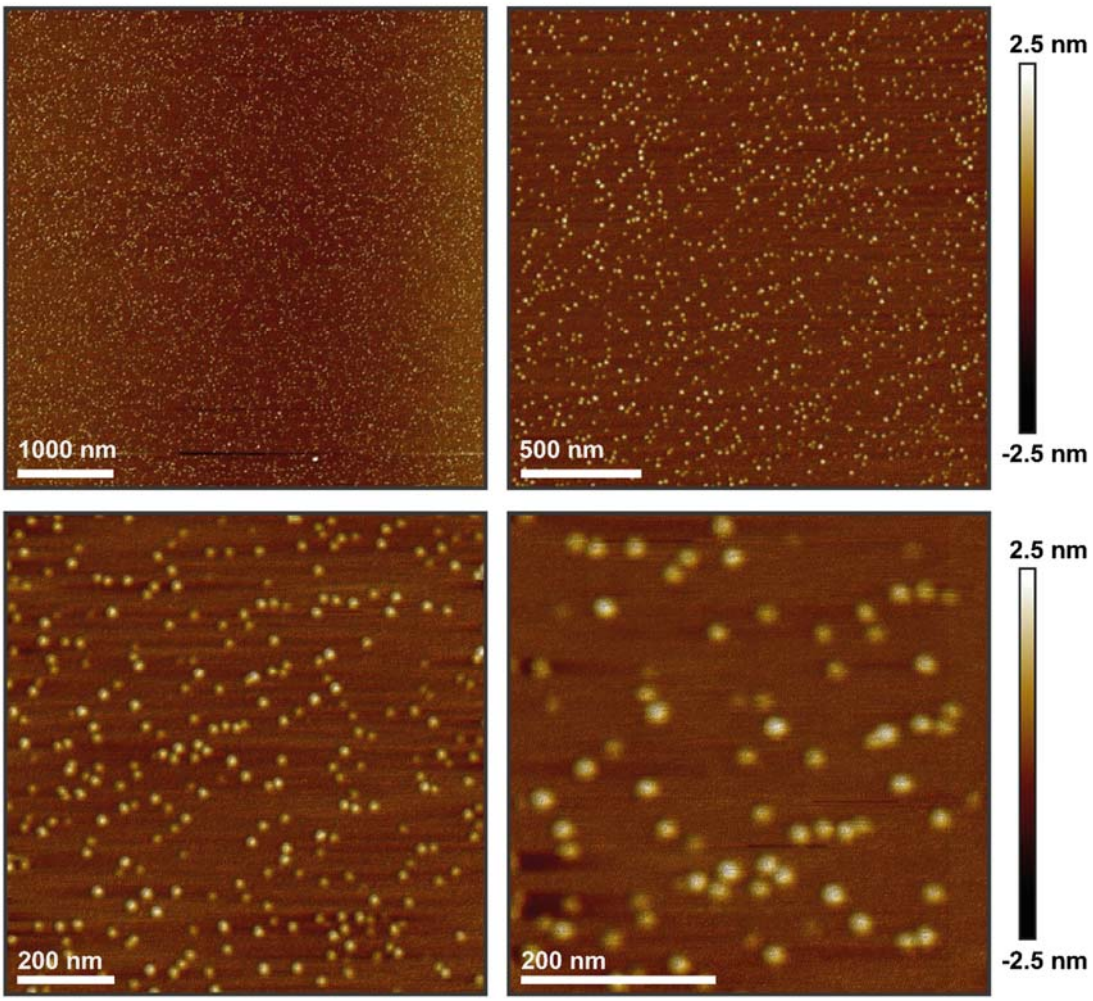

Figure 3.20 - Additional AFM images of HE_6-DNA micelles under dry conditions. Average height 1.7 ± 0.4nm and width 17.8 ± 1.8nm. This flat and wide morphology is due to deformation of the micelles upon surface adsorption and drying.

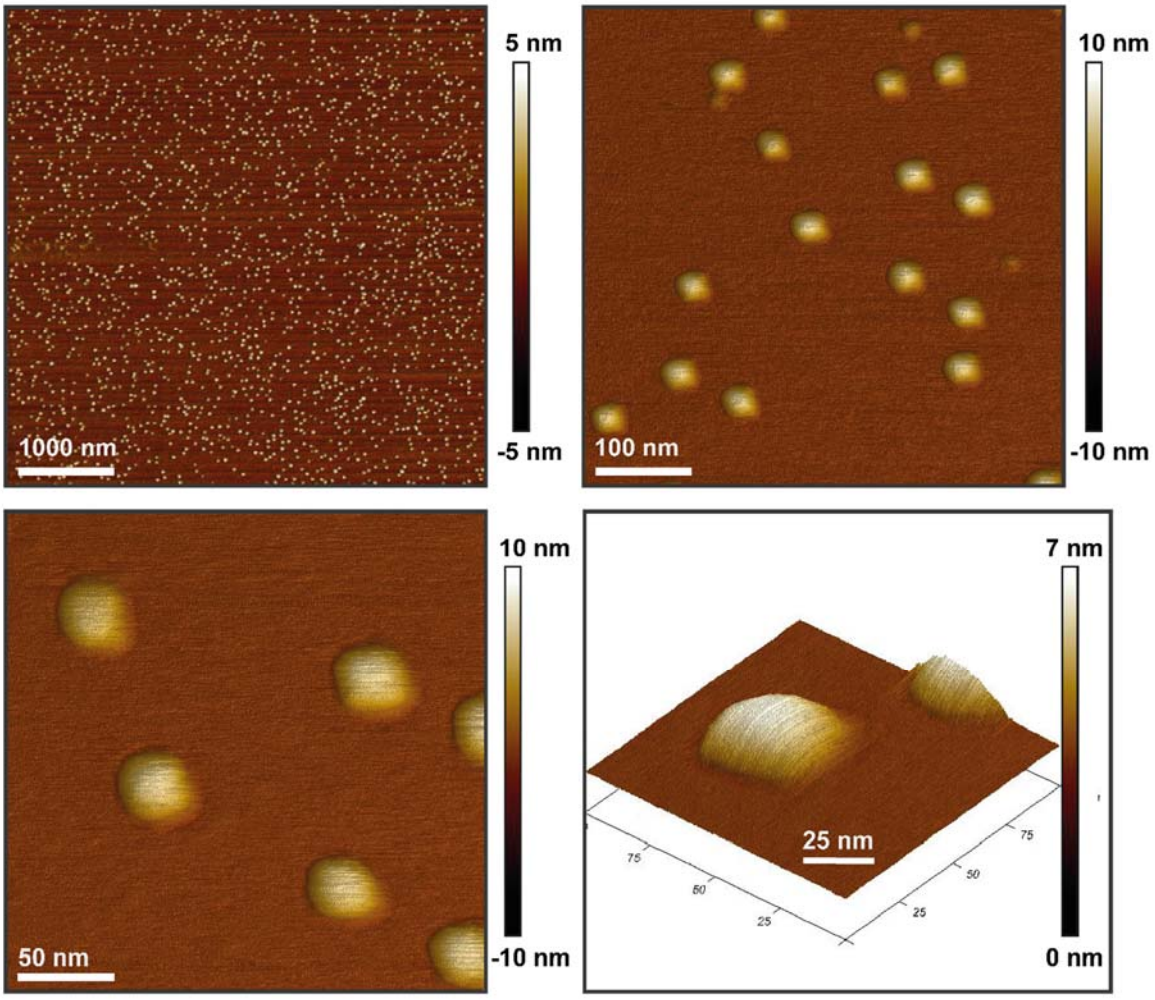

Figure 3.21 - Additional AFM images of HE_{12}-DNA micelles under dry conditions. Average height 6.0 ± 0.6nm and width 23.4 ± 4.4nm. This size is larger in than the **HE_6-DNA** sample, consistent with the other characterization data. Again, the flat and wide morphology is due to deformation of the micelles upon surface adsorption and drying.

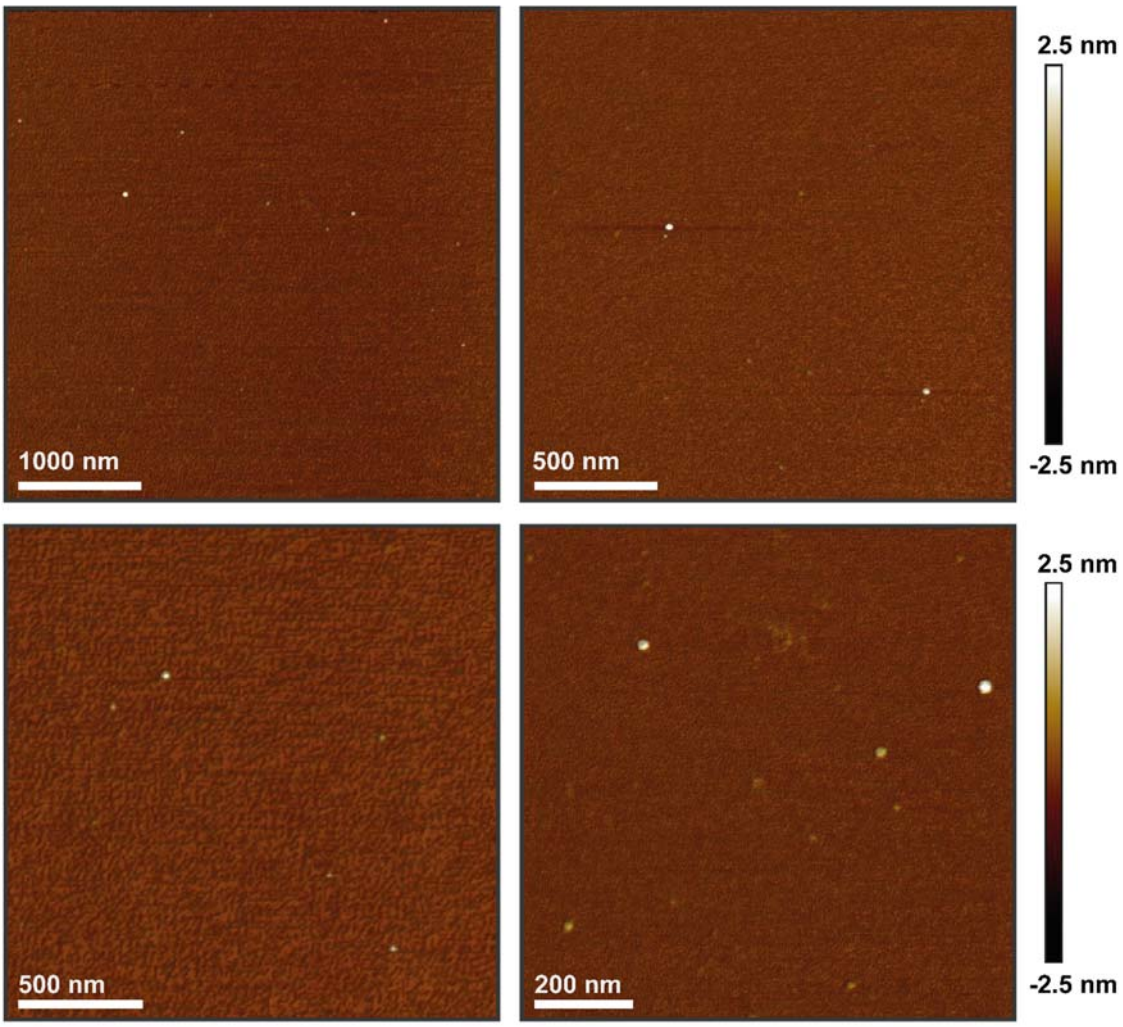

Figure 3.22 - AFM images of HE_6-HEG_6-DNA micelles under dry conditions. The poor surface adsorption of **HE_6-HEG_6-DNA** micelles results in a very sparse coating of the surface with particles. This is most likely due to the presence of the **HEG** blocks as the **HE_x-DNA** showed rapid and robust adsorption the mica surface. The few particles that were observed do fall in the range expected for these aggregates (height 2.7 ± 1.1nm, width 22.2 ± 3.3nm) by comparison with the other micelle samples, however the DLS, fluorescence and PAGE results remain more conclusive for characterization of the self-assembly.

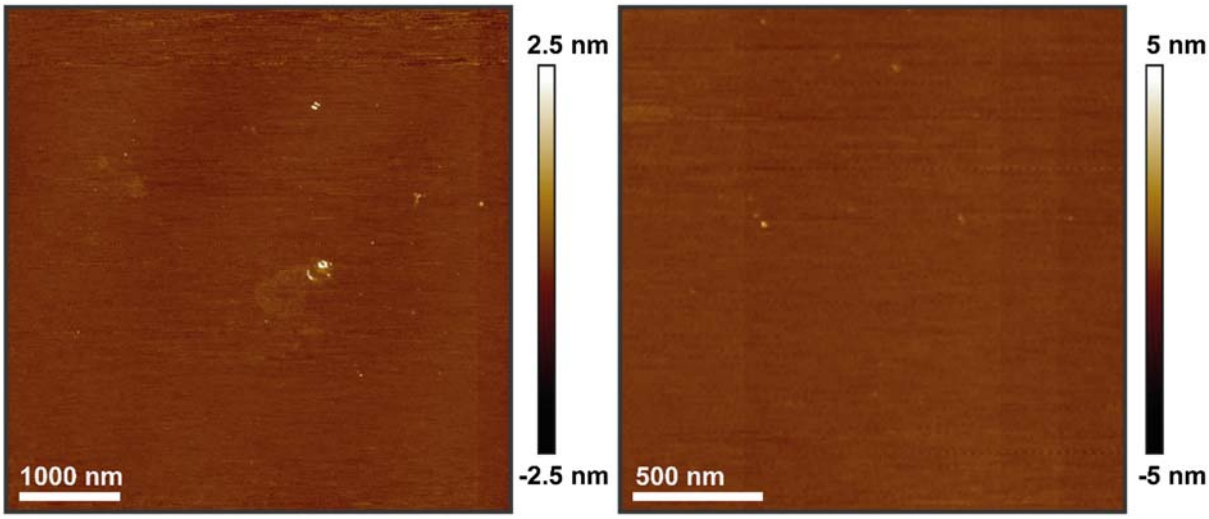

Figure 3.23 - AFM images of HEG_6-HE_6-DNA control under dry conditions.

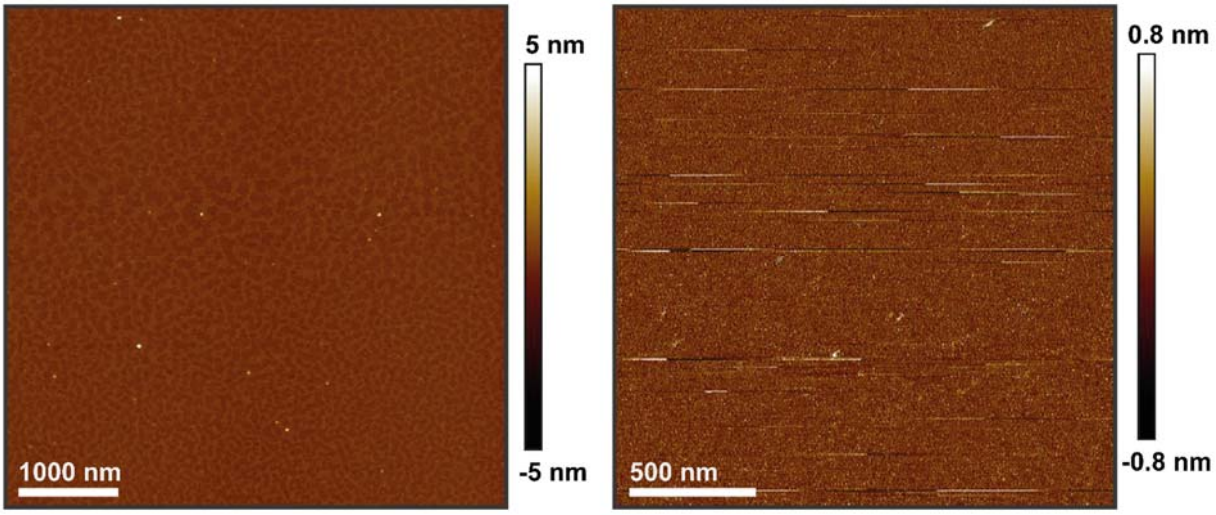

Figure 3.24 - AFM images of DNA control under dry conditions.

3.5.14 Atomic force microscopy in the liquid state

Fluid AFM was carried out using a MultiMode8™ SPM connected to a Nanoscope™ V controller from Veeco. All images were obtained using ScanAsyst mode in fluid with ScanAsyst-FLUID cantilevers (Nominal values: Tip radius – 20nm, Resonant frequency – 150kHz, Spring constant – 0.7N/m) from Bruker. Samples were diluted to 1μM in TAMg buffer (0.2 μm filtered) and 5μL of this solution was deposited on a freshly cleaved mica surface (ca. 15 x 15mm) and allowed to adsorb for 1-2 seconds. Then 50μL of 0.22μm filtered Millipore water was dropped on the surface and instantly removed with filter paper. The surface was then washed with a further 200μL of water and the excess removed with a strong flow of nitrogen. Finally, 50μL of 0.22μm filtered Millipore water was added to the cantilever on the fluid cell. The cell was immediately mounted on the sample.

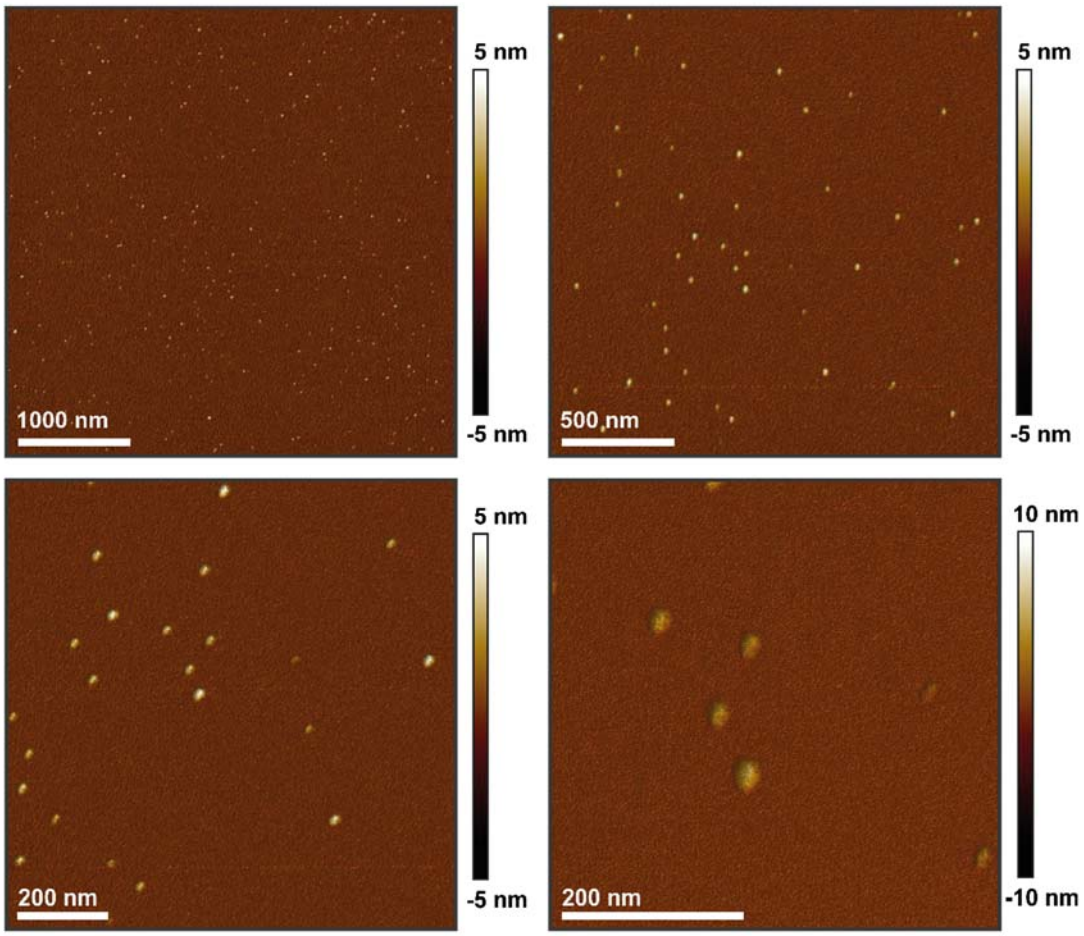

Figure 3.25 - Additional AFM images of HE_6-DNA micelles in fluid conditions.

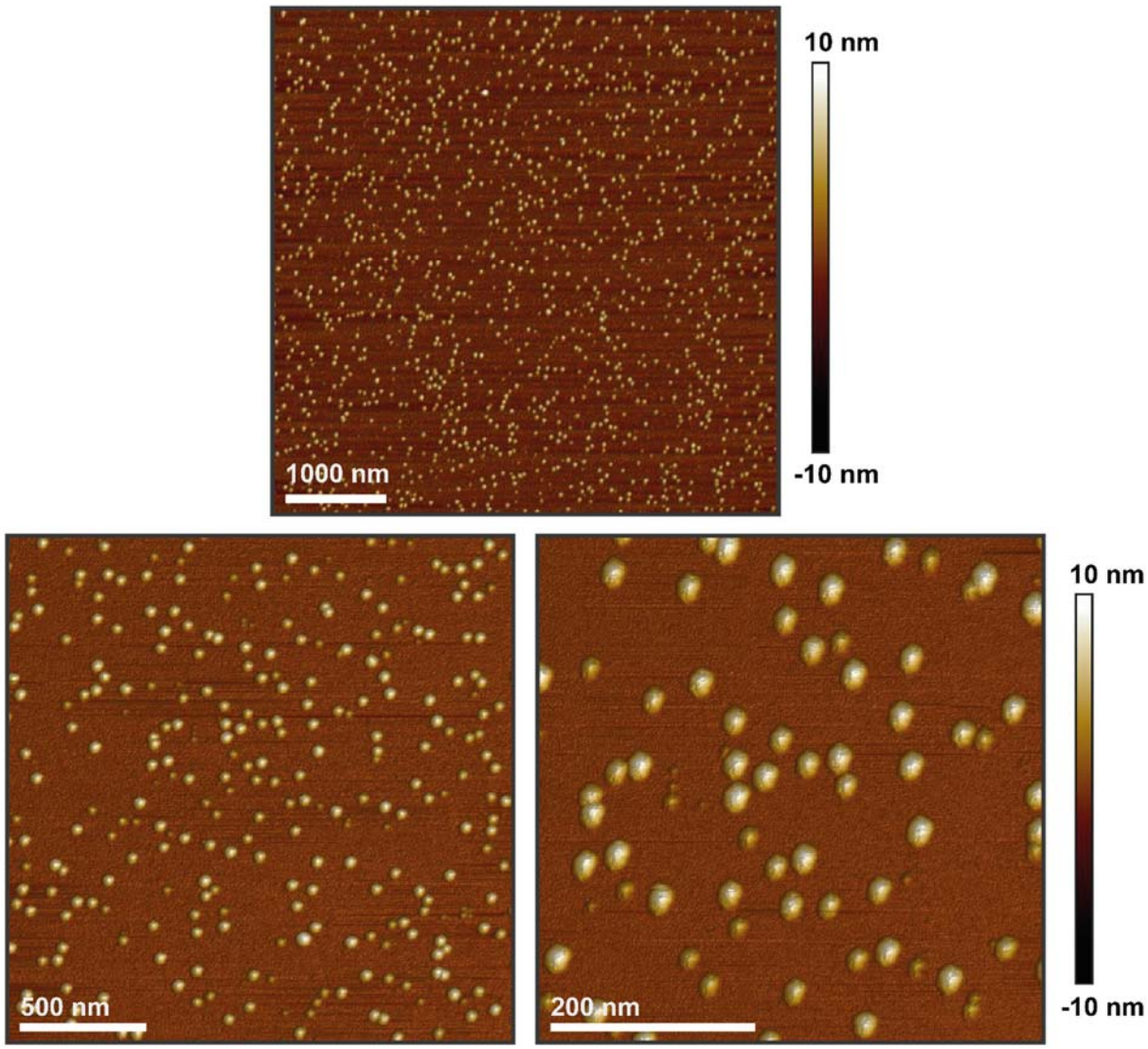

Figure 3.26 - Additional AFM images of HE_{12}-DNA micelles in fluid conditions

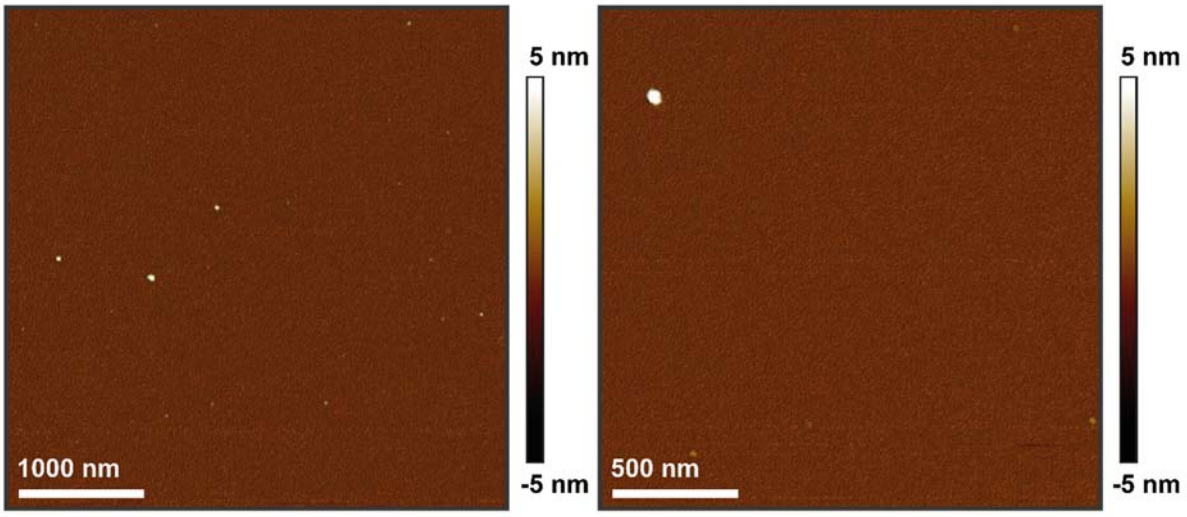

Figure 3.27 - AFM images of HE_6-HEG_6-DNA micelles in fluid conditions. Similarly to the dry AFM of **HE_6-HEG_6-DNA** micelles poor surface adsorption results in a very sparse coating of the surface with particles. The DLS, fluorescence and PAGE data give a more conclusive picture of the self-assembly characteristics of this molecule.

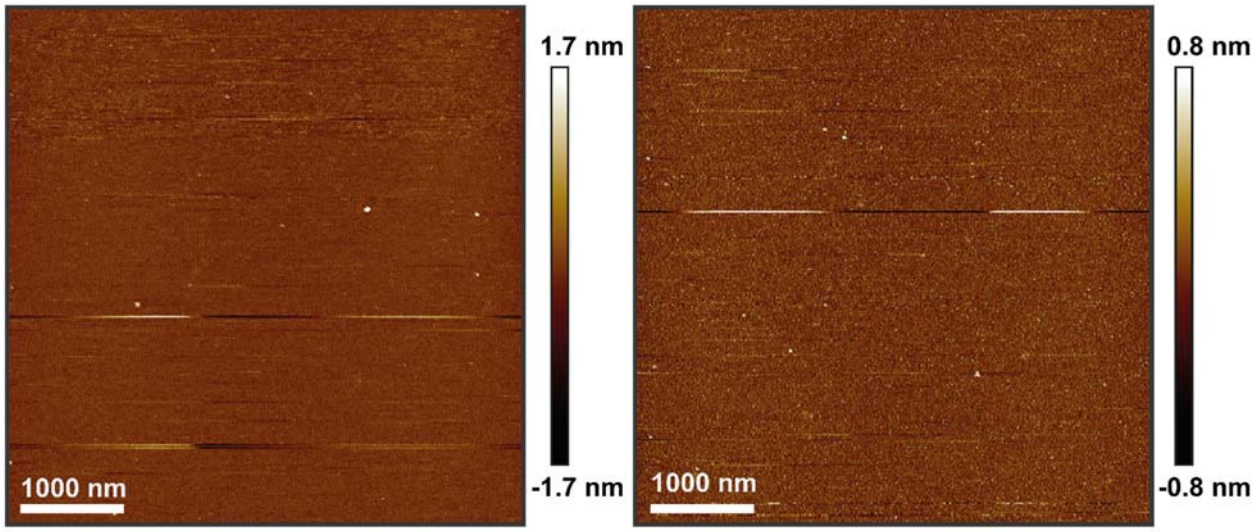

Figure 3.28 - AFM images of HEG_6-HE_6-DNA control in fluid conditions.

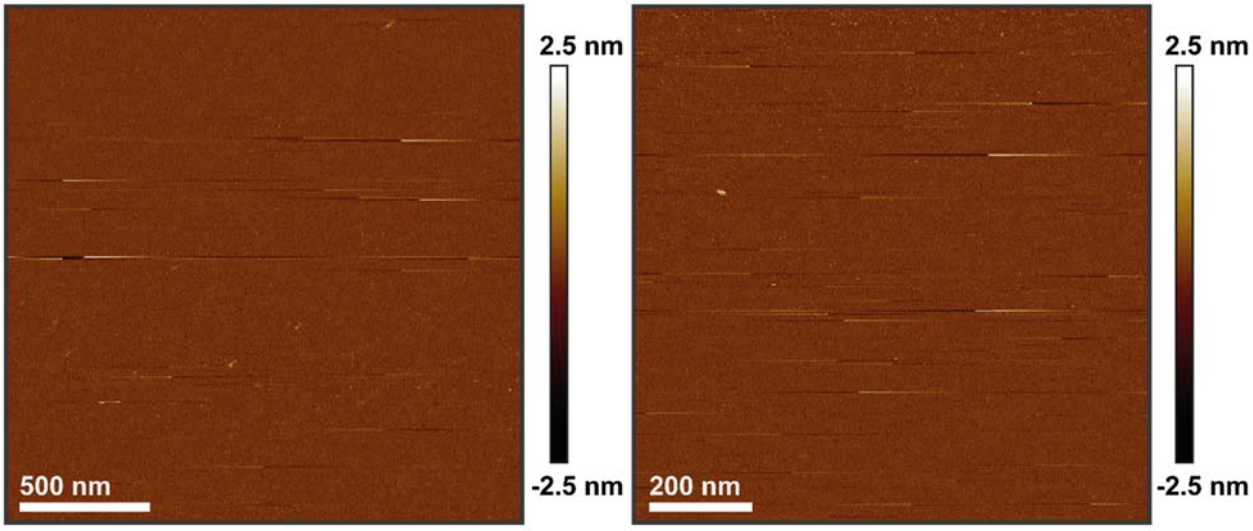

Figure 3.29 - AFM images of DNA control in fluid conditions.

3.6 References

1 Lutz, J.-F., Ouchi, M., Liu, D. R. & Sawamoto, M. "Sequence-Controlled Polymers." *Science* **341**, (2013).

2 Lutz, J.-F. "Writing on Polymer Chains." *Accounts of Chemical Research* **46**, 2696-2705, (2013).

3 Pfeifer, S. & Lutz, J.-F. "A Facile Procedure for Controlling Monomer Sequence Distribution in Radical Chain Polymerizations." *Journal of the American Chemical Society* **129**, 9542-9543, (2007).

4 Benoit, D., Hawker, C. J., Huang, E. E., Lin, Z. & Russell, T. P. "One-Step Formation of Functionalized Block Copolymers." *Macromolecules* **33**, 1505-1507, (2000).

5 Minoda, M., Sawamoto, M. & Higashimura, T. "Sequence-regulated oligomers and polymers by living cationic polymerization. 2. Principle of sequence regulation and synthesis of sequence-regulated oligomers of functional vinyl ethers and styrene derivatives." *Macromolecules* **23**, 4889-4895, (1990).

6 Merrifield, R. B. "Solid Phase Peptide Synthesis. I. The Synthesis of a Tetrapeptide." *Journal of the American Chemical Society* **85**, 2149-2154, (1963).

7 Letsinger, R. L. & Mahadevan, V. "Oligonucleotide synthesis on a polymer support [19]." *Journal of the American Chemical Society* **87**, 3526-3527, (1965).

8 Milnes, P. J. *et al.* "Sequence-specific synthesis of macromolecules using DNA-templated chemistry." *Chemical Communications* **48**, 5614-5616, (2012).

9 Niu, J., Hili, R. & Liu, D. R. "Enzyme-free translation of DNA into sequence-defined synthetic polymers structurally unrelated to nucleic acids." *Nat Chem* **5**, 282-292, (2013).

10 Lewandowski, B. *et al.* "Sequence-Specific Peptide Synthesis by an Artificial Small-Molecule Machine." *Science* **339**, 189-193, (2013).

11 Gody, G., Maschmeyer, T., Zetterlund, P. B. & Perrier, S. "Rapid and quantitative one-pot synthesis of sequence-controlled polymers by radical polymerization." *Nat Commun* **4**, (2013).

12 Schaffert, D. *et al.* "Solid-Phase Synthesis of Sequence-Defined T-, i-, and U-Shape Polymers for pDNA and siRNA Delivery." *Angewandte Chemie International Edition* **50**, 8986-8989, (2011).
13 Kwak, M. & Herrmann, A. "Nucleic acid amphiphiles: synthesis and self-assembled nanostructures." *Chem. Soc. Rev.* **40**, 5745-5755, (2011).
14 Shu, J. Y., Panganiban, B. & Xu, T. "Peptide-Polymer Conjugates: From Fundamental Science to Application." *Annual Review of Physical Chemistry* **64**, 631-657, (2013).
15 Chien, M.-P., Rush, A. M., Thompson, M. P. & Gianneschi, N. C. "Programmable Shape-Shifting Micelles." *Angewandte Chemie International Edition* **49**, 5076-5080, (2010).
16 Pokholenko, O. *et al.* "Lipid oligonucleotide conjugates as responsive nanomaterials for drug delivery." *Journal of Materials Chemistry B* **1**, 5329-5334, (2013).
17 Wang, L. *et al.* "Reversibly controlled morphology transformation of an amphiphilic DNA-dendron hybrid." *Chemical Communications* **48**, 3715-3717, (2012).
18 Carneiro, K. M. M. *et al.* "Stimuli-responsive organization of block copolymers on DNA nanotubes." *Chem. Sci.* **3**, 1980-1986, (2012).
19 Edwardson, T. G. W., Carneiro, K. M. M., McLaughlin, C. K., Serpell, C. J. & Sleiman, H. F. "Site-specific positioning of dendritic alkyl chains on DNA cages enables their geometry-dependent self-assembly." *Nat Chem* **5**, 868-875, (2013).
20 Wu, Y., Sefah, K., Liu, H., Wang, R. & Tan, W. "DNA aptamer–micelle as an efficient detection/delivery vehicle toward cancer cells." *Proceedings of the National Academy of Sciences* **107**, 5-10, (2010).
21 Raouane, M., Desmaële, D., Urbinati, G., Massaad-Massade, L. & Couvreur, P. "Lipid Conjugated Oligonucleotides: A Useful Strategy for Delivery." *Bioconjugate Chemistry*, (2012).
22 Woller, J. G., Hannestad, J. K. & Albinsson, B. "Self-Assembled Nanoscale DNA–Porphyrin Complex for Artificial Light Harvesting." *J. Am. Chem. Soc.* **135**, 2759-2768, (2013).
23 Lundberg, E. P., Feng, B., Saeid Mohammadi, A., Wilhelmsson, L. M. & Nordén, B. "Controlling and Monitoring Orientation of DNA Nanoconstructs on Lipid Surfaces." *Langmuir* **29**, 285-293, (2012).
24 Chan, Y.-H., Lengerich, B. & Boxer, S. "Lipid-anchored DNA mediates vesicle fusion as observed by lipid and content mixing." *Biointerphases* **3**, FA17-FA21, (2008).
25 Beaucage, S. L. & Caruthers, M. H. "Deoxynucleoside phosphoramidites—A new class of key intermediates for deoxypolynucleotide synthesis." *Tetrahedron Letters* **22**, 1859-1862, (1981).
26 Greenspan, P., Mayer, E. P. & Fowler, S. D. "Nile red: a selective fluorescent stain for intracellular lipid droplets." *The Journal of Cell Biology* **100**, 965-973, (1985).
27 Greenspan, P. & Fowler, S. D. "Spectrofluorometric studies of the lipid probe, nile red." *Journal of Lipid Research* **26**, 781-789, (1985).
28 van Hest, J. C. M. & Tirrell, D. A. "Protein-based materials, toward a new level of structural control." *Chemical Communications*, 1897-1904, (2001).
29 Altintas, O. & Barner-Kowollik, C. "Single Chain Folding of Synthetic Polymers by Covalent and Non-Covalent Interactions: Current Status and Future Perspectives." *Macromolecular rapid communications* **33**, 958-971, (2012).

30 Serpell, C. J., Edwardson, T. G. W., Chidchob, P., Carneiro, K. M. M. & Sleiman, H. F. "Precision Polymers and 3D DNA Nanostructures: Emergent Assemblies from New Parameter Space." *Journal of the American Chemical Society* **136**, 15767-15774, (2014).

Introduction to Chapter 4

Chapters 2 and 3 have described the synthesis of novel DNA-conjugates and their organization on 3D-DNA prisms. One motivation for this work was to develop simple and modular synthetic routes to DNA-amphiphiles. Another motivation is that the organization of these DNA amphiphiles on the 3D-DNA nanostructure could be used to add functionality, such as creating encapsulation environments and revealing new modes of tuneable self-assembly. Finally, the incorporation of these amphiphiles with DNA nanostructures was investigated with the aim of modulating the amphiphilic assembly via templation on a nanoscaffold. Overall, this research highlighted the advantages of combining additional supramolecular assembly motifs with DNA nanotechnology.

The concept of DNA nanostructures as templates to regulate intermolecular interactions is taken further in chapter 4. Another novel DNA conjugate is synthesized, which does not display amphiphilic properties, but is instead designed to bind strongly to gold surfaces. Using the same cubic scaffold introduced in chapter 2 as a template, these reactive groups are organized into a predetermined geometry. This active DNA nanostructure template is used to transfer well-defined numbers and patterns of DNA to a gold nanoparticle. The transfer of structural information to the gold nanoparticle breaks the isotropic nature of these interesting nanomaterials, creating building blocks for advanced DNA-mediated gold nanoparticle assembly. In chapter 2 the use of a DNA nanostructure as template for controlling hydrophobic interactions was described, in chapter 4 this concept is extended to a hybrid DNA-gold nanoparticle system highlighting the general applicability of hybrid DNA nanostructures as templates.

4 DNA nanostructures as templates to control the number, geometry and sequence asymmetry of DNA strands on gold nanoparticles

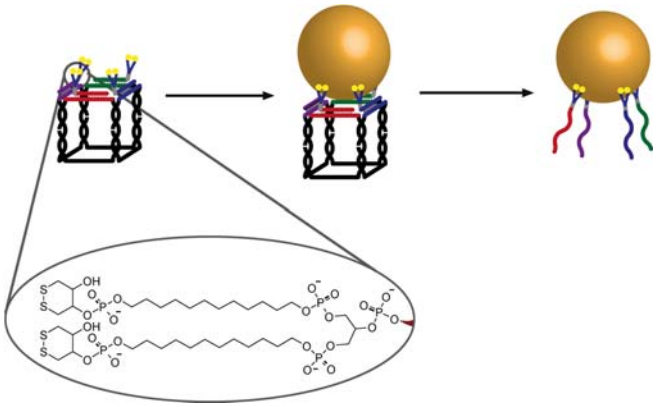

This chapter is composed mainly of work submitted for publication as "Pattern transfer from DNA nanostructures to gold nanoparticles: anisotropic control of directionality, number, geometry and sequence asymmetry", Edwardson, T. G. W.; Lau, K. L.; Bousmail, D. B.; Serpell, C. J. and Sleiman, H. F. *Nature Nanotechnology* (submitted Dec 12th, 2014).

4.1 Abstract

The self-assembly of nanoparticles into structures of predetermined size and shape is valuable for nanophotonics, nanoelectronics, catalysis and biological sensing. DNA-mediated nanoparticle assembly has produced functional materials, most often by attaching isotropically functionalized particles to DNA nanostructures. On the other hand, the ability to place DNA strands directly on spherical nanoparticles with arbitrary control of their geometry is more challenging. This can give anisotropic particles that behave as 'atoms' with specific valences, resulting in finer control of particle assembly with minimal DNA strands. In this chapter, a method to efficiently transfer a pattern of DNA strands from a 3D-DNA prismatic structure onto a gold nanoparticle is described. This strategy produces highly stable particles labelled with strands of controlled number, geometry, and asymmetric placement of different DNA sequences. The

approach is potentially scalable as the DNA templates are recovered, and the resulting particles display directional patterns with additional potential in cellular recognition and therapy.

4.2 Introduction

A major challenge in nanoparticle and colloidal assembly is the introduction of asymmetry to spherical particles.[1,2] The potential of nanoparticles as building blocks for advanced materials is currently restricted by our limited control over the interactions between individual components. In particular, the construction of both discrete and extended architectures of arbitrary geometries is challenging due to the inherent isotropic nature of nanoparticles.[3] In a bid to overcome this, there has been much effort aimed at controlling the size, shape and surface chemistry of noble metal nanoparticles.[4-10]

Since the power of DNA as a chaperone for the assembly of AuNPs was first exemplified,[11,12] it has been applied in the 1D, 2D and 3D organization of AuNPs.[13,14] However, there are limitations to the range of assemblies that can be achieved using strictly mono- or poly-functionalized AuNPs. Recently, the ability to impart particles themselves with the geometries and valences that we take for granted in molecular self-assembly has been proposed as a solution, and it may open doors to new levels of control over nanoparticle assembly.[15,16]

With this in mind, the creation of AuNPs which possess anisotropic DNA patterns has been highly sought after.[16,17] To date, advances towards these types of particles are coming ever closer to producing building blocks with the information needed for complex self-assembly. For example, controlled spacing between two or three DNA strands on the AuNP surface has been achieved using 1D DNA templates.[18-20] Microsphere clustering with in situ polymerization has been used to create DNA patches on polymer colloids.[21] Surface immobilization has also been used, creating Janus particles with localized patches of DNA strands.[22-25] The combination of surface techniques with a stepwise approach exploiting electrostatic repulsion has produced geometrically defined DNA-AuNPs with a controlled number of up to six strands.[26] More recently, amphiphilic polymers have been used to allow regioselective DNA functionalization on gold nanoparticles.[27]

While these methods have produced AuNPs with a significant measure of anisotropic regioselectivity, the ability to position many different strands with individual sequences into geometrically controlled patterns has remained elusive; this is the keystone for accessing the full potential of DNA programmability for the creation of predictable and well-defined aggregates via self-assembly.

DNA nanotechnology has been established as a powerful tool for the nanoscale organization of materials.[28-30] The broad applicability of DNA nanostructures as templates for the arrangement of other functional molecules and macromolecules makes them well suited as scaffolds for nanoparticles.[31] By site-specifically binding AuNPs at desired positions on DNA scaffolds, a wide range of DNA-AuNP architectures have been realized, from small discrete structures[32-34] to long range assemblies[35-39] and chiral structures.[40-43]

A potentially powerful strategy to impart complex assembly information to nanoparticles is to transfer the information contained in a template DNA nanostructure directly and irreversibly to the nanoparticle. DNA nanostructures are ideal candidates for this as they are monodisperse and can be assembled into arbitrary shapes and sizes with tuneable physical characteristics. A template structure must also display strongly binding chemical anchors, allowing irreversible and robust conjugation to the AuNP surface. To facilitate the production of DNA-patterned AuNPs, surface passivation and simple high-throughput methods to remove the template and isolate the desired products must also be developed. The aim would be to produce a patterning technology which provides control over the number, geometry, anisotropy and sequence asymmetry of DNA on the nanoparticle surface.

In this chapter, a general method for transferring pattern information from a parent three-dimensional DNA template to AuNPs is described. This represents a new approach, the direct 'printing' of a DNA pattern onto gold nanoparticles from a 3D nanoscaffold, and provides control over the number of strands, their relative placement, directionality and sequence asymmetry. This creates directionally functionalized AuNPs,[15] which can be used as components for the self-assembly of complex DNA programmed architectures.

4.3 Results and Discussion

4.3.1 Novel gold binding moieties

The goal is to produce a robust patterning of a well-defined number of DNA strands on the nanoparticle surface. This requires anchoring groups appended to the oligonucleotide which can bind strongly to the gold surface and remain so after downstream processing and manipulation of the samples.[17] With this in mind, a novel DNA-conjugate was synthesized,[44,45] terminated with two cyclic disulfide (**CD**) moieties to allow AuNP-DNA conjugation, Figure 4.1. A divergent synthetic strategy using standard automated DNA chemistry on a solid support was employed to produce the bis-disulfide-DNA (**Dx**, where x refers to the unique sequence) in good yield. Pure **Dx** were isolated easily by reverse-phase HPLC and characterized by LC-ESI-MS (*Experimental Sections 4.54-8*).

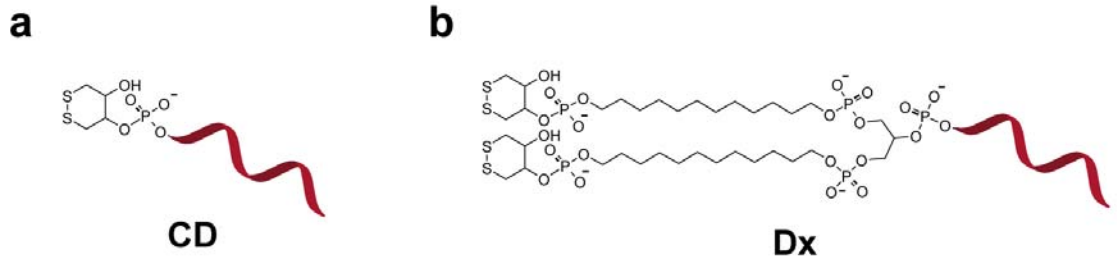

Figure 4.1 – Chemical structure of cyclic disulfide modifications. a) The structure of single CD-DNA (**CD)** which is often used for DNA-AuNP conjugation. b) The structure of bis-CD-DNA (**Dx,** where **x** will refer to a unique DNA sequence), has two cyclic disulfide moieties positioned at the end of symmetrically branched dodecane-diol spacers. .

To compare the chemical stability of AuNPs functionalized with the bis-chelating **Dx** vs. simple cyclic disulfide modified DNA (**CD**), a displacement assay was carried out using 1,4-dithiothreitol (DTT).[46] Figure 4.2 shows the absorption spectra of 10nm AuNPs poly-functionalized with **CD** and **Dx**s in the presence of 10mM DTT. The redshift of the plasmon resonance band coupled with its eventual loss in intensity is evident of aggregation of the AuNPs as the DTT displaces the DNA strands. It was found that **Dx** conjugation produced considerably more stable AuNPs than the equivalent **CD** strands.

The **Dx-AuNPs** remained in solution for around 2 hours compared to less than 15 minutes for the **CD-AuNPs** (full experimental details in *Experimental Section 4.5.11*).

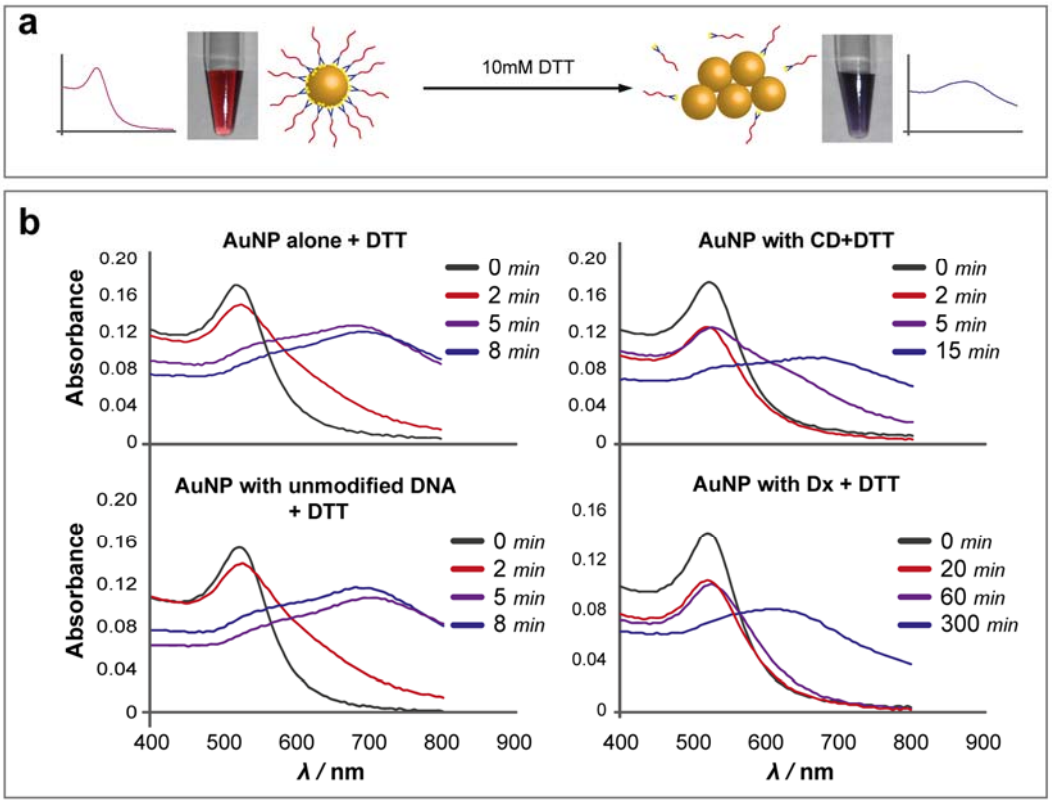

Figure 4.2 – Stability assay for DNA-AuNPs. a) Schematic of DTT displacement assay used to assess the stability of **Dx** stabilized AuNPs compared to **CD**. b) Time resolved UV-vis measurements of **Dx** compared to **CD** with controls of naked AuNP and unmodified DNA. At time zero there is no DTT in solution, upon addition of DTT (10mM) spectra were obtained at various intervals. The **Dx** stabilized AuNPs exhibit substantially enhanced stability. Measurements were carried out at 20°C in 1xTBE, 150mM NaCl.

Comparison of the gold binding ability of **CD** and **Dx** revealed that **Dx** bound to AuNPs more efficiently with faster binding kinetics, Figure 4.3. The extending C12 portion may help to orient the DTPA moieties away from the highly charged DNA backbone thus reducing electrostatic repulsion, which is a key factor in the chemisorption of DNA strands to gold nanoparticles.[47] Additionally, the ability of **Dx** to hybridize to a partner strand was confirmed by thermal denaturation studies (*Experimental Section 4.5.10*). It was found that 5' modification with the bis-disulfide moiety did not affect duplex formation with a complementary DNA strand. These results

suggested that the **Dx** conjugates are well-suited to use in the patterning experiments to follow.

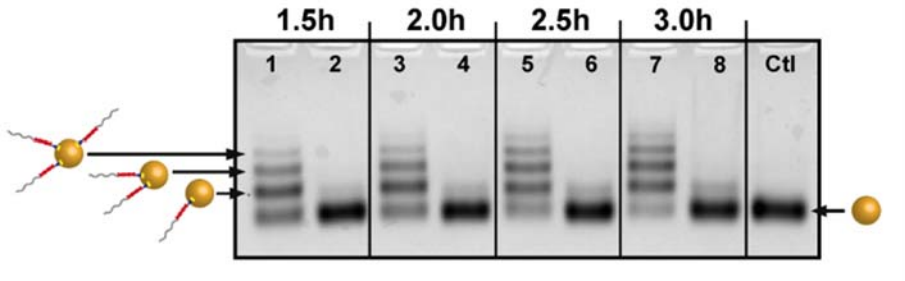

Figure 4.3 – Conjugation kinetics. Comparative binding assay of **CD** vs. **Dx** with AuNPs. Five equivalents of **CD** or **Dx** were incubated with 10nm AuNPs (100nM) for different times and the conjugation yields revealed by agarose gel electrophoresis (AGE). 3% AGE, odd numbered lanes correspond to **Dx** and even numbers to **CD**.

4.3.2 DNA nanostructure template

The criteria set for the DNA nanostructure used as a template are as follows; it has the potential for 1) geometric variation, 2) introduction of sequence asymmetry, 3) positioning of different numbers of **Dx** and 4) can be removed easily after pattern transfer. In chapter 2, and in other work from Sleiman's group it has been shown that DNA minimal 'clip-by-clip' based structures can be efficiently used to site-specifically position hydrophobic DNA-conjugates and DNA-polymer conjugates.[45,48,49] Here, the same strategy is employed to precisely arrange gold binding DNA conjugates for pattern transfer to a nanoparticle.

An important practical consideration for the DNA nanostructure is that it does not require Mg^{2+} for assembly, as gold nanoparticles with labile surface passivation (bis(p-sulfonatophenyl)phenylphosphine (BSPP) or citrate) can undergo irreversible aggregation in the presence of divalent cations. The cubic scaffold, shown in Figure 2, self-assembles efficiently in buffers containing ≥100mM NaCl. This salt concentration was found to be compatible with phosphine ligand stabilized gold nanoparticles up to 13nm in size (*Experimental Section*, Figure 4.24).

The first step in the patterning process is to prepare the template, in this case a 3D DNA scaffold decorated with the desired **Dx** for transfer to the AuNP substrate. As such,

the organization of different numbers of **Dx** on the DNA scaffold was carried out to produce a range of different letters for the printing process.

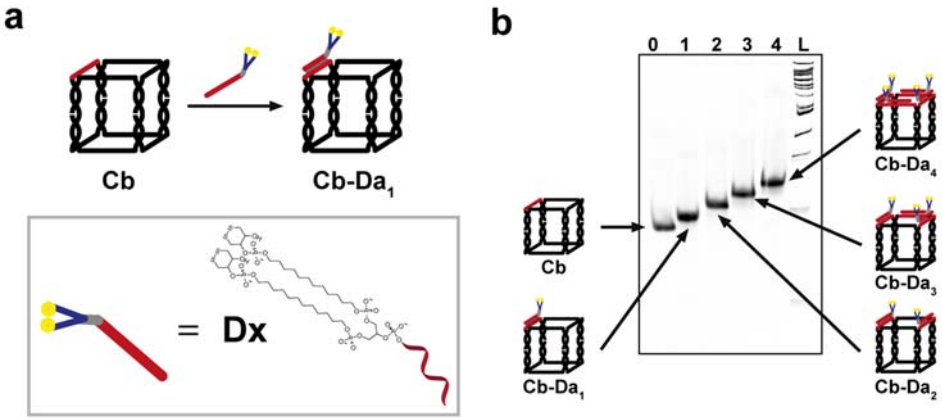

Figure 4.4 – Dx Decorated DNA scaffold. a) The DNA cube, **Cb**, has eight ssDNA binding sites which can be addressed site specifically to organize **Da** molecules. **b)** Native 6% PAGE analysis of **Da** addition to the cube scaffold: Lane 0, **Cb**; Lane 1, **Cb-Da$_1$**; Lane 2, **Cb-Da$_2$**; Lane 3, **Cb-Da$_3$**; Lane 4, **Cb-Da$_4$**; Lane L, 25-700bp DNA ladder

The same design strategy described in chapter 2 was used. The single-stranded regions of the cubic scaffold **Cb** are 20 nucleotides (nt) in length, with only the central 14 nt were used for the binding of the **Dx** which have a spacer of 5 nt to orient them away from the crowded corners of the structure. It was expected that by orienting the **Dx** away from the DNA scaffolds binding to AuNPs would be more favourable, considering electrostatic and steric influences. This design also lowers the melting temperature of this region to facilitate removal of the template after pattern transfer.

The structures shown in Figure 4.4b were assembled by one-pot thermal annealing of appropriate molar equivalents of the component DNA strands in a TBE buffer containing 100mM Na^+ (1xTBEN). Near quantitative yields of the desired products **Cb-Da$_x$** (x=1-4, cubes with 1-4 **Da** strands positioned on one face) eliminated the need for purification of the DNA nanostructure prior to AuNP patterning (Figure 4.4b).

4.3.3 Pattern transfer using symmetric cubic scaffold

Next, the ability of the functionalized DNA nanoscaffolds, **Cb-Da$_x$**, to bind to AuNPs and transfer the desired number of **Da** strands was investigated. Based on geometry calculations, 10nm AuNPs (**NP^{10}**) were used as they represent the best size match for the cubic scaffold (*Experimental Section 4.5.15*). These systems may exhibit a cooperative binding of the bis-disulfide moieties, due to the close proximity of the reactive groups upon binding of the first unit. Gold nanoparticles (10nm, BSPP coated) were incubated with **Cb-Da$_x$** at a 1:1 molar ratio for 16 hours at room temperature (1xTBEN buffer, 2mM BSPP). The resulting hybrid DNA cage-AuNP assemblies, **NP^{10}-Cb-Da$_x$**, were analyzed by AGE with reference to a control of BSPP coated AuNPs.

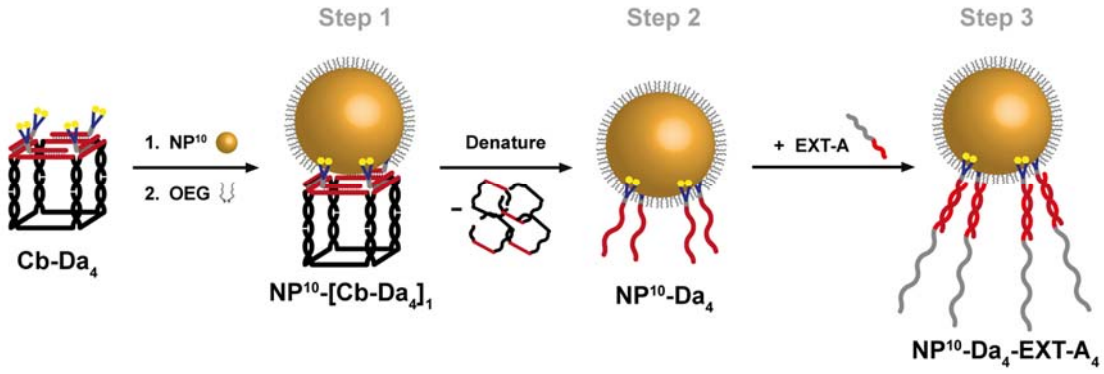

Figure 4.5 – Overview of patterning process. a) Exemplary reaction scheme showing the binding of **Cb-Da$_4$** to **NP^{10}** to produce the template bound **NP^{10}-[Cb-Da$_4$]**, which is treated with octaethylene glycol disulfide (**OEG**) for surface passivation before removal of the template by denaturing to produce **NP^{10}-Da$_4$**, which can then hybridize to four **EXT-A** strands to produce the structure **NP^{10}-Da$_4$-EXT-A$_4$**.

Electrophoretic mobility data for the reaction mixtures of **Cb-Da$_x$** with **NP^{10}** (*step 1*) are shown in Figure 4.6. The structure **Cb-Da$_1$** (cube with one DNA strand **Da** containing the chelating bis-disulfide) exhibits negligible binding to **NP^{10}**, while for **Cb-Da$_2$** a bound product with a small mobility difference is seen, which may be too small to be the expected cube-bound nanoparticle **NP^{10}-[Cb-Da$_2$]**. However, in the case of both **Cb-Da$_3$** and **Cb-Da$_4$** a product with mobility consistent with the **NP^{10}-[Cb-Da$_x$]** complex is observed (see below for elucidation). Furthermore, the trend of increasing conjugation yield with increasing number of **Da** positioned on the cube suggests a cooperative effect

due to the spatial organization on the template. Controls of cubic scaffolds unmodified with **Dx** strands showed no interaction with the AuNP, confirming that the binding was mediated by the **Dx** organized on the DNA cube (*Experimental Section*, Figure 4.25).

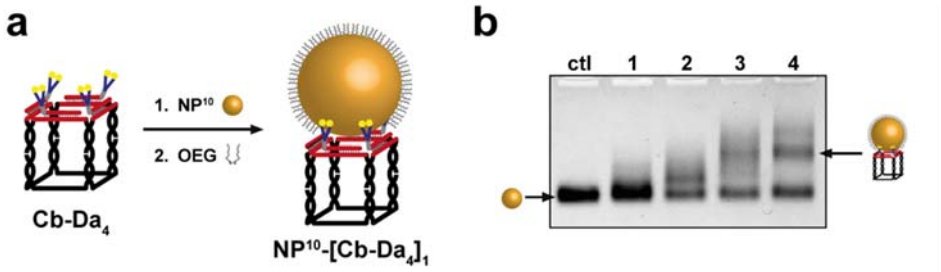

Figure 4.6 – Cube patterning analysis at step 1. a) Exemplary scheme showing *step 1* patterning stage. b) 3% AGE analysis of products obtained at *step 1* for the **Cb-Da$_x$** variants: Lane ctl, **NP^{10}**; Lane 1, **Cb-Da$_1$** + **NP^{10}**; Lane 2, **Cb-Da$_2$** + **NP^{10}**; Lane 3, **Cb-Da$_3$** + **NP^{10}**; Lane 4, **Cb-Da$_4$**+ **NP^{10}**.

To further stabilize the structures for downstream processing, the passivation of the remaining surface of the AuNPs with a stable ligand was carried out. Short carboxyl terminated octaethylene glycol disulfide (OEG) chains were used to cover the AuNP surface and furnish particles that are resilient to higher salt concentrations and divalent cations, in order to facilitate DNA assembly. It was found that this surface passivation step could be carried out before or after removal of the template scaffold with no observable difference to the assemblies (*Experimental Section*, Figure 4.26). Interestingly, after this stage the patterned AuNPs were found to be remarkably stable in sodium and even magnesium containing buffers (for weeks when stored at 7°C).

After surface passivation, samples were run on AGE and the product bands excised and isolated by electroelution. The template scaffold was removed by disrupting all DNA hybridization under denaturing conditions (3M urea, 1xTBE), followed by centrifugation to isolate AuNPs. This process afforded purified **NP^{10}-Da$_x$**, *step 2* products, shown in Figure 4.7, with average isolated yields of 35% with respect to **NP^{10}**.

To determine the number of **Dx** strands transferred to the AuNP, and thus the fidelity of the patterning process, extension strands (**EXT-X**, where **X** is complementary to the **Dx** strands bound to the AuNP) were used to provide greater gel mobility differences and aid characterization, see *step 3* in Figure 4.7. Importantly, these also probe the addressability of the **Dx** strands bound to the AuNP surface.

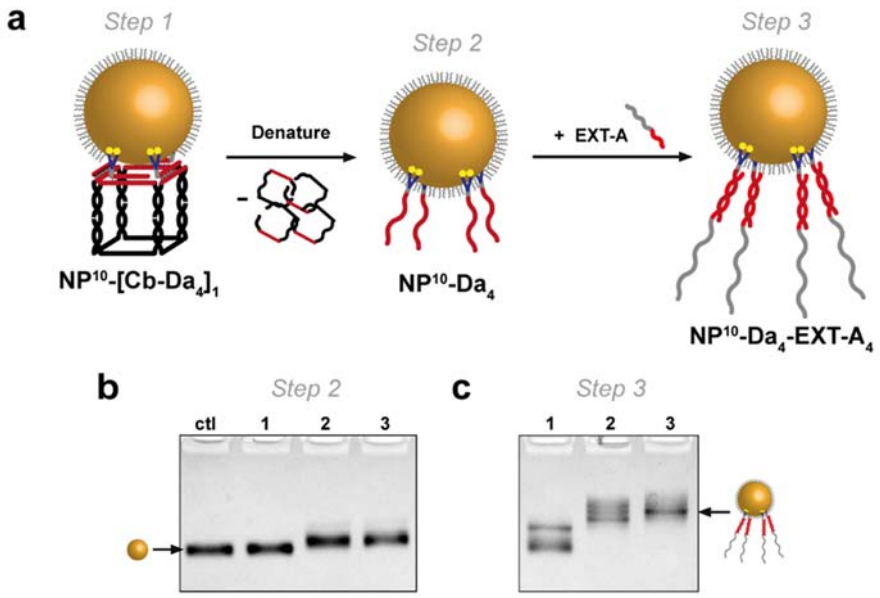

Figure 4.7 – Cube patterning analysis at steps 2 and 3. a) Exemplary scheme showing *step 2* and *3* patterning stage. b) 3% AGE analysis at *step 2* for denatured product bands: Lane ctl, **NP^{10}**; Lane 1, **NP^{10}-Da$_2$**; Lane 2, **NP^{10}-Da$_3$**; Lane 3, **NP^{10}-Da$_4$**. c) 3% AGE analysis at *step 3* after addition of **EXT-A** for resolution of products: Lane 1, **NP^{10}-Da$_2$-EXT-A$_2$**; Lane 2, **NP^{10}-Da$_3$-EXT-A$_3$**; Lane 3, **NP^{10}-Da$_4$-EXT-A$_4$**.

The **EXT-X** strands were designed to have a 17nt region of complementarity with each **Dx** strand and an extending ssDNA tail of 43nt to provide sufficient resolution on AGE. We will focus first on the coupling product **NP^{10}-Da$_4$**. This product was isolated from the major band in Figure 4.6b (lane 4), and was characterized (Figure 4.7b, lane 3). Aliquots of the samples were incubated with an excess of **EXT-A** strands (25 molar equivalents) in tris-acetate-magnesium (1xTAMg) buffer for 2 hours at 25°C. The resulting sample exhibits decreased mobility in comparison with **NP^{10}-Da$_4$** starting material, revealing that the **Da** strands transferred to the AuNP surface remain available for duplex formation and retain practical hybridization kinetics (Figure 4.7c, lane 3).

The process was repeated for **NP^{10}-Da$_3$** and **NP^{10}-Da$_2$** in which the cube is bound to the nanoparticle via three or two bis-disulfide DNA strands. Comparison of mobility differences with the tetra-patterned sample **NP^{10}-Da$_4$** revealed that higher fidelity pattern transfer was achieved with higher numbers of **Da** on the scaffold, Figure 4.7. **Cb-Da$_3$** and **Cb-Da$_2$** gave a distribution of patterned products, while the sample created from the **Cb-Da$_4$** template gave one major product **NP^{10}-Da$_4$-EXT-A**, exhibiting mobility consistent with four **Da** strands bound to the surface, Figure 4.7c (the faint band above the major product in Figure 4.7c (lane 3) is a result of the addition of excess **EXT-A** and some non-specific binding, see Figure 4.12a).

To highlight the advantage of using a template scaffold to control the number of strands transferred to the AuNP, a non-templated control sample was prepared. For this, 1 to 4 molar equivalents of **Da** were incubated with 10nm BSPP coated AuNPs under the same conditions used for the preparation of **NP^{10}-Da$_x$**. These samples were then incubated with **EXT-A** and analyzed by AGE. A statistical distribution of products with between one and four **Da** strands bound to the AuNP was observed (Figure 4.8), which is very different from the behavior of **NP^{10}-Da$_x$**.

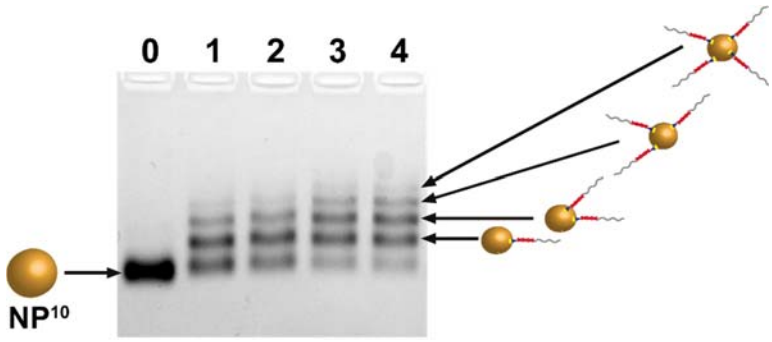

Figure 4.8 - Non-patterned control. Without organization on a template a statistical distribution of products is seen, 3% AGE: Lane 0 – **NP^{10}**, Lane 1 – **NP^{10} + 1x [Da-EXT-A]**, Lane 2 – **NP^{10} + 2x [Da-EXT-A]**, Lane 3 – **NP^{10} + 3x [Da-EXT-A]**, Lane 4 – **NP^{10} + 4x [Da-EXT-A]**.

Additionally, DLS analysis of **NP^{10}-Da$_4$** in comparison to non-templated control, which had four **Da** strands randomly distributed on the AuNP surface, was carried out, Figure 4.9. The templated sample, **NP^{10}-Da$_4$**, exhibited less than 10% polydispersity compared to the control sample which gave more than 20%, corroborating the AGE

results and suggesting regioselective control via the cube template (see *Experimental Section 4.5.18* for details).

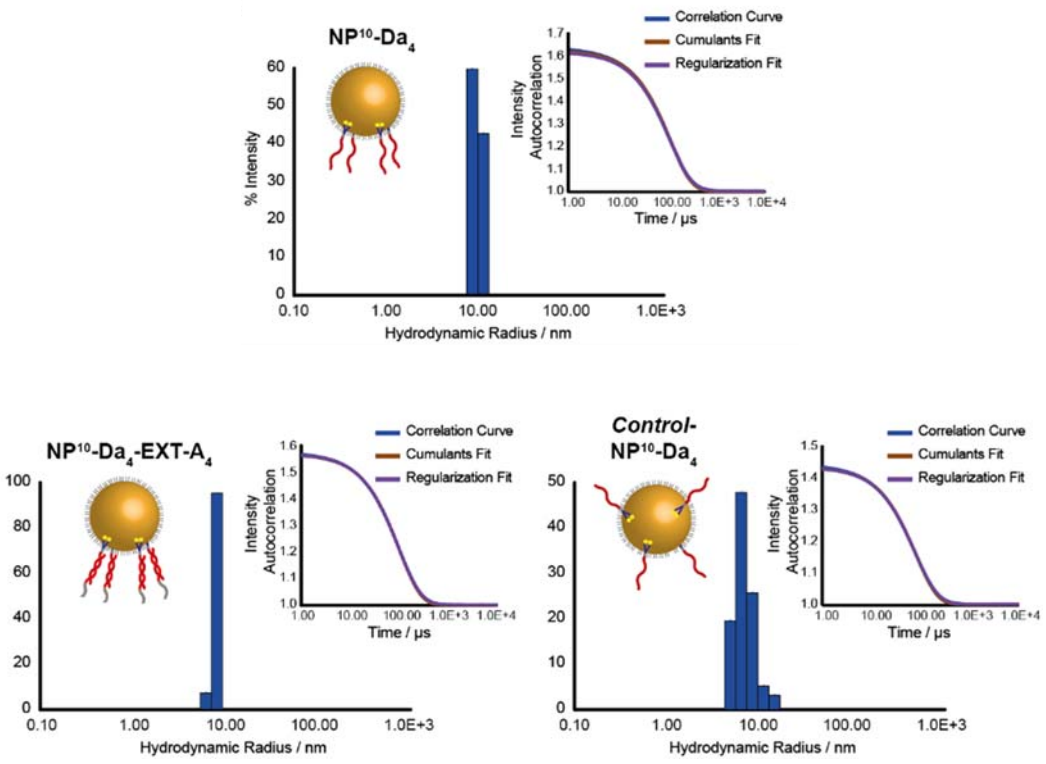

Figure 4.9 – DLS of anisotropically DNA-functionalized AuNPs. DLS measurements of the templated product **NP^{10}-Da$_4$** at *steps 2* and *3* in comparison to a control sample in which four **Da** are positioned randomly on the nanoparticle reveals lower polydispersity, consistent with regioselectivity.

Another important consideration of this approach is that not only the number of **Dx** strands bound to the AuNP is controlled by the parent template, but also the directionality and spacing of the **Dx** on the AuNP surface, which are the direct result of the geometry of the DNA template (see below). The preparation of Janus particles as a strategy to introduce anisotropy to spheres has been used to produce a range of asymmetrically functionalized AuNPs.[22,23,25,27,50] Although hemispherical separation can be obtained, the number and placement of DNA strands on the AuNP is not precisely controlled.

4.3.4 Patterning using geometric variants

Based on the data showing that full decoration of one face of the DNA scaffold with **Da** provided the best patterning templates, extension of the method to other prism geometries was investigated. To probe the applicability of the patterning of different numbers and geometries of scaffold, triangular (**TP**) and pentagonal prism (**PP**) templates were synthesized in the same manner as for the cube. The **TP** and **PP** scaffolds were decorated with **Da** strands to produce **TP-Da$_3$** and **PP-Da$_5$** which were incubated with 10nm BSPP coated AuNPs and then passivated with **OEG**.

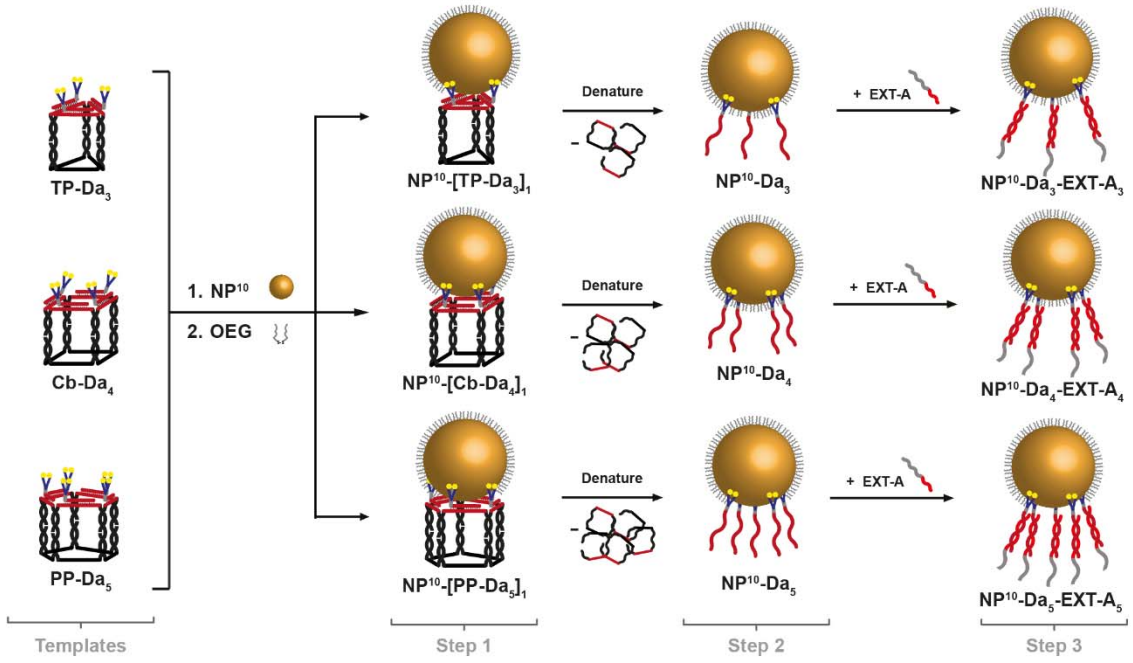

Figure 4.10 – Overview of patterning with geometric prism series. General scheme for the patterning of AuNP using the DNA scaffolds **TP-Da$_3$**, **Cb-Da$_4$** and **PP-Da$_5$** to produce tri-, tetra- and pentavalent DNA-AuNPs **NP^{10}-Da$_3$**, **NP^{10}-Da$_4$** and **NP^{10}-Da$_5$**.

The resulting assemblies were compared to the products obtained from cubic patterning. The prism-AuNP constructs were analyzed by AGE and a decrease in electrophoretic mobility was seen with increasing DNA scaffold size, consistent with the binding of the prisms to the AuNPs, Figure 4.11. In each case the second bands, highlighted in Figure 4.10b, were determined to be the 1:1 complexes, e.g. **NP^{10}-[TP-Da$_3$].** The band of lowest mobility was assigned as the 2:1 product, e.g. **NP^{10}-[TP-Da$_3$]$_2$**,

based on gel mobility (Figure 4.12b) and a titration assay (*Experimental Section*, Figure 4.27).

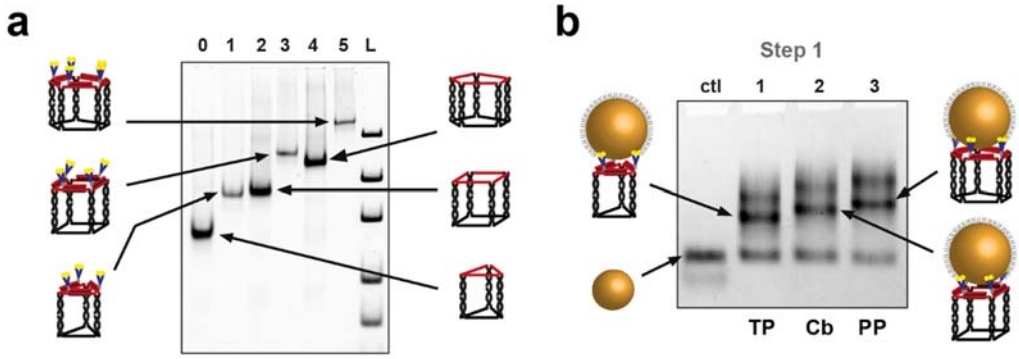

Figure 4.11 – Step 1 products of geometric patterning. a) Native 6% PAGE analysis of **Da** decorated prisms: Lane 0, **TP**; Lane 1, **TP-Da$_3$**; Lane 2, **Cb**; Lane 3, **Cb-Da$_4$**; Lane 4, **PP**; Lane 5, **PP-Da$_5$**; Lane L, 75-300bp DNA ladder. **c)** 3% AGE analysis of crude products at step 1: Lane ctl, **NP^{10}**; Lane 1, **TP-Da$_3$ + NP^{10}**; Lane 2, **Cb-Da$_4$ + NP^{10}**; Lane 3, **PP-Da$_5$ + NP^{10}**.

After purification and removal of the prism strands by denaturation, **EXT-A** was added to resolve the number of strands transferred to the AuNP. In Figure 4.12a, electrophoretic mobility patterns reveal that 3, 4 and 5 strands were transferred by **TP-Da$_3$**, **C-Da$_4$** and **PP-Da$_5$**, respectively. Additionally, products isolated from the band of lower mobility in *step 1*, which corresponds to 2:1 prism:AuNP complexes are shown in Figure 4.12b.

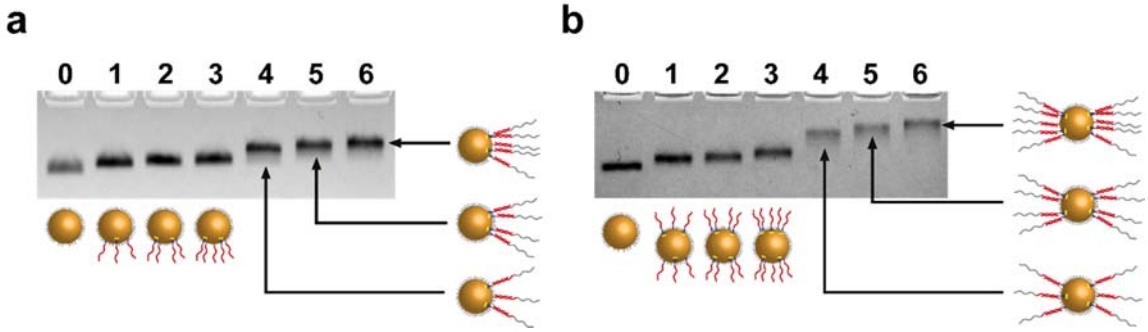

Figure 4.12 – Single and double geometric products. a) Products which are derived from the binding of one prism to one AuNP, with and without **EXT-A** strands: Lane 0, **NP^{10}(OEG)**; Lane 1, **NP^{10}-Da$_3$**; Lane 2, **NP^{10}-Da$_4$**; Lane 3, **NP^{10}-Da$_5$**.; Lane 4, **NP^{10}-Da$_3$-EXT-A$_3$**; Lane 5, **NP^{10}-Da$_4$-EXT-A$_4$**; Lane 6, **NP^{10}-Da$_5$-EXT-A$_5$**. **b)** Products which are derived from the binding of two prisms to one AuNP, with and without **EXT-A** strands: Lane 0, **NP^{10}(OEG)**; Lane 1, **NP^{10}-Da$_6$**; Lane 2, **NP^{10}-Da$_8$**; Lane 3, **NP^{10}-Da$_{10}$**; Lane 4, **NP^{10}-Da$_6$-EXT-A$_6$**; Lane 5, **NP^{10}-Da$_8$-EXT-A$_8$**; Lane 6, **NP^{10}-Da$_{10}$-EXT-A$_{10}$**.

The expected trend and increase in mobility correspond the transfer of 6, 8 and 10 **Da** to the AuNP. This shows that the AuNP can be patterned from both sides and has implications for the patterning of more complex 3D arrangements of DNA strands.

For additional characterization, the R_h of the patterned products, with and without extension strands, were determined by DLS, Figure 4.13. In reference to **NP^{10}**(OEG), R_h = 6.9 ± 0.2nm, a slight increase in hydrodynamic radii is seen with increasing number of strands in the series **TP-Da$_3$**, **C-Da$_4$** and **PP-Da$_5$** with R_h of 7.4 ± 0.2nm, 7.6 ± 0.2nm and 7.7 ± 0.1nm, respectively. The addition of **EXT-A** strands accentuated the trend, with R_h of 7.8 ± 0.1nm, 8.8 ± 0.1nm and 9.6 ± 0.1nm, for **NP^{10}-Da$_3$-EXT-A$_3$**, **NP^{10}-Da$_4$-EXT-A$_4$** and **NP^{10}-Da$_5$-EXT-A$_5$**, respectively. Moreover, comparing R_h data of samples with 3, 4 or 5 **Da** per particle but no spatial control revealed that templated products were less polydisperse than their non-patterned counterparts, (*Experimental Section*, Figures 4.31-4.34 and Table 4.5). These data, obtained for each step of the patterning process, demonstrate that well-defined numbers of DNA strands can be transferred to the AuNPs by geometric variation of the parent template.

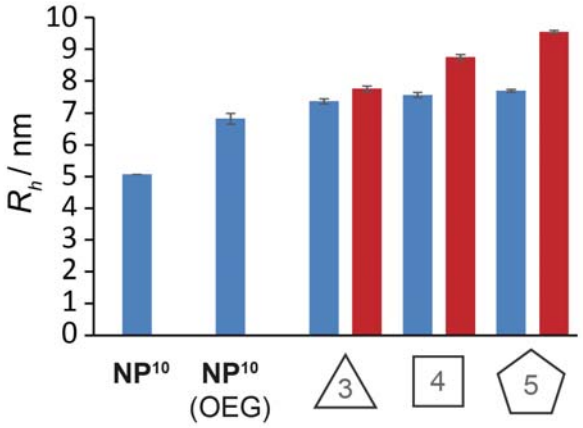

Figure 4.13 – Summary of DLS results for geometric series. DLS study of the products at step 2 and 3 of the patterning process - blue bars refer to *step 2* products and red bars to *step 3*, after addition of **EXT-A**. (Full DLS data can be found in the *Experimental Section 4.5.18*)

4.3.5 Transfer of sequence asymmetry

Finally, the potential of this strategy to transfer a specific number of strands to the nanoparticle, where the DNA sequence asymmetry can be varied, was investigated. The preparation of DNA-AuNPs with a defined number of strands, each of which has a unique sequence, has to date been unachievable using current techniques. These truly asymmetric particles represent building blocks with great potential in the field of self-assembled advanced materials.[15,16]

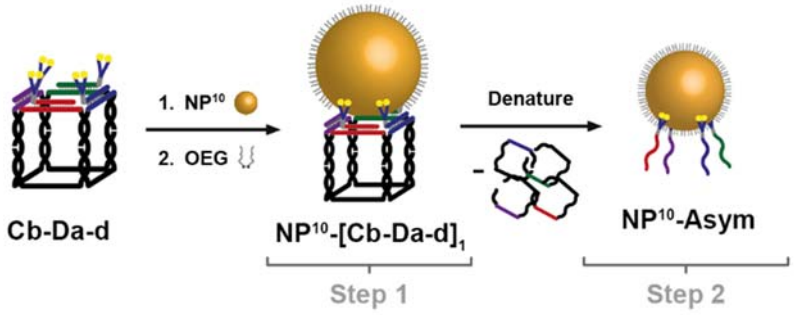

Figure 4.14 – Transfer of sequence asymmetry. General strategy for the production of sequence specifically patterned AuNPs using asymmetric DNA scaffolds **Cb-Da-d** to transfer four unique **Dx** strands to the AuNP.

A cubic scaffold with eight unique ssDNA binding sites **Cb-Da-d** was assembled and decorated with four unique gold binding conjugates; **Da**, **Db**, **Dc**, and **Dd,** on the top face. Incubation with 10nm AuNPs followed by **OEG** surface passivation, isolation of the major product, **NP^{10}-[Cb-Da-d]$_1$**, and subsequent removal of the cubic scaffold, produced sequence asymmetric **NP^{10}-Da$_1$-Db$_1$-Dc$_1$-Dd$_1$ (NP^{10}-Asym)**.

To confirm the correct four strand DNA sequence code had been transferred to the AuNP, stepwise addition of four unique **EXT** strands, **EXT-A** to **EXT-D**, was carried out as before. In Figure 4.15b, the stepwise binding and site selective addressability of **NP^{10}-Asym** is shown, in lane 3 the addition of **EXT-A** produces a particle with one extension strand bound and **Db**, **Dc** and **Dd** available for further hybridization, **E1**. The subsequent addition of the remaining three extension strands reveals a ladder of decreasing mobility as each additional **EXT** binds to its specific site on **NP^{10}-Asym**. This

confirmed that the asymmetric pattern had been correctly transferred to the AuNP and the **Dx** are individually addressable due to their unique sequences.

A control sample of AuNP incubated with one molar equivalent of each **Dx** strand (**Da**-**Dd**) without organization on a template was prepared under the same conditions as the patterned sample. This should produce a statistical mixture of number and identity of **Dx** on the AuNP. Stepwise addition of the **EXT** strands **A**-**D** reveals this in 4.15c. This highlights the control of information transfer achieved by the use of the DNA nanoscaffold template.

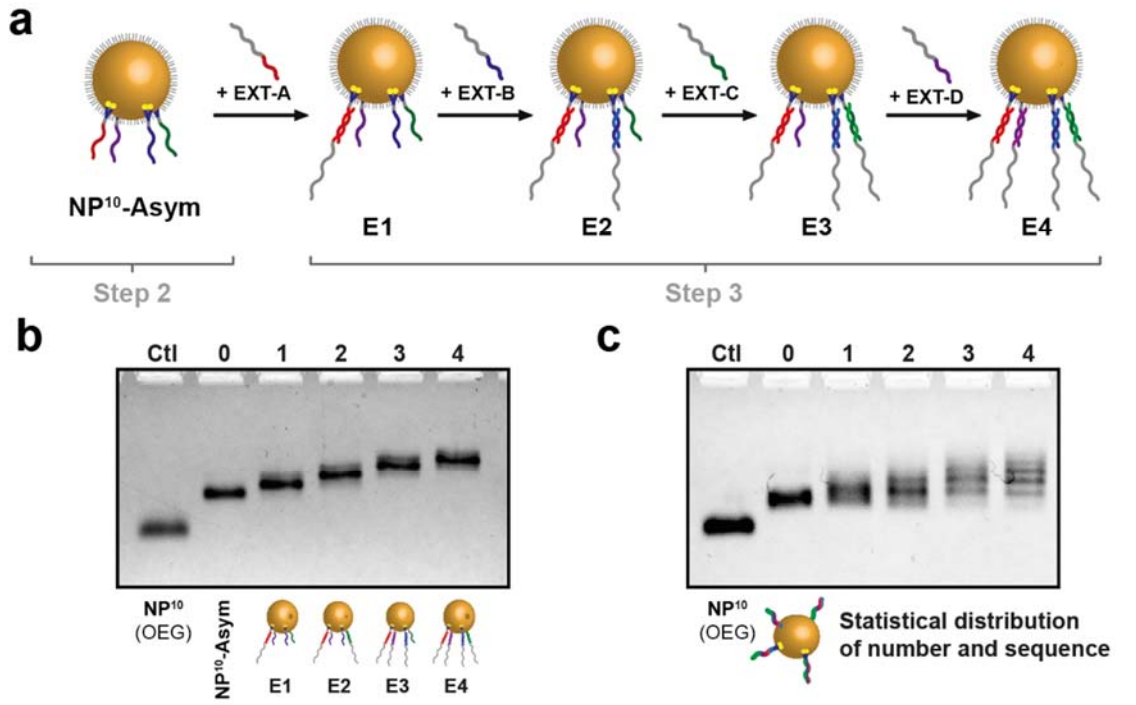

Figure 4.15 – Uniquely addressable anisotropic AuNPs. a) Each **Dx** strand on **NP^{10}-Asym** can be targeted individually to produce **E1-4**. b) 3% AGE analysis of purified **NP^{10}-Asym** showing the site-specific binding of each unique **EXT** strand: Lane ctl, **NP^{10}**; Lane 0, **NP^{10}-Da-d**; Lane 1, **E1**; Lane 2, **E2**; Lane 3, **E3**.; Lane 4, **E4**. c) 3% AGE analysis of template free control where one equivalent of each **Da**-**Dd** was incubated with **NP^{10}**, the addition of specific **EXT** strands reveals the statistical distribution of number and sequence: Lane ctl, **NP^{10}**; Lane 0, **NP^{10}-Dx$_n$**; Lane 1, **NP^{10}-Dx$_n$** + **EXT-A**; Lane 2, **NP^{10}-Dx$_n$** + **EXT-A/B**; Lane 3, **NP^{10}-Dx$_n$** + **EXT-A/B/C**; Lane 4, **NP^{10}-Dx$_n$** + **EXT-A/B/C/D**.

To visualize the asymmetric pattern and regioselectivity by TEM, 6nm AuNPs (**NP^{6}**) bearing complementary sequences (**a'**-**d'**) to the patterned **NP^{10}-Asym** were used as site-selective probes. The parent particle **NP^{10}-Asym** was incubated with an excess of

different **NP⁶-Dx'** to produce the structures shown in Figure 4.16. The decrease in mobility upon sequential addition of **NP⁶-Dx'** to **NP¹⁰-Asym** is analogous to that seen with addition of extension strands, revealing the binding of the 6nm AuNPs to each unique site on the parent particle, **NP¹⁰-Asym**. The bands highlighted were excised and electroeluted for TEM analysis. The lower yields seen for the higher order structures are not unexpected as there will be increased steric and electrostatic repulsion, this could be overcome by varying the DNA length to optimizing the spacing between the particles.

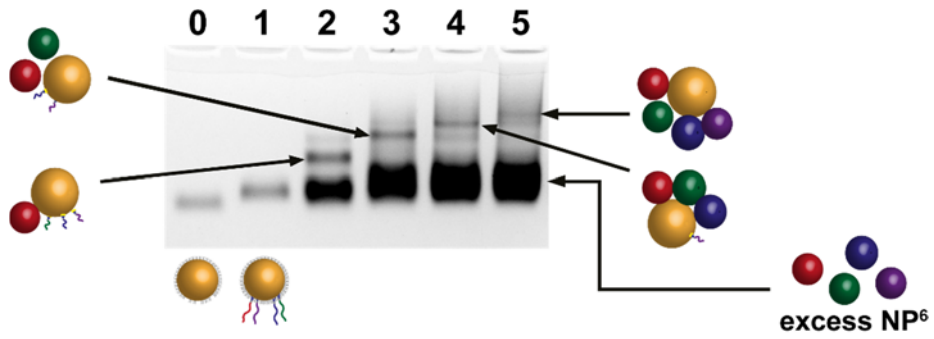

Figure 4.16 - AGE analysis of asymmetric satellite structures. Poly-functionalized **NP⁶** can bind selectively to each specific strand on the asymmetrically patterned nanoparticle, **NP¹⁰-Asym.** 3% AGE: Lane 0, **NP¹⁰(OEG)**; Lane 1, **NP¹⁰-Asym**; Lane 2, **NP¹⁰-Asym + NP⁶-Da'**; Lane 3, **NP¹⁰-Asym + NP⁶-Da' + NP⁶-Db'**; Lane 4, **NP¹⁰-Asym + NP⁶-Da' + NP⁶-Db' + NP⁶-Dc'**; Lane 5, **NP¹⁰-Asym + NP⁶-Da' + NP⁶-Db' + NP⁶-Dc' + NP⁶-Dd'**. The large band at highest mobility corresponds to the excess 6nm AuNPs.

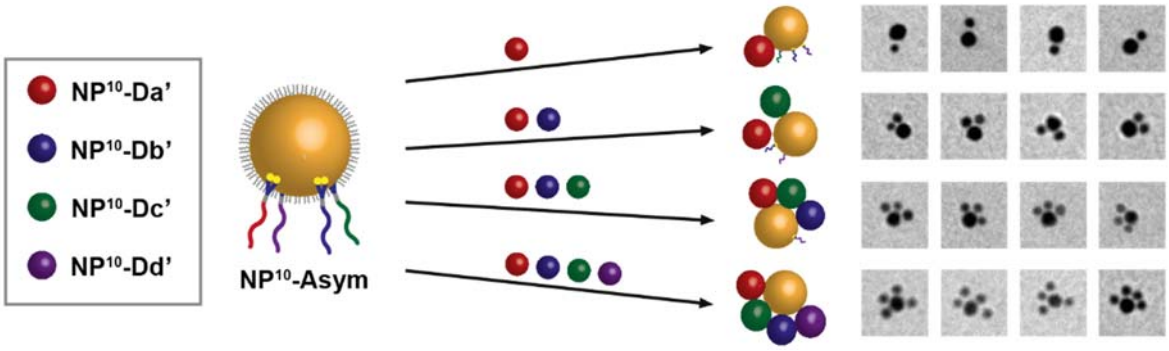

Figure 4.17 - TEM images of asymmetric satellite structures. TEM images show the site-specific addressability of the structure **NP¹⁰-Asym** by hybridization of **NP⁶** labelled with complementary strands **Da'**, **Db'**, **Dc'** or **Dd'**, the structure of these satellite structures shows the anisotropic nature of the patterning (for additional TEM images and statistics see *Experimental Section 4.5.19*).

To further investigate the sequence specificity imparted to the **NP^{10}-Asym** particles a fluorescence assay was employed. Two fluorophores were used; 6-carboxyfluorescein (6-FAM) and cyanine 3 (Cy3), which have discernible excitation/emission properties. We synthesized four 5' dye- labelled DNA sequences a' – d'; **Cy3-a'**, **Cy3-b'**, **6-FAM-c'** and **6-FAM-d'**. Incubation of 1.5 molar equivalents of fluorophore to each unique binding site on **NP^{10}-Asym** was carried out at room temperature for 12 hours. This was followed by three centrifugation and washing cycles, under native conditions, to remove any traces of unbound dyes, and produce **F4** (Figure 4.18a).

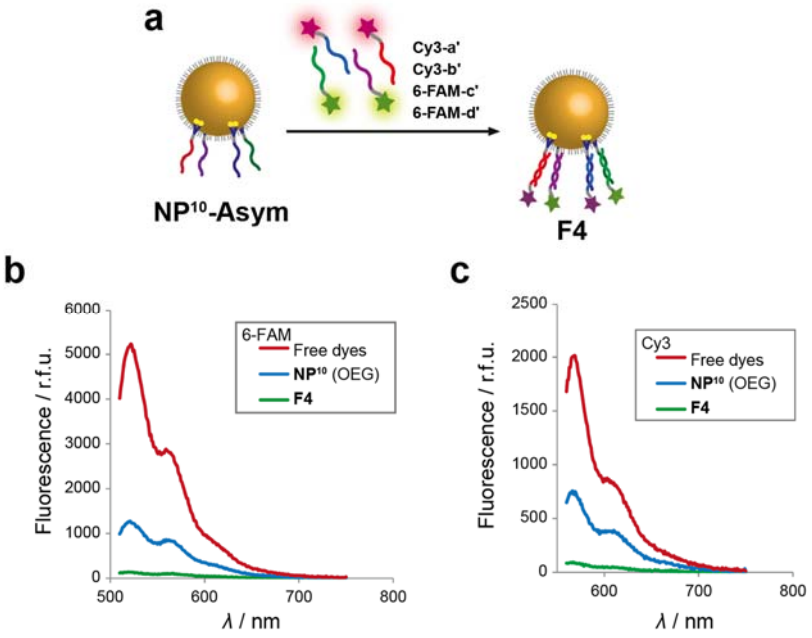

Figure 4.18 – Fluorescent labelling of AuNPs. a) Scheme showing the preparation of a fluorophore 'barcode' on the sequence asymmetric **NP^{10}-Asym** using Cy3 and 6-FAM labelled oligonucleotides. b) Fluorescence emission spectra of 6-FAM free in solution, in the presence of **NP^{10}**(OEG) and when bound to the AuNP in structure **F4** (Excitation; 490nm) c) Spectra for Cy3 free in solution, in the presence of **NP^{10}**(OEG) and when bound to the AuNP in structure **F4** (Excitation; 545nm).

Steady-state fluorescence spectra of the nanoparticle bearing all four dye-labelled DNAs (**F4**) were measured, Figure 4.18b-c, and compared to control samples which contained the same concentration of dyes free in solution and in the presence of an AuNP without complementary DNA strands, **NP^{10}**(OEG). Firstly, a small decrease in fluorescence is seen in the presence of **NP^{10}**(OEG) compared to the free dyes, suggesting some non-specific binding occurs. In contrast, for the sample **F4**, a large decrease in emission is observed when the dye-labelled DNAs are bound to the nanoparticle by

hybridization to their surface bound complements. The fluorescence quenching observed is likely caused by both the AuNP as well as the close proximity of the dyes to each other. [51]

The efficient fluorescence quenching of the AuNP bound dyes allowed a displacement assay to be monitored directly without the need for separation of the AuNPs and liberated fluorophores at each step, Figure 4.19a. Four specific eraser strands, $\mathbf{E_a}$ to $\mathbf{E_d}$, were designed to remove the dye-tagged strands one-by-one from **F4** by strand displacement, utilizing a 10nt toehold region for specificity and rapidity. Figure 5d shows the cumulative addition of the different eraser strands, which will release the dyes from the AuNP sequentially, giving an increase in fluorescence emission of a specific dye at each step. For example, $\mathbf{E_a}$ is added to **F4** to liberate **Cy3-a'** and produce the structure **F3**. At this step an increase in Cy3 fluorescence is observed with negligible change in the 6-FAM fluorescence. The following displacement steps were carried out by alternating between the two dyes, in each case an increase in fluorescence for one dye was seen.

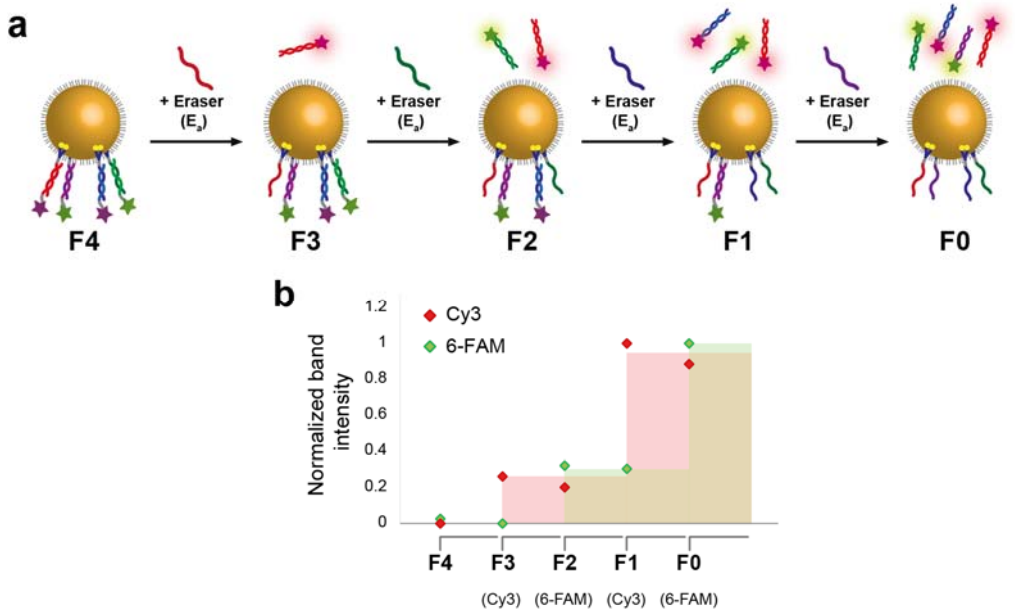

Figure 4.19 – Selective liberation of fluorophores. a) Scheme showing the sequential, site-specific release of fluorophores 'by stand displacement. b) Histogram produced from AGE analysis of sequential strand displacement of dyes from **F4** to finally produce **F0.** The order of eraser strands added was: E_a, E_c, E_b then E_d. This corresponds to alternating removal of the two dyes starting with Cy3. The resulting increase in fluorescence at each step was seen to be dye specific, through the sequence specific eraser strands. (refer to *Experimental Section 4.5.21* for additional details).

These results further support that four DNA strands with unique sequences have been transferred to the AuNP by the patterning method and presents a platform with unique properties well-suited to biosensing. In particular, this method can result in a very large and diverse set of 'barcoded' gold nanoparticles from a minimum number of dyes of different colors, allowing efficient multiplexing of bioanalyte sensing platforms.[52]

4.4 Conclusions

In this chapter, a method to encode gold nanoparticles with complex patterns comprising number, geometry and positioning of different unique DNA strands was described. The use of DNA nanostructures as transient templates for the creation of patterned AuNPs is a general strategy which could be applied to a variety of inorganic nanoparticles. For example, the application of this approach to non-spherical particles could be used as a strategy for furthering complexity. As well as allowing the transfer of different geometrical patterns to the AuNP, it is possible that the size ratio between the different DNA scaffolds and the AuNP could be used to further control the surface spacing and angle between DNA strands. In principle, this strand transfer should give a chiral arrangement of the DNA strands on the gold nanoparticles, which will be useful for the development of chiral plasmonic structures.

This method also presents the advantage of potential recycling of the template or solid-support immobilization for high throughput, scalable generation of patterned structures. The products of the templation, AuNPs with regioselective sequence specific patterning of precise numbers of DNA strands have the potential to be used as building blocks for the creation of designer nano-, meso- and macroscopic architectures. The ability to program nanoparticle assemblies using the patterned building blocks has the potential to provide access to advanced materials with pre-determined functionality through rational design.

As well as applications in colloidal crystallization and biocomputing,[53] it is likely that this method could also be applied to surfaces to guide nanoelectronic or photonic circuitry or create robust anchors for positioning other functional components such as aptamers and enzymes. It is becoming well understood that surface structure and ligand placement are key factors to the cellular uptake of nanoparticles *in vitro* and their fate *in*

vivo. This patterning creates a platform for exploring site-specific multivalent ligand-receptor or cell-surface interactions in combination with nucleic acid functionalized nanoparticles, for regulation of gene expression.[54]

4.5 Experimental Section

4.5.1 General

PEG acid disulfide (**OEG**) (cas # 873013), magnesium acetate and triethylamine were purchased from Sigma and used without further purification. Acetic acid and boric acid were used as purchased from Fisher Scientific. Acrylamide/Bis-acrylamide (40% 19:1 solution), ammonium persulfate, TEMED, tris(hydroxymethyl)-aminomethane (Tris), urea, EDTA and agarose were obtained from Bioshop Canada Inc. and used as supplied. Universal 1000Å LCAA-CPG supports with loading densities of 25-40 μmol/g and standard reagents used for automated DNA synthesis were purchased through Bioautomation. Gold colloids were purchased from Ted Pella. Sephadex G-25 (super fine, DNA grade) was purchased from Glen Research. GelRed™ nucleic acid stain was purchased from Biotium Inc. 1xTBE buffer is composed of 90mM Tris and Boric acid and 2 mM EDTA with pH 8.3. 1xTBEN buffer is composed of 90mM Tris and Boric acid, 2 mM EDTA and 100mM NaCl with pH 8.3. 1xTAMg buffer is composed of 45 mM Tris and 12.5 mM $Mg(OAc)_2 \cdot 6H_2O$ with pH adjusted to 7.8 using glacial acetic acid.

4.5.2 Instrumentation

DNA synthesis was performed on a Mermade MM6 synthesizer from Bioautomation. HPLC purification was carried out on an Agilent Infinity 1260. DNA quantification measurements were performed by UV absorbance with a NanoDrop Lite spectrophotometer from Thermo Scientific. A Varian Cary 300 Bio spectrophotometer was used for melting temperature studies. Polyacrylamide gel electrophoresis experiments were carried out on a 20 X 20 cm vertical Hoefer 600 electrophoresis unit and for agarose gel electrophoresis experiments Thermo Scientific™ Owl™ EasyCast™ B1 Mini Gel Electrophoresis Systems were used. Gel images were captured using a ChemiDoc™ MP System from Bio-Rad Laboratories. Electroelution employed an Elutrap® Electroelution System from Whatman®. Thermal annealing of all DNA structures was conducted using an Eppendorf Mastercycler® 96 well thermocycler.

Oligonucleotide mass determination by Liquid Chromatography Electrospray Ionization Mass Spectrometry (LC-ESI-MS) was carried out using a Dionex Ultimate 3000 coupled to a Bruker MaXis Impact™ QTOF. DLS experiments were carried out using a DynaPro™ Instrument from Wyatt Technology. TEM Micrographs were obtained using a Phillips Tecnai 12 120 kV microscope.

4.5.3 Synthesis of DNA-conjugates

The DNA synthesis was performed on a 1 μmole scale, using universal 1000 Å CPG solid-supports (BioAutomation, cat.# MM1-3500-1). Dithiol phosphoramidite (cat.# 10-1937), Cy3 and fluorescein (6-FAM) phosphoramidites (cat.# 10-5913 and 10-1963) were purchased from Glen Research. Symmetrical branching (cat.# CLP-5215) and DMT-dodecane-diol (cat.# CLP-1114) phosphoramidites were purchased from ChemGenes. All non-standard amidites were dissolved to 0.1M in anhydrous acetonitrile, extended coupling times of 10 minutes using manual 'syringe technique' under argon atmosphere were employed. Coupling efficiency was monitored after removal of the dimethoxytrityl (DMT) 5′-OH protecting groups, using 3% DCA in dichloromethane. Completed syntheses were deprotected in 28% aqueous ammonium hydroxide solution for 16-18 hours at 65°C. The crude deprotected solution was separated from the solid support and concentrated under reduced pressure at 60°C. This crude solid was re-suspended in 0.5mL Millipore water and filtered through a 0.45μm syringe filter for HPLC purification. The resulting solution was quantified by absorption at 260nm.

Table 4.1 - Sequences used for DNA-conjugates, unmodified cube binding strands and EXT. Non-standard amidite codes: (***C***=Cyclic Dithiol), (***D***=DMT-dodecane-diol), (***S***=Symmetrical branching).

Name	Sequence (5'-xx-3')
AT	TTTTTCAGTTGACCATATA
BT	TTTTACCATCTGGTATTAC
CT	TTTTTGCCAGTATAGAAGA
DT	TTTTTCTCGCAGTCGCGGT
Da	***CDS***TTTTTCAGTTGACCATATA
Db	***CDS***TTTTACCATCTGGTATTAC
Dc	***CDS***TTTTTGCCAGTATAGAAGA
Dd	***CDS***TTTTTCTCGCAGTCGCGGT
Da'	***CDS***TTTATATGGTCAACTGAAA

Db'	***CDS***TTGTAATACCAGATGGTAA
Dc'	***CDS***TTTCTTCTATACTGGCAAA
Dd'	***CDS***TTACCGCGACTGCGAGAAA
CD-a	***C***TTTTTCAGTTGACCATATA
EXT-A	TTTTTTTTTTTTTTTTTTTTTTTTTTTTTTTTTTTTTTTTTTTTTTTATATGGTCAACTGAAA
EXT-B	TTTTTTTTTTTTTTTTTTTTTTTTTTTTTTTTTTTTTTTTTTTTTTTGTAATACCAGATGGTAA
EXT-C	TTTTTTTTTTTTTTTTTTTTTTTTTTTTTTTTTTTTTTTTTTTTTTTCTTCTATACTGGCAAA
EXT-D	TTTTTTTTTTTTTTTTTTTTTTTTTTTTTTTTTTTTTTTTTTTTTTTACCGCGACTGCGAGAAA
Cy3-a'	***Cy3***GGACGGATGTTATATGGTCAACTGAAA
Cy3-b'	***Cy3***CTAGCTTTCGGTAATACCAGATGGTAA
6-FAM-c'	***6-FAM***TACTCACTTTTCTTCTATACTGGCAAA
6-FAM-d'	***6-FAM***CGCTCATCATACCGCGACTGCGAGAAA
E_a	TTTCAGTTGACCATATAACATCCGTCC
E_b	TTACCATCTGGTATTACCGAAAGCTAG
E_c	TTTGCCAGTATAGAAGAAAAGTGAGTA
E_d	TTTCTCGCAGTCGCGGTATGATGAGCG

4.5.4 HPLC Purification

For Dx modifications. Solvent system; A:TEAA buffer, B:Acetonitrile. TEAA buffer (50mM Triethylammonium acetate, pH 8.0) was filtered through 0.22μm cellulose membrane before use. The elution gradient was 3-40% solvent B over 30 minutes. Column: Hamilton PRP-C18 5 μm 100 Å 2.1 x 150 mm. For each separation approximately 0.5 OD_{260} of crude DNA in Millipore water was injected and the absorbance monitored at 260nm. The typical retention times for the **Dx** products were around 36-37 minutes in contrast to unmodified DNA which eluted at around 9-10 minutes.

For dye-labelled DNA. Solvent system; A:TEAA buffer, B:Acetonitrile. TEAA buffer (50mM Triethylammonium acetate, pH 8.0) was filtered using through 0.22□m cellulose membrane before use. The elution gradient was 3-30% solvent B over 20 minutes, then 30-95% over 50 minutes. Column: Hamilton PRP-C18 5 μm 100 Å 2.1 x 150 mm. For each separation approximately 0.5 OD_{260} of crude DNA in Millipore water was injected and the absorbance monitored at 260, 488 and 556nm. The Cy3 strands exhibited longer retention times than 6-FAM consistent with the more hydrophobic character of the dye.

4.5.5 HPLC traces of crude Dx product mixtures

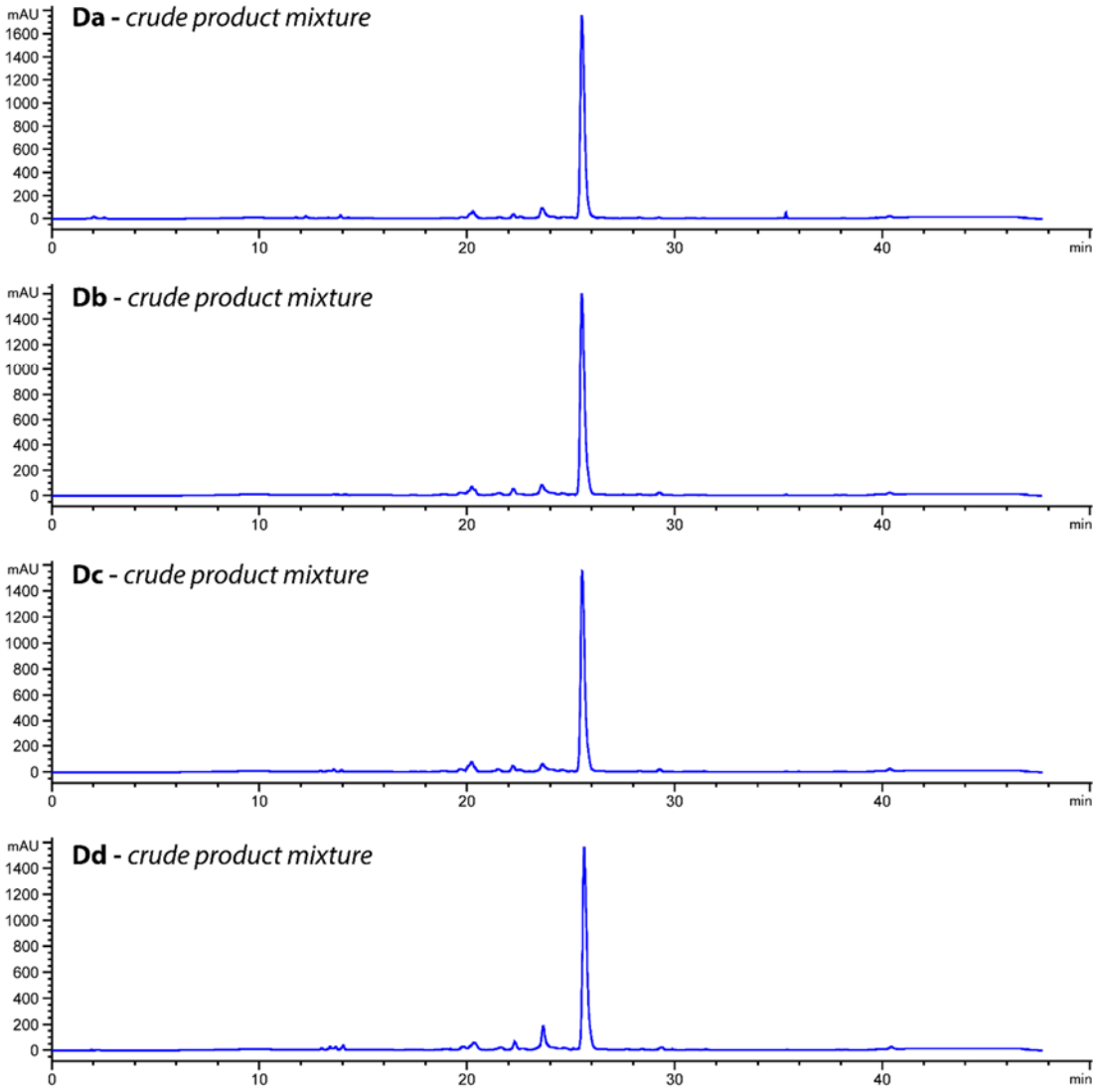

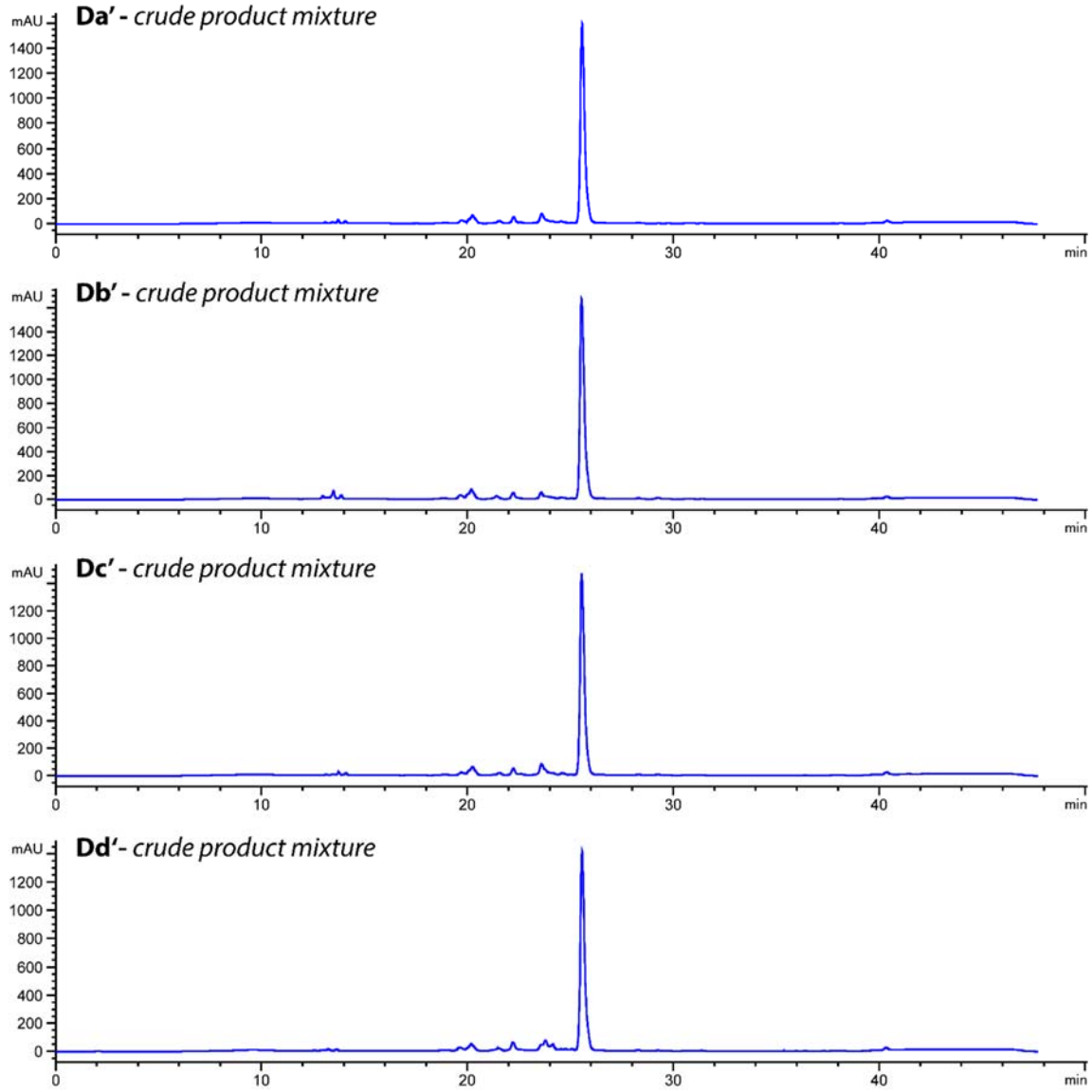
Da' - crude product mixture
Db' - crude product mixture
Dc' - crude product mixture
Dd'- crude product mixture
mAU
min

4.5.6 HPLC traces of isolated Dx products

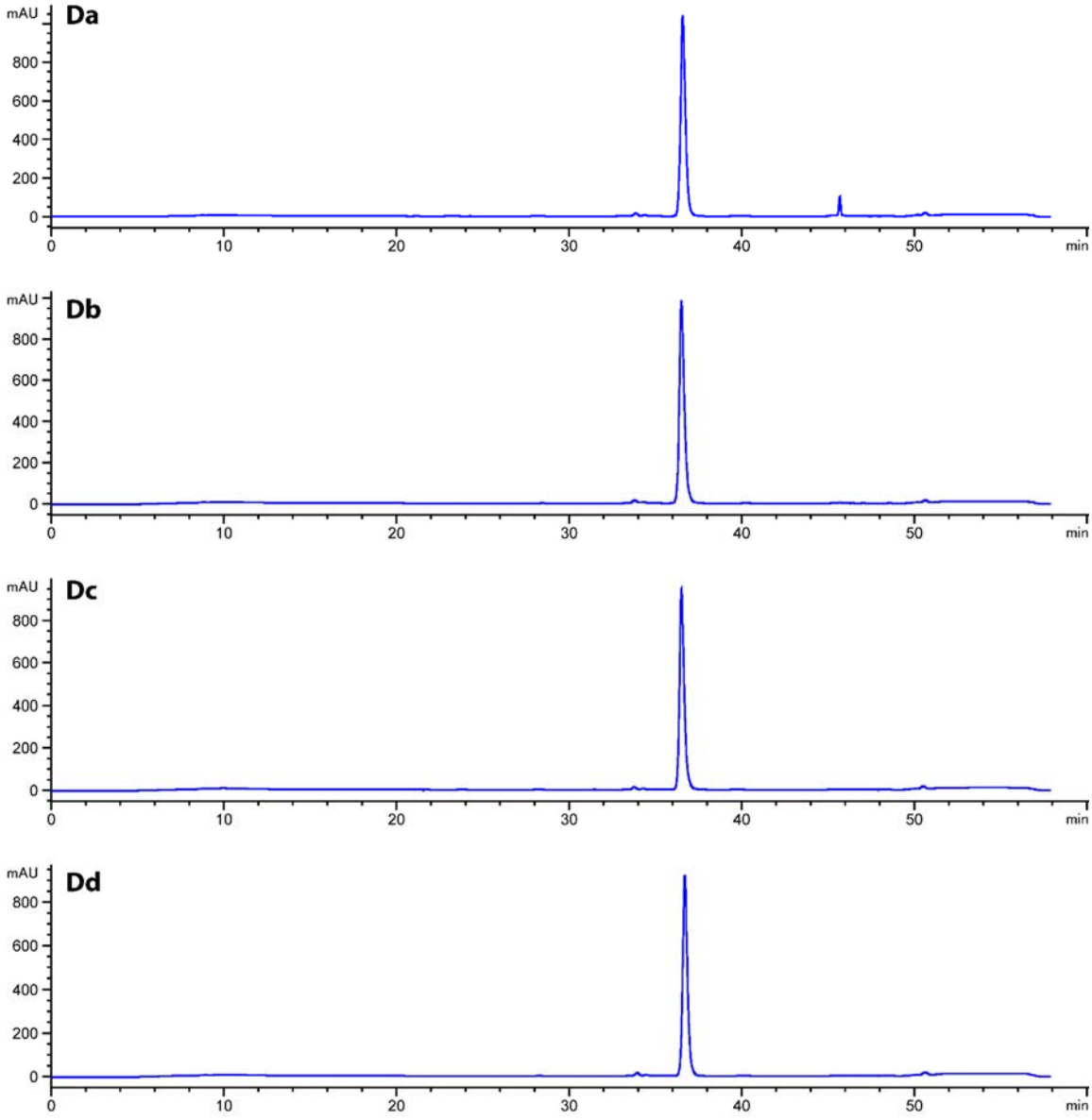

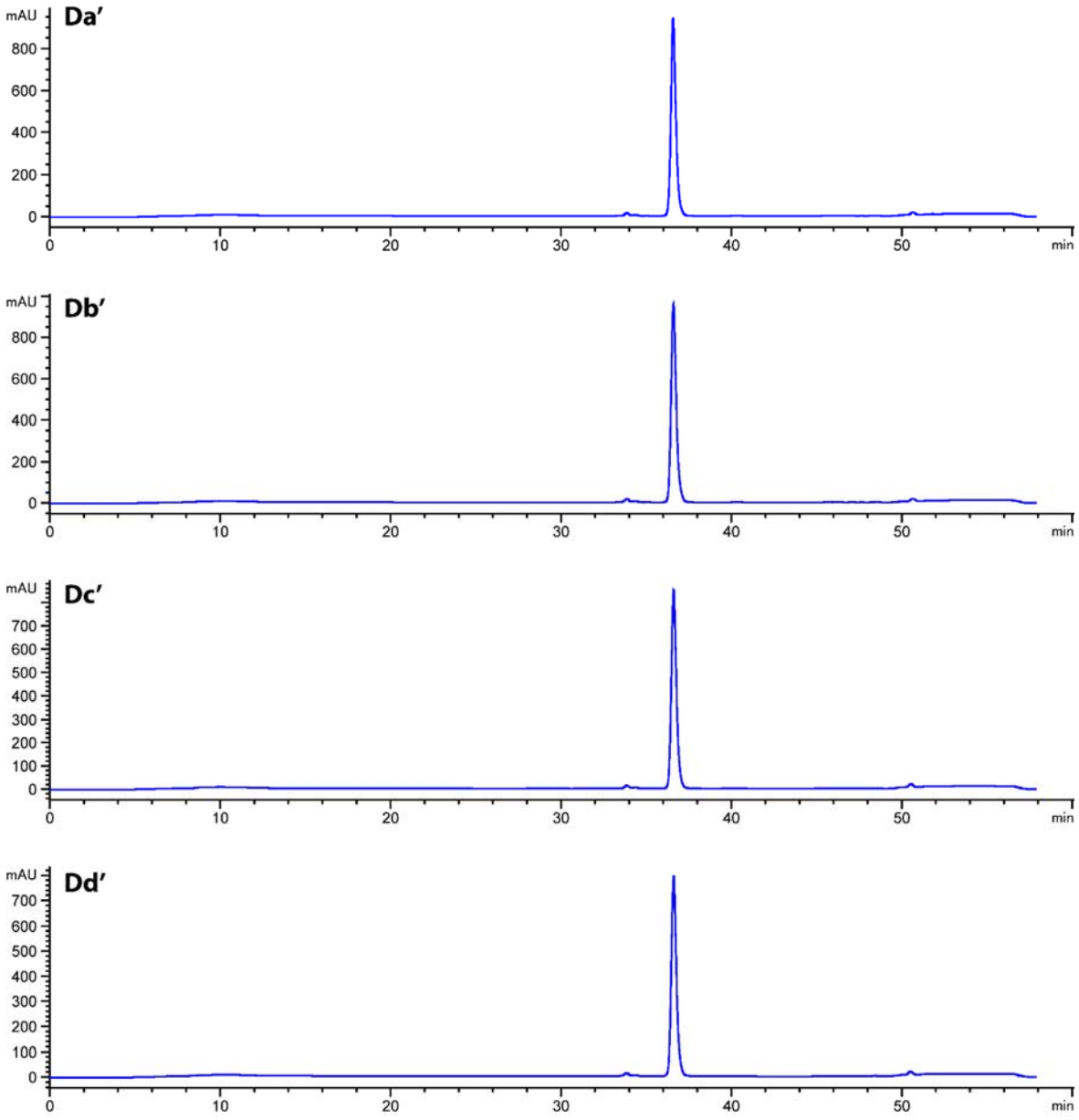
Da′
mAU
800
600
400
200
0
0
10
20
30
40
50
min
Db′
mAU
800
600
400
200
0
0
10
20
30
40
50
min
Dc′
mAU
700
600
500
400
300
200
100
0
0
10
20
30
40
50
min
Dd′
mAU
700
600
500
400
300
200
100
0
0
10
20
30
40
50
min

4.5.7 HPLC traces of crude Dye-labelled DNA

Asterisks highlight the product peak which is characterized by LC-ESI-MS in Section 4.5.8.

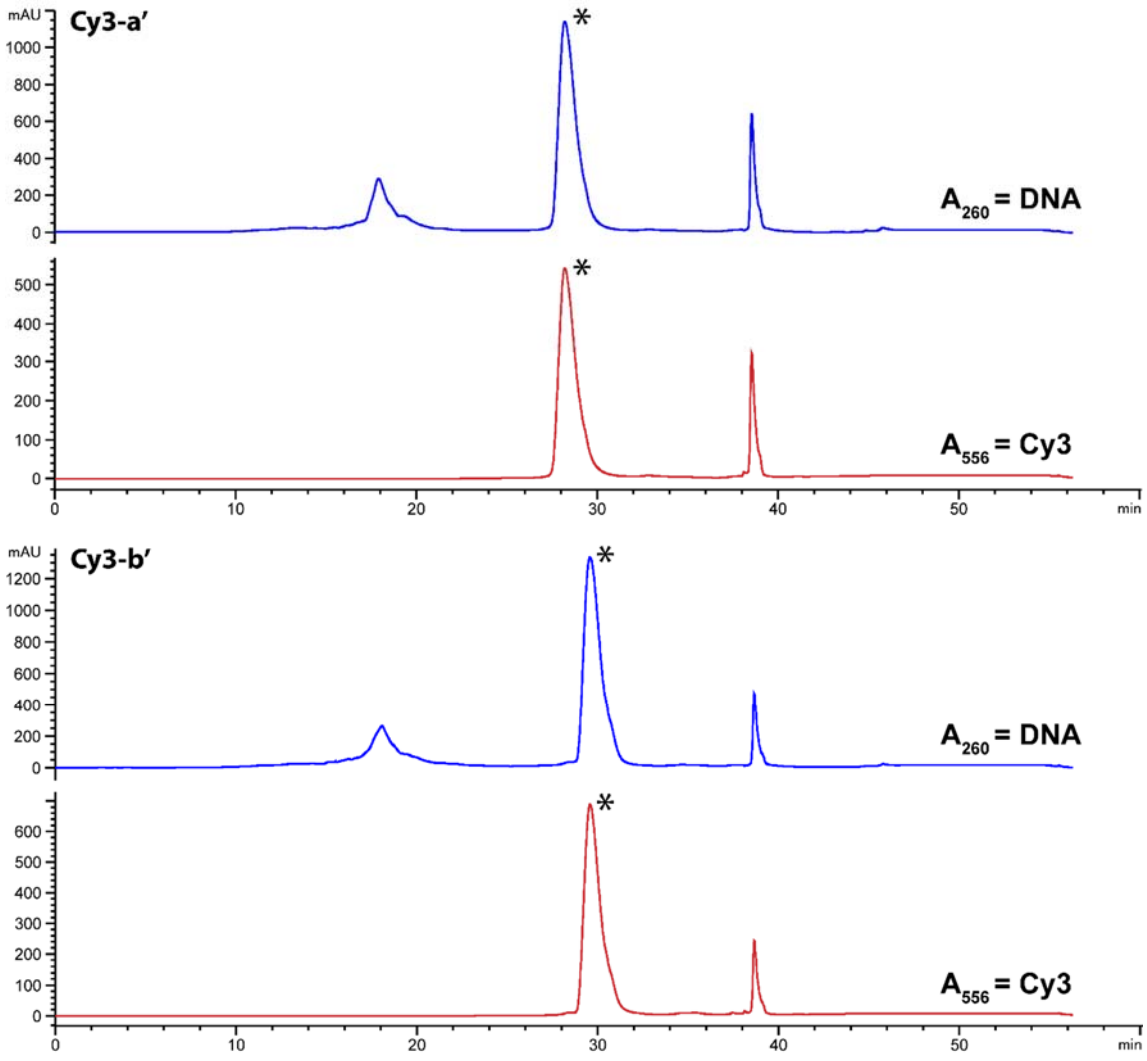

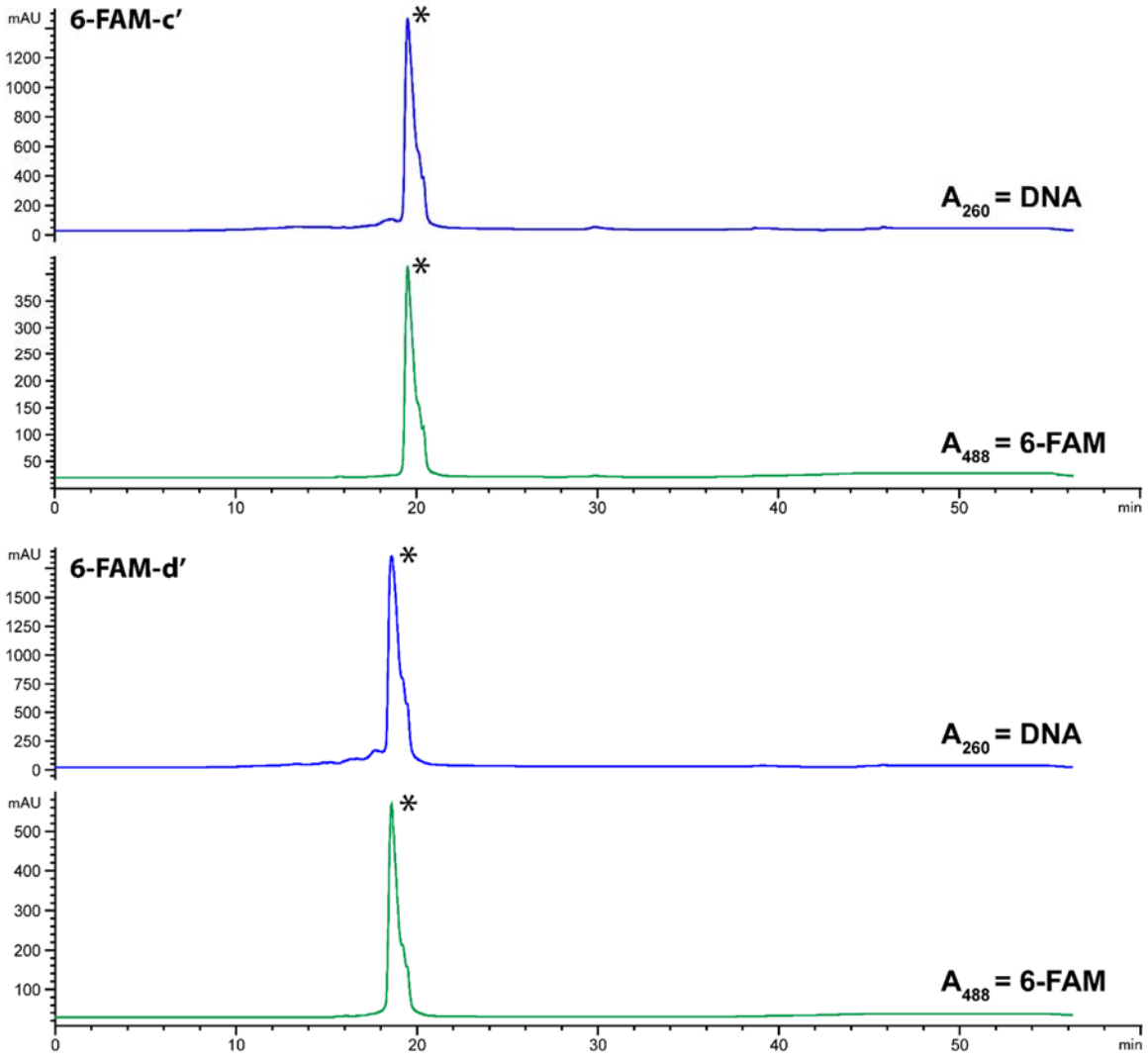
6-FAM-c'
mAU
1200
1000
800
600
400
200
0
*
A260 = DNA
350
300
250
200
150
100
50
*
A488 = 6-FAM
0
10
20
30
40
50
min
6-FAM-d'
mAU
1500
1250
1000
750
500
250
0
*
A260 = DNA
mAU
500
400
300
200
100
*
A488 = 6-FAM
0
10
20
30
40
50
min

4.5.8 LC-ESI-MS characterization

The oligonucleotides were analyzed by LC-ESI-MS in negative ESI mode. Samples were run through an Acclaim RSLC 120 C18 column (2.2μM 120Å 2.1 x 50mm) using a gradient of 98% mobile phase A (100mM 1,1,1,3,3,3-hexafluoro-2-propanol and 5mM triethylamine in water) and 2 % mobile phase B (Methanol) to 40 % mobile phase A and 60% mobile phase B in 8 minutes. The data was processed and de-convoluted using the Bruker DataAnalysis software version 4.1.

Table 4.2 - LC-ESI-MS data for all DNA-conjugates.

Molecule	Calculated (exact mass/Da)	Found (exact mass/Da)
Da	6875.2022	6875.0875
Db	6851.1902	6851.1125
Dc	6949.2282	6949.1062
Dd	6884.1752	6884.1062
Da'	6933.2332	6933.1000
Db'	6958.2402	6958.1250
Dc'	6860.2022	6860.0562
Dd'	6929.2352	6929.1187
CD-a	5978.1822	5978.9875
Cy3-a'	8889.7100	8889.6875
Cy3-b'	8800.6840	8800.5625
6-FAM-c'	8722.5140	8722.4875
6-FAM-d'	8801.5540	8801.4625

4.5.9 LC-ESI-MS data

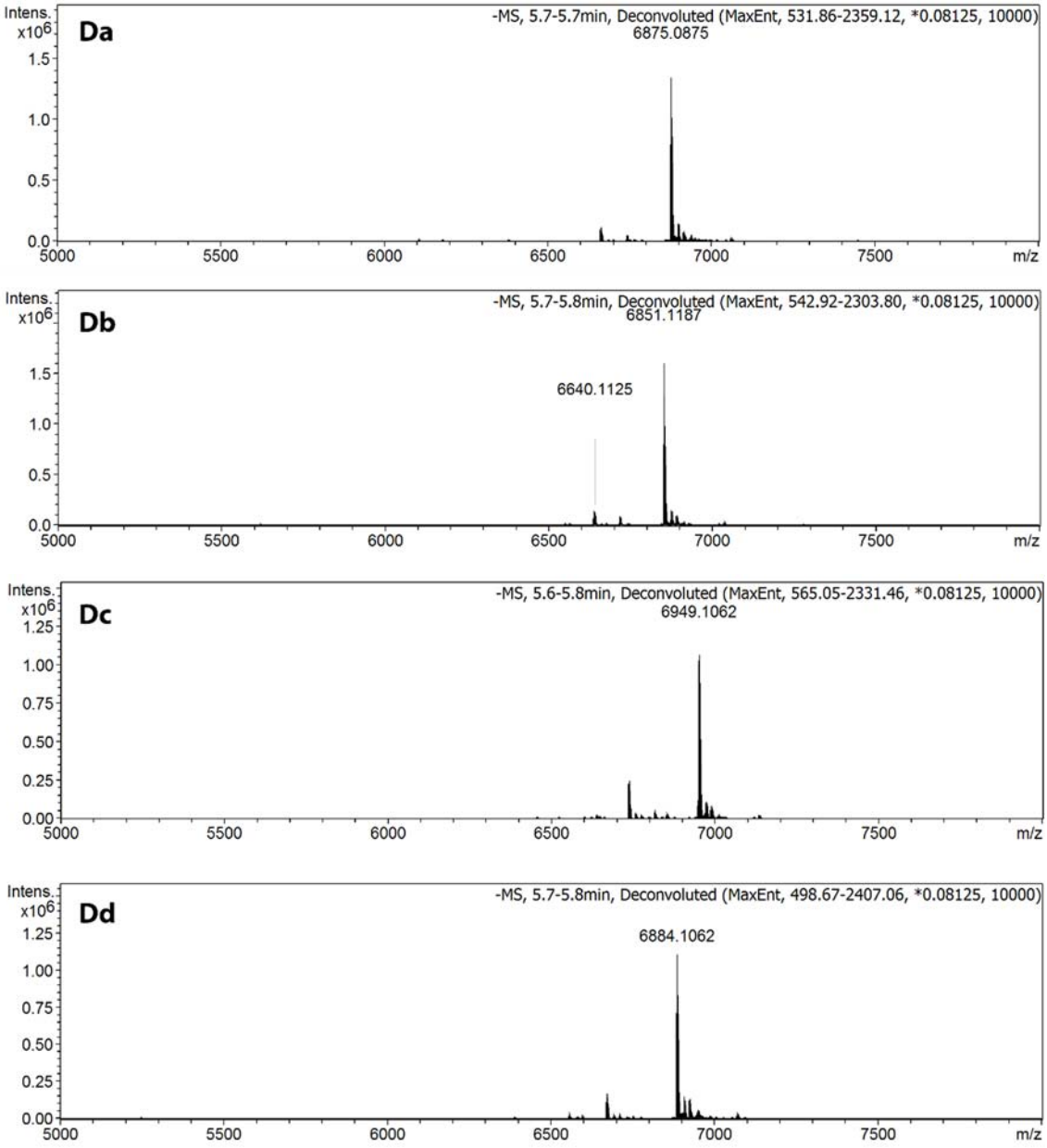

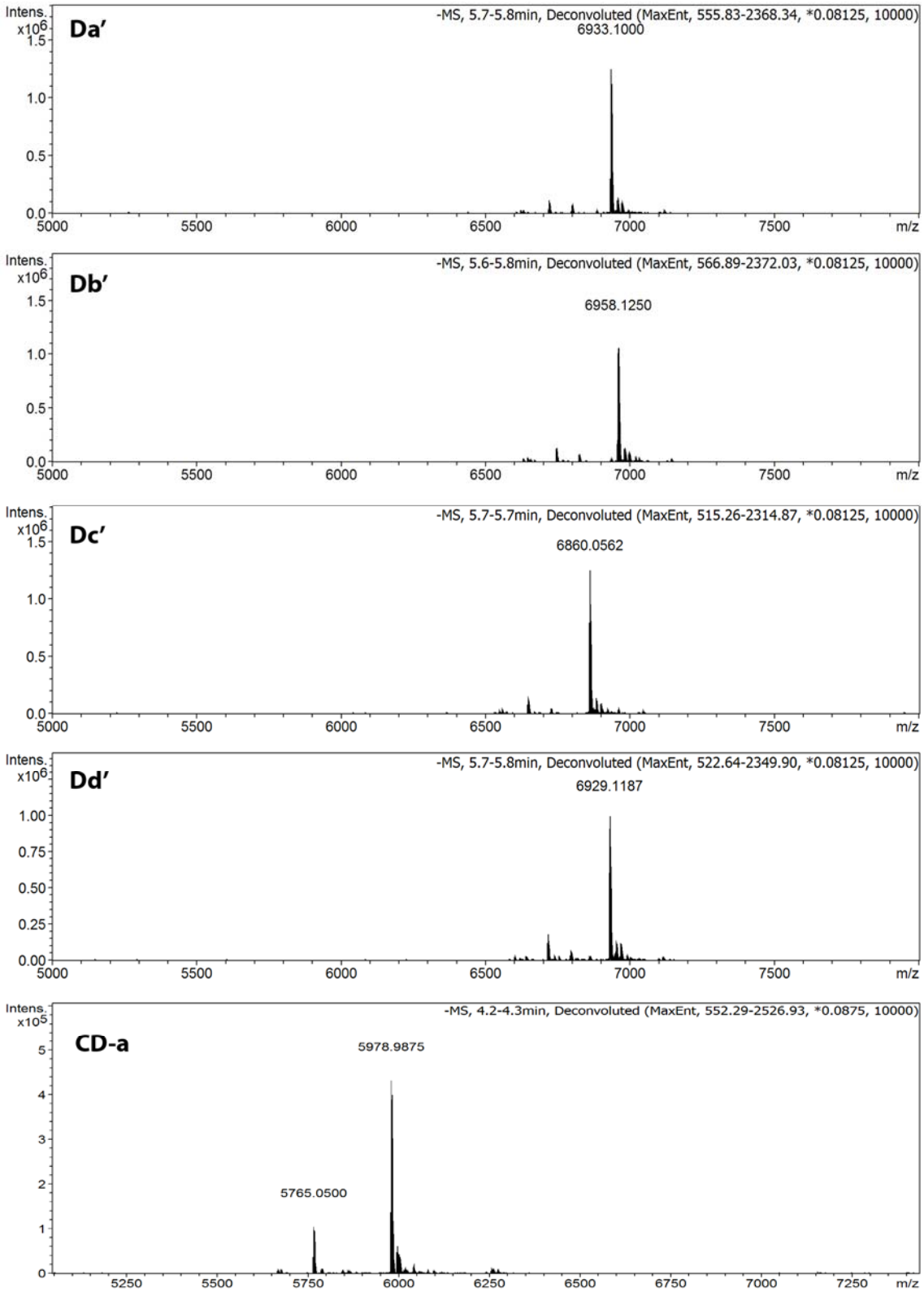
Da'
-MS, 5.7-5.8min, Deconvoluted (MaxEnt, 555.83-2368.34, *0.08125, 10000)
6933.1000
Db'
-MS, 5.6-5.8min, Deconvoluted (MaxEnt, 566.89-2372.03, *0.08125, 10000)
6958.1250
Dc'
-MS, 5.7-5.7min, Deconvoluted (MaxEnt, 515.26-2314.87, *0.08125, 10000)
6860.0562
Dd'
-MS, 5.7-5.8min, Deconvoluted (MaxEnt, 522.64-2349.90, *0.08125, 10000)
6929.1187
CD-a
-MS, 4.2-4.3min, Deconvoluted (MaxEnt, 552.29-2526.93, *0.0875, 10000)
5978.9875
5765.0500
Intens.
m/z

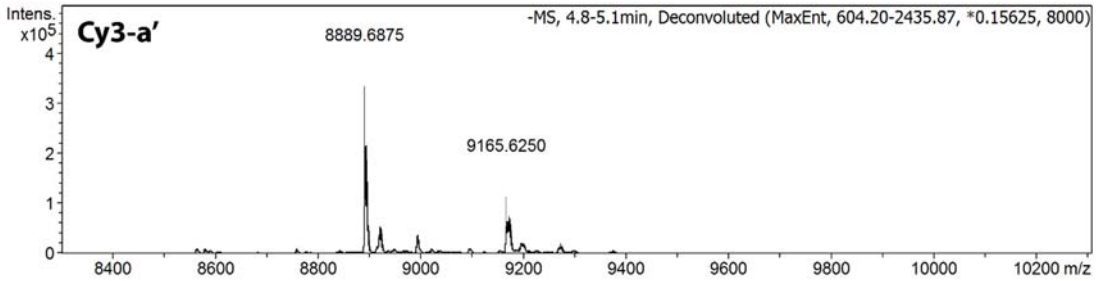
Intens.
x10^5
Cy3-a'
-MS, 4.8-5.1min, Deconvoluted (MaxEnt, 604.20-2435.87, *0.15625, 8000)
8889.6875
9165.6250
8400
8600
8800
9000
9200
9400
9600
9800
10000
10200 m/z

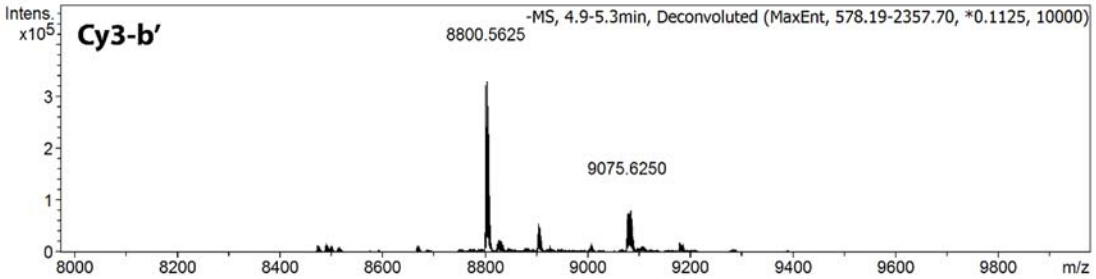
Intens.
x10^5
Cy3-b'
-MS, 4.9-5.3min, Deconvoluted (MaxEnt, 578.19-2357.70, *0.1125, 10000)
8800.5625
9075.6250
8000
8200
8400
8600
8800
9000
9200
9400
9600
9800
m/z

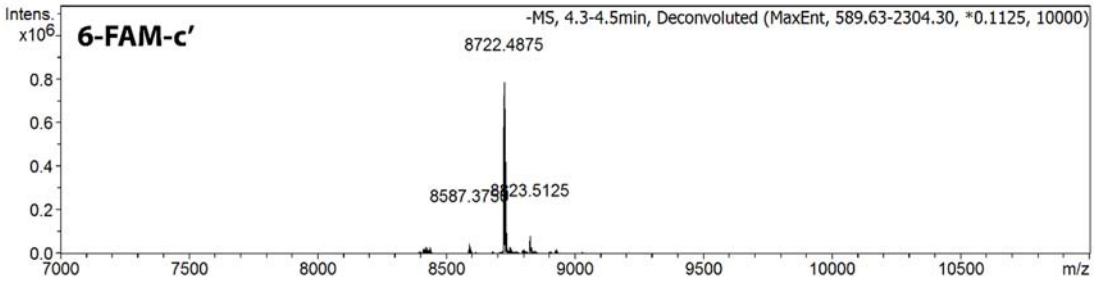
Intens.
x10^6
6-FAM-c'
-MS, 4.3-4.5min, Deconvoluted (MaxEnt, 589.63-2304.30, *0.1125, 10000)
8722.4875
8587.3750
8823.5125
7000
7500
8000
8500
9000
9500
10000
10500
m/z

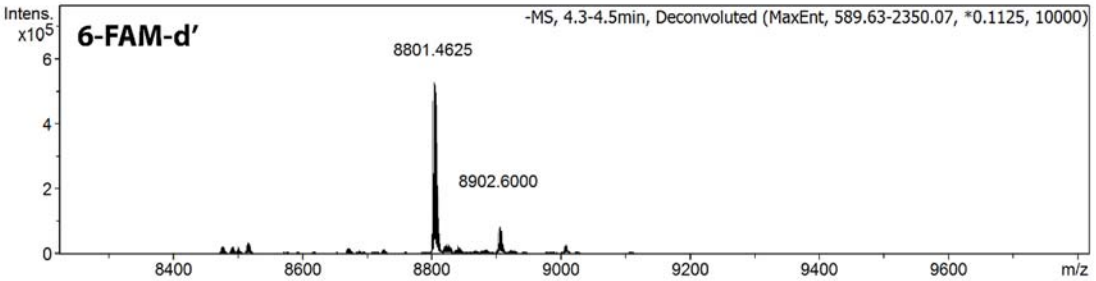
Intens.
x10^5
6-FAM-d'
-MS, 4.3-4.5min, Deconvoluted (MaxEnt, 589.63-2350.07, *0.1125, 10000)
8801.4625
8902.6000
8400
8600
8800
9000
9200
9400
9600
m/z

4.5.10 Melting temperatures

To confirm that the hybridization of the **Dx** conjugates was not impaired by the 5' modification, thermal denaturation study of duplexes was carried out by UV absorption. For each experiment equimolar amounts of **Da** and complement strand, either **EXT-A** or **A14** were combined in 1xTBEN buffer to give a final volume of 150 µL with a duplex concentration of 2.5 µM. Samples were annealed by heating to 95 °C and cooling to 4 °C over 2 hours, then transferred to a quartz cuvette. The absorbance at 260 nm was monitored between 10 °C and 60 °C.

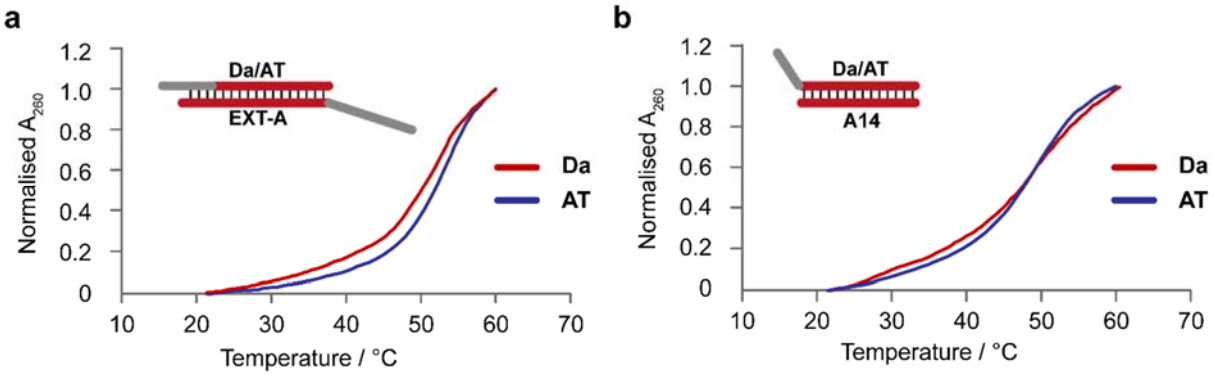

Figure 4.20 - Hybridization of Dx compared to unmodified DNA. a) Characteristic sigmoidal melting curves are seen for the 17 nt binding of **EXT-A** to unmodified **AT** and **Da**. **b)** Melting curves for the hybridization of the 14 nt region which is used to bind **Da** to the prismatic scaffolds. The negligible change in T_m between **Da** and **AT** in both cases reveals that the **Dx** modification does not disrupt the duplex formation of the DNA portion.

4.5.11 Stability assay

The chemical stability assay was adapted from previous work by Mirkin et al.[46] Polyvalent 10nm AuNPs were first prepared by incubating 15 pmol of BSPP coated AuNPs with 1.5 µmol of DNA (**CD** or **Da**) in 1xTBEN, final volumes were ca. 20 µL. The samples were 'salt-aged' up to 300mM NaCl over 2 hours with intermittent sonication and left overnight at room temperature.[47] Samples were then centrifuged (15000 x *g*) and the supernatant removed and replaced with fresh 1xTBEN. This was repeated three times to remove all excess unbound DNA strands. Samples were then quantified by absorbance at 450nm. Samples were then diluted to 350 nM in 45 µL of 1xTBEN and the absorption spectra measured. Then 5 µL of 0.1 M DTT solution (pre-prepared, Life

Technologies) was added and absorption spectra were measured at time intervals over 4 hours.

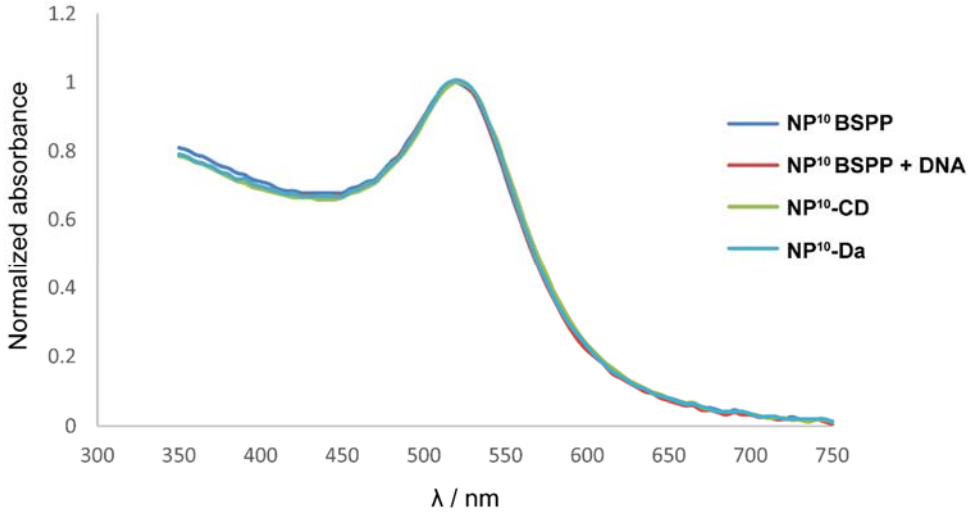

Figure 4.21 - Absorption spectra of polyvalent AuNPs. Shown here are the samples used for the stability assay shown in Figure 4.2, before the addition of DTT. Spectra were recorded 1xTBE, 150mM NaCl. A slight redshift was observed for the samples **CD** and **Da** compared to the controls (BSPP and DNA) which is indicative of conjugation to the surface through the DTPA moieties.

4.5.12 Synthesis of clip strands

The DNA synthesis was performed on a 1 μmole scale, using universal 1000 Å CPG solid-supports (BioAutomation, cat.# MM1-3500-1). DMT-hexaethyloxy-Glycol phosphoramidite (cat# CLP-9765) was purchased from ChemGenes. Removal of the DMT protecting group was carried out using 3% DCA in dichloromethane and monitored for coupling efficiency. Completed sequences were deprotected in 28% ammonium hydroxide solution for 16-18 hours at 65 ˚C. The crude deprotected solution was separated from the solid support and concentrated under reduced pressure at 60 ˚C. This crude solid was re-suspended in 0.2mL Millipore water ready for purification.

Table 4.3 - List of clip sequences used. Non-standard amidite code: (**H**=hexaethyloxy-glycol), these spacers are used as flexible junctions to allow the cube structure to form.

Name	Sequence (5'-xx-3')
CC1-AB	TCGCTGAGTA**H**TCCTATATGGTCAACTGCTC**H**GCAAGTGTGGGCACGCAC AC**H**GTAGTAATACCAGATGGAGT**H**CACAAATCTG
CC2-AB	CTATCGGTAGT**H**CCTATATGGTCAACTGCTCT**H**ACTCAGCGACAGATTTGT G**H**GTAGTAATACCAGATGGAGT**H**CAACTAGCGG
CC3-AB	CACTGGTCAG**H**TCCTATATGGTCAACTGCTC**H**CTACCGATAGCCGCTAGT TG**H**GTAGTAATACCAGATGGAGT**H**GGTTTGCTGA
CC4-AB	CCACACTTGC**H**TCCTATATGGTCAACTGCTC**H**CTGACCAGTGTCAGCAAA CC**H**GTAGTAATACCAGATGGAGT**H**GTGTGCGTGC
TC3-AB	CCACACTTGC**H**TCCTATATGGTCAACTGCTC**H**CTACCGATAGCCGCTAGT TG**H**GTAGTAATACCAGATGGAGT**H**GTGTGCGTGC
PC4-AB	TACCGGATCG**H**TCCTATATGGTCAACTGCTC**H**CTGACCAGTGTCAGCAAA CC**H**GTAGTAATACCAGATGGAGT**H**CCGTAATTGC
PC5-AB	CCACACTTGC**H**TCCTATATGGTCAACTGCTC**H**GATCCGGTAGCAATTACG G**H**GTAGTAATACCAGATGGAGT**H**GTGTGCGTGC
CC1-AS	TCGCTGAGTA**H**GCCTGGCCTTGGTCCATTTG**H**GCAAGTGTGGGCACGCA CAC**H**CGCACCGCGACTGCGAGGAC**H**CACAAATCTG
CC2-AS	CTATCGGTAG**H**AAAACTCTGCCGTAAGAGGA**H**TACTCAGCGACAGATTTG TG**H**TCCTATATGGTCAACTGCTC**H**CAACTAGCGG
CC3-AS	CACTGGTCAG**H**CCACCAGCTAGATGTTGAAG**H**CTACCGATAGCCGCTAGT TG**H**CGCTCTTCTATACTGGCGGA**H**GGTTTGCTGA
CC4-AS	CCACACTTGC**H**TACAGGTACGATTCACCACT**H**CTGACCAGTGTCAGCAAA CC**H**GTAGTAATACCAGATGGAGT**H**GTGTGCGTGC

4.5.13 Purification of clip strands

The clip strands were purified on 8 % polyacrylamide/8 M urea PAGE (one third of a crude 1 µmol synthesis was loaded per gel) at constant current of 30 mA for 1.5 hours (30 min at 250 V followed by 1 hr at 500 V), in TBE buffer. The product bands were excized under UV shadowing on silica plates, and the gel pieces were crushed and incubated in 12 mL of sterile water at 60 °C for 12-16 hours. Samples were then dried to ca. 1.5 mL, desalted using size exclusion chromatography (Sephadex G-25), and quantified (OD_{260}) using UV-Vis spectroscopy.

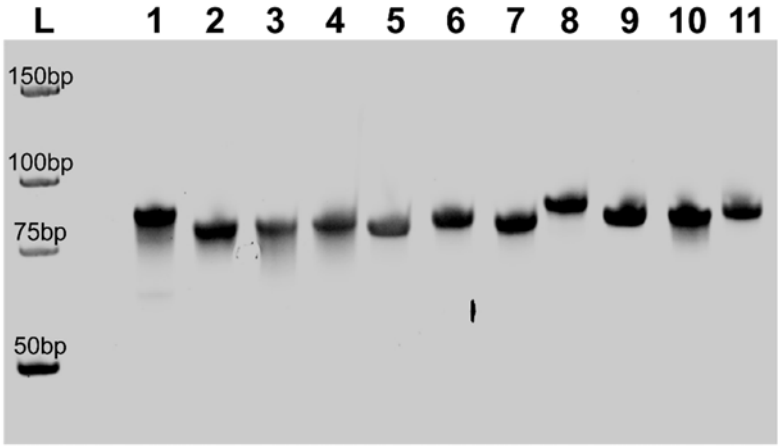

Figure 4.22 - Analytical PAGE on purified clip strands. Gel: 8% polyacrylamide/8 M urea analytical PAGE. Run at constant current of 30 mA for 1.5 hours (30 min at 250 V followed by 1 hr at 500 V). Loading is 10 pmol of DNA per lane and bands were visualized using GelRed™. Lane L – DNA ladder**,** Lane 1 - **CC1-AB**, Lane 2 - **CC2-AB**, Lane 3 - **CC3-AB**, Lane 4 - **CC4-AB**, Lane 5 – **TC3-AB**, Lane 6 - **PC4-AB**, Lane 7 - **PC5-AB**, Lane 8 - **CC1-AS**, Lane 9 - **CC2-AS**, Lane 10 - **CC3-AS**, Lane 11 - **CC4-AS**.

4.5.14 Preparation of 3D structures.

In each case, equimolar amounts of appropriate clips were combined in 1xTBEN buffer with a total DNA concentration of 5 μM (giving a final prism concentrations of 1.67, 1.25 and 1.00 μM for TP, Cb and PP respectively). Samples were annealed by heating to 95 °C for 5 minutes and cooling to 4 °C over 6 hours. For each of the scaffold variants reported in the manuscript, different combinations of the clip strands were used as shown in Table 4.4.

Table 4.4| Clip combinations required for different DNA prisms.

Scaffold	Clip strands	Sequence structure
TP	CC1-AB, CC2-AB, TC3-AB	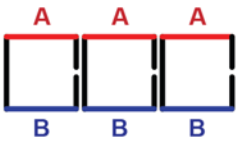
Cb	CC1-AB, CC2-AB, CC3-AB, CC4-AB	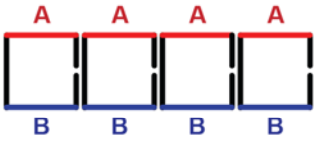
PP	CC1-AB, CC2-AB, CC3-AB, PP4-AB, PP5-AB	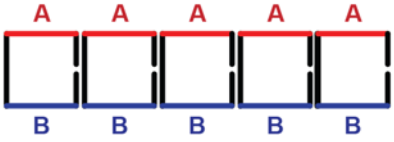
Cb^{AS}	CC1-AS, CC2-AS, CC3-AS, CC4-AS	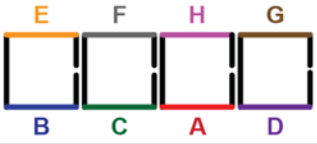

4.5.15 Additional Geometry calculations

The dimensions of DNA structures shown here are based on idealized rigid B-form DNA, e.g. 0.34nm per base pair. Gold nanoparticles are sized as perfect spheres of 6, 10 or 13 nm in diameter.

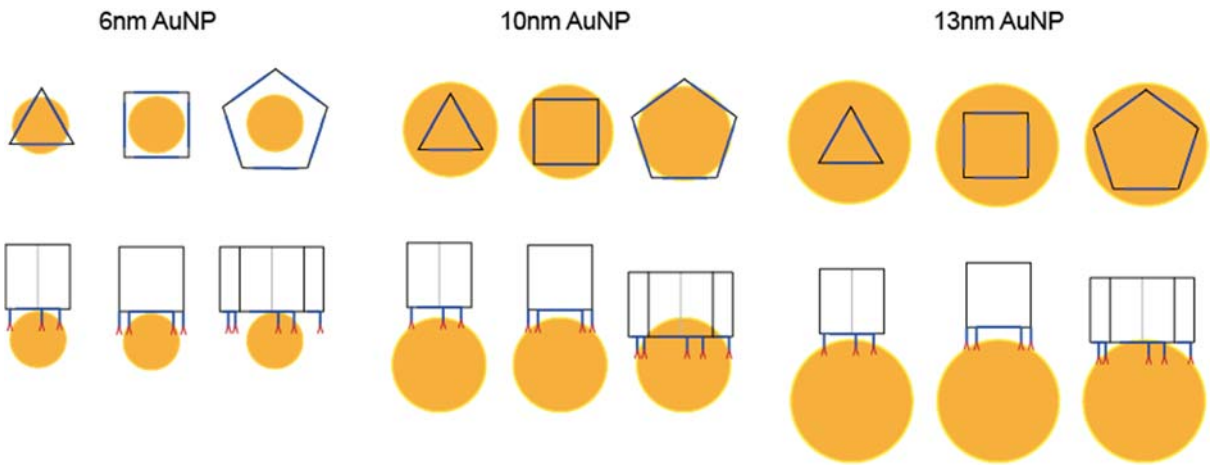

Figure 4.23 - To scale drawings of different prism variants and AuNPs.

4.5.16 Protocol for AuNP patterning

The 10 nm AuNPs were purchased from Ted Pella, 6 nm and 13 nm AuNPs were synthesized through Turkevich-Frens syntheses, described in previous work.[39] All nanoparticles were subject to BSPP surface passivation before use in experiments.[55] In a typical patterning experiment 20 pmol of BSPP coated AuNPs were incubated with 20 pmol of DNA scaffold bearing **Dx** conjugates. Final sample concentrations were *ca.* 300 nM in 1xTBE with 100-150 mM NaCl and 2mM BSPP. Following Incubation at room temperature overnight, 20,000 equivalents of OEG (*ca.* 0.2 M in 1xTBEN) was added to stably passivate the surface. After a 30 minute incubation with OEG at room temperature, samples were centrifuged (12000 x *g*) at 4 °C, the supernatant was removed and fresh buffer added. This process was repeated at least twice before loading the samples on gel. Gel bands were assigned, see Figures 2 and 3, and the desired band carefully excised. Samples were extracted by electroelution in 1xTBE buffer and subsequently concentrated by centrifugation (15000 x g) at 30 °C and removal of supernatant. The 'pellet' was then washed with 3 M urea in 0.625xTBE three times. This was followed by three washes with sterile de-ionized water. Finally, sample

solutions were quantified by absorption spectroscopy, monitoring absorbance at 450 nm.

4.5.17 Gel Mobility shift assays

Agarose gel electrophoresis AGE was used as the primary analytical method to follow the patterning experiments. In each case AGE was carried out at 25 °C for 1-2 hours at a constant voltage of 80 V. Typical sample loading is between 0.5 and 2 pmol, with respect to AuNPs, per lane. A variety of studies were carried out to investigate the patterning process, selected experiments are shown below.

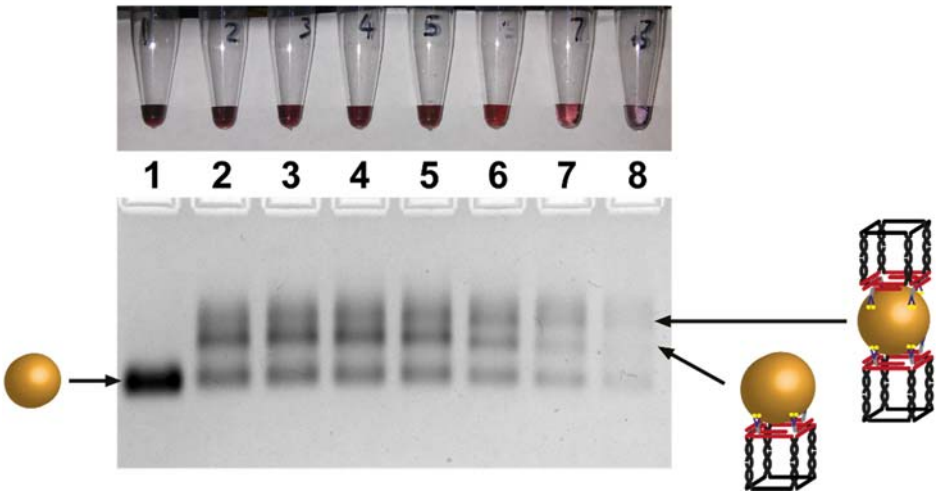

Figure 4.24 - Effect of salt concentration on the binding efficiency of cube to AuNPs. Increasing salt concentration is known to aid maximal loading of oligonucleotides AuNPs.[47] Although maximal surface loading is not required here, the effect of [Na^+] on the products of the prism-AuNP binding was investigated using the symmetric cube **Cb-Da$_4$**. Samples were incubated overnight at 1:1 molar ratio in 1xTBE buffer at room temperature with [Na^+] between 100mM and 300mM. Lane 1 - **NP^{10}**, Lane 2 – **100mM** NaCl, Lane 3 – **125mM** NaCl, Lane 4 – **150mM** NaCl, Lane 5 – **175mM** NaCl, Lane 6 – **200mM** NaCl, Lane 7 – **225mM** NaCl, Lane 8 – **250mM** NaCl. The photograph above the gel shows the samples after overnight incubation, the colour change seen for samples 6,7 and 8 is a good indicator of aggregation at this high Na^+ concentration. Based on these results DNA structures and patterning experiments were carried out between 100 and 150mM to avoid aggregation and conserve yield.

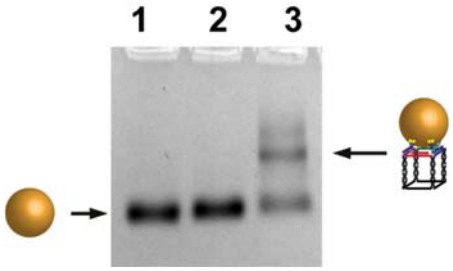

Figure 4.25 - Naked cube control. Cubic scaffolds without gold binding conjugates, **Dx**, do not exhibit binding to BSPP coated AuNPs, 3 % AGE: Lane 1 – **NP^{10}**, Lane 2 – **NP^{10}** + **Cb**, Lane 3 – **NP^{10}** + **Cb-Da$_4$**.

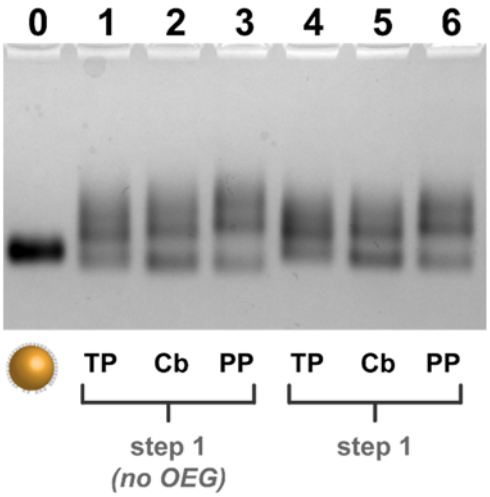

Figure 4.26 - Effect of OEG treatment on prism-AuNP complexes. The effect of surface passivation with **OEG** on the prism-AuNP complexes was probed comparing mobility patterns of patterning reaction mixtures, *step1*, pre- and post-treatment: Lane 0 – **NP^{10}**(**OEG**), Lane 1 – **NP^{10}** + **TP-Da$_3$** Lane 2 – **NP^{10}** + **Cb-Da$_4$**, Lane 3 – **NP^{10}** + **PP-Da$_5$**, Lane 4 - **NP^{10}** + **TP-Da$_3$**(**OEG**)**,** Lane 5 – **NP^{10}** + **Cb-Da$_4$**(**OEG**), Lane 6 - **NP^{10}** + **PP-Da$_5$**(**OEG**). (3 % AGE). The most obvious change in mobility is seen for **NP^{10}** + **TP-Da$_3$** (Lanes 1 and 4) which may be due to the fact it is the smallest prism and therefore more surface area is available for **OEG** binding.

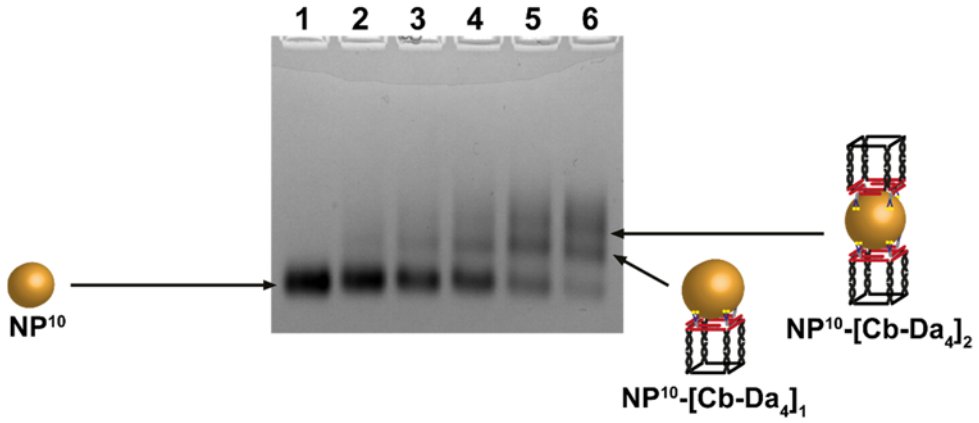

Figure 4.27 - Titration of NP^{10} against Cb-Da_4. The effect of stoichiometry on the product distribution was investigated by titrations of **Dx** bearing prisms with **NP^{10}**. Here **Cb-Da_4** is used as an example: Lane 1 – **NP^{10}**, Lane 2 – **NP^{10}** + 0.125x **Cb-Da_4**, Lane 3 – **NP^{10}** + 0.25x **Cb-Da_4**, Lane 4 - **NP^{10}** + 0.5x **Cb-Da_4,** Lane 5 – **NP^{10}** + 1x **Cb-Da_4**, Lane L - **NP^{10}** + 2x **Cb-Da_4**. (3 % AGE). It should be noted that the complex consisting of two prisms bound to one AuNP (**NP^{10}**-[**Cb-Da_4**]$_2$) is more favoured at higher **Cb-Da_4**: **NP^{10}** ratio. This suggests that the higher order structures are in fact two prisms to one AuNP (**NP^{10}**-[**Cb-Da_4**]$_2$) and not two AuNP on one prism ([**NP^{10}**]$_2$-[**Cb-Da_4**]). This is also consistent with the cooperative binding of **Dx** moieties, which would disfavour formation of a 2:1 complex of AuNP:cube.

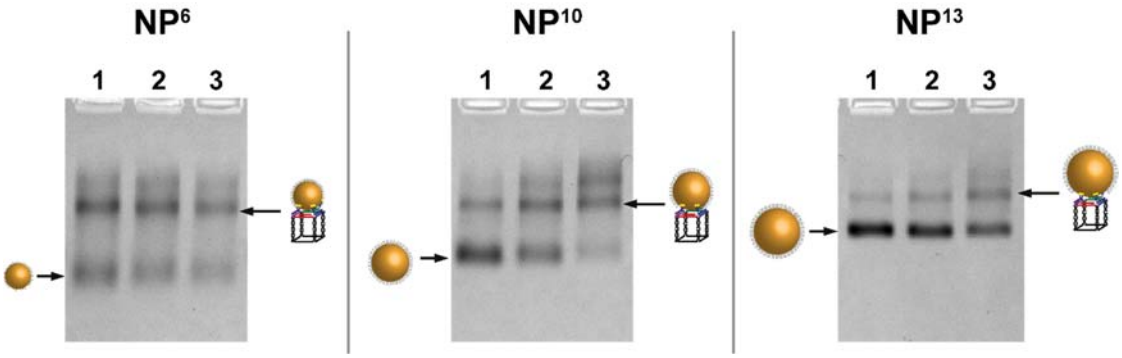

Figure 4.28 - Variation of particle size. Gel mobility comparison of cube **Cb-Da-Dd** binding to 6, 10 and 13 nm AuNPs (**NP^6**, **NP^{10}** and **NP^{13}**). Different equivalents of **Cb-Da-Dd** to AuNP were used to see any differences in binding efficiency. In each case: Lane 1, **0.5 equiv. Cb-Da-Dd** ; Lane 2, **1.0 equiv. Cb-Da-Dd**; Lane 3, **2.0 equiv. Cb-Da-Dd**. There is an inverse relationship between the binding efficiency and particle size, likely due to electrostatic reasons.

4.5.18 Dynamic light scattering

All samples, water and buffer were filtered using a 0.45 µm nylon syringe filter before use in DLS sample preparation. All measurements were carried out at 25 °C. A cumulants fit model was used to determine the size of monomodal populations of nanoparticles. The non-patterned controls were obtained from incubation of **NP^{10}** (30 pmol) with **Da** (210 pmol) and **EXT-A** (840) pmol overnight at 25 °C in 1xTBEN, final volume ca. 50 µL. The samples were worked up as for patterned samples described in Experimental Section 4.5.16.

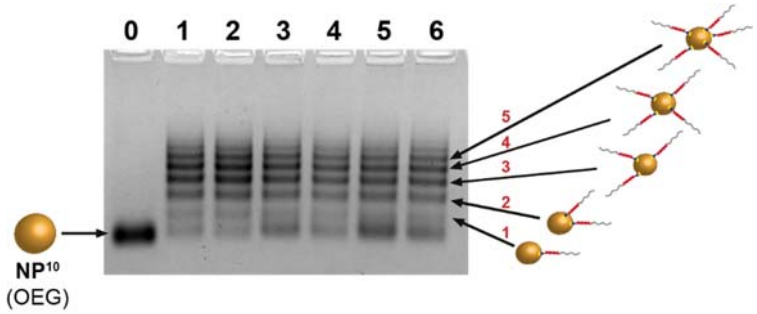

Figure 4.29 - Preparation of DLS controls. Shown here is the agarose gel of the crude samples from incubation of 7 equivalents of **Da** with **NP^{10}**, in the presence of **EXT-A**. The bands corresponding to 3, 4 and 5 **Da** on the AuNP were used as number defined, but randomly positioned, control samples in the DLS experiments shown below.

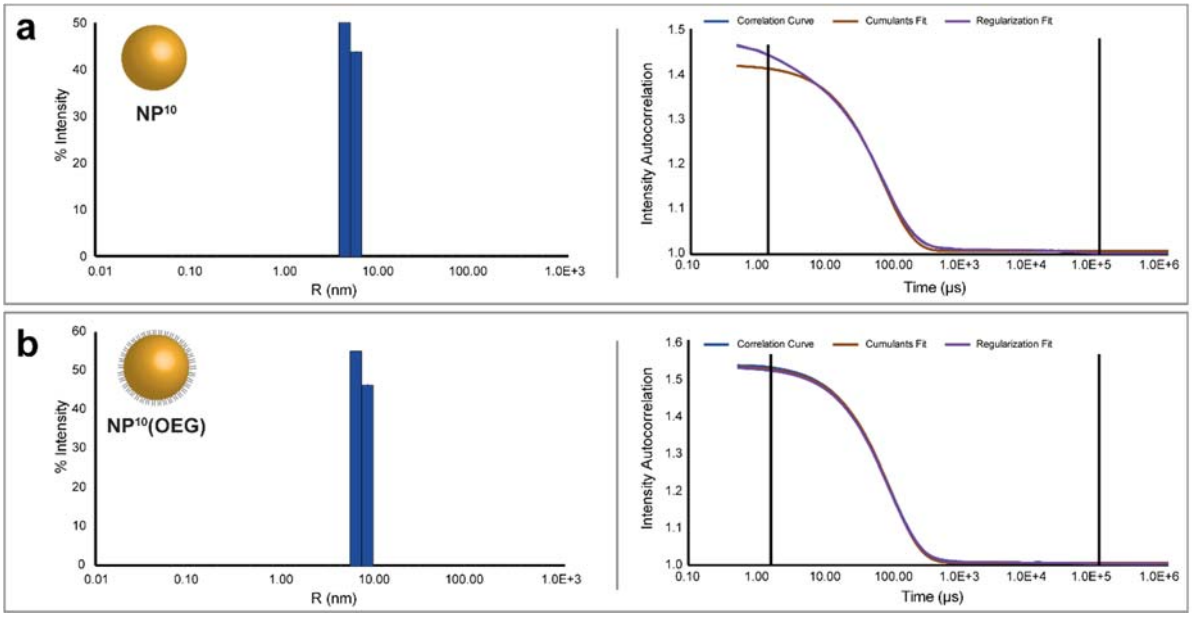

Figure 4.30 - DLS measurements of AuNP controls. Shown here are representive DLS regularization distribution histograms and the related correlation functions. a) **NP^{10}**, b) **NP^{10} (OEG)**. The increase in R_h in consistent with surface passivation with the carboxylate terminated oligoethylene glycol disulfide.

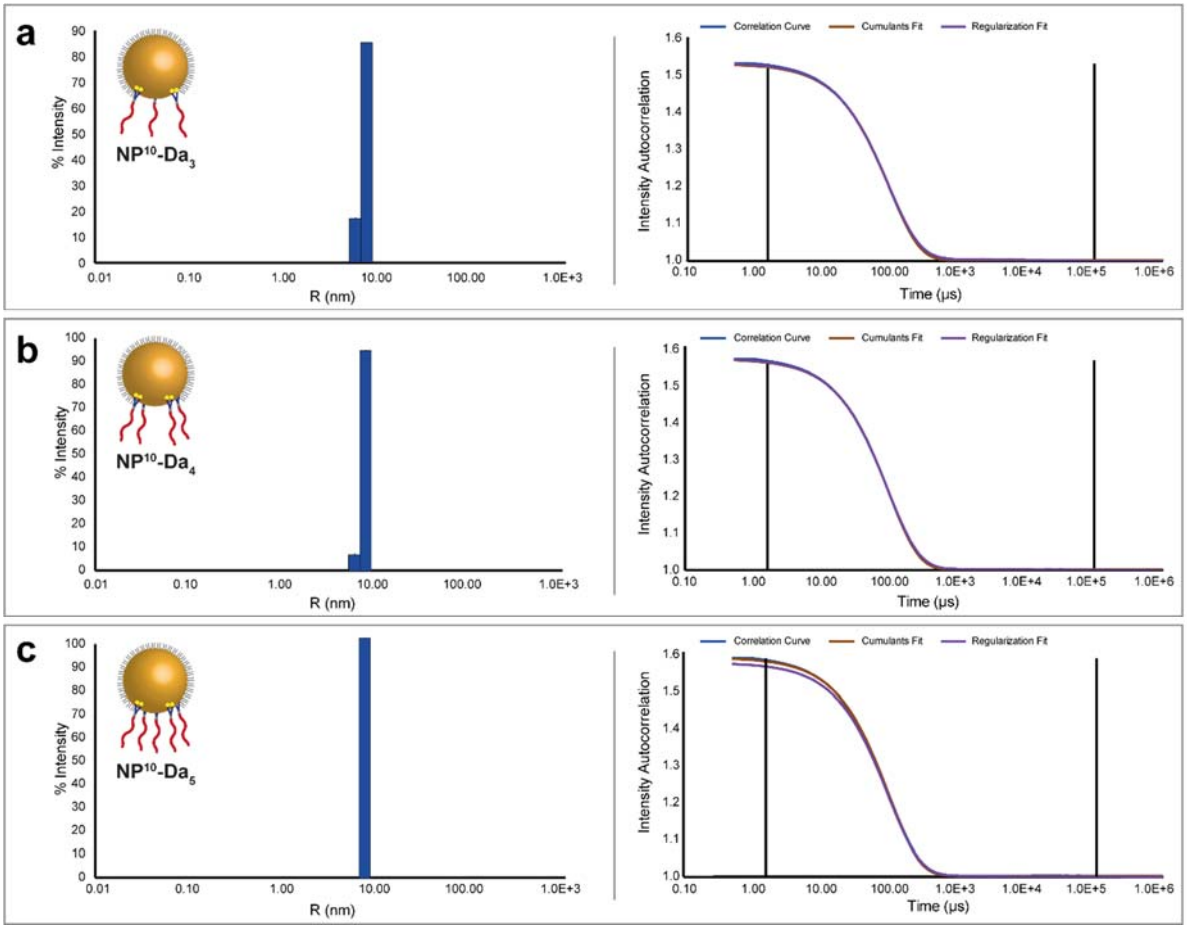

Figure 4.31 - DLS measurements of geometric series at step 2. Shown here are representive DLS regularization distribution histograms and the related correlation functions. a) **NP^{10}-Da$_3$**, b) **NP^{10}-Da$_4$**, c) **NP^{10}-Da$_5$**. There is little change in R_h without the extension strands bound, see table ST5 below for a summary of results.

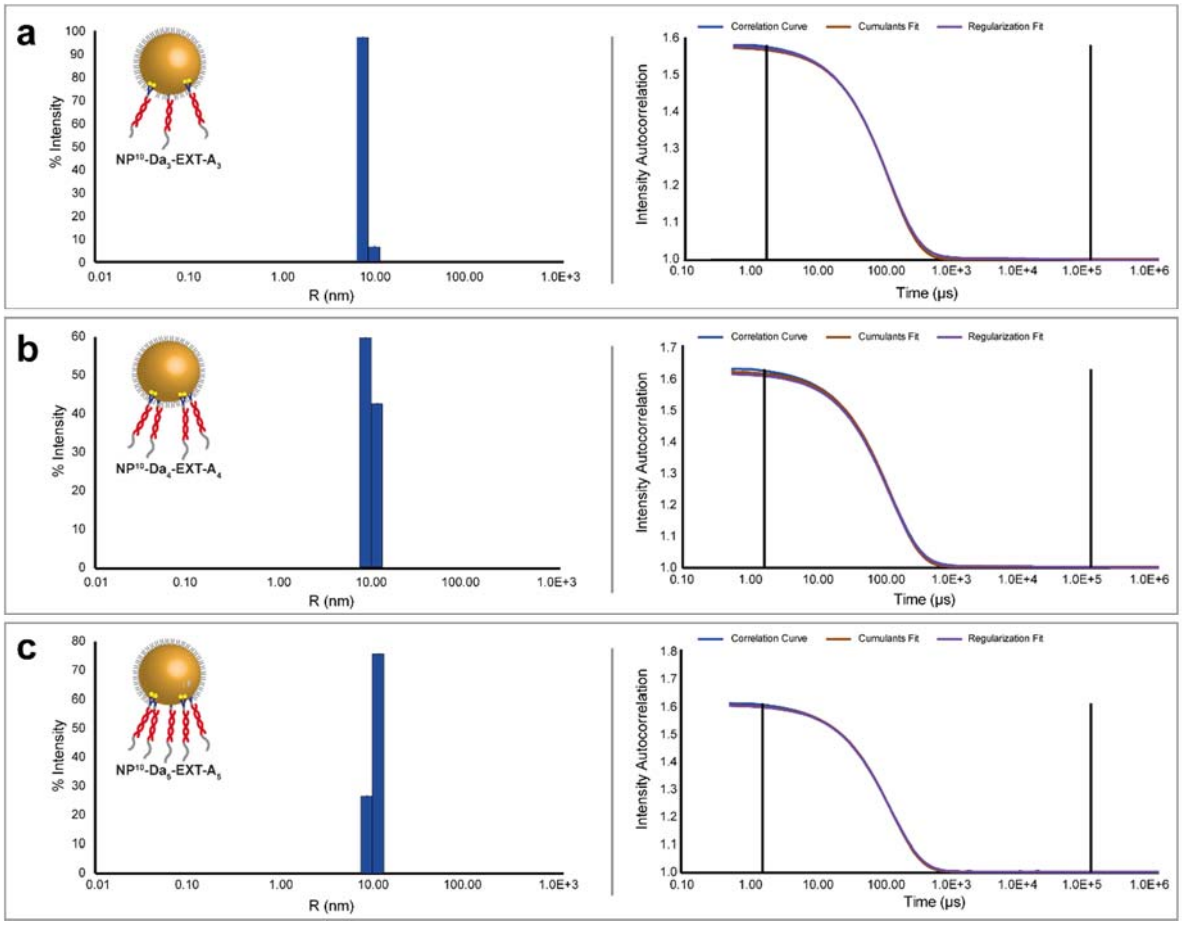

Figure 4.32 - DLS measurements of geometric series at step 3. Shown here are representive DLS regularization distribution histograms and the related correlation functions. a) **NP^{10}-Da$_3$-EXT-A$_3$**, b) **NP^{10}-Da$_4$-EXT-A$_4$**, c) **NP^{10}-Da$_5$-EXT-A$_5$**. An increase in R_h is seen as the number of **Da** increases, see table ST5 below for a summary of results.

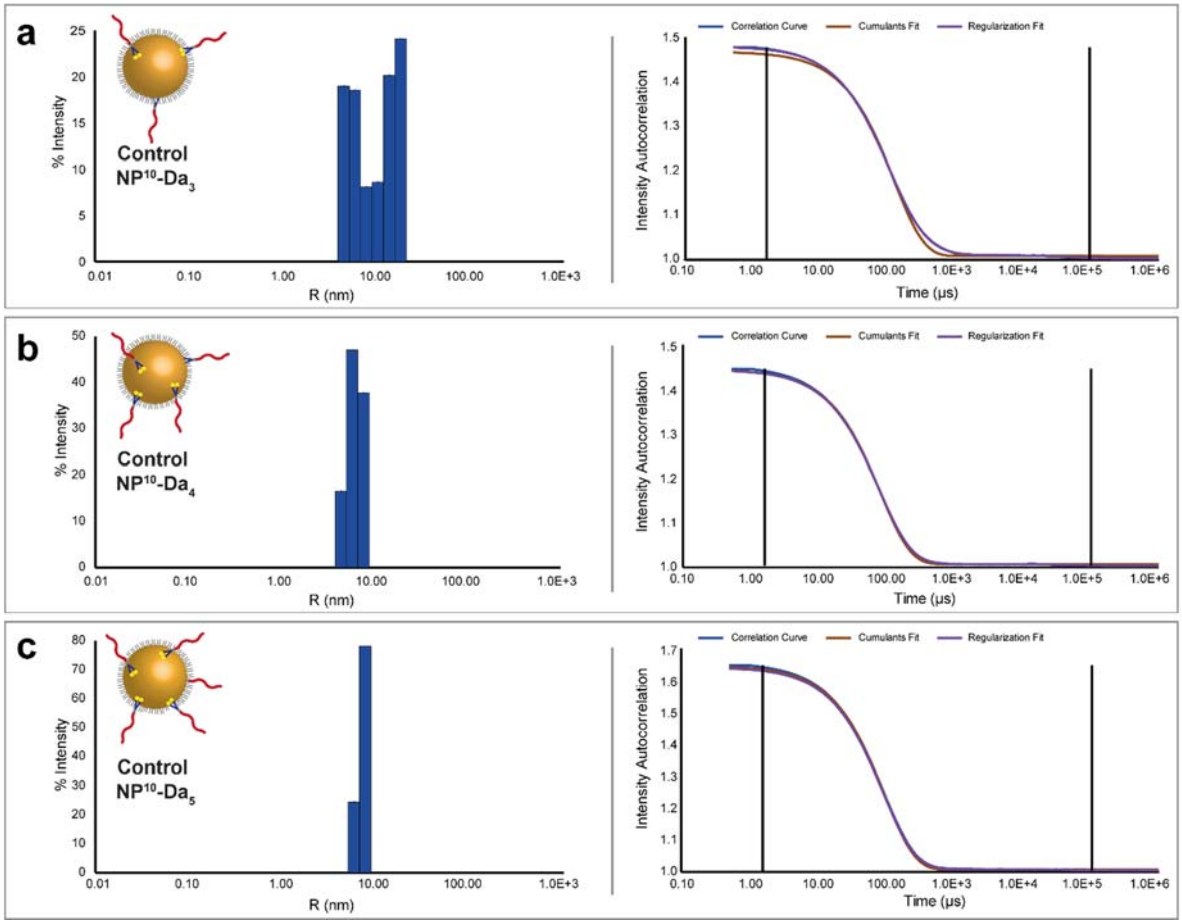

Figure 4.33 - DLS measurements of non-patterned control samples. Shown here are representive DLS regularization distribution histograms and the related correlation functions. a) **Control- NP^{10}-Da$_3$**, b) **Control-NP^{10}-Da$_4$**, c) **Control-NP^{10}-Da$_5$**. These samples exhibit smaller Rh with higher polydispersity than their anisotropic templated counterparts, see table ST5 below for a summary of results.

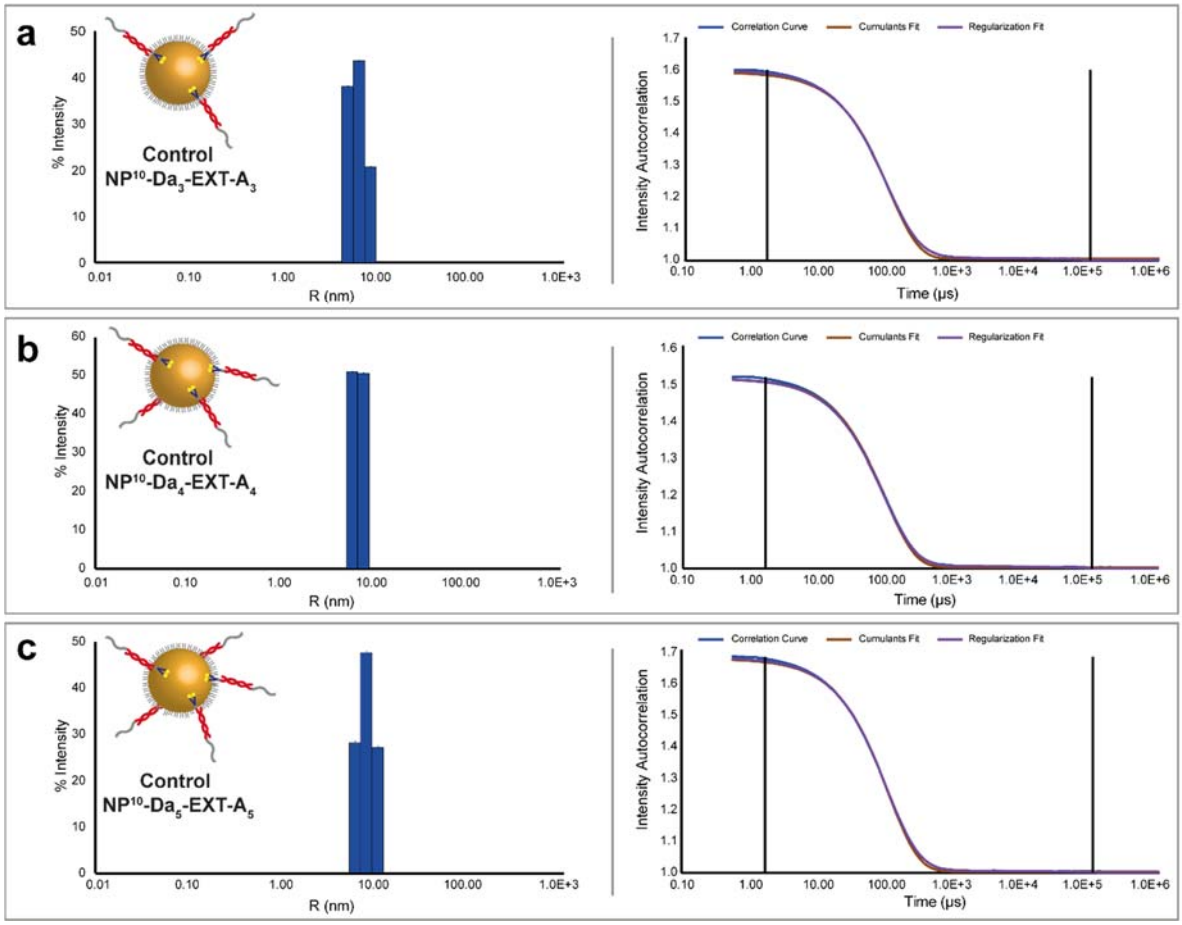

Figure 4.34 - DLS measurements of non-patterned control samples with EXT-A. Shown here are representive DLS regularization distribution histograms and the related correlation functions. a) **Control-NP^{10}-Da$_3$-EXT-A$_3$**, b) **Control-NP^{10}-Da$_4$-EXT-A$_4$**, c) **Control-NP^{10}-Da$_5$-EXT-A$_5$**. These samples exhibit smaller Rh with higher polydispersity than their anisotropic templated counterparts, see table ST5 below for a summary of results.

Table 4.5 - Summary of DLS measurements. Triplicate measurements were obtained for each sample, mean values for hydrodynamic radii and polydispersity of each are shown below. Error margins are derived from the standard deviation of the triplicate measurements.

Sample	Mean hydrodynamic radius (nm)	Mean polydispersity (%)
NP^{10}	5.1 ± 0.00	14.0 ± 1.1
NP^{10}(OEG)	6.9 ± 0.36	12.8 ± 0.4
NP^{10}-Da_3	7.4 ± 0.08	10.5 ± 0.69
NP^{10}-Da_4	7.6 ± 0.08	9.8 ± 4.42
NP^{10}-Da_5	7.7 ± 0.05	5.2 ± 0.05
NP^{10}-Da_3-EXT-A_3	7.8 ± 0.08	4.3 ± 3.18
NP^{10}-Da_4-EXT-A_4	6.4 ± 0.08	14.0 ± 0.08
NP^{10}-Da_5-EXT-A_5	9.6 ± 0.05	11.7 ± 0.05
Control NP^{10}-Da_3	5.6 ± 0.12	21.6 ± 3.11
Control NP^{10}-Da_4	6.5 ± 0.09	22.6 ± 4.89
Control NP^{10}-Da_5	7.2 ± 0.05	11.8 ± 0.60
Control NP^{10}-Da_3-EXT-A_3	6.7 ± 0.19	13.7 ± 0.33
Control NP^{10}-Da_4-EXT-A_4	7.6 ± 0.12	23.5 ± 1.96
Control NP^{10}-Da_5-EXT-A_5	8.1 ± 0.12	22.9 ± 0.36

4.5.19 TEM sample preparation

For the preparation of satellite structures polyvalent 6 nm AuNPs were used. Typically, to 100 pmol of 6 nm BSPP coated AuNP was added 1 µmol of **Dx'** (complement to Dx on the patterned AuNP) in 1xTBEN at a final volume of ca. 50 µL. Samples were held at 50 °C for 1 hour and cooled to 20 °C over 30 minutes. Next, 10,000 equivalents of **OEG** (*ca.* 0.5 M in 1xTBEN) was added. After a 30 minute incubation with **OEG** at room temperature, samples were centrifuged (12000 x *g*) at 30 °C, and the supernatant removed and replaced with fresh 1xTBEN. This washing step was repeated three times to ensure removal of any excess **OEG** and DNA strands. Four different polyvalent particles were made, functionalized with either **Da'**, **Db'**, **Dc'** or **Dd'**. Satellite structures were then assembled by incubating 5 pmol of **NP^{10}-Asym** with 50 pmol of each required **NP^{6}-Dx'** overnight at room temperature in 1xTAMg buffer, total volume

ca. 20 µL. Samples were then purified by 3% AGE and the product bands excised and gel slices soaked in 1xTAMg buffer at 7°C overnight to extract the samples with minimal disruption to the assembly.

Samples were prepared for imaging as follows; 5 µL of aqueous bacitracin solution (0.5 mg/mL) was deposited onto the carbon-coated grid, after 1 minute the droplet was removed using filter paper. A washing step was carried out by dropping 5 µL of sterile water (0.45 µm filtered) and wicking away immediately. Next, 5 µL of sample ([AuNP] = 10-30 nM) was deposited onto the grid and left for 1 minute before removal with filter paper. Finally, another wash step was carried out and the grid was put under vacuum for 16 hours before microscopy.

Tabe 4.6 - TEM Statistics. The satellite structures imaged by TEM were purified by AGE before sample deposition. As such TEM yields shown here are a representation of those samples which remain intact after sample deposition and drying. The lower yields with increasing structural complexity correlate with the AGE analysis suggesting lower stability of these more demanding structures. The yields were calculated based on the fraction of **NP^{10}** found in product structures versus the number of **NP^{10}** found in other structures, ignoring clusters of multiple 10nm particles. Due to low particle numbers for the 3:1 and 4:1 structures, the percent yield has low statistical significance.

Sample	Yield	Particles screened
NP^{10}-Asym + NP^{6}-Da' 	70%	128
NP^{10}-Asym + NP^{6}-Da', NP^{6}-Db' 	87%	162
NP^{10}-Asym + NP^{6}-Da', NP^{6}-Db', NP^{6}-Dc' 	36%	28
NP^{10}-Asym + NP^{6}-Da', NP^{6}-Db', NP^{6}-Dc', NP^{6}-Dd' 	38%	45

4.5.20 Additional TEM micrographs

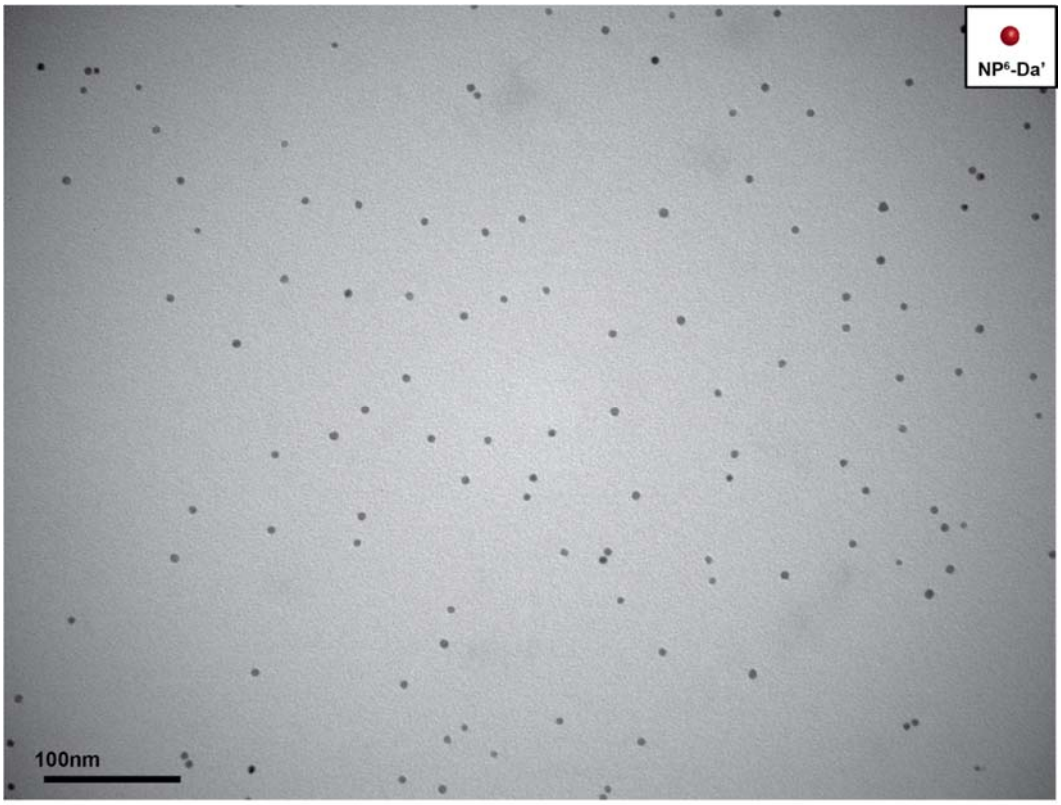

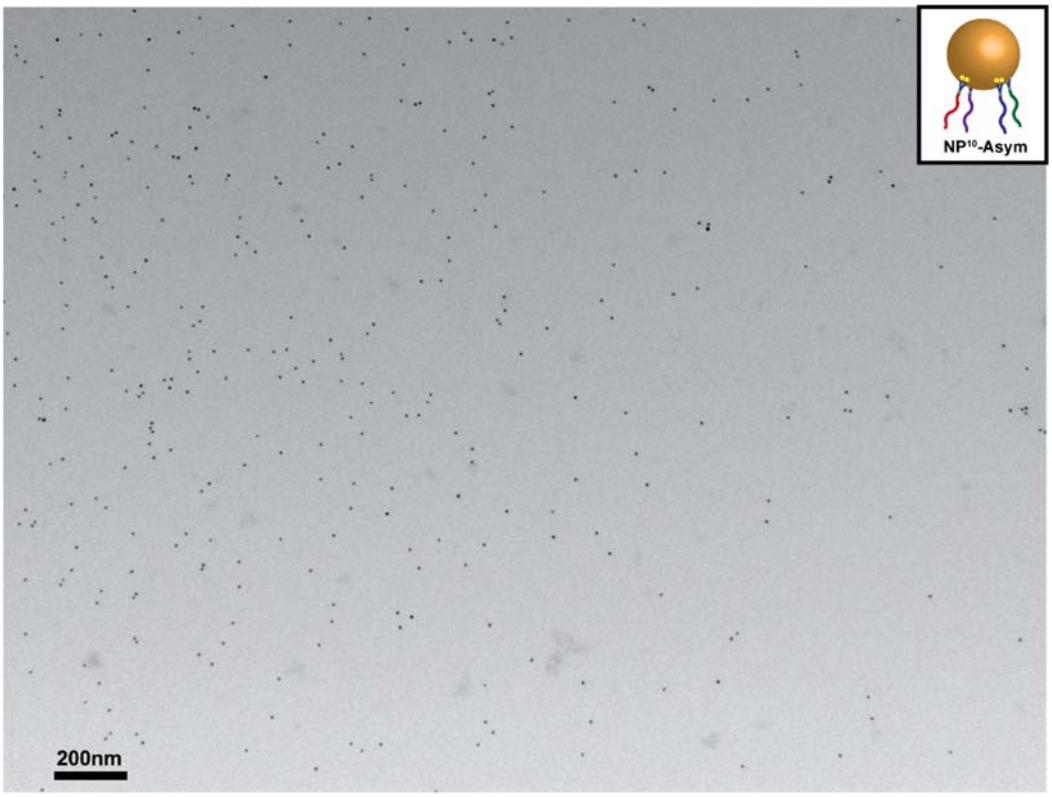
NP10-Asym
200nm

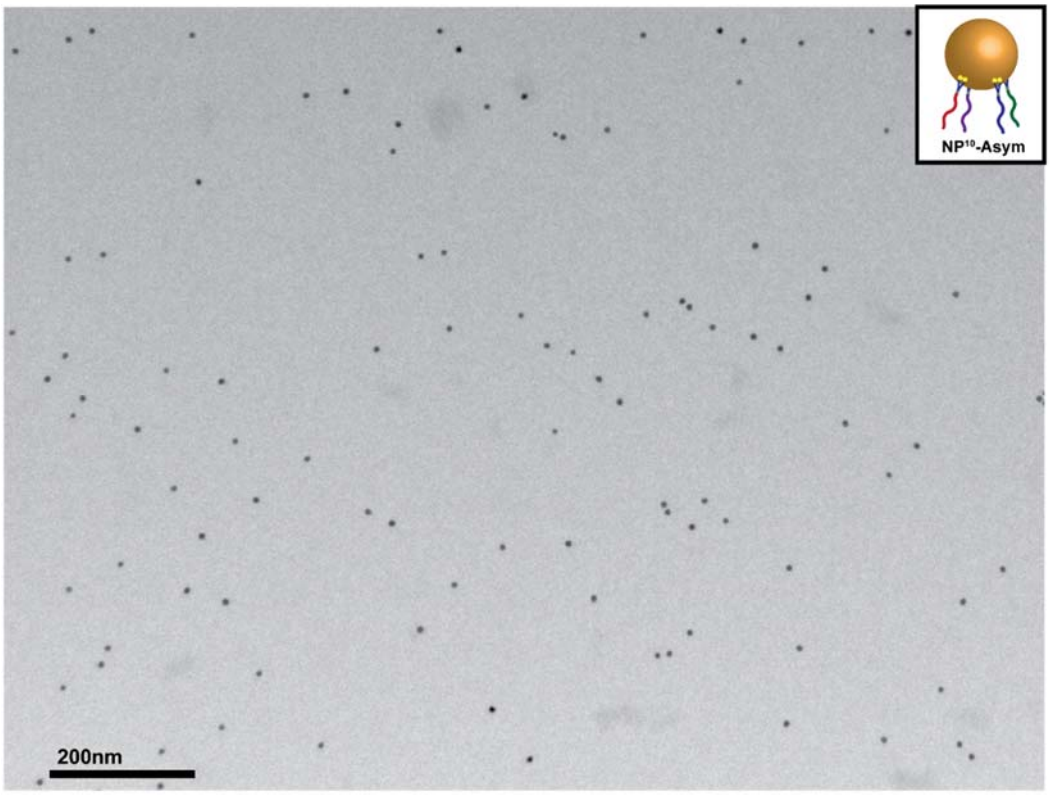
NP19-Asym
200nm


200nm

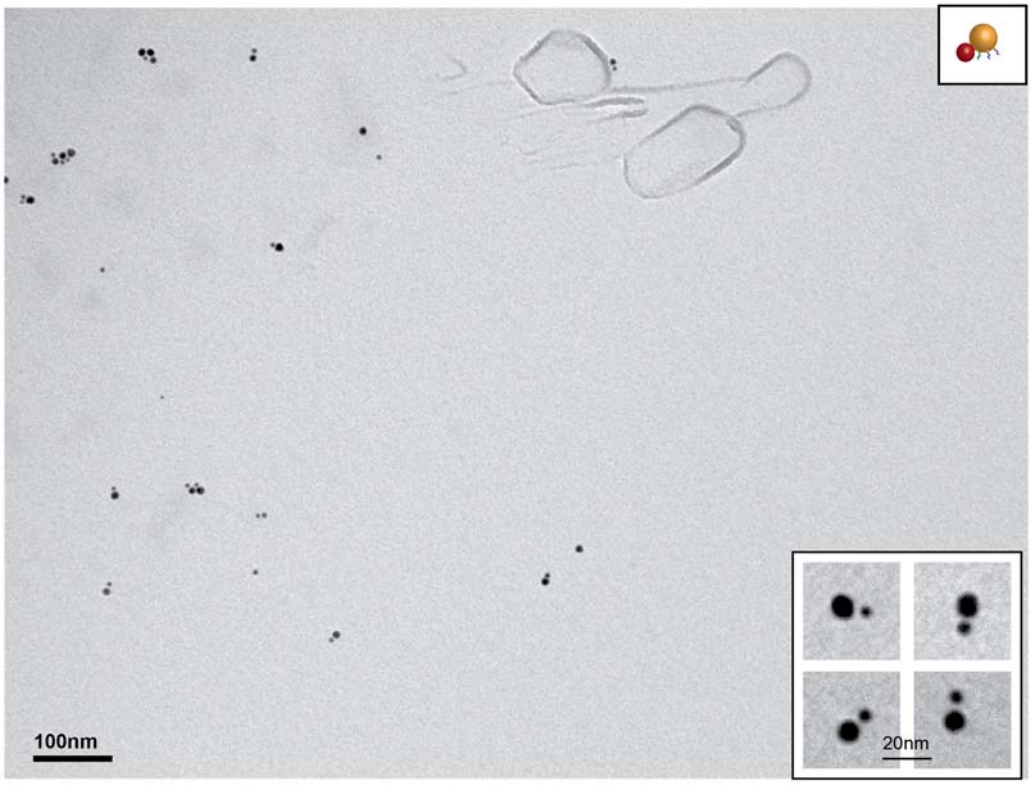
100nm
20nm


200nm

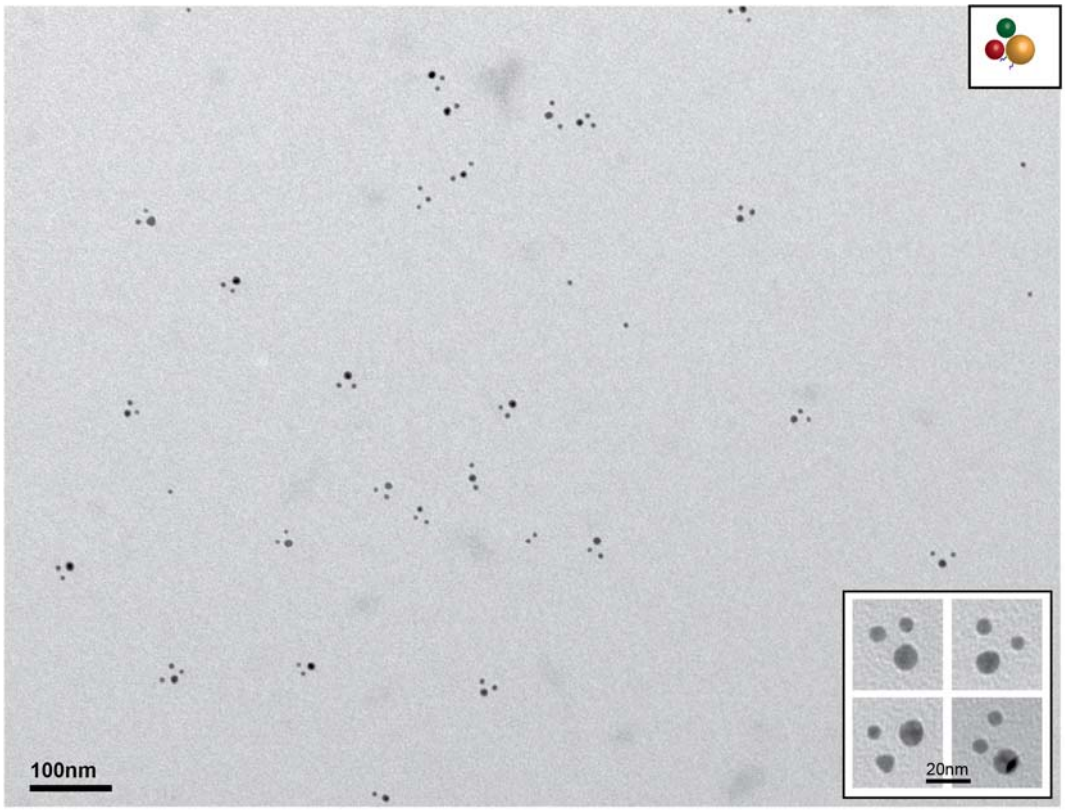
100nm
20nm


200nm


200nm

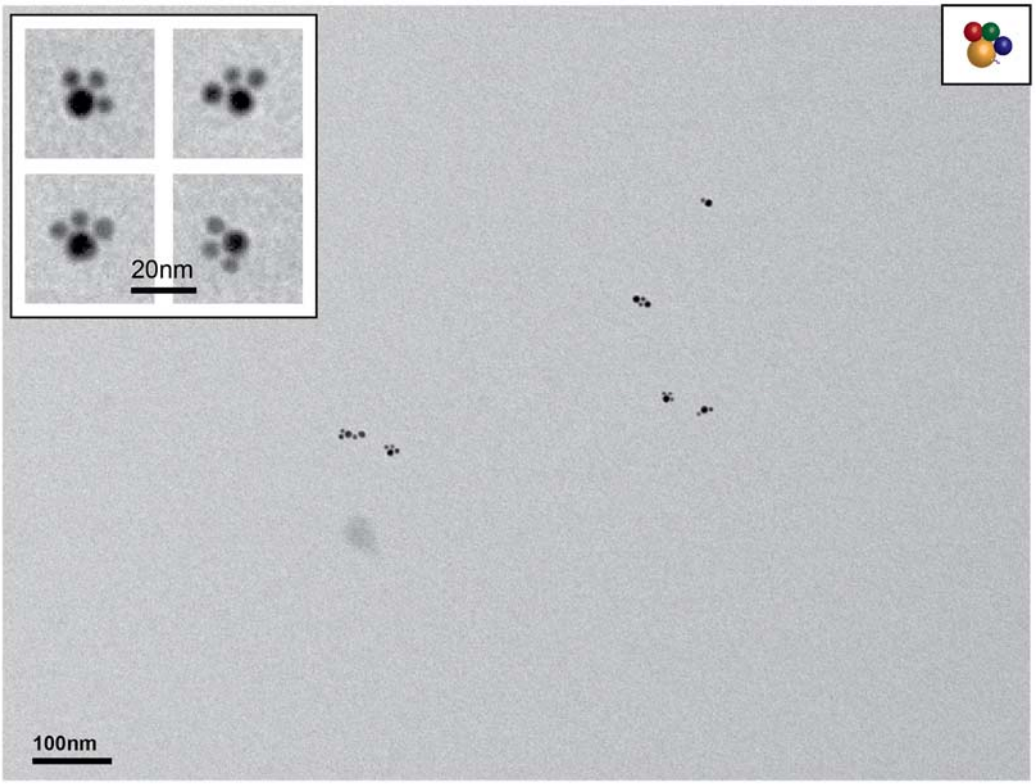
20nm
100nm


200nm

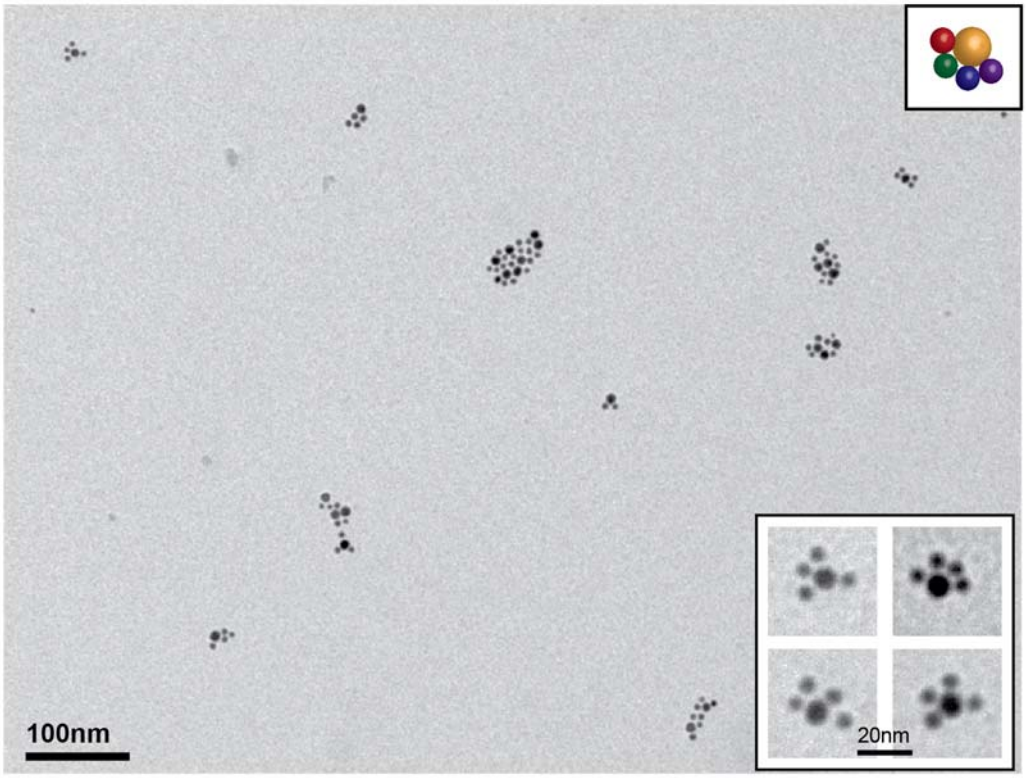
100nm
20nm

4.5.21 Fluorescence assays

Fluorescently tagged sample (**F4**) was prepared as follows. To 3 pmol of **NP^{10}-Asym** in 1xTAMg buffer was added 4.5 pmol of each dye-labelled DNA strand (**Cy3-a'**, **Cy3-b'**, **6-FAM-c'**, **6-FAM-d'**) in 1xTAMg at a final concentration of *ca.* 100 nM with respect to the AuNP. The mixture was incubated at room temperature overnight. After centrifugation (12000 x *g*) at 4°C the supernatant was removed, and 30 µL of 1xTAMg was added. This process was repeated 3 times to remove any unbound dye-labelled DNA strands.

For liberation of the dye-labelled DNA by strand displacement an excess of required eraser strands was added to each sample. For example, to remove **Cy3-a'**: to 1 pmol of **F4** in 1xTAMg was added 10 pmol of $\mathbf{E_a}$ in 1xTAMg, total volume *ca.* 10 µL, and the mixture incubated at room temperature for 1.5 hours.

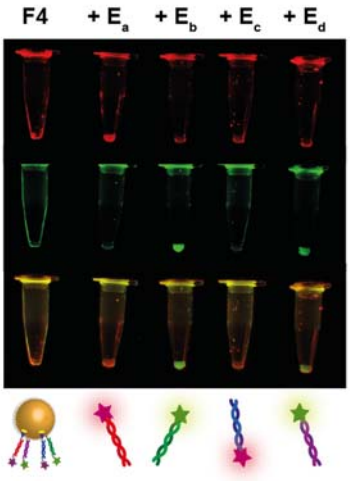

Figure 4.35 - Fluorescence imaging upon addition of single erasers. Single eraser strands ($\mathbf{E_a}$-$\mathbf{E_d}$) were added to **F4** as individual samples to monitor the specificity of dye-tagged DNA release. Samples were imaged directly using a fluorescence gel imaging system (ChemiDoc™ MP System, Bio-Rad Laboratories). The excitation wavelength was by blue or green epi illumination and filters used were 538/28 and 605/50 for 6-FAM and Cy3, respectively.

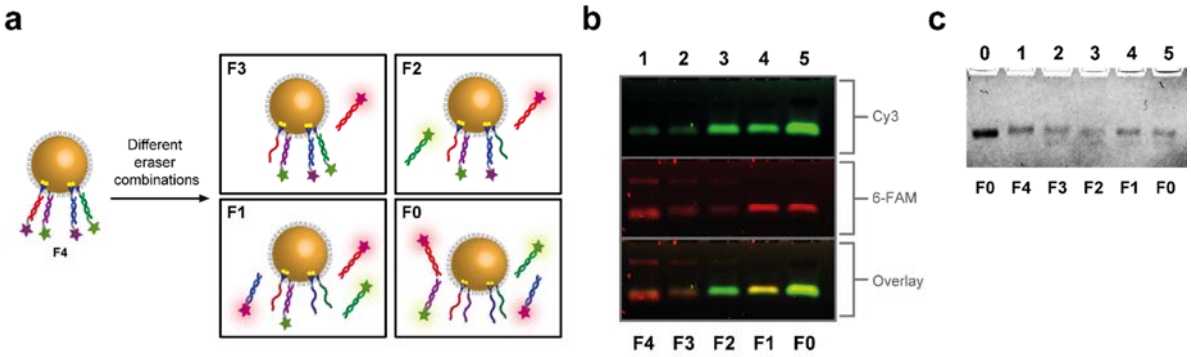

Figure 4.36 - AGE analysis of sequential fluorophore displacement. a) To monitor the cumulative effect of dye-tagged DNA release different eraser strand combinations ($\mathbf{E_a}$-$\mathbf{E_d}$) were added to **F4** as four individual samples, producing **F3**, **F2**, **F1** and **F0**, shown in panel. **b)** AGE analysis of the five samples confirmed the release of the desired dye at each step: Lane 1 – **F4**, Lane 2 – **F3**, Lane 3 – **F2**, Lane 4 – **F1,** Lane 5 – **F0.** The presence of Cy3 and 6-FAM in **F4** (lane 1) is likely due to excess dye-labelled strands not fully removed in the washing step. This was supported by careful analysis of the band mobility, which revealed that the fluorescent bands in lane 1 have higher mobility than in the other lanes, thus suggesting that they are indeed free Cy3/6-FAM strands not bound to an eraser. For this reason, to summarize the data in Figure 5d these bands were ignored. For dye monitoring the excitation was by blue or green epi illumination and filters used were 538/28 and 605/50 for 6-FAM and Cy3, respectively. **c)** AGE analysis of the five samples looking at the AuNP under white light: Lane 0 – **F0**, Lane 1 – **F4**, Lane 2 – **F3**, Lane 3 – **F2**, Lane 4 – **F1,** Lane 5 – **F0**. The ladder of increasing mobility is expected as dye-labelled strands are removed from the AuNP sequentially from left to right. The small change in mobility is expected as the dye-labelled strands have an overhang of 10nt, compared to 43nt for the extension strands used in other experiments.

4.6 References

1 Zhang & Glotzer, S. C. 'Self-Assembly of Patchy Particles'. *Nano Letters* **4**, 1407-1413 (2004).

2 Pawar, A. B. & Kretzschmar, I. 'Fabrication, Assembly, and Application of Patchy Particles'. *Macromolecular rapid communications* **31**, 150-168 (2010).

3 Velev, O. D. 'Patchy nanoparticles: Curvature makes a difference'. *Nat Nano* **8**, 620-621 (2013).

4 Murphy, C. J. *et al.* 'Anisotropic Metal Nanoparticles: Synthesis, Assembly, and Optical Applications'. *The Journal of Physical Chemistry B* **109**, 13857-13870 (2005).

5 DeVries, G. A. *et al.* 'Divalent Metal Nanoparticles'. *Science* **315**, 358-361 (2007).
6 Gong, J., Li, G. & Tang, Z. 'Self-assembly of noble metal nanocrystals: Fabrication, optical property, and application'. *Nano Today* **7**, 564-585 (2012).
7 Wang, Z., Tang, L., Tan, L. H., Li, J. & Lu, Y. 'Discovery of the DNA "Genetic Code" for Abiological Gold Nanoparticle Morphologies'. *Angewandte Chemie International Edition* **51**, 9078-9082 (2012).
8 Li, N., Zhao, P. & Astruc, D. 'Anisotropic Gold Nanoparticles: Synthesis, Properties, Applications, and Toxicity'. *Angewandte Chemie International Edition* **53**, 1756-1789 (2014).
9 Helmi, S., Ziegler, C., Kauert, D. J. & Seidel, R. 'Shape-Controlled Synthesis of Gold Nanostructures Using DNA Origami Molds'. *Nano Letters* (2014).
10 Sun, W. *et al.* 'Casting inorganic structures with DNA molds'. *Science* **346** (2014).
11 Mirkin, C. A., Letsinger, R. L., Mucic, R. C. & Storhoff, J. J. 'A DNA-based method for rationally assembling nanoparticles into macroscopic materials'. *Nature* **382**, 607-609 (1996).
12 Alivisatos, A. P. *et al.* 'Organization of 'nanocrystal molecules' using DNA'. *Nature* **382**, 609-611 (1996).
13 Tan, S. J., Campolongo, M. J., Luo, D. & Cheng, W. 'Building plasmonic nanostructures with DNA'. *Nat Nano* **6**, 268-276 (2011).
14 Barrow, S. J., Funston, A. M., Wei, X. & Mulvaney, P. 'DNA-directed self-assembly and optical properties of discrete 1D, 2D and 3D plasmonic structures'. *Nano Today* **8**, 138-167 (2013).
15 Halverson, J. D. & Tkachenko, A. V. 'DNA-programmed mesoscopic architecture'. *Physical Review E - Statistical, Nonlinear, and Soft Matter Physics* **87** (2013).
16 Kim, J.-W. & Deaton, R. 'Molecular Self-Assembly of Multifunctional Nanoparticle Composites with Arbitrary Shapes and Functions: Challenges and Strategies'. *Particle & Particle Systems Characterization* **30**, 117-132 (2013).
17 Zhang, T., Yang, Z. & Liu, D. 'DNA discrete modified gold nanoparticles'. *Nanoscale* **3**, 4015-4021 (2011).
18 Suzuki, K., Hosokawa, K. & Maeda, M. 'Controlling the Number and Positions of Oligonucleotides on Gold Nanoparticle Surfaces'. *Journal of the American Chemical Society* **131**, 7518-7519 (2009).
19 Zhang, T. *et al.* 'DNA Bimodified Gold Nanoparticles'. *Langmuir : the ACS journal of surfaces and colloids* **28**, 1966-1970 (2011).
20 Zhang, C., Ma, J., Yang, J., Liu, S. & Xu, J. 'Binding Assistance Triggering Attachments of Hairpin DNA onto Gold Nanoparticles'. *Analytical Chemistry* **85**, 11973-11978 (2013).
21 Wang, Y. *et al.* 'Colloids with valence and specific directional bonding'. *Nature* **491**, 51-55 (2012).
22 Xu, X., Rosi, N. L., Wang, Y., Huo, F. & Mirkin, C. A. 'Asymmetric functionalization of gold nanoparticles with oligonucleotides'. *Journal of the American Chemical Society* **128**, 9286-9287 (2006).
23 Maye, M. M., Nykypanchuk, D., Cuisinier, M., van der Lelie, D. & Gang, O. 'Stepwise surface encoding for high-throughput assembly of nanoclusters'. *Nature materials* **8**, 388-391 (2009).
24 Feng, L., Dreyfus, R., Sha, R., Seeman, N. C. & Chaikin, P. M. 'DNA Patchy Particles'. *Advanced Materials* **25**, 2779-2783 (2013).
25 Xing, H. *et al.* 'DNA-Directed Assembly of Asymmetric Nanoclusters Using Janus Nanoparticles'. *ACS Nano* **6**, 802-809 (2011).

26 Kim, J.-W., Kim, J.-H. & Deaton, R. 'DNA-Linked Nanoparticle Building Blocks for Programmable Matter'. *Angewandte Chemie International Edition* **50**, 9185-9190 (2011).
27 Tan, L. H., Xing, H., Chen, H. & Lu, Y. 'Facile and Efficient Preparation of Anisotropic DNA-Functionalized Gold Nanoparticles and Their Regioselective Assembly'. *Journal of the American Chemical Society* **135**, 17675-17678 (2013).
28 Seeman, N. C. 'DNA in a material world'. *Nature* **421**, 427-431 (2003).
29 Aldaye, F. A., Palmer, A. L. & Sleiman, H. F. 'Assembling materials with DNA as the guide'. *Science* **321**, 1795-1799 (2008).
30 Zhang, F., Nangreave, J., Liu, Y. & Yan, H. 'Structural DNA Nanotechnology: State of the Art and Future Perspective'. *Journal of the American Chemical Society* **136**, 11198-11211 (2014).
31 Pinheiro, A. V., Han, D., Shih, W. M. & Yan, H. 'Challenges and opportunities for structural DNA nanotechnology'. *Nat Nano* **6**, 763-772 (2011).
32 Loweth, C. J., Caldwell, W. B., Peng, X., Alivisatos, A. P. & Schultz, P. G. 'DNA-Based Assembly of Gold Nanocrystals'. *Angewandte Chemie International Edition* **38**, 1808-1812 (1999).
33 Aldaye, F. A. & Sleiman, H. F. 'Sequential self-assembly of a DNA hexagon as a template for the organization of gold nanoparticles'. *Angewandte Chemie - International Edition* **45**, 2204-2209 (2006).
34 Aldaye, F. A. & Sleiman, H. F. 'Dynamic DNA templates for discrete gold nanoparticle assemblies: Control of geometry, modularity, write/erase and structural switching'. *Journal of the American Chemical Society* **129**, 4130-4131 (2007).
35 Li, H., Park, S. H., Reif, J. H., LaBean, T. H. & Yan, H. 'DNA-Templated Self-Assembly of Protein and Nanoparticle Linear Arrays'. *Journal of the American Chemical Society* **126**, 418-419 (2003).
36 Le, J. D. *et al.* 'DNA-Templated Self-Assembly of Metallic Nanocomponent Arrays on a Surface'. *Nano Letters* **4**, 2343-2347 (2004).
37 Zhang, J., Liu, Y., Ke, Y. & Yan, H. 'Periodic Square-Like Gold Nanoparticle Arrays Templated by Self-Assembled 2D DNA Nanogrids on a Surface'. *Nano Letters* **6**, 248-251 (2006).
38 Sharma, J. *et al.* 'Control of Self-Assembly of DNA Tubules Through Integration of Gold Nanoparticles'. *Science* **323**, 112-116 (2009).
39 Lau, K. L., Hamblin, G. D. & Sleiman, H. F. 'Gold nanoparticle 3D-DNA building blocks: High purity preparation and use for modular access to nanoparticle assemblies'. *Small* **10**, 660-666 (2014).
40 Mastroianni, A. J., Claridge, S. A. & Alivisatos, A. P. 'Pyramidal and Chiral Groupings of Gold Nanocrystals Assembled Using DNA Scaffolds'. *Journal of the American Chemical Society* **131**, 8455-8459 (2009).
41 Chen, W. *et al.* 'Nanoparticle Superstructures Made by Polymerase Chain Reaction: Collective Interactions of Nanoparticles and a New Principle for Chiral Materials'. *Nano Letters* **9**, 2153-2159 (2009).
42 Shen, X. *et al.* 'Rolling Up Gold Nanoparticle-Dressed DNA Origami into Three-Dimensional Plasmonic Chiral Nanostructures'. *Journal of the American Chemical Society* **134**, 146-149 (2011).
43 Kuzyk, A. *et al.* 'DNA-based self-assembly of chiral plasmonic nanostructures with tailored optical response'. *Nature* **483**, 311-314 (2012).

44 Carneiro, K. M. M., Aldaye, F. A. & Sleiman, H. F. 'Long-range assembly of DNA into nanofibers and highly ordered networks using a block copolymer approach'. *Journal of the American Chemical Society* **132**, 679-685 (2010).
45 Edwardson, T. G. W., Carneiro, K. M. M., McLaughlin, C. K., Serpell, C. J. & Sleiman, H. F. 'Site-specific positioning of dendritic alkyl chains on DNA cages enables their geometry-dependent self-assembly'. *Nat Chem* **5**, 868-875 (2013).
46 Li, Z., Jin, R., Mirkin, C. A. & Letsinger, R. L. 'Multiple thiol-anchor capped DNA-gold nanoparticle conjugates'. *Nucleic Acids Research* **30**, 1558-1562 (2002).
47 Hurst, S. J., Lytton-Jean, A. K. R. & Mirkin, C. A. 'Maximizing DNA Loading on a Range of Gold Nanoparticle Sizes'. *Analytical chemistry* **78**, 8313-8318 (2006).
48 McLaughlin, C. K. *et al.* 'Three-dimensional organization of block copolymers on "DNA- minimal" scaffolds'. *Journal of the American Chemical Society* **134**, 4280-4286 (2012).
49 Serpell, C. J., Edwardson, T. G. W., Chidchob, P., Carneiro, K. M. M. & Sleiman, H. F. 'Precision Polymers and 3D DNA Nanostructures: Emergent Assemblies from New Parameter Space'. *Journal of the American Chemical Society* **136**, 15767-15774 (2014).
50 Huo, F., Lytton-Jean, A. K. R. & Mirkin, C. A. 'Asymmetric Functionalization of Nanoparticles Based on Thermally Addressable DNA Interconnects'. *Advanced Materials* **18**, 2304-2306 (2006).
51 Reineck, P. *et al.* 'Distance and Wavelength Dependent Quenching of Molecular Fluorescence by Au@SiO2 Core–Shell Nanoparticles'. *ACS Nano* **7**, 6636-6648 (2013).
52 De, M., Ghosh, P. S. & Rotello, V. M. 'Applications of Nanoparticles in Biology'. *Advanced Materials* **20**, 4225-4241 (2008).
53 Nikitin, M. P., Shipunova, V. O., Deyev, S. M. & Nikitin, P. I. 'Biocomputing based on particle disassembly'. *Nat Nano* **9**, 716-722 (2014).
54 Rosi, N. L. *et al.* 'Oligonucleotide-modified gold nanoparticles for infracellular gene regulation'. *Science* **312**, 1027-1030 (2006).
55 Wen, Y., McLaughlin, C. K., Lo, P. K., Yang, H. & Sleiman, H. F. 'Stable gold nanoparticle conjugation to internal DNA positions: Facile generation of discrete gold nanoparticle-DNA assemblies'. *Bioconjugate Chemistry* **21**, 1413-1416 (2010).

5 Conclusions and Future Work

5.1 Conclusions and contributions to original knowledge

The work described in this thesis aimed to address the design and synthesis of DNA-conjugates and their integration with DNA nanostructures. Overall it is found that the introduction of DNA-conjugates to DNA nanostructures can introduce unprecedented modes of assembly and provide new functionality. A key concept is that the introduction of orthogonal supramolecular interactions to DNA nanostructures expands the palette of interactions without increasing the DNA sequence space.

The research presented in chapter 2 addressed the integration of dendritic DNA amphiphiles with DNA cages. The use of phosphoramidite chemistry to produce dendritic alkyl-DNA was described. The development of the synthetic, purification and characterization methods needed to produce D-DNA was a large part of the work presented in chapter 2. Due to the accessibility and reliability of these methods, they are now currently being applied by our group to produce DNA-conjugates for a variety of different research projects. The integration of the DNA-amphiphiles with a 3D DNA scaffold was shown to create a tunable platform which displayed a wide range of assembly behaviors, dependent on the number, positioning and chemical structure of the amphiphiles on the scaffold. This was used to drive intermolecular association through hydrophobic residues, analogous to quaternary protein structure. The intermolecular hydrophobically mediated association represents a new assembly method for bringing together DNA nanostructures. The hydrophobic groups were also shown to undergo intramolecular assembly, creating an encapsulation environment for small molecule drugs. This is the first example of a DNA nanostructure which can load and release small molecule cargo, and is therefore an important contribution to the field of drug-delivery.

In chapter 3, the development of a facile, modular and high yielding synthetic approach for the production of DNA-polymer conjugates was introduced. The implementation of phosphoramidite chemistry for the production of phosphate punctuated polymer modifications was shown to be a powerful strategy for the creation of monodisperse polymer-DNA conjugates with tunable self-assembly properties. Hydrophobic DNA-polymer conjugates are typically difficult to produce. The development of this efficient, and importantly, accessible method will expedite the production of these interesting nanomaterials which have great potential in the areas of drug and nucleic acid delivery. Additionally, the applicability of the method to create different polymer sequences is an exciting discovery, which can be used to create a wide variety of sequence-defined polymers with ease. The discovery of sequence-dependent self-assembly properties is an important finding and can be used to create designer self-assembling materials.

In chapter 4, the potential of DNA nanostructures to act as templates for the transfer of assembly information to gold nanoparticles was investigated. The development of a novel gold binding moiety which produced highly stable gold nanoparticle conjugates was described. The positioning of the reactive groups on a 3D DNA scaffold was shown to create templates which could effectively transfer a specific pattern of DNA strands to gold nanoparticles. This represents the first example of gold nanoparticles with defined number, geometry, directionality and sequence asymmetry of bound DNA strands. The resulting 'smart' nanoparticles are ready for use as building blocks in the self-assembly of discrete nanoclusters with arbitrary shapes. This technology will be valuable for the creation of plasmonic architectures which could not be created with isotropically functionalized particles.

5.2 Suggestions for future work

The encapsulation of small molecules in DNA cages as described in chapter 2 has great implications for DNA-based drug delivery devices. As such, future work will be focused on investigating the ability of these systems to carry and deliver therapeutic cargo. This will involve scale-up and optimization of small molecule loading, work which is already underway in our group. The generality of the approach to encapsulate a range of different small molecule drugs would also be an important aspect to explore

as well as the potential of integrating nucleic acid therapeutics into the structure to create dual-purpose delivery vehicles. To determine the cellular uptake profiles and internalization pathway *in vitro* studies will be an important step for the further development of these systems, as will an investigation into their stability in biological media. Additionally, the hydrophobically mediated intermolecular assembly discovered in chapter 2 could be investigated further. The specificity of the geometry and number of hydrophobic residues needed to give intermolecular self-assembly can be used to create dynamic DNA assemblies with unique molecular recognition properties.

In chapter 3, a new method to create DNA-polymer conjugates and sequence-defined polymers was described. The resulting polymers were shown to assemble into very well-defined micelles, which are capable of encapsulating small molecule cargo. The development of these as drug-delivery vehicles is currently being investigated in our lab with promising results. Additionally, the method can be expanded to the creation of RNA-polymer conjugates, an exciting platform for carrier-free delivery of nucleic acid therapeutics. The initial synthesis of sequence-controlled polymers focused on the use of only two polymer building blocks, hexaethylene and hexaethylene glycol. With these hydrophobic and hydrophilic monomers sequence-dependent self-assembly was observed. However, the method is highly modular and applicable to a wide range of different monomer units. This could be used to introduce other molecular recognition motifs, such as metal-coordination centers, fluorophilic chains, chromophores or redox active units. The incorporation of these can be used to create artificial protein mimics, with potential applications in catalysis, light-harvesting and fundamental studies of supramolecular foldamers.

The work in chapter 4 introduced the concept of DNA nanostructures as templates for the printing of DNA strands on gold nanoparticles with specific number, directionality and sequence asymmetry. The modularity of the approach opens up a number of possibilities which can be rationally investigated. For example the effect of DNA prism size and surface curvature of the particle on the relative spacings and angles of the surface bound DNA strands could be investigated. For the asymmetric patterning, the question of stereoselectivity remains unanswered and this would be an important avenue to pursue. The extension of the printing method to gold surfaces could be used as a tool to determine the chiral purity of the clip-by-clip DNA cages. The use of the patterned nanoparticles, especially the asymmetric version, in the creation of discrete of

long range plasmonic architectures will also be an important next step, as these nanoparticles have the potential to create a variety of different 2D and 3D structures which are not be accessible via other methods. Additionally, an investigation into the multiplex sensing potential of the multiple fluorophore labelled nanoparticles will have interesting implications for biosensing.

5.3 Publications

Author contributions are provided for work included in this thesis for clarity.

1 Edwardson, T. G. W., Carneiro, K. M., McLaughlin, C. K., Serpell, C. J. & Sleiman, H. F. 'Dendritic Alkyl Chains on DNA Cages: A Geometry-Dependent Inter- or Intramolecular "Handshake"'. **2013** *Journal of Biomolecular Structure & Dynamics* 31, 87-87. – *Published Conference Abstract*

2 Edwardson, T. G. W., Carneiro, K. M. M., McLaughlin, C. K., Serpell, C. J. & Sleiman, H. F. 'Site-specific positioning of dendritic alkyl chains on DNA cages enables their geometry-dependent self-assembly'. **2013** *Nature Chemistry*, 5, 868-875.

Covered in chapter 2. *Author contributions:* **Thomas G. W. Edwardson** helped develop the project and primarily contributed to the production of experimental data from DNA synthesis, HPLC, mass spectrometry, electrophoresis, dynamic light scattering, atomic force microscopy and absorption and fluorescence spectroscopies and writing of the paper. **Karina M. M. Carneiro** helped design the project, developed the synthesis of modified DNA, aided data interpretation and co-wrote the paper. **Christopher K. McLaughlin** designed and synthesized the sequences for the DNA scaffold and additional unmodified DNA, data interpretation and co-wrote the paper. **Christopher J. Serpell** aided in the interpretation of data, discussion of results and co-wrote the paper. **Hanadi F. Sleiman** designed the project, guided interpretation of data, discussion of results and concepts and co-wrote the paper.

3 Fakhoury, J. J., McLaughlin, C. K., Edwardson, T. G. W., Conway, J. W. & Sleiman, H. F. 'Development and Characterization of Gene Silencing DNA Cages'. **2013** *Biomacromolecules*, 15, 276–282.

4 Bujold, K. E., Fakhoury, J. J., Edwardson, T. G.W., Carneiro, K. M. M., Neves Briard, J., Godin, A. G., Amrein, L., Hamblin, G. D., Panasci, L. C., Wiseman, P.,

Sleiman, H.F. 'Sequence-Responsive Unzipping DNA Cubes with Tunable Cellular Uptake Profiles'. **2014**, *Chemical Science*, 5, 2449-2455.

5 Edwardson, T. G. W., Carneiro, K. M. M., Serpell, C. J. & Sleiman, H. F. 'An Efficient and Modular Route to Sequence-Defined Polymers Appended to DNA'. **2014** *Angewandte Chemie International Edition*, 53, 4567–4571.

Covered in chapter 3. *Author contributions:* **Thomas G.W. Edwardson** contributed to the synthesis, characterization and self-assembly studies of the DNA-polymer conjugates, production of experimental data, interpretation of results and co-wrote the paper. **Karina M. M. Carneiro** contributed to the synthesis of modified DNA, interpretation of data and co-wrote the paper. **Christopher J. Serpell** designed the project, carried out fluorescence experiments, aided in the interpretation of data, discussion of results and concepts and co-wrote the paper. **Hanadi F. Sleiman** designed the project, guided interpretation of data, discussion of results and concepts and co-wrote the paper.

6 Serpell, C. J., Edwardson, T. G. W., Chidchob, P., Carneiro, K. M. M. & Sleiman, H. F. 'Precision Polymers and 3D DNA Nanostructures: Emergent Assemblies from New Parameter Space'. **2014** *Journal of the American Chemical Society*, 136, 15767-15774.

Summarized without discussion of any experimental details in chapter 3. *Author contributions:* **Christopher J. Serpell** helped develop the project and primarily contributed to the production of experimental data and writing of the paper. **Thomas G.W. Edwardson** designed and synthesized DNA-polymer conjugates, clip strands and prism linking strands. **Pongphak Chidchob** carried out AFM analysis and helped write the paper. **Karina M.M. Carneiro** assisted in DNA-polymer conjugate synthesis. **Hanadi F. Sleiman** designed the project, guided interpretation of data, discussion of results and concepts and co-wrote the paper.

7 Conway, J. W. et al. 'Dynamic Behavior of DNA Cages Anchored on Spherically Supported Lipid Bilayers'. **2014** *Journal of the American Chemical Society*, 136, 12987-12997.

Submitted publication:

8 Edwardson, T. G. W.; Lau, K. L.; Bousmail, D. B.; Serpell, C. J. and Sleiman, H. F. 'Pattern transfer from DNA nanostructures to gold nanoparticles: anisotropic control of directionality, number, geometry and sequence asymmetry', *Nature Nanotechnology* (submitted Dec 12th, 2014)

Covered in chapter 4. *Author contributions:* **Thomas G. W. Edwardson** helped develop the project and primarily contributed to the production of experimental data from DNA synthesis, HPLC, gel electrophoresis, dynamic light scattering, fluorescence spectroscopy and writing of the paper. **Kai Lin Lau** carried out gold nanoparticle synthesis, the majority of transmission electron microscopy analysis, prepared patterned gold nanoparticles for fluorescence spectroscopy, aided data interpretation and co-wrote the paper. **Danny Bousmail** carried out all dynamic light scattering experiments and data interpretation and co-wrote the paper. **Christopher J. Serpell** synthesized clip strands TC3-AB, PC4-AB and PP5-AB. **Hanadi F. Sleiman** designed the project, guided interpretation of data, discussion of results and concepts and co-wrote the paper.

Appendix:

Serum protein interactions of DNA amphiphiles on DNA cages

This appendix is comprised of preliminary investigations into the serum protein interactions of the D-DNA decorated cubes introduced in chapter 2. **Thomas G.W. Edwardson** helped design the project and carried out all experimental work. **Hanadi F. Sleiman** designed the project and guided interpretation of data, discussion of results and concepts.

A.1 Abstract

DNA nanotechnology has shown great potential for the construction of smart, stimuli responsive biomedical tools. There are major challenges which must be addressed however. One of these challenges is to understand, and ideally be able to control, the interactions of DNA nanostructures with biological systems. This appendix describes preliminary studies into serum protein interactions of a cubic DNA scaffold. It is found that DNA amphiphiles mediated the interaction with serum albumin and that there is the potential to tune this interaction by spatial positioning of hydrophobic residues on the DNA cage and the chemical identity of those hydrophobic groups.

A.2 Introduction

DNA nanostructures have emerged as a promising candidate for the production of targeted drug-delivery vehicles. It is the complete control over structural parameters such as size, shape, rigidity and presentation of functional groups which makes these systems very valuable. There are however issues which must be addressed for the successful development of DNA nanostructures in nanomedicine. The main challenges are cellular uptake, serum stability and immunogenicity. As nucleic acids are negatively charged macromolecules they exhibit minimal cellular uptake, this has been addressed in the area of nucleic acid therapeutics in two main ways. One approach is the synthesis of

nucleic acid amphiphiles, conjugating the nucleic acid to a hydrophobic group which aids uptake via inclusion in lipoproteins and receptor mediated uptake.[1,2] Another approach is to package the nucleic acid in a nanostructure, such as a spherical nucleic acid or 3D nanostructure.[3] These structures have been shown to exhibit enhanced cellular uptake, which is shape dependent.[4]

The stabilization of DNA and RNA in biological media is largely achieved by chemical modification, particularly to the sugar ring or phosphate backbone. A range of chemical modifications have been shown to increase stability and potency of nucleic acid therapeutics. Another method used to stabilize nucleic acid therapeutics *in vivo* relies on the encapsulation of nucleic acids within liposomal systems or stable nucleic acid lipid particles (SNALPs). Additionally, the close packing of nucleic acids in the corona of spherical nucleic acids (SNAs) has shown to prevent access to nucleases, thus increasing the stability in biological media.[5]

One consideration for any nanoparticle which is to be introduced to the biological milieu is the interaction with proteins, this is especially important for molecules with hydrophobic regions.[6] Biological serum contains high concentrations of proteins which have the potential to interact specifically, or non-specifically, with exogenous nanomaterials. With this in mind, the possibility to control interactions with proteins by structural design is a powerful concept. In this appendix the discovery of a supramolecular interaction between an amphiphile decorated DNA nanostructure and bovine serum albumin (BSA) is presented. Preliminary investigations are shown which suggest that the interaction is mediated by the DNA amphiphiles and could be due to specific binding. This is a promising step towards understanding the role that size, shape and surface functionality on nanostructures plays on their interactions with biological systems.

A.3 Results and Discussion

A.3.1 DNA nanostructure

The DNA nanostructure used in this study is the same system described in chapter 2. This consists of a 3D DNA cubic scaffold decorated with differing numbers and spatial orientations of dendritic DNA amphiphiles (**D-DNA**). Figure A.1 shows the structure of the DNA amphiphiles **D1** and **D2**.

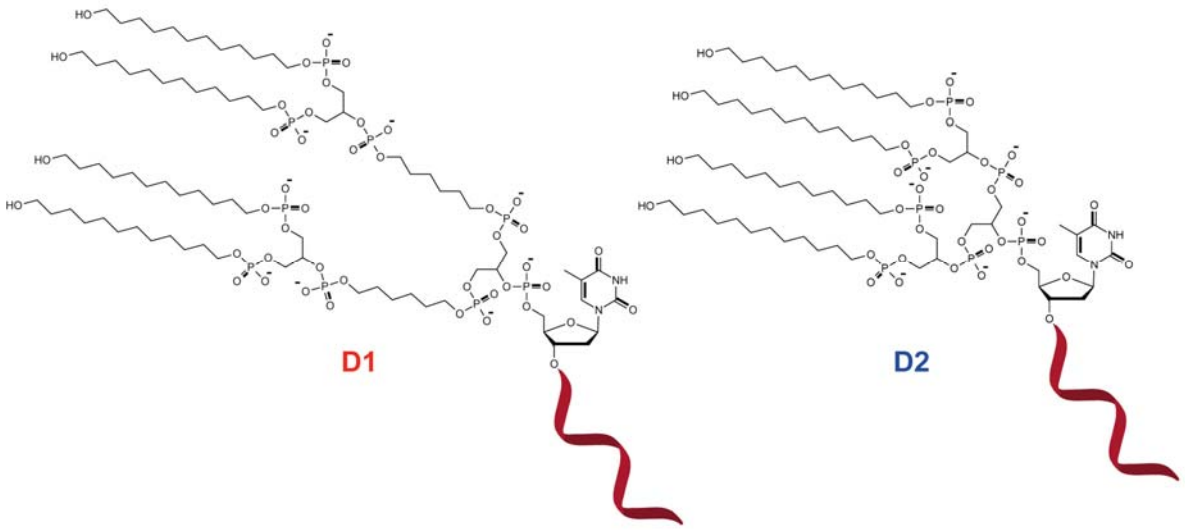

Figure A.1 – Chemical structure of D-DNA. The structure of dendritic DNA amphiphiles **D1** and **D2** is shown, see chapter 2 for full details of synthesis, characterization and self-assembly properties.

The nuclease resistance of DNA nanostructures is commonly studied by means of a fetal bovine serum (FBS) stability assay.[7] FBS consists of a mixture of non-specific exo- and endo-nucleases, as well as other proteins. The first experiment described here is the FBS stability assay of **D-DNA** decorated cubic scaffolds. Three samples were prepared for this purpose, shown in Figure A.2. The first structure (**C-A$_4$B$_4$**) is an unmodified DNA cube with eight single-stranded regions. The second and third samples are cube-core structures formed from the intramolecular association of eight **D-DNA** conjugates hybridized to the single-stranded regions. The structure **2** has eight **D1** amphiphiles and the structure **3** has eight **D2** amphiphiles. It is important to note that **D1** and **D2** exhibit different self-assembly behavior, described fully in chapter 2.

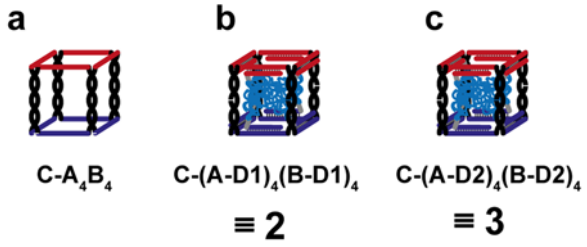

Figure A.2 – DNA nanostructures. The structure of a) single stranded cube **C-A$_4$B$_4$**, b) Cube-core structure **2**, with **D1** amphiphiles and c) Cube-core structure **3**, with **D2** amphiphiles.

The cubic scaffold (200nM) was incubated with 10% FBS in Dulbecco's modified Eagle's medium (DMEM) at 37°C and aliquots were taken at time points of 0, 1, 5, 12 and 24 hours. At each timepoint the aliquot was treated with either EDTA (for native study) or formamide (denaturing study) to deactivate the enzymes, and the sample kept at 4°C until loading on gel. Figure A.3 shows the native and denaturing PAGE analysis of the **C-A$_4$B$_4$** FBS digestion assay. Panel *a* shows the native PAGE which reveals that the 3D construct is mostly degraded after 1 hour. The denaturing analysis shown in panel *b* reveals a typical degradation pattern over the course of 24 hours. It is noteworthy that these iterations of the clip-cy-clip structures are not expected to be resistant to enzymatic cleavage, methods to increase the serum stability have been previously reported by the Sleiman group. [7]

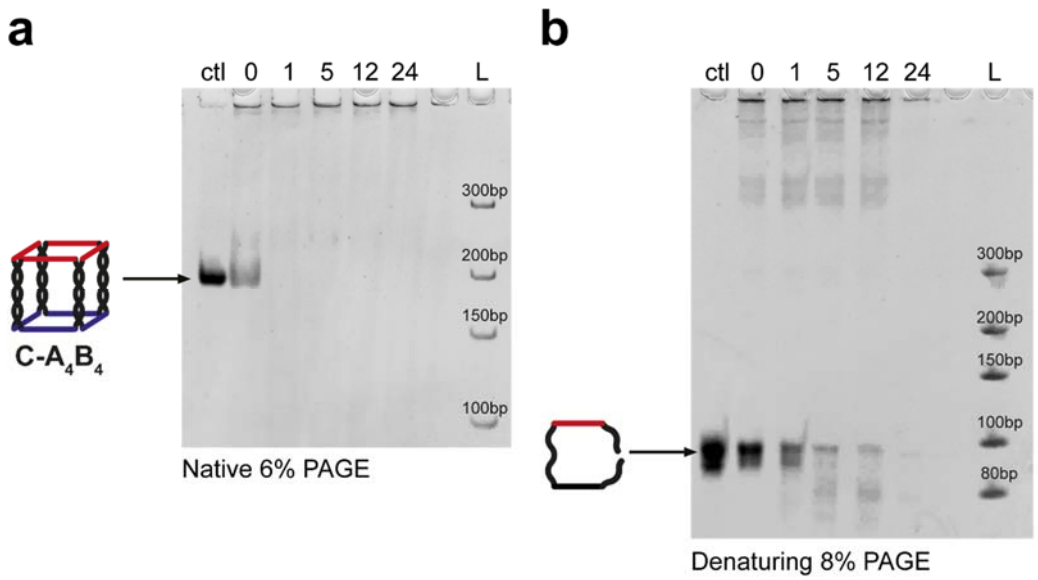

Figure A.3 – FBS assay on single stranded cubic scaffold. a) Native PAGE analysis reveals rapid degradation of **C-A$_4$B$_4$**, b) Denaturing analysis shows the degradation of the clip strands, apparent from the loss of intensity of the highlighted clip band and appearance of higher mobility digested fragments.

Next, the cube-core structures were subjected to the same conditions and analyzed by tandem native and denaturing gels. The resulting gel mobility patterns revealed some unexpected behavior. Figure A.4a shows the native gel analysis of both **2** and **3** FBS digestion assays. The control samples (lane ctl) correspond to DNA structures without the addition of FBS and exhibit the expected gel mobility for these structures based on previous work. However, at time point 0 a mobility shift to a higher molecular

weight assembly is observed (lanes 0). At the later time points the degradation of the 3D structures is still observed, as it was for **C-A$_4$B$_4$**. The denaturing analysis shown in Figure A.4b reveals more interesting band patterns. It should be noted that the amphiphiles **D1** and **D2** should not be visible on this gel as they are low molecular weight oligonucleotides of 19 nt (see ladder, lane L). The degradation pattern for the clips strands is as expected and is the same as was observed with the single-stranded cube **C-A$_4$B$_4$**. However the appearance of a band at lower mobility is unexpected and must be due to the **D-DNA** based on the control. Since the mobility of this band is too low to correspond to the individual strands it was hypothesized that it was due to an interaction between the **D-DNA** and some component of the FBS. It is worth noting here that there is a stronger band for **D1** amphiphiles compared to **D2**, suggesting that the binding may be sensitive to the structure of the hydrophobic moiety.

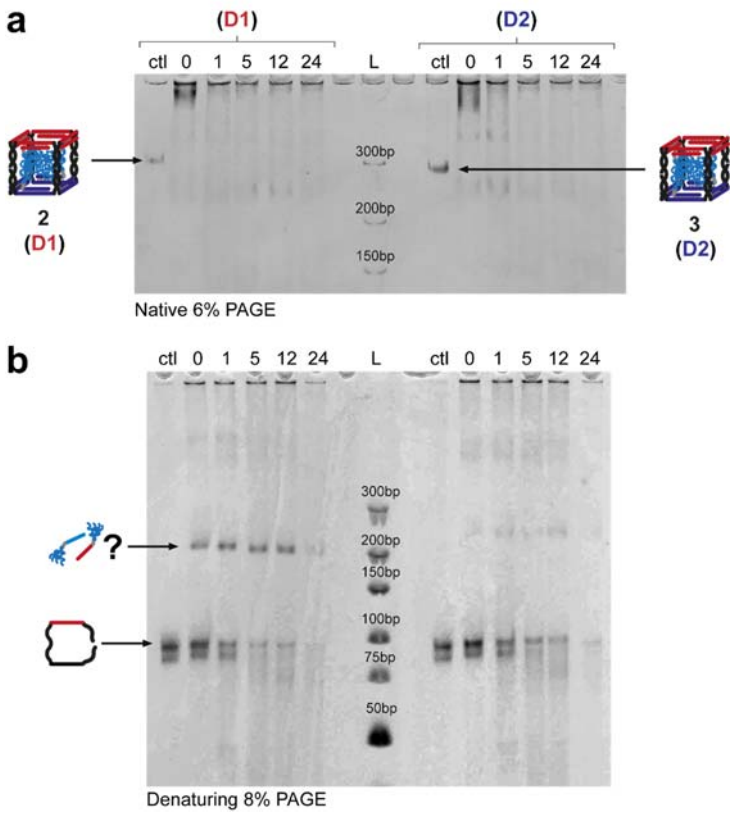

Figure A.4 – FBS assay on cube-core structures. Numbers above lanes correspond to time points (hours). a) Native PAGE analysis reveals unexpected low mobility band for structures **2** and **3**, (lanes 0) suggesting an interaction with serum components. b) Denaturing analysis shows the degradation of the clip strands, and the appearance of another low mobility band which is too large to be single D-DNA strands, further suggesting serum protein binding.

To ensure that the behavior observed was in fact due to serum proteins and not any other assay variable a control experiment was carried out. For this experiment only the zero time point was investigated as the degradation pattern was not the focus. In Figure A.5 the incubation of DNA structures with the same DMEM and EDTA concentrations but differing percentages of FBS are shown in relation to a control sample which is DNA structure assembled in 1xTAMg buffer. For the cubic scaffold **C-A$_4$B$_4$**, an increase in FBS concentration causes some band smearing but no higher-order assemblies, consistent with only weak non-specific interactions. However, for **2** and **3** the intensity of low mobility bands increases with increasing percentage of FBS showing that the assemblies are likely mediated by serum proteins.

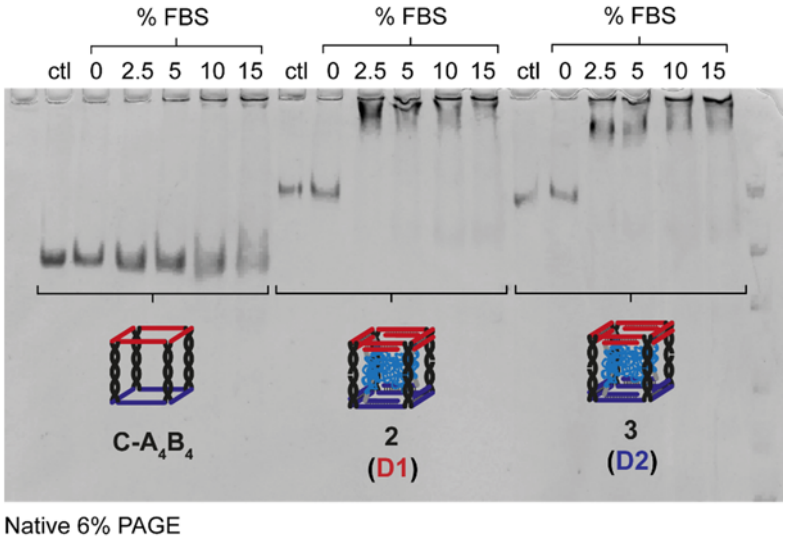

Figure A.5 – FBS assay on single stranded cubic scaffold. The lanes ctl refer to the DNA structures in 1xTAMg buffer without the addition of DMEM and EDTA. Other lanes contain a varying percentage (v/v) of FBS, indicated by the number above each lane. Cubic scaffold **C-A$_4$B$_4$** shows negligible interaction with the FBS whereas the cube-core structures **2** and **3** show a strong interaction which is clearly due to a component of the FBS.

With a clear indication that there was an interaction between the **D-DNA** containing nanostructures and some component of the FBS, the next step was to determine which specific component was causing this effect. The major protein component of FBS is bovine serum albumin (BSA). This globular 65kDa transport protein is present at concentrations of up to 1mM in FBS. Serum albumin transports fatty acids to cells for lipid biosynthesis as a source of energy. Figure A.6 shows the crystal structure of human serum albumin (HSA) bound to dodecanoic acid.[8] As both **D-DNA** amphiphiles

are terminated with dodecanol chains it seemed a likely hypothesis that this may be the interacting component in the FBS and that the binding may be specific and mediated by the dodecanol chains. The different binding affinity between **D1** and **D2** shown earlier further suggested a specific binding interaction, which is sensitive to small structural changes in the alkyl dendron.

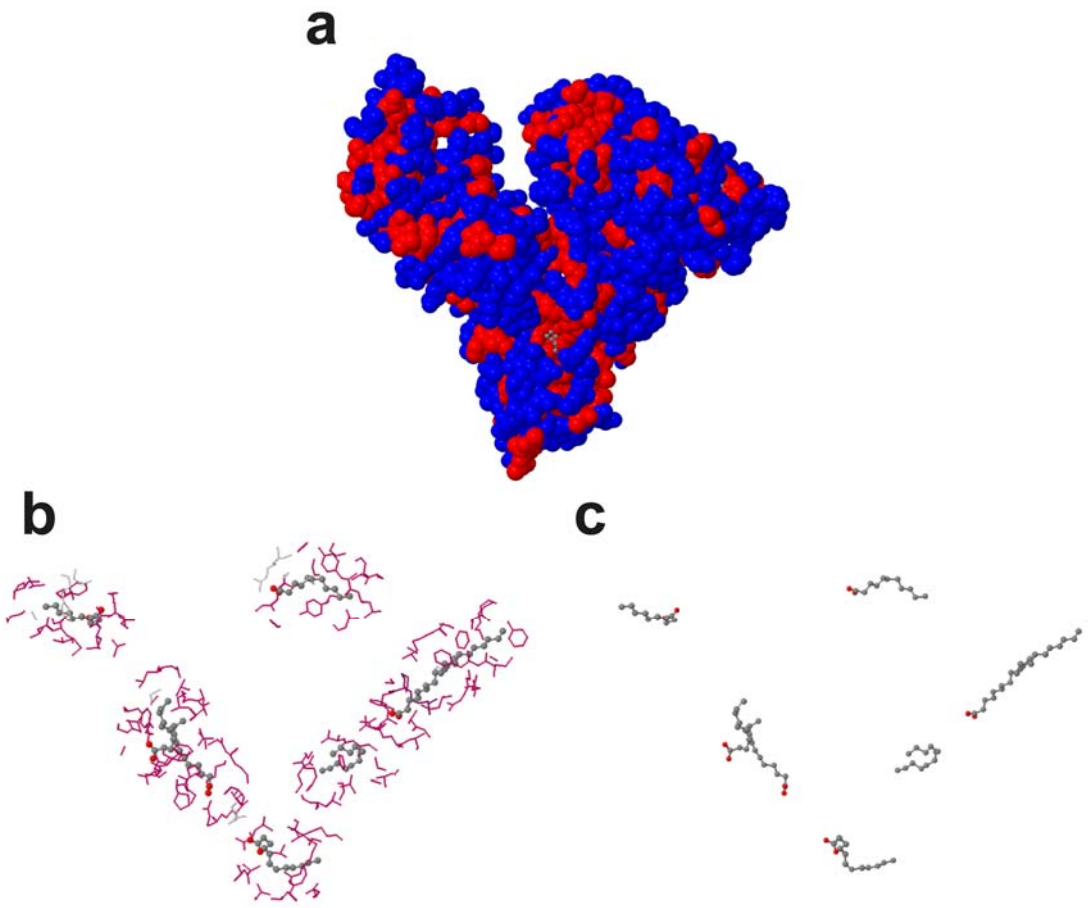

Figure A.6 – Crystal structure of HSA. The structure of HSA bound to dodecanoic acid. a) Space-filling model - hydrophobic regions are red and hydrophilic are blue. b) dodecanoic acid in binding pockets. c) orientation of dodecanoic acid molecules in the complex. (Protein data bank code 1E7F[8])

With this in mind the DNA structures were incubated with BSA and compared to the results obtained with FBS. The same experimental conditions were used with the FBS being replaced by a 40mg/mL solution of BSA in 1xPBS buffer, this is approximately the equivalent concentration. Shown in Figure A.7 is the result of the incubation of cube-core structure **2** with BSA and FBS. As expected the same mobility pattern is seen as for the FBS confirming that BSA is the interacting component in the serum.

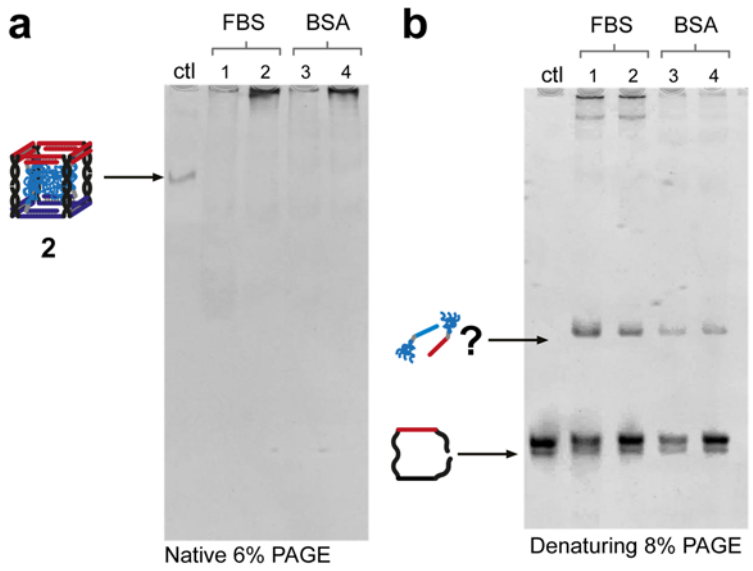

Figure A.7 – Comparison of FBS and BSA. The interaction of the **D1** functionalized cube with FBS and BSA is compared to determine if BSA is the interacting component in serum. Similar mobility patterns are seen for the incubation of cube-core structure **2** with FBS and with BSA, confirming that BSA binds to **D-DNA**. a) Native analysis: Lane ctl, **2** in 1xTAMg, Lane 1, FBS, Lane 2, **2**+ FBS, Lane 3, BSA, Lane 4, **2** + BSA and b) Denaturing anallyis: Lane ctl, **2** in 1xTAMg (denatured), Lane 1, 0.5 x **2** + FBS, Lane 2, **2**+ FBS, Lane 3, 0.5 x **2** + BSA, Lane 4, **2** + BSA.

With the interacting component of FBS established as BSA, a preliminary study of the relative binding affinities of **D1** and **D2** was carried out. As noticed in the earlier experiments, **D1** appeared to exhibit a stronger interaction with BSA than **D2**. An electrophoretic mobility shift assay (EMSA) was used to probe the relative binding affinities of **D1** and **D2** to BSA. Aliquots of **D1** and **D2** (500nM) were incubated with increasing equivalents of BSA in 1xPBS buffer at 37°C for 1 hour and run on non-denaturing 12% PAGE. Figure A.8 shows the results of this assay which reveal that the **D1** conjugate has a higher binding affinity than **D2**. This is an interesting finding which suggests that the structure of the alkyl dendron is important for the binding interaction, suggesting specificity which may be due to the insertion of the dodecanol chains into the fatty acid binding pockets. **D1** is the more flexible of the two DNA amphiphiles and may be able to adopt a more favourable conformation for binding to the protein.

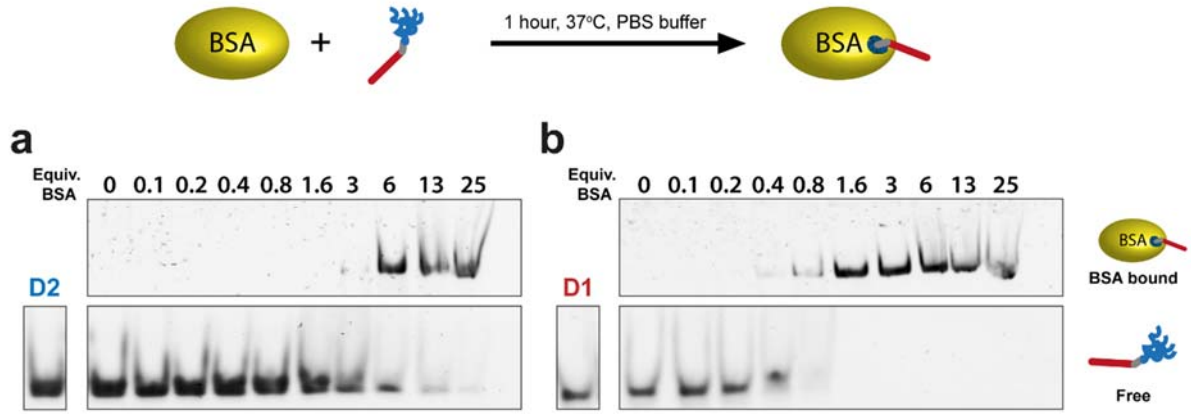

Figure A.8 – BSA binding comparison of D1 and D2. a) Titration of **D2** with increasing equivalents of BSA. The bottom portion of the gel shows the free **D2** conjugates while the top portion shows the **D2-**BSA complex. B) The same data is shown for **D1** which exhibits a higher binding affinity.

Finally, the effect of differing orientations of **D-DNA** on the cubic scaffold on BSA binding was investigated. In chapter 2, it was shown that site-specific positioning of the **D-DNA** had a strong effect on the inter and intramolecular association of the hydrophobic residues. As **D1** exhibited a stronger interaction with BSA than **D2** and does not undergo intermolecular self-association it was used as for the initial experiments to probe the effect of spatial organization. Figure A.9c shows preliminary evidence that changing the orientation of **D1** conjugates on the cubic scaffold alters the interaction with BSA. The single-stranded cube control shows no interaction with BSA and exhibits the expected mobility for the free DNA cube, lane 0. However, for the **D1** decorated cubes, lanes 1-4, a disappearance of the band corresponding to free DNA structures is observed. Additionally, a ladder of decreasing mobility is observed with increasing number of **D1** strands per cube. Although definitive assignments of the identity of these complexes cannot be made at this point, mobility patterns suggest that cubes may bind to more than one BSA molecule. Future work will focus on a systematic study of these complexes using different characterization techniques to elucidate the structures of the complexes. Furthermore the effect of number and positioning of **D1** on the scaffold on the resulting complexes will be studied.

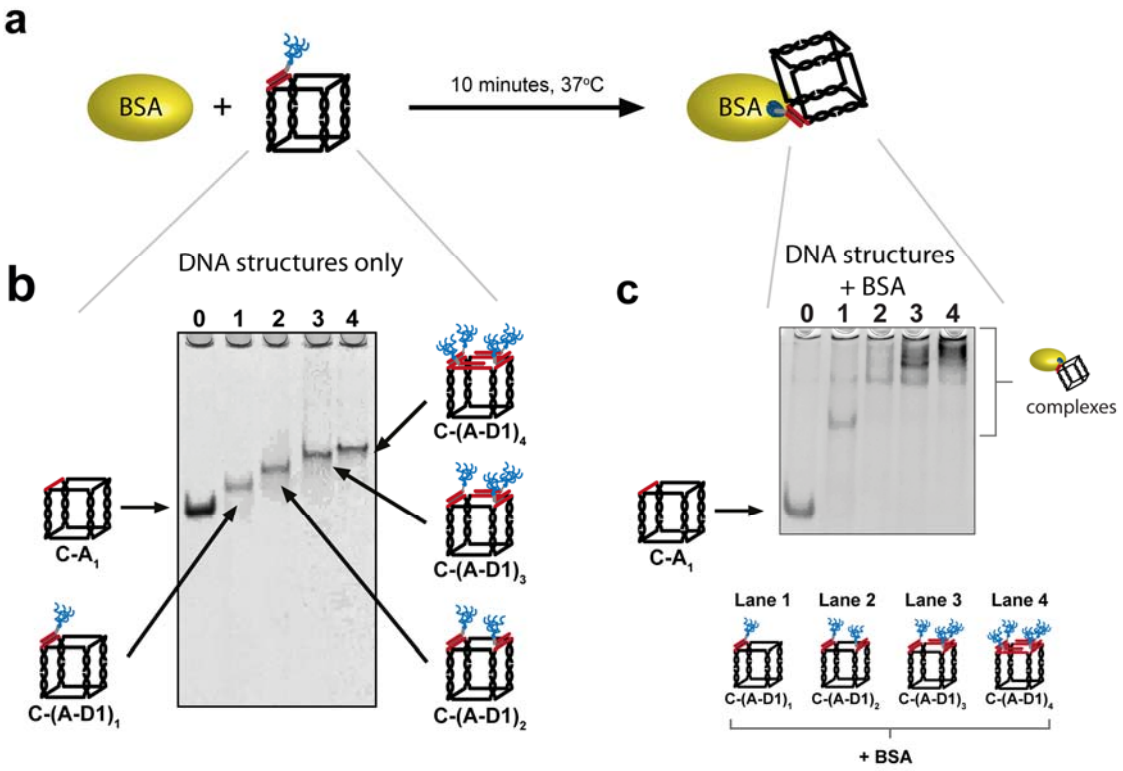

Figure A.9 – Effect of spatial organization on BSA binding. a) Example scheme of **D1** decorated cube binding to BSA. b) Native PAGE analysis of different numbers of **D1** on the cubic scaffold, revealing the expected mobility shift with addition of each **D1** to the top face of the cubic scaffold. c) The products of the BSA + DNA nanostructure are shown. The single-stranded cube **C-A$_4$B$_4$** does not bind to BSA an acts as a reference for gel mobility of the other structures, lane 0. The other structures shown in lanes 1-4 show high molecular weight products which correspond to cube-BSA complexes.

A.4 Conclusions

In this appendix an initial study into the binding of DNA-cages to serum albumin was presented using BSA as a model. It was found that while an unmodified DNA cube did not bind to BSA, the decoration of the structure with **D-DNA** resulted in strong binding. The **D-DNA** present dodecanal chains which may insert into the fatty acid binding pockets of the protein. It was found that slight modification to the chemical structure of the **D-DNA** modulates the binding affinity and the positioning of different numbers of **D-DNA** on the cubic scaffold produced a different binding pattern. This suggests that polyvalency plays an important role in the binding, and this may be used as a tool to alter the interaction strength. It has been shown previously that strong binding of therapeutics to albumin sequesters them, thus modulating bioavailability.[9] The preliminary results shown here suggest that DNA nanostructures that present hydrophobic chains could be used as a

platform to rationally tune serum protein interactions and therefore pharmacokinetics. This is especially promising in the area of nucleic acid delivery as albumin has been presented as a potential delivery vehicle for therapeutics.[10-12] The ability to combine serum albumin binding motifs with integration of siRNA or antisense oligonucleotides to the DNA cage could be used as a tool to explore the effect of album in the transport on therapeutic nucleic acids and develop new delivery strategies.

A.5 Experimental Section

The synthesis of DNA conjugates **D1** and **D2**, assembly protocols for cubic scaffolds and hybrid assemblies can be found in chapter 2, experimental section 2.5. All general information pertaining to instrumentation and chemicals can also be found in in chapter 2, experimental section 2.5.

A.5.1 FBS digestion assay

Fetal bovine serum was purchased from Wisent corporation and Dulbecco's Modified Eagle Medium (DMEM) was purchased from Invitrogen. DNA nanostructures were prepared as described in chapter 2, section 2.5.13. Samples were adjusted to 250nM in 1xTAMg for the FBS assay. In a typical assay a cubic scaffold (200nM) was incubated with 10% FBS in Dulbecco's modified Eagle's medium (DMEM) at 37°C and aliquots were taken at time points of 0, 1, 5, 12 and 24 hours. At each timepoint the aliquot was treated with either 50mM EDTA (for native study) or 25% (v/v) formamide (denaturing study) to deactivate the enzymes. Samples were loaded on either 6% PAGE in 1xTAMg for native conditions or 8% PAGE 1xTBE/8M urea for denaturing analysis. The bands were visualized with stains-all.

A.5.2 BSA binding assay

BSA was purchased from Bioshop and used without further purification. Working solutions of BSA were prepared by dilution in 1xPBS buffer (pre-prepared, Bioshop) to 40mg/mL. This concentration of albumin is approximately the same as FBS serum. For the initial assays of 3D structures with BSA the same protocol described above was used but FBS was replaced with BSA solution. For the assay shown Figure A.9 1μL of BSA solution was added to 2μL of 1μM 3D construct and total volume was made up to 10μL

with 1xTAMg. Samples were loaded on 6% PAGE in 1xTAMg and the bands visualized with stains-all.

A.5.3 EMSA for D-DNA and BSA

For the assay of single-stranded D1 and D2 against BSA the same working solution was used as described above. To each 2μL aliquot of 500nM **D-DNA** in 1xPBS was added the desired number of equivalents of BSA in 1xPBS and the final volume made up to 10μL with 1xPBS buffer for each sample. The solutions were incubated at 37°C for 1 hour before adding 2uL of 70%(v/v) glycerine solution to aid loading on a 12% non-denaturing PAGE gel, 1xTBE running buffer, and run at 250V for 30 minutes and 500V for 1 hour. Gel bands were visualized by staining with GelRed.

1 Raouane, M., Desmaële, D., Urbinati, G., Massaad-Massade, L. & Couvreur, P. "Lipid Conjugated Oligonucleotides: A Useful Strategy for Delivery." *Bioconjugate Chemistry*, (2012).

2 Wolfrum, C. *et al.* "Mechanisms and optimization of in vivo delivery of lipophilic siRNAs." *Nat Biotech* **25**, 1149-1157, (2007).

3 Rosi, N. L. *et al.* "Oligonucleotide-modified gold nanoparticles for infracellular gene regulation." *Science* **312**, 1027-1030, (2006).

4 Alemdaroglu, F. E., Alemdaroglu, N. C., Langguth, P. & Herrmann, A. "Cellular Uptake of DNA Block Copolymer Micelles with Different Shapes." *Macromolecular rapid communications* **29**, 326-329, (2008).

5 Rush, A. M., Thompson, M. P., Tatro, E. T. & Gianneschi, N. C. "Nuclease-Resistant DNA via High-Density Packing in Polymeric Micellar Nanoparticle Coronas." *ACS Nano* **7**, 1379-1387, (2013).

6 Felber, A. E. *et al.* "The interactions of amphiphilic antisense oligonucleotides with serum proteins and their effects on in vitro silencing activity." *Biomaterials* **33**, 5955-5965, (2012).

7 Conway, J. W., McLaughlin, C. K., Castor, K. J. & Sleiman, H. "DNA nanostructure serum stability: Greater than the sum of its parts." *Chemical Communications* **49**, 1172-1174, (2013).

8 Bhattacharya, A. A., Grune, T. & Curry, S. "Crystallographic analysis reveals common modes of binding of medium and long-chain fatty acids to human serum albumin." *Journal of molecular biology* **303**, 721-732, (2000).

9 Otagiri, M. "A molecular functional study on the interactions of drugs with plasma proteins." *Drug metabolism and pharmacokinetics* **20**, 309-323, (2005).

10 Lau, S. *et al.* "Enhanced Extravasation, Stability and in Vivo Cardiac Gene Silencing via in Situ siRNA–Albumin Conjugation." *Molecular Pharmaceutics* **9**, 71-80, (2011).

11 Weecharangsan, W. *et al.* "Efficient Delivery of Antisense Oligodeoxyribonucleotide G3139 by Human Serum Albumin-Coated Liposomes." *Molecular Pharmaceutics* **6**, 1848-1855, (2009).

12 Wartlick, H., Spänkuch-Schmitt, B., Strebhardt, K., Kreuter, J. & Langer, K. "Tumour cell delivery of antisense oligonuclceotides by human serum albumin nanoparticles." *Journal of Controlled Release* **96**, 483-495, (2004).